Diazopeptide chemistry

Thesis

DIAZOPEPTIDE CHEMISTRY

By

Michael Andrew Potterton

Thesis Submitted

for

the Degree of

DOCTOR OF PHILOSOPHY

at

THE OPEN UNIVERSITY

Department of Chemistry

The Open University

Walton Hall

Milton Keynes

March 1997

Date of submission: 7 November 1996
Date of award: 21 March 1997

ProQuest LLC.
789 East Eisenhower Parkway
P.O. Box 1346
Ann Arbor, MI 48106 – 1346

This Thesis is

Dedicated to My Family

Acknowledgements

I would like to express my sincere gratitude to Professor Brian Challis for his excellent supervision and his encouragement throughout the course of this work.

I would like to thank the technical staff in the Chemistry Department. In particular, Pravin Patel, Graham Geffs, Jim Gibbs, Gordon Howell and Brandon Cook for their support and good advice on technical matters during three years of research.

I would also like to thank Dr. Judy Challis for her expert assistance in supplying and interpreting many of the mass spectra required for structure elucidation of reaction products.

Finally, I must also thank my friends and colleagues at the Open University for providing some light, but welcome relief from research.

Abbreviations

Ac	Acetyl
AcOH	Acetic acid
anhyd.	Anhydrous
amu	Atomic mass units
Ar	Aromatic
aq.	Aqueous
br.	Broad peak
Bz	Benzyl
$\delta^{13}C$	Carbon 13 chemical shift
d.	Day
d	Doublet
DCM	Dichloromethane
dd	Doublet of doublets
ddd	Doublet of doublet of doublets
DECP	Diethylcyanophosphonate
DMF	Dimethylformamide
DMSO	Dimethylsulphoxide
DNA	Deoxyribonucleic acid
DPPA	Diphenylphosporylazide
EI	Electron impact
equiv.	Equivalent
Et	Ethyl
EtOH	Ethanol
FAB	Fast atom bombardment
FTIR	Fourier transform infra red
$\delta^{1}H$	Proton Chemical shift
h.	Hour

hplc	High performance liquid chromatography
Hz	Hertz
i.r.	Infra red
J	Coupling constant
LDA	Lithium diisopropylamide
λ	Wavelength
M	Mol dm^{-3}
m	Multiplet
Me	Methyl
MeOH	Methanol
min.	Minute
mM	Millimole dm^{-3}
mmol	Millimole
mol	Mole
m.p.	Melting point
m/s	Mass spectrometry
m/z	Mass to charge ratio
NEt_3	Triethylamine
nmr	Nuclear magnetic resonance
Ph	Phenyl
ppm	Parts per million
q	Quartet
R	Alkyl
s	Second/singlet
S_N	Nucleophilic substitution
sat.	Saturated
t	triplet
t	tertiary
tlc	Thin layer chromatography

THF	Tetrahydrofuran
TMS	Tetramethylsilane
TSP	Tetramethylsilanepropionate
uv	ultra violet
ν	Wavenumber
VT	Variable temperature
v/v	Volume/volume
w/v	Weight/volume

Abstract

The decomposition of diazopeptides in buffer-acid solutions (formate, acetate and phosphate) are general-acid-catalysed, but the catalysis for these reactions is attenuated at high buffer-acid concentrations and non-linear second-order plots are observed. This behaviour is evident for both glycyl and non-glycyl diazopeptides, which decompose *via* different mechanisms *i.e.* A-2 and A-S_E2 mechanisms, respectively. Hence, an explanation for this unusual kinetic behaviour, based on a change in the rate-limiting step with increasing [HA] must be excluded. Further, unlike glycyl diazopeptides, non-glycyl diazopeptides decompose to give products whose structure and yield is independent of the acid-catalyst. Thus, the acid-catalysis and non-linear kinetics observed can neither relate to product forming steps. The only plausible mechanistic explanation for this behaviour must, therefore, relate to the existence of a competing nucleophilic addition pathway of the buffer-acid across the diazo group to form azo-ester compounds. Good evidence was also found *via* kinetic and product studies, for the occurrence of similar reactions of diazopeptides with amines to form analogous triazene compounds. Such diazopeptide addition reactions may be biologically significant, as the compounds formed may have the potential to act as more stabilised, transportable forms of the cytotoxic diazonium ion. This study also includes the synthesis and spectroscopic characterisation of novel triazene-peptide compounds and metal-triazene-peptide complexes.

The above mechanisms for the decomposition of non-glycyl diazopeptides (where elimination, substitution and neighbouring group reactions arise) are supported by product studies involving spectroscopic analyses and the synthesis of novel, authentic compounds. The formation of cyclic products *i.e.* epoxides and lactams, from the acid-catalysed decompositions of *N*-(2-diazo-3-hydroxybutanoyl)glycine ethyl ester (2.1) and *N*-(2-diazo-3-carbamoylpropanoyl)glycine benzyl ester (4.1), respectively, are reported.

Ring-strained compounds are highly reactive especially towards nucleophiles, and therefore, could possibly be cytotoxic, acting as stabilised alkylating agents. Epoxide alkyl-oxygen bond fission to generate an alkylating agent, and stability for absorption intact from the gastric tract, are two fundamental requirements for the carcinogenic activity of epoxides. Hence, kinetic and product studies for epoxides *cis*-(4.10), (4.14) and *cis*-(4.15), derived *via* the nitrosation of α-amino threonyl and seryl residues, were carried out for reactions in dilute acidic and basic solutions and in aqueous morpholine. Further, independent studies have shown that epoxide (4.14) is mutagenic by Ames Test.

KEY STRUCTURES

DIAZOPEPTIDES

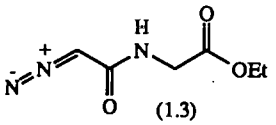
(1.3)

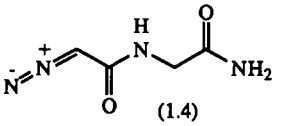
(1.4)

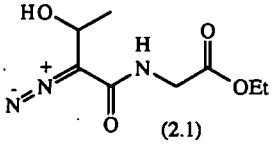
(2.1)

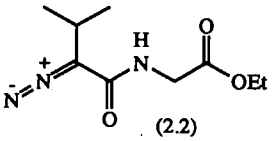
(2.2)

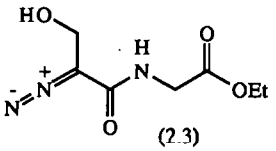
(2.3)

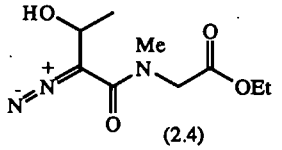
(2.4)

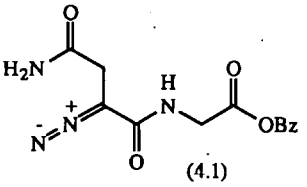
(4.1)

DIAZOPEPTIDE ADDITION PRODUCTS

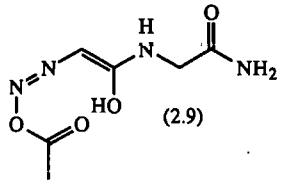
(2.9)

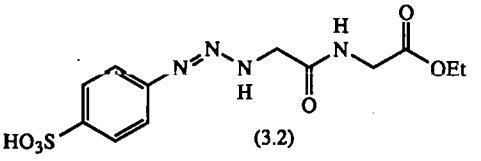
(3.2)

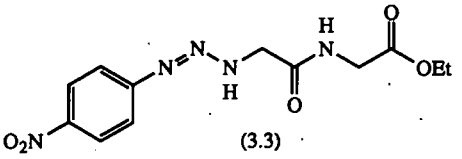
(3.3)

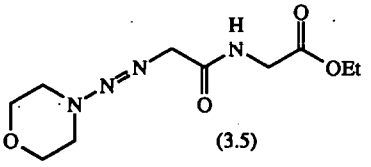
(3.5)

DIAZOPEPTIDE DECOMPOSITION PRODUCTS

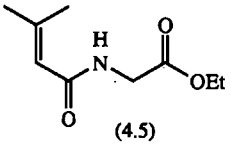
(4.5)

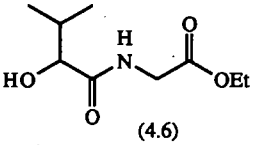
(4.6)

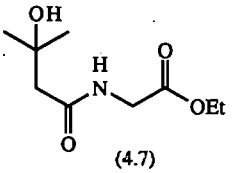
(4.7)

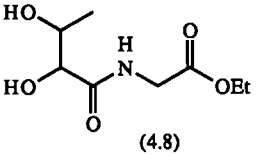
(4.8)

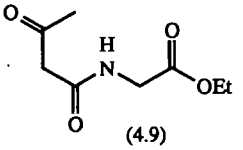
(4.9)

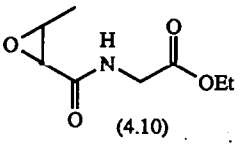
(4.10)

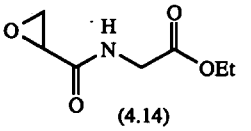
(4.14)

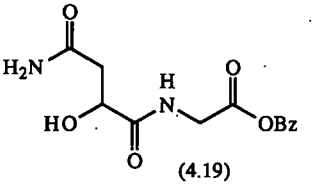
(4.19)

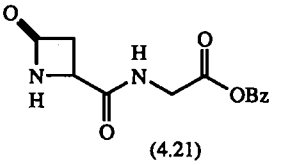
(4.21)

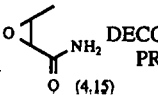
DECOMPOSITION PRODUCTS

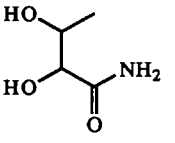
(5.3)

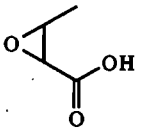
(5.4)

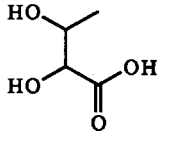
(5.5)

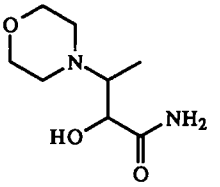
(5.6)

CONTENTS

1. Historical Review

1.1 Introduction

Because many *N*-nitroso-compounds are carcinogenic there is much interest in nitrosation as a causal factor in human cancer.[1] Early work focused on exposure to exogenously formed *N*-nitroso-compounds, which are frequently found in some food, beverages and tobacco products.[2] Once it became known that nitrosation proceeds in the human stomach, interest extended to endogenous formation of *N*-nitroso-compounds both in the respiratory tract by inhaled nitrogen oxides[2] and in the stomach by ingested nitrite.[3]

There is much evidence that diet[3] is an important factor in the incidence of human cancer. The stomach provides suitable conditions (pH 1-5, 37°C) for nitrosation reactions,[4] both nitrite and nitrate salts are present in the diet[5] and an estimated 20 % of ingested nitrate is reduced to nitrite by bacteria in the oral cavity.[5] High gastric nitrite concentrations (> 0.2 mM) are found in conjunction with elevated gastric pH (6.5-9.0) and they relate to an overgrowth of nitro-reductase bacteria in the high pH stomach. Patients with clinical conditions such as pernicious anaemia and gastrectomy have an elevated incidence of stomach cancer,[6] but it is conjectural whether this translates into an increased endogenous synthesis of *N*-nitroso-compounds.[7]

N-nitroso-derivatives are most readily produced by the nitrosation of secondary amino compounds, and *N*-nitroso compounds have been found in gastric aspirates.[53] The risks posed by endogenous nitrosation of secondary amines may be small, however, because their dietary intake is only 6-8 g/day.[8] The endogenous nitrosation of peptides, from a protein intake of 70-250 g/day,[8] may pose a greater risk because of their larger availability in the diet. The aim of the present work was to investigate the diazotisation of peptides by nitrous acid and to ascertain the structure and properties of the products formed.[9, 10]

1.2 Nitrosation of Peptides

The nitrosation of peptides can occur at either the terminal primary amino group to effect deamination (loss of N_2) *via* a diazopeptide (*Path 1*) or the peptide N-atom to give an *N*-nitrosopeptide (*Path 2*). Subsequently, the *N*-nitrosopeptide may react with a nucleophile resulting in cleavage of the peptide linkage (Scheme 1.1).[11]

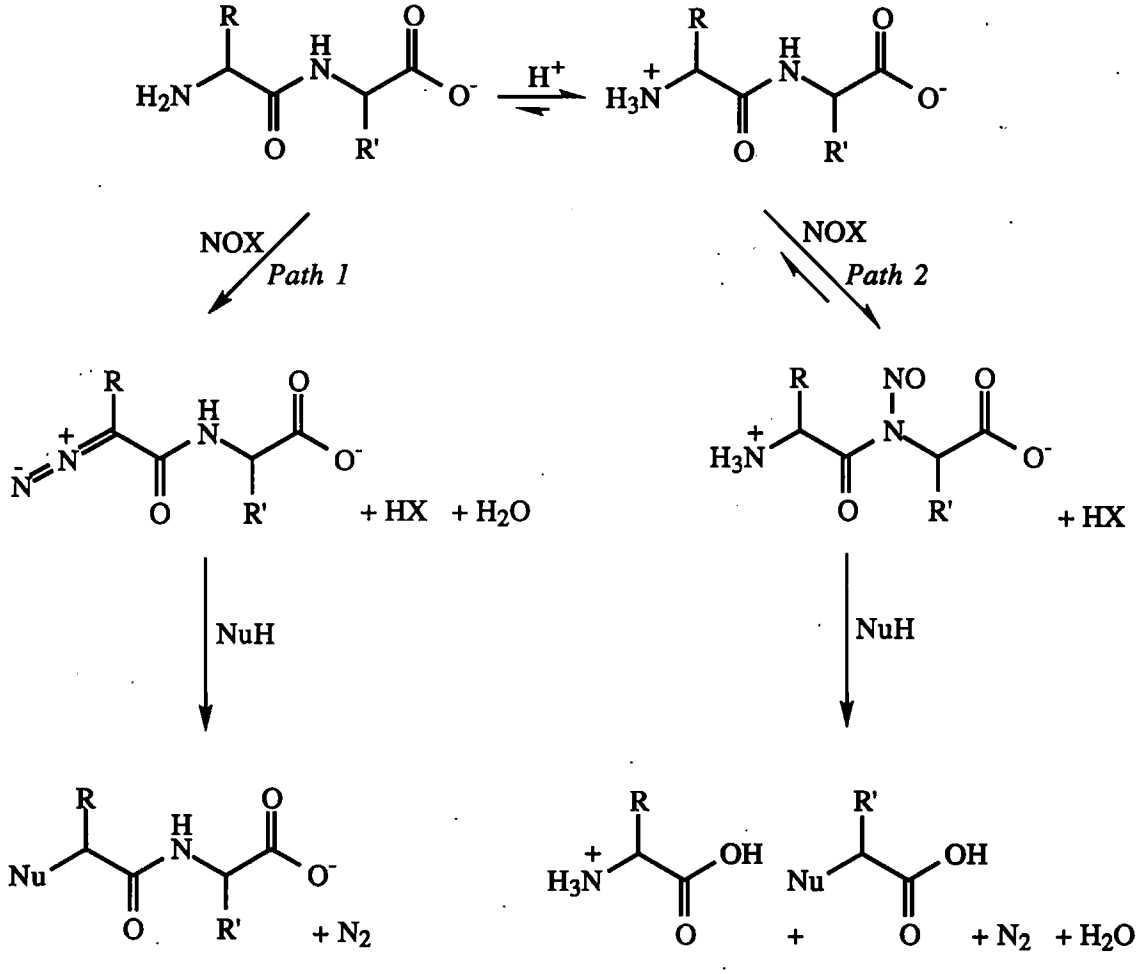

NuH = HCl, H_2O, DNA etc.

Scheme 1.1 *Nitrosation of Peptides*

Diazopeptides were discovered by Curtius in 1883,[37] although this early work only produced derivatives of glycylpeptides without a free carboxylic acid terminus. Other

diazopeptides, including those with a free carboxylic acid terminus were not synthesised until 1990, *via* aprotic nitrosation procedures.[42]

In 1966, Baldini and Brambilla[12] discovered that some of the Curtius diazopeptide derivatives expressed antineoplastic properties and subsequently, it was shown that they are mutagenic,[13] immunodepressive[14] and antibacteriostatic,[15] with a complex pattern of cytotoxic properties including tumour induction,[14] tumour suppression,[12] and antimetastatic activity.[16]

Diazopeptides are labile, decomposing rapidly at gastric pH. For this reason, they may not be absorbed intact following endogenous formation in the stomach. Diazopeptides are relatively stable at blood pH (*ca.* pH 7), however, and have been shown to be carcinogens.[13, 17] Challis *et. al.* also demonstrated that diazopeptides form readily from dilute, gaseous NO_2 in both aqueous buffers and human blood from several peptides.[19]

N-Nitrosopeptides were first synthesised in 1984.[22, 23] These were derived from N-protected substrates, such as (*N*-acetyl-*L*-prolyl)glycine, alanine and phenylalanine (1.1a-c) and several protected peptide esters, to avoid concurrent diazotisation. N-nitrosation was effected aprotically in organic solvents using N_2O_4[22] or dilute gaseous NO_2.[23] Subsequently, some of these compounds were shown to be direct acting mutagens[20, 21] and to alkylate DNA *in vitro*. In aqueous media between pH 1-8 at 37 °C, nitrosopeptides have half-lives of the order of a few hours, decomposing *via* a deaminative pathway to generate a diazo compound (Scheme 1.2).[11]

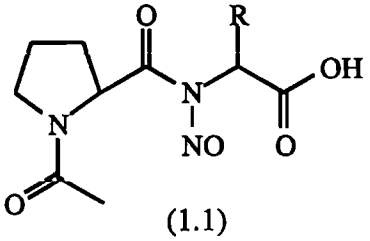

(1.1)

a, R = H; b, R = Me; c, R = CH_2Ph

Thus, it is probable that diazo derivatives readily form *in vivo* by endogenous nitrosation of dietary peptides either directly, *via* nitrosation at the terminal primary amino group, or indirectly, *via* nitrosation at the peptide N-atom to give an *N*-nitrosopeptide which subsequently decomposes to a diazopeptide.

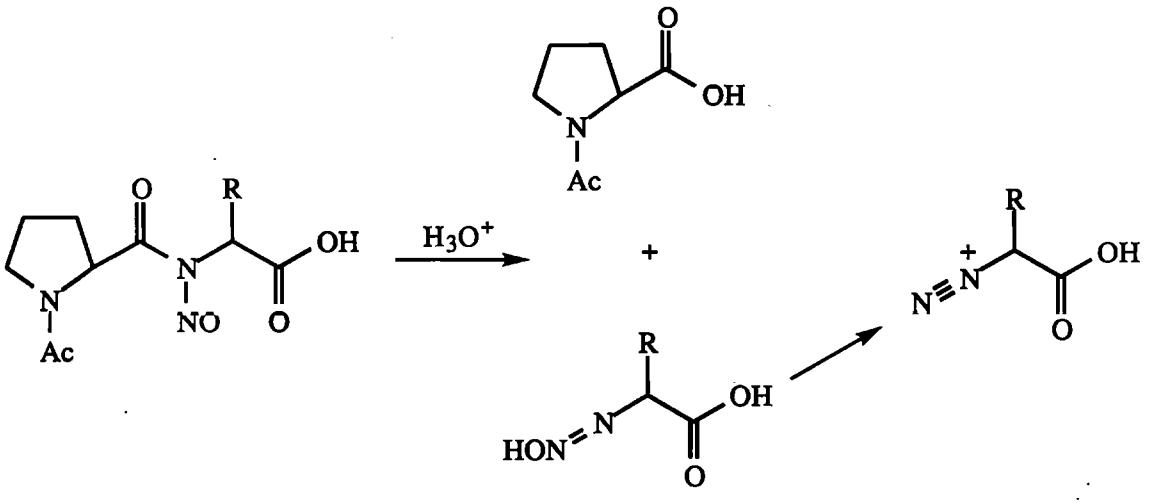

Scheme 1.2 *Decomposition of N-Nitrosopeptides*

1.3 Synthesis of Diazopeptides

Except under very special circumstances, reviewed by Bott,[24] aliphatic diazonium ions are too unstable to be isolated. The unprotonated form, however, is well known and many aliphatic diazo compounds have been prepared and characterised. Diazo compounds have attracted much interest as reliable, widely applicable precursors of both carbenes[25] and C=N=N synthons.[26] Several excellent reviews of this chemistry exist[27-29] and many procedures for the synthesis of aliphatic diazo compounds have been reviewed by Regitz.[30] These include the nitrosation of primary amines (Equation 1.1),[31] the Forster Reaction (Equation 1.2),[32] dehydration of hydrazones (Equation 1.3),[33] the Bamford-Stevens Reaction (Equation 1.4),[34] deacylation of *N*-nitrosocarboxamides (Equation 1.5),[35] nitrogen-transfer reactions (Equation 1.6)[34, 35] and triazene decomposition reactions (Equation 1.7).[36, 50]

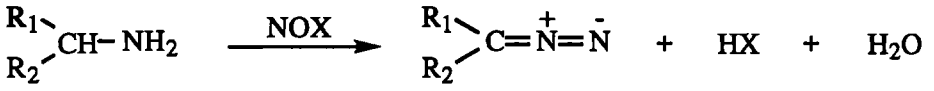

(1.1)

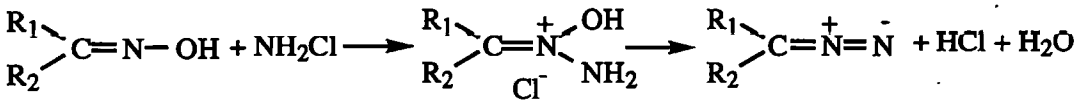

(1.2)

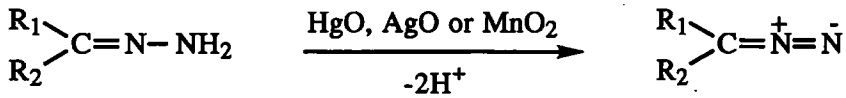

(1.3)

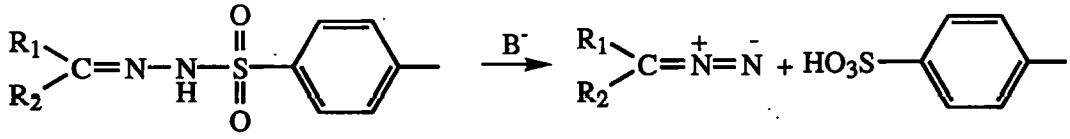

(1.4)

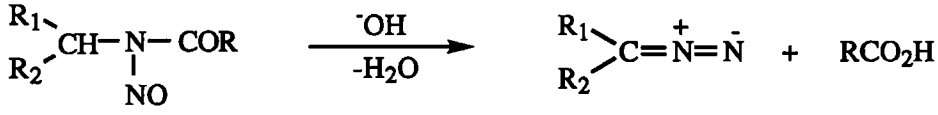

(1.5)

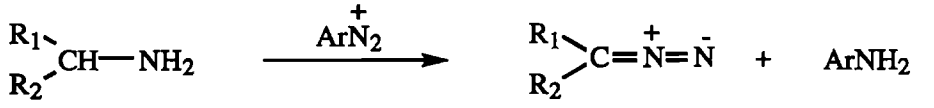

(1.6)

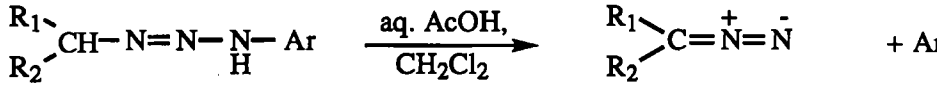

(1.7)

Many of these methods are unsuitable for the synthesis of diazopeptides because either the reaction conditions lead to product decomposition or the precursor compounds are too difficult to synthesise.[25] Two methods involving transformation of the native peptide under relatively mild conditions are the nitrosation (diazotisation) reaction (Equation 1.1) and the nitrogen-transfer and related triazene decomposition reactions (Equations 1.6 and 1.7). Using the second of these, McGarrity[51] reported the preparation of several diazo amino esters in yields of up to 70 % by treating amino acid esters with either 4-nitrobenzenediazonium tetrafluoroborate or 2,4-dinitrobenzene-diazonium tetrafluoroborate in the presence of base. The reaction proceeds *via* base

induced cleavage of the triazene intermediate (Scheme 1.3). The corresponding reaction with peptide ethyl esters gave only low yields of diazopeptides.[18, 52]

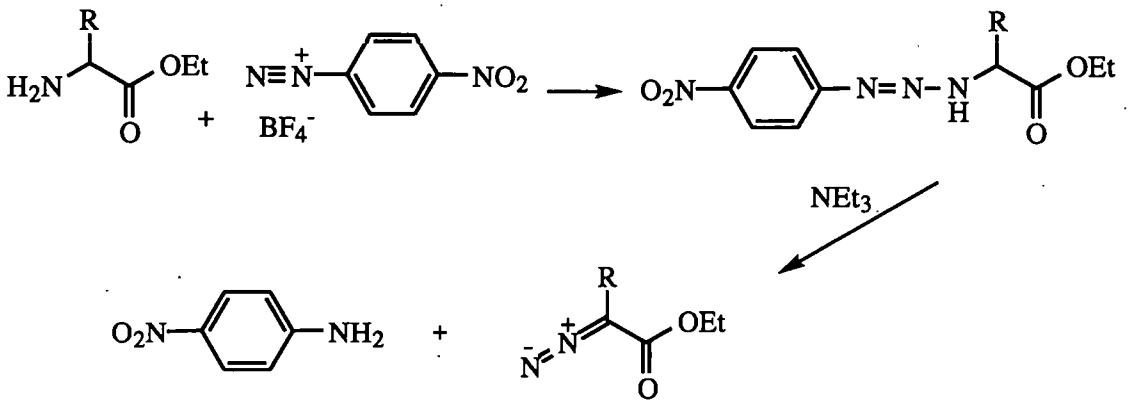

Scheme 1.3 *Synthesis of Diazoesters via the Nitrogen Transfer Reaction*

To date, the most successful method of preparing diazopeptides is *via* nitrosation. This reaction was first described by Curtius[37] in 1883 to prepare *N*-(2-diazoacetyl)triglycine ethyl ester (1.2) from the peptide ester in an aqueous acetate buffer at 0 °C using HNO_2 generated from the nitrite salt (Equation 1.8).

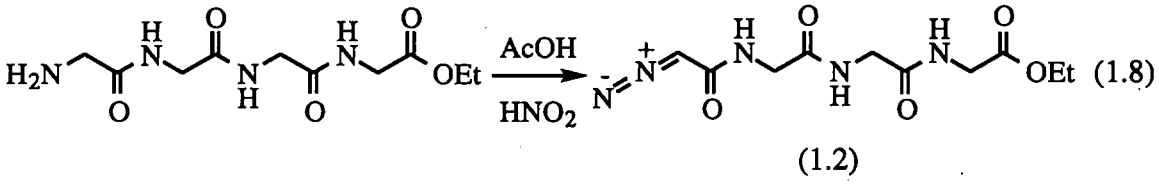

(1.2)

Subsequently, a number of other diazo compounds (1.3-1.5) derived from glycyl-peptide compounds were prepared using the same procedure.[38-40] In all cases, the terminal carboxyl terminus was protected, and isolation of the diazo compound relied upon precipitation from the reaction mixture on the basis of their low aqueous solubility. A subsequent modification[41] of the Curtius *et. al.* procedure involving a biphasic system, where the diazopeptide was continually extracted into an organic solvent as it formed in the aqueous phase, reduced acid-catalysed decomposition of the diazopeptide, and increased the yield significantly.

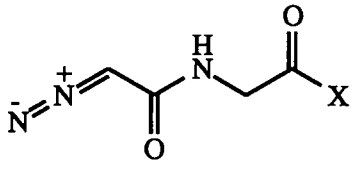

X = OEt (1.3); NH_2 (1.4); $NHNH_2$ (1.5)

Protic nitrosation was found to be unsuitable for the synthesis of non-glycyl diazopeptides because of their greater lability. In 1990, Challis and Latif[42] reported the synthesis of several diazopeptide ethyl esters *via* aprotic nitrosation using liquid nitrogen dioxide at -40 °C (Equation 1.9). This followed the procedure of White[43] for the synthesis of *N*-nitrosoamides which was also used for the synthesis of nitrosopeptides.[21] Reactions were carried out in an organic solvent (e.g. $CHCl_3$, EtOAc) with triethylamine to keep the mixture non-acidic, and $NaSO_4$ to remove water (Equation 1.9).

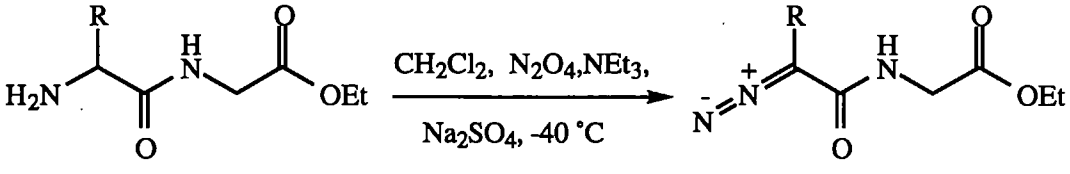

CH_2Cl_2, N_2O_4,NEt_3, Na_2SO_4, -40 °C

+ NO_3^- (1.9)

R = H, CH_3, $CH(OH)CH_3$, CH_2OH, $CH_2CH(CH_3)_2$ etc.

This aprotic method was extended to synthesis of glycyl diazopeptides with an unprotected carboxyl terminus from native peptides by a simple adaptation. Thus, the highly polar peptide substrate was solubilised as the tetra-*N*-butylammonium salt and after reaction, the diazopeptide was precipitated as the calcium salt. All the diazopeptides could be purified by silica-column chromatography and were obtained in yields of 20-80 %.

1.4 Structure and Spectroscopic Properties of Diazopeptides

In diazoalkanes, the C-N (1.28-1.32 Å) and the N-N (1.12-1.13 Å)[44] bond lengths are slightly longer than the C=N and N=N bond lengths of imines and nitrogen, respectively.

This suggests that the diazo group exists as a resonance hybrid between the canonical forms (X), (Y) and (Z) {Figure 1.1}. Structures (X) and (Y) have been confirmed by i.r. spectroscopy.[45] Structure (Z) probably makes a smaller contribution than structures (X) and (Y) to the resonance hybrid because it has fewer covalent bonds and greater charge separation. The three hybrid forms account for all the chemistry of diazo compounds, which under appropriate conditions, may behave as either acids, bases, nucleophiles, electrophiles, 1,3-dipoles or sources of carbene radicals.

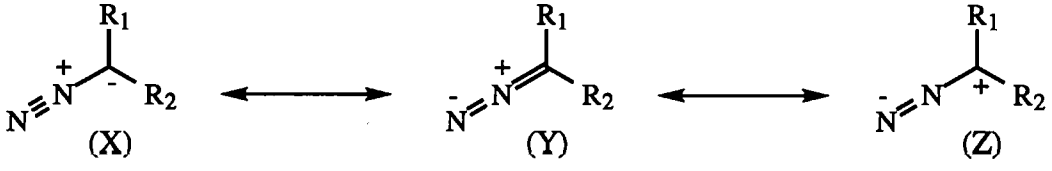

Figure 1.1

It can be anticipated that the less widely studied diazopeptides have similar properties to diazoalkanes, and results reported for several diazopeptides by Challis and Latif[42] support this contention. Thus, as for diazoalkanes, diazopeptides have a highly characteristic i.r. band at ν_{max} *ca.* 2100 cm^{-1} corresponding to the C=N=N stretching vibration, a strong ultraviolet absorbance at λ_{max} *ca.* 250-260 nm (log ε *ca.* 4) corresponding to the π->π^* transition, and a weaker visible absorbance accounting for their yellow colour at λ_{max} *ca.* 370-380 nm (log ε *ca.* 1.3) corresponding to the n->π^* transition.[42] In the ^{1}H-nmr spectra of diazopeptides there is pronounced deshielding, relative to the parent peptide, of protons α and β to the diazo group *i.e.* 0.83-1.50 ppm for the α glycyl-H of *N*-(2-diazoacetyl) peptides and 0.39-0.60 ppm for the β-H of non-glycyl diazopeptides.[42] In electron impact mass spectrometry, the diazopeptide molecular ions are either unobservable or extremely weak, because of facile loss of N_2. Good spectra are obtained, however, with fast atom bombardment (FAB) techniques.[42]

1.5 Stabilities and Acid-Catalysed Decomposition Reactions

The decomposition reactions of free diazoamino acids and diazopeptides and the corresponding esters have been examined in connection with H^+-transfer studies.

Either one of two steps in the acid-catalysed reactions may be rate-limiting (Scheme 1.4).

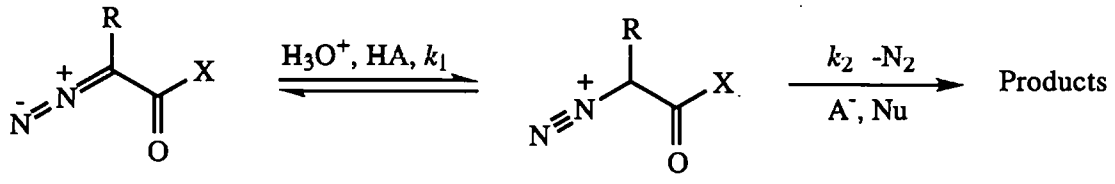

X = O^-, NH_2, OR, NHR

Scheme 1.4 *Decomposition of Diazoamino acids and Diazopeptides*

If k_1 is slow and H^+-transfer rate-limiting, decomposition proceeds *via* an A-S_E2 mechanism. The reaction is subject to general-acid-catalysis but not to nucleophilic-catalysis, and a normal solvent deuterium isotope effect {$k_1(H_3O^+) / k_1(D_3O^+) > 1$)}is expected. Such kinetic behaviour has been observed for α-C-substituted diazopeptide ethyl esters (R = Ph, CH_2OH, $CHCH_3OH$ and $CH_2CH(CH_3)_2$; X = $NHCH_2CO_2Et$)[86] and for ethyl-2-diazopropionate (R = CH_3; X = OEt).[73] Since the initial H^+-transfer is rate-limiting, information about subsequent rapid steps is inaccessible from kinetic data. It is not known, for example, whether decomposition of the diazonium ion intermediate is unimolecular (S_N1) or bimolecular (S_N2). Alternatively, k_2 can be rate-limiting *via* A1 or A2 mechanisms following rapid equilibrium protonation of the neutral diazo substrate. These reactions exhibit specific acid-catalysis, an inverse deuterium isotope effect {$k_2(H_3O^+) / k_2(D_3O^+) < 1$}, and catalysis by nucleophiles if the A2 mechanism applies. Such behaviour has been observed for *N*-(2-diazoacetyl)-peptides (R = H, X = $NHCH_2CO_2X'$)[86] and ethyldiazoacetate (R = H, X = OEt)[87-89] which decompose *via* A-2 pathways in dilute aqueous acidic media. Kreevoy and Konasewich,[90] however, found that diazoacetate ion (R = H, X = O^-) decomposed *via* an A-S_E2 pathway in dilute aqueous acid and alkali solutions, but *via* an A-1 pathway in concentrated alkali. Their data in aqueous alkali are also consistent with an A-2 pathway involving intramolecular nucleophilic-catalysis by the carboxylate ion (Scheme 1.5), which would avoid formation of a primary carbocation.

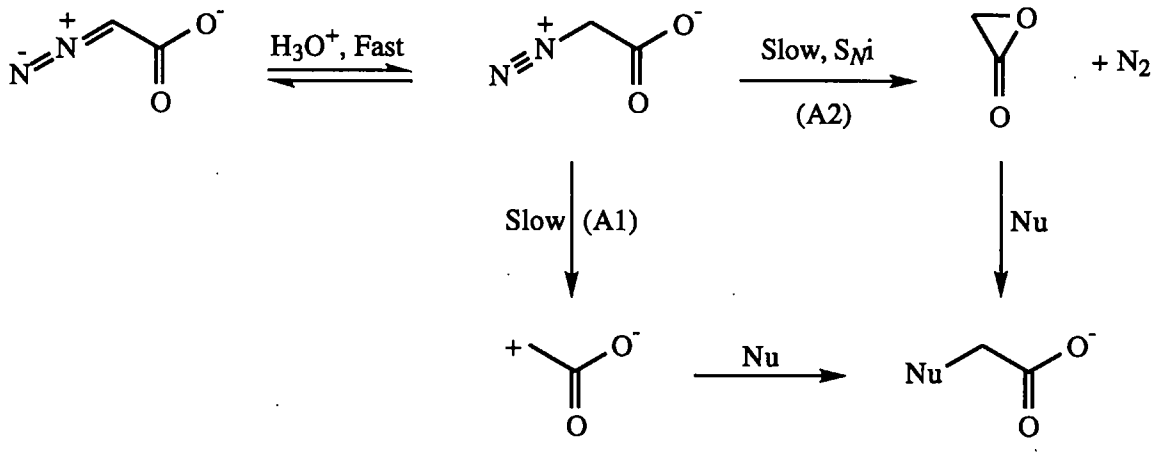

Scheme 1.5 *Decomposition of Ethyldiazoacetate in Aqueous Solution*

The decomposition of diazopeptides is general-acid-catalysed, occuring in both buffer solutions and dilute acid.[18] However, Shuja reported that some of these reactions in buffer solutions were unusual with a non-linear dependence of the rate of diazopeptide decomposition on the buffer-acid concentration *i.e.* attenuation of the rate was observed at high [HA], where HA = formic acid and acetic acid in formate and acetate buffers, respectively.

Initial investigations of diazopeptides carried out by Glover,[91] suggested that their stabilities lie somewhere in between those of diazoamino acid esters and free diazoamino acids. *N*-(2-Diazoacetyl)glycine ethyl ester (1.3), for example, gave $t_{1/2}$ *ca.* 11min. and 54 h. at 25 °C and pH 4.75 and 7.21, respectively.[91] More detailed studies have shown that diazoacetyl-peptides (R = H) are more stable than those with electron-donating substituents (R = alkyl) adjacent to the alkyl group. Since protonation of diazoacetyl peptides and subsequent cleavage of the C-N bond generates an unstable primary carbocation, C-N bond cleavage is more difficult and indeed rate-limiting. But for non-glycyl diazopeptides ($R \neq H$), protonation and C-N bond fission generates a more stable secondary carbocation, hence C-N bond cleavage is faster and the initial H^+-transfer is rate-limiting.

1.6 Deamination Products

Nitrosation is a standard procedure for deaminating primary amines including amino acids and peptides. The initial diazo product (e.g. amino acid or peptide with a protected terminal carboxylate moiety) is often isolable (see Section 1.3), but it generates a reactive diazonium ion intermediate under acidic conditions which readily expels N_2 (Scheme 1.4). There has been much interest in the stereochemistry of deamination of amino acids. With chiral substrates, deamination has been shown to proceed with retention of stereochemistry.[92] As mentioned earlier, this has been attributed to interaction between the carboxylate moiety and the diazonium ion[93] to form an α-lactone intermediate (1.6), which is subsequently ring-opened by the incoming nucleophile to give net retention of configuration (Scheme 1.6).

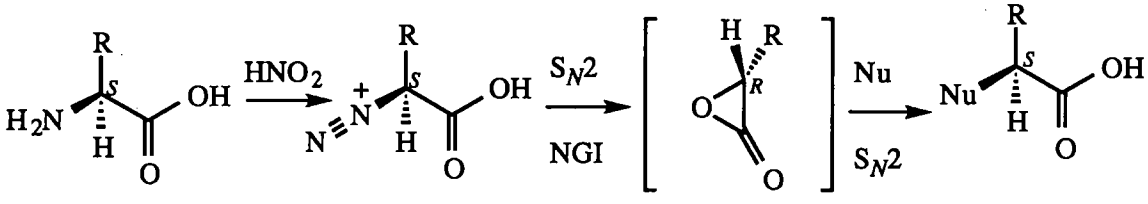

(1.6)

Scheme 1.6 *Carboxylate Neighbouring Group Effect in the Deamination of Amino acids*

Thus, deamination of the amino acids serine, aspartic acid and asparagine by nitrous acid gave glyceric acid (1.7), malic acid (1.8) and β-malamidic acid (1.9), respectively, all with retention of stereochemistry.[94-97]

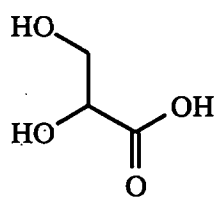

(1.7)

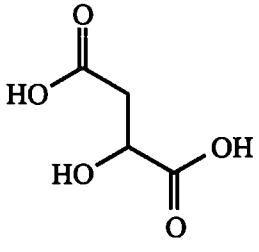

(1.8)

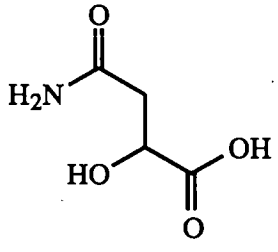

(1.9)

Since a similar neighbouring group interaction is less likely (see Scheme 1.13), the deamination of peptides may be expected to proceed *via* direct S_N reaction of the

diazonium ion intermediate to substitution products with inverted stereochemistry at the α-C-atom for S_N2 like product forming steps.

It follows that diazopeptides are alkylating agents and that peptide nitrosation will lead to a spectrum of substitution, elimination and rearrangement products characteristic of carbocation intermediates. For glycyl peptides, where elimination and rearrangement reactions are impossible, substitution products resulting from the alkylation of water and other nucleophilic substances predominate as shown in Table 1.1 for both the diazotisation of glycylglycine ethyl ester (1.10) and the decomposition of authentic *N*-(2-diazoacetyl)glycine ethyl ester (1.3) in 1 M HCl and 1 M HOAc buffer at 37 °C.[98]

Table 1.1 Products and % Yield for the Nitrosation of Glycylglycine ethyl ester (1.10) and the Decomposition of *N*-(2-Diazoacetyl)glycine ethyl ester (1.3)

Substrate	Reaction	Product 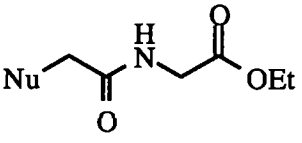 and % Yield*		
		Nu = $^-$OH	Nu = Cl^-	Nu = AcO^-
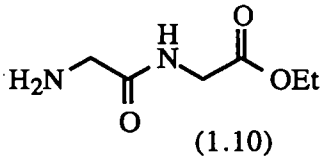 (1.10)	in 1 M HCl	42	46	-
+ HNO_2	in 1 M AcOH	68	-	31
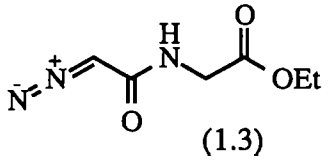 (1.3)	in 1 M HCl	45	47	-
	in 1M AcOH	68	-	31

**Relative to HNO_2 or diazopeptide*

The formation of cyclic products *via* deamination has been reported for a number of amino acids. For example, Austin[99] showed that deamination of glutamic acid gave γ-lactone (1.11) in 93 % yield with retention of stereochemistry. Thus, cyclisation by the γ-carboxylate moiety must be proceeded by an S_N2 displacement of nitrogen by the α-carboxylate moiety to form the α-lactone intermediate (1.12) {Scheme 1.7}.[99, 100]

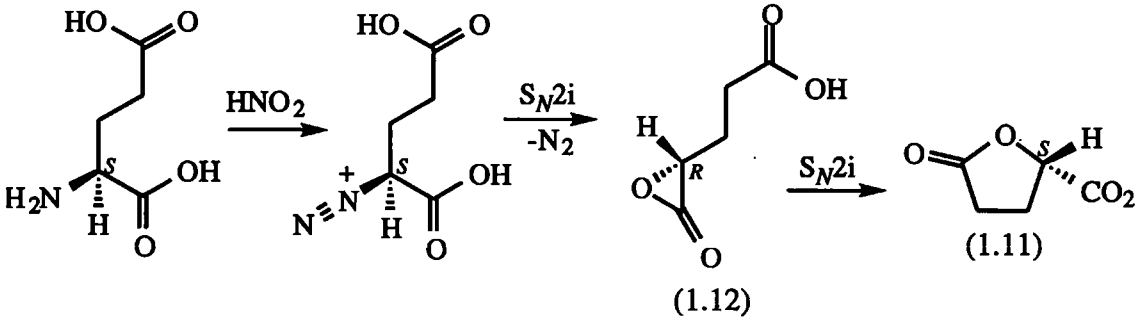

Scheme 1.7 *γ-Lactone Formation from L-Glutamic acid*

Treatment of *L*-glutamine with nitrous acid also gave γ-lactone (1.11) as the final product, plus an abnormally large amount of nitrogen (two moles per mole of *L*-glutamine in the Van-Slyke determination).[101] This has been attributed to formation of an imidate ester intermediate (1.13) which reacts with a second mole of nitrous acid to liberate a second mole of nitrogen (Scheme 1.8).[99-102]

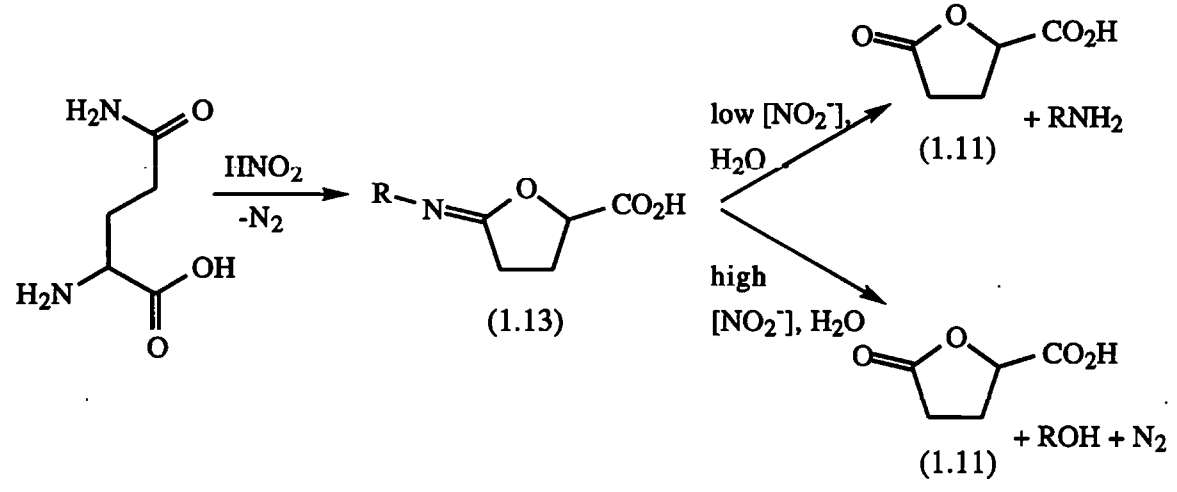

Scheme 1.8 *γ-Lactone Formation from L-Glutamine*

Again, the reaction proceeds with net retention of stereochemistry at the α-C-atom, implying γ-lactone formation *via* an α-lactone intermediate. Cyclic products were not observed for the deamination of asparagine nor aspartic acid,[103] presumably because the corresponding β-lactone is less stable due to ring-strain.

Treatment of *L*-cysteine with nitrous acid gave a 3:1 mixture of the (*R*) and (*S*) enantiomers, respectively, of thiiran carboxylic acid (1.14) in 55 % yield.[104, 105] The major (*R*) isomer resulted from ring-opening of the α-lactone intermediate by sulphur (*PATH 1*), whilst the minor (*S*) isomer resulted from nucleophilic displacement of the nitrogen directly by the sulphur (*PATH 2*) {Scheme 1.9}.

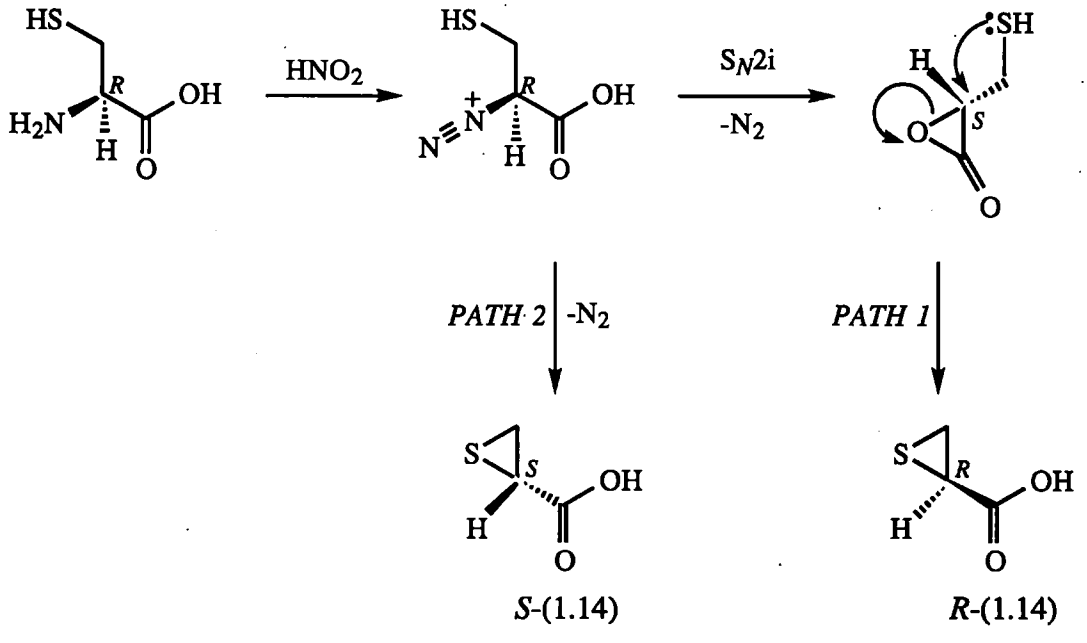

Scheme 1.9 *Thiiran Formation from L-Cysteine*

Consistent with this rationalisation, methyl (*R*)-cysteinate gave only the methyl (*S*)-thiiran carboxylate (1.15) in 47 % yield.[104, 105] Comparable epoxide products from the deamination of serine and threonine amino acids have not been reported.

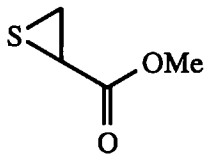

(1.15)

Similar, intramolecular neighbouring group interactions may also be anticipated for the deamination of peptides bearing amino, carbonyl, thiol and possibly hydroxyl groups adjacent to the primary amino terminus. These interactions are of interest in the present context insofar as some of the resultant cyclic products are likely to be more robust alkylating agents than their relatively unstable diazopeptide precursors. Some of these expectations have been realised for the diazotisation of cysteinyl and aspartyl dipeptides. For example, the diazotisation of *L*-cysteinylglycine methyl ester (1.16) by $NaNO_2$ in dilute HCl at 0 °C gave the thiiran peptide derivative (1.17) in 44 % yield (Scheme 1.10),[106] presumably with inversion of stereochemistry at the α-C-atom.

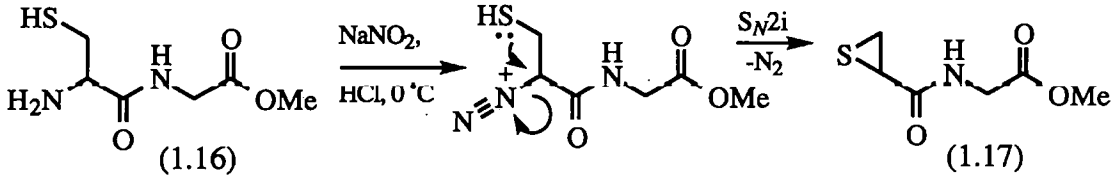

Scheme 1.10 *Thiiran Formation from L-Cysteinylglycine methyl ester (1.16)*

The diazotisation of *L*-aspartyl-*L*-phenylalanine methyl ester (1.18) {the artificial sweetener, aspartame} under similar conditions yielded β-lactone (1.19) in a maximum yield of *ca.* 27 % after 2 h. (Scheme 1.11). On forming, the β-lactone (1.19) decomposed to hydrolysis products.[107]

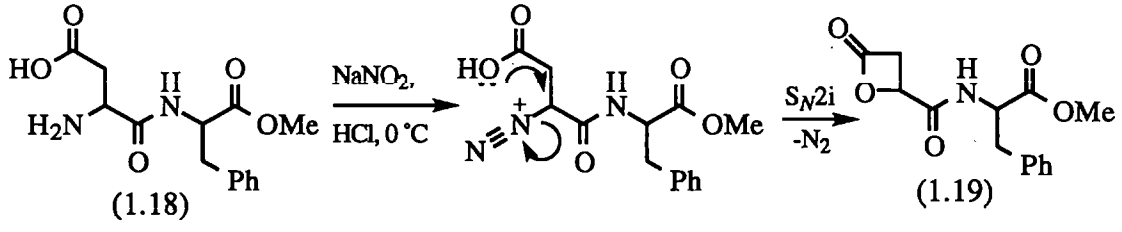

Scheme 1.11 β *Lactone Formation from L-Aspartyl-L-phenylalanine methyl ester (1.18)*

Further, recent work by Shuja indicated that the decomposition of *N*-(2-diazo-3-hydroxypropanoyl)glycine ethyl ester (2.3) in dilute $HClO_4$ gave virtually equal amounts of diol (1.32) and epoxide (4.14) products, although authentic compounds were unavailable to confirm their identity (Scheme 1.12).[18] A similar epoxide product may also be anticipated from the deamination/decomposition of threonyl peptide/diazopeptide residues.

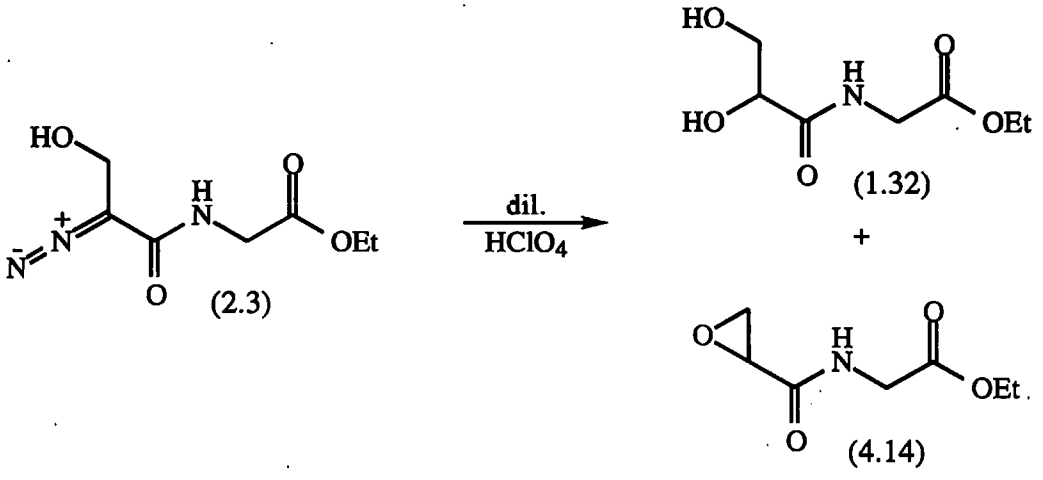

Scheme 1.12 *Products from the Decomposition of N-(2-Diazo-3-hydroxypropanoyl)glycine ethyl ester (2.3) in $HClO_4$*

Three other neighbouring group interactions may be common to all peptide diazotisations, irrespective of their amino acid constituents. The first involves cyclisation by the terminal carboxylic acid of native dipeptides to produce diketomorpholines (1.20), as observed for the nitrosation of glycylglycine in dilute acid (Scheme 1.13).[108]

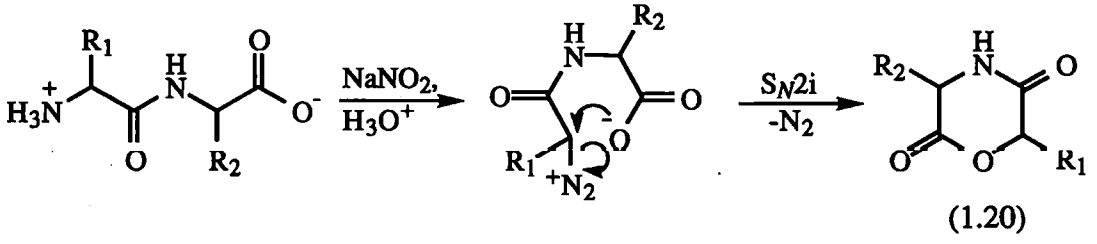

Scheme 1.13 *Diketomorpholine (1.20) Formation from Native Dipeptides*

The second involves the peptide N-atom to form an α-lactam intermediate (1.21), which is first hydrolysed to an iminodialkanoic acid (1.22) and then further nitrosated at the peptide N-atom to form an *N*-nitrosoiminodialkanoic acid (1.23) {Scheme 1.14}.[91, 109-111] This neighbouring group interaction is analogous to substitution by the α-carboxylate at the α-C-atom observed for the deamination of amino acids (see Scheme 1.5). Pollock reported the formation of *N*-nitrosoimino dialkanoic acids *via* the nitrosation of dipeptides at high nitrite concentrations, but in low yields (0.1-10 %).[109]

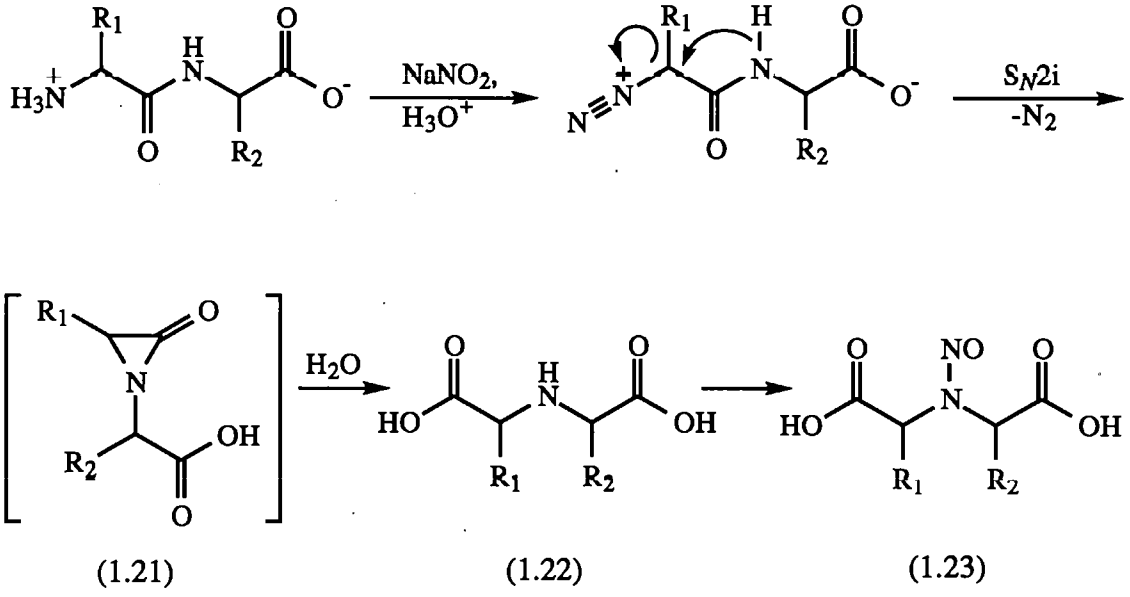

Scheme 1.14 *Formation of N-Nitrosoiminodialkanoic acids*

The third neighbouring group interaction involves cyclisation of the diazo group with the peptide N-atom to form a triazene intermediate and then a triazole product (1.24) under alkaline conditions (pH > 10) {Scheme 1.15}. This interesting reaction, discovered by Curtius and Thompson[112] for *N*-(2-diazoacetyl)glycine ethyl ester (1.3), is probably common to all diazopeptides. The cyclisation is reversible in acid, and the reverse reaction (*i.e.* conversion of triazoles to diazoamides) was studied extensively by Dimroth at the turn of the century.[113] However, for triazoles derived from diazopeptides, conversion back to the diazopeptide proceeds only in very concentrated acids,[114] and there is no evidence that triazoles react with genetic material under physiological conditions.

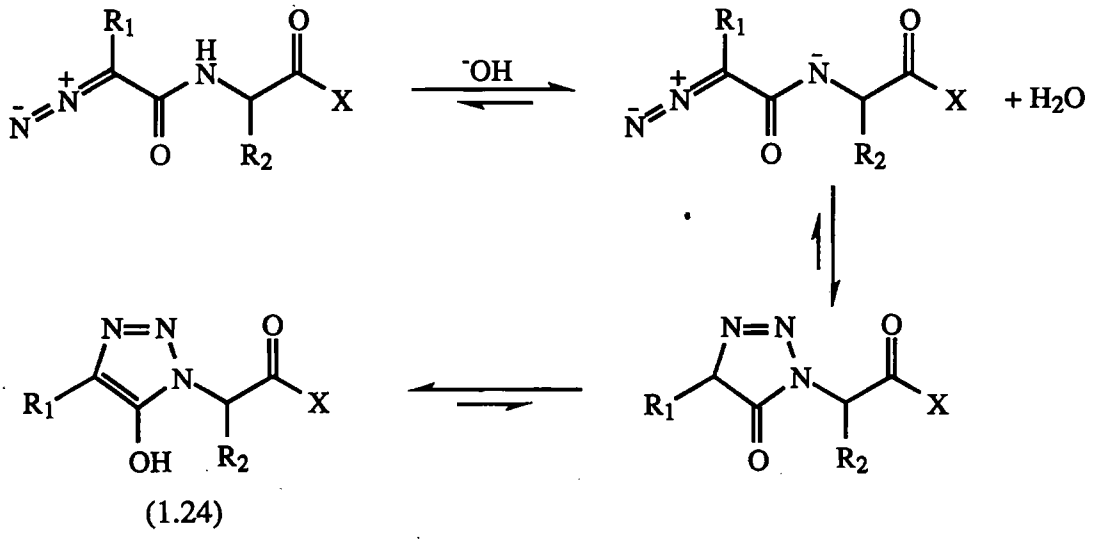

(1.24)

X = OEt, NH_2, O^-, NHR

Scheme 1.15 *Cyclisation of Diazopeptides to Triazoles in Base*

1.7 Other Reactions of Diazopeptides

Whilst reactions of diazo compounds (including diazopeptides) with nucleophiles usually result in displacement of N_2 (*i.e.* deamination), it is conceivable that the NuH entity may add across the diazo group (Equation 1.10). These reactions are not well known and are likely to be reversible. Hydroxide ions and acetate ions, however, are known to add reversibly to aryldiazonium ions,[132] and the triazole formation discussed above (Scheme 1.15) is an intramolecular example of amide addition. The reactions of primary amines to produce triazenes are the most common addition reactions of diazo compounds, as discussed in more detail in Sections 1.9-1.11.

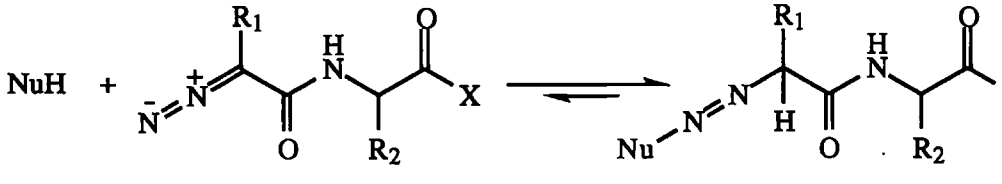

(1.10)

1.8 Biological Properties of Diazopeptides

The biological properties of *N*-(2-diazoacetyl)glycine compounds have been well studied. Compounds (1.3), (1.4) and (1.5) all show similar mutagenic activity towards strains of *Salmonella typhimuruim* bacteria (Ames Test),[17, 13] which is susceptible to base-pair substitution inducing agents.

As no biological activity is observed for frame-shift mutation-susceptible strains of Salmonella, these results suggest that *N*-(2-diazoacetyl)glycine compounds induce mutation *via* alkylation of bacterial DNA. These diazopeptides also produce a mutagenic *in vitro* response against Chinese hamster cells,[115] and induced dose-dependent, unscheduled DNA synthesis *in vivo*.[119]

N-(2-Diazoacetyl)-peptides possess anti-tumour properties.[12] Reference has already been made to the original study of Baldini and Brambilla,[12] which reported inhibition of several different tumour implants in mice.[12] Subsequently, inhibitory effects were observed against leukaemia,[116] melanoma,[116] the Ehrlich carcinoma in mice[117] and cultured human KB cells *in vitro*.[115] *N*-(2-Diazoacetyl)-peptides, however, proved to be poor inhibitors of lung-tumour implants in mice,[118] but both *N*-(2-diazoacetyl)glycinamide (1.4) and *N*-(2-diazoacetyl)glycylglycinamide inhibited lung metastases.[118] Brambilla *et. al.*[120] also showed that high doses of (1.4) in new born and adult Swiss mice induced both pulmonary tumours and leukaemia in a relatively short time. Further, compound (1.4) exerted marked, long lasting immunodepressive effects.[121] The last two findings suggest that the tumourgenic effects may arise from inhibition of processes by which mutant, somatic cells are eliminated.

More recently, three other diazopeptides have been tested for mutagenicity *in vitro*. Thus, *N*-(2-diazoacetyl)glycine and *N*-(2-diazoacetyl)glycylglycine (both with free

terminal carboxylic acid groups) have proven to be mutagenic in the Ames Test,[122] whereas *N*-(2-diazo-4-methylvaleryl)glycine ethyl ester (1.25) {the only diazopeptide to be tested with substitution at the α-C-atom}, was non-mutagenic.[122] Compound (1.25) is *ca.* 8-fold more labile than (1.4), so biological activity may be linked to compound stability.

1.9 Synthesis of Alkylaryltriazenes (ArN=N-NHR)

Two general methods are known for the preparation of alkylaryltriazenes. The first, attributed to Dimroth,[46] reacts a Grignard reagent with an aryl azide followed by hydrolysis (Equation 1.11).

$$ArN_3 + RMgX \longrightarrow [ArN(MgX)N{=}NR] \xrightarrow{H_2O} ArNH\text{-}N{=}NR \quad (1.11)$$

The second involves coupling of an aryldiazonium ion with an alkylamine in aqueous media (Equation 1.12). Isolation of the diazonium ion prior to amine coupling is not necessary.

$$\overset{+}{Ar}N_2 + H_2NCH_2Y \longrightarrow ArN{=}N\text{-}NHCH_2Y \quad (1.12)$$

Where Y= CO_2Et for e.g., but not CO_2^-

Even when the alkylamine contains an electron-withdrawing group Y such as CO_2R, the diazonium ion attacks the NH_2 moiety with no tendency to react at the activated CH_2 to produce hydrazones (Equation 1.13).

$$\overset{+}{Ar}N_2 + H_2NCH_2Y \not\longrightarrow ArNH\text{-}N{=}C\begin{matrix}NH_2\\ \diagdown\\ Y\end{matrix} \quad (1.13)$$

The corresponding reaction with free α-amino acids is unsuccessful, however, and results only in the deamination of the α-amino acid because the $ArN{=}N\text{-}NHCHRCO_2H$ triazene formed initially is unstable.[47]

Attempts to couple the phenyldiazonium ion with glycine ethyl ester were also unsuccessful,[47] probably because the triazene reacts with a second mole of the phenyldiazonium ion to give a penta-azadiene (1.26) {Equation 1.14}.

$$PhN_2^+ + RNH_2 \longrightarrow PhN^1{=}N^2\text{-}N^3HR \xrightarrow{PhN_2^+} \underset{(1.26)}{PhN{=}N\text{-}\overset{\overset{R}{|}}{N}\text{-}N{=}NPh} \quad (1.14)$$

Aryldiazonium ions containing strong electron-withdrawing substituents, however, react cleanly with primary aliphatic amines to give penta-azadiene free triazenes. This difference has been attributed to resonance effects of the aryl substituent, which reduces electron density at the N^3-atom and prevents further coupling with diazonium ion.[48]

1.10 Spectroscopic Characterisation of Alkylaryltriazenes

Alkylaryltriazenes have been widely examined by i.r. and nmr spectroscopy, and the results have proven invaluble in elaborating the tautomeric equlibrium (Ia) $\rightleftharpoons$ (Ib).

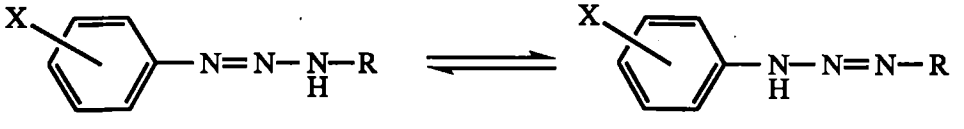

(Ia) (Ib)

For example, ^{1}H-nmr studies show that the tautomerism is both solvent dependent and strongly influenced by substituents (X) in the aryl ring.[68-71] Tautomers (Ia) and (Ib) can

be clearly distinguished by ^{1}H-nmr when the aryl ring contains electron-withdrawing groups.[69] Significant broadening of both the *N*-methylene and the aromatic proton resonances is observed for the ^{1}H-nmr spectrum of triazene (1.27) in $CDCl_3$, suggesting interconversion between (Ia) and (Ib) is rapid in this solvent at room temperature.[47]

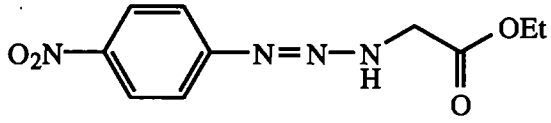

(1.27)

The i.r. spectra of alkylaryltriazenes usually show two NH stretching bands, one at 3480-3440 cm^{-1} assigned to tautomer (Ia), and the other at *ca.* 3338 cm^{-1} assigned to tautomer (Ib).[72] Alkylaryltriazenes also absorb in the near ultraviolet spectrum, generally strongly and often as more than one band.[74] There are few detailed studies of the mass spectra of alkylaryltriazenes,[66] but frequently observed fragmentation pathways (Scheme 1.16) appear to be: Loss of an alkyl radical (Path a); loss of an alkylamino radical (Path b); and loss of the diazoalkane moiety (Path c). Surprisingly, loss of N_2 (Path d) is not a common fragmentation unless the aryl group contains an electron-withdrawing group.[67]

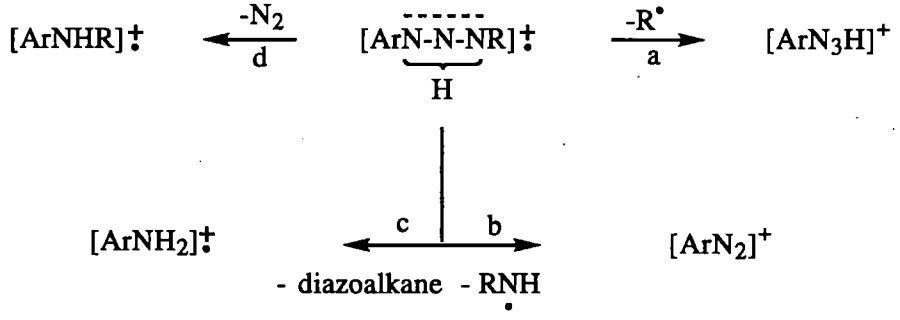

Scheme 1.16 *Mass Spectral Fragmentation of Alkylaryltriazenes*

1.11 Chemical Properties of Alkylaryltriazenes

Alkylaryltriazenes are alkylating agents,[49] which may account for their carcinogenicity (Scheme 1.17).

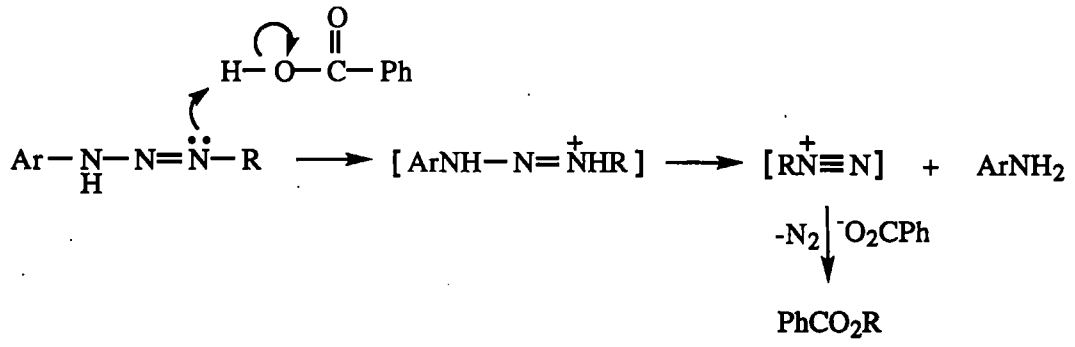

Scheme 1.17

These reactions, which can be brought about under both acidic and basic conditions, probably proceed *via* diazo intermediates (Scheme 1.17) and triazenes are intermediates in diazo-transfer reactions (see Equation 1.6 and Scheme 1.3).

In strongly alkaline solutions, alkylaryltriazenes can be alkylated. Because the anion intermediate is ambident, alkylation can occur at either terminal nitrogen atom (Equation 1.15).[54]

(1.15)

The nucleophilic character of alkylaryltriazenes is also demonstrated by the formation of penta-azadienes as co-products of triazenes during N-diazo coupling reactions (see Section 1.9). Dimroth[46] showed that an identical, unsymmetrical penta-azadiene (1.28) arises from two different coupling reactions of diazonium ions with monomethyltriazene (Equation 1.16). Because of its greater nucleophilicity, diazo coupling occurs at the N-atom adjacent to the methyl not the aryl group. The same effect is also evident for acylation with acetic anhydride, which affords 3-aryl derivatives.[55]

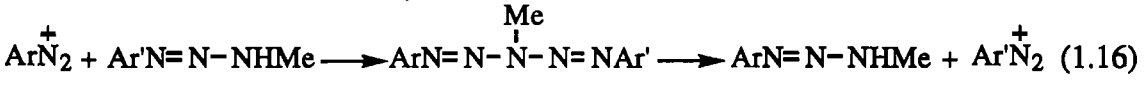

(1.16)

(1.28)

The nucleophilic character of triazenes is also evident by their ability to act as

co-ordination compounds in the formation of triazenido-metal complexes. These complexes were discovered and investigated by Dimroth as early as 1905.[56] In 1969, Rukhadze *et. al.*[57] reported the preparation of 3-*t*-butyl-1-aryltriazene complexes with Ag^{I}, Hg^{I}, Hg^{II} and Cu^{II}, but their structures have not been defined. Complexation was effected by simply mixing the triazene, in aqueous ethanol, with an ethanolic or ammonical (in the case of copper) solution of the metal salts, which gave an immediate precipitate.[57] Most complexes were insoluble in water, alcohol and other organic solvents (apart from DMF), were thermally unstable above 100 °C and decomposed with loss of N_2 on treatment with conc. HCl.[57] The bright yellow silver complexes, however, decomposed on standing. Complexation with mercury resulted in the disappearance of the i.r. absorption band at *ca.* 3200 cm^{-1} related to the NH stretching vibration of the triazene group.[57]

Subsequently, three co-ordination modes have been identified for metal-triazene complexes. The monodentate mode (X) for complex formation by diaryltriazenes with platinum[58] and palladium[59] has been verified by X-ray analysis. The more common bidentate mode or chelation (Y) occurs for ruthenium[58] and cobolt[60] complexes of 1,3-diphenyltriazene. The third mode (Z) has a bridging triazinido group between two metal atoms which sometimes are bonded to each other. The (Z) mode has been characterised for complexes of 1,3-dimethyltriazene with rhodium and copper,[61] and for diaryltriazenes with copper[62] and palladium.[63]

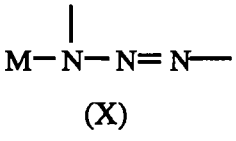

(X)

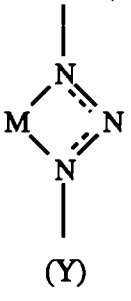

(Y)

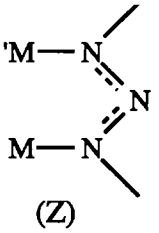

(Z)

All three co-ordination modes have not been observed for complexes of alkylaryl-triazenes. However, chelation of molybdenum and tungsten by 1-(*p*-chlorophenyl)-3-

isopropyltriazene, {mode (Y)}, has been reported[64] and 3-methyl-1-*p*-tolyl-triazene acts as a bridging ligand, {mode (Z)}, in complexes with silver/rhodium, silver/indium and mercury/iridium.[65]

1.12 Biological Properties of Alkylaryltriazenes

Alkylaryltriazenes are cytotoxic with carcinogenic,[75] mutagenic,[76] teratogenic,[77] anti-fungal,[78] and anti-tumour activity.[79] They have attracted interest because of their possible role as active metabolites and proximate carcinogens of anti-tumour 3,3-dialkyltriazenes. Anti-tumour activity of dimethyltriazenes was first reported in 1955,[80] and 5-(3,3-dimethyl-1-triazene)imidazole-4-carboxamide (1.29) {DTIC} is clinically useful in the treatment of malignant melanoma.[81] It has been suggested that DTIC is a stabilised form of diazo-IC (1.30), the active component liberated in target cells.[82] Simple 3,3-dialkyl-1-aryltriazenes (1.31) without an imidazole moiety, however, are equally effective as anti-tumour agents as DTIC. Not all of the diazonium ions derived from these compounds are active,[83] but this has been attributed to unfavourable transport characteristics of the diazonium compounds.[84]

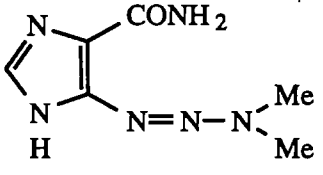

(1.29)

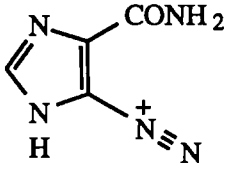

(1.30)

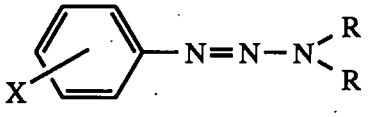

(1.31)

The correlation between the rate of hydrolysis of dimethyltriazenes and their ability to induce tumours at the site of administration,[85] supports an hypothesis that triazenes may be transportable forms of the toxic diazonium ion (Equation 1.18).

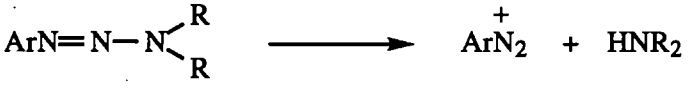

(1.18)

1.13 Summary

The largest dietary intakes of nitrosatable material are amino acids, peptides and proteins. *In vitro* studies show that the nitrosation of amino acids and small peptides occur under gastric conditions to yield, initially, the corresponding diazo compound. This, itself, may be carcinogenic as shown for several diazo derivatives of glycyl compounds, but diazoamino acids and peptides are highly acid-labile and therefore may not persist in the gastric environment to undergo interaction with genetically sensitive material.

Alternatively, other factors may govern their potency as carcinogens. For example, deamination of peptides bearing terminal α-amino nucleophilic side groups may lead to the formation of cyclic products *via* acid-catalysed decomposition of the diazonium ion intermediate (e.g. thiirans, epoxides and lactones from cysteine & methionine, serine & threonine and aspartic & glutamic acid, amino residues, respectively). Such ring-strained, heterocyclic compounds are highly reactive, especially towards nucleophiles, and therefore could be cytotoxic, acting as stabilised alkylating agents.

The work presented in this thesis investigates the formation of both non-cyclic and cyclic products from the acid-catalysed decomposition of the three non-glycyl diazopeptides *N*-(2-diazo-3-hydroxybutanoyl)glycine ethyl ester (2.1), *N*-(2-diazo-3-methylbutanoyl)glycine ethyl ester (2.2) and *N*-(2-diazo-3-carbamoylpropanoyl)glycine benzyl ester (4.1).

As mentioned earlier (see Section 1.7), diazopeptides may also react with nucleophiles, such as carboxylate and amino groups, across the diazo group to give azo-ester and

triazene compounds, respectively. This may be biologically significant, as such compounds have potential to act as transportable forms of the cytotoxic diazonium ion. These reactions were realised to some extent by Shuja, who reported non-linear general-acid-catalysis for the decomposition of diazopeptides in carboxylic acid buffers (see Section 1.5).[18] His results can only be rationalised by the existence of an equilibrium pathway leading to azo-ester formation, competing with the acid-catalysed diazopeptide decomposition pathway at high buffer-acid concentration. This unexpected result was checked and investigated further, along with the analogous reaction of diazopeptides with amines to form triazene compounds.

2. Kinetics for the Acid-Catalysed Decomposition of Diazopeptides in Aqueous Buffer-Acid Solutions

2.1 Decomposition of Diazopeptides

Previous work has shown that the decomposition of diazopeptides is acid-catalysed, occurring in both buffer solutions and dilute acid.[18] Some of the reactions in buffer solutions were unusual, however, insofar as the rate of decomposition gave a non-linear dependence on the buffer-acid concentration. The present work was aimed at confirming these effects and seeking a mechanistic explanation. It involved kinetic studies of the decomposition of *N*-(2-diazoacetyl)glycinamide (1.4), *N*-(2-diazo-3-hydroxybutanoyl)glycine ethyl ester (2.1), *N*-(2-diazo-3-methylbutanoyl)glycine ethyl ester (2.2), *N*-(2-diazo-3-hydroxypropanoyl)glycine ethyl ester (2.3) and *N*-(2-diazo-3-hydroxybutanoyl)sarcosine ethyl ester (2.4) in several buffer solutions and in dilute $HClO_4$.

2.2 Decomposition in Aqueous Buffers

These reactions were followed by monitoring the decrease in the diazopeptide absorbance at λ_{max} *ca.* 250 or 380 nm (depending on the absorbance of the buffer solution). They were carried out in a uv cuvette thermostatted at 25 °C within a uv/visible spectrophotometer for relatively slow reactions ($t_{1/2} > 60$ sec), and *via* a stopped-flow procedure for relatively fast reactions ($t_{1/2} < 60$ sec) as described in more detail in Section 7.3.1. The absorbance changes were monitored against time over at least four half-lives, and the infinity value was obtained either at ten half-lives or for slow reactions ($t_{1/2} > 10$ h.) by the addition of conc. HCl to the contents of the cuvette.

Previous work[106, 121, 124] showed that the acid-catalysed decomposition of diazopeptides follow *pseudo* first-order kinetics (Equation 2.1) and this was confirmed

in the present study. Thus, k_o was evaluated from the slope of $\ln(A_t-A_\infty)$ *vs.* time plots, where A_t and A_∞ are absorbances of the reaction solution at time t and infinity, respectively. These plots showed good linearity as exemplified for the decomposition of (1.4) in 0.5 M phosphate buffers shown in Figure 2.1 (see Section 7.3.1.1). Values of k_o were reproducible to ± 5 % for slow reactions ($t_{1/2}$ > 60 sec) and to ± 10 % for faster reactions ($t_{1/2}$ < 60 sec).

$$\text{Rate} = k_o\,[\text{Diazopeptide}] \qquad (2.1)$$

Figure 2.1 *First-Order Plot for the Decomposition of N-(2-diazoacetyl)-glycinamide (1.4) in 0.5 M Phosphate Buffer at 25 °C and pH = 6.10; Initial [(1.4)] ca. 10 $^{-4}$ M; μ = 1.25*

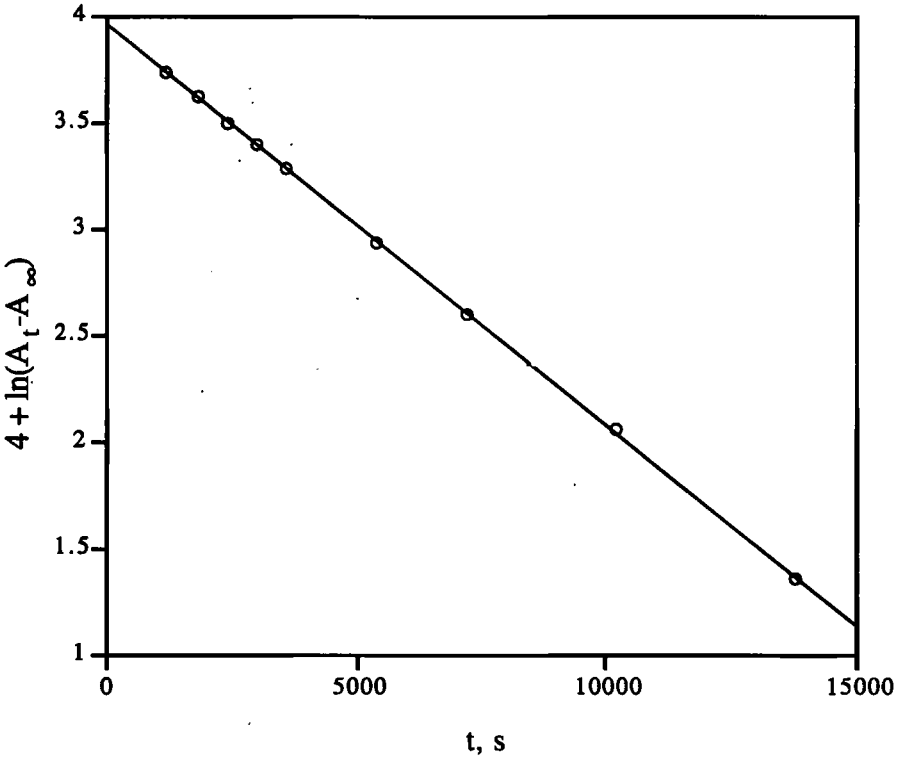

2.2.1 Decomposition of *N*-(2-Diazoacetyl)glycinamide (1.4)

This compound was examined as a typical diazo derivative of a glycyl peptide. Values of k_o (Equation 2.1) for its decomposition at 25 °C in several concentrations up to 1 M of formate, acetate, pyridine and phosphate buffer solutions are reported in Tables 2.1-2.4,

respectively. Most of the reactions were carried out in duplicate or more, and the mean value of k_o is reported. Each buffer was at a constant pH and adjusted to a constant ionic strength of 1 (1.25 for phosphate buffers) by the addition of solid $NaClO_4$. Also listed in the Tables are values of k_o at [Buffer-acid] = 0, estimated for the particular pH from the measurements in dilute $HClO_4$ reported in Section 2.4.

The variation of k_o with [Buffer-acid] for the data in Tables 2.1-2.4 are shown graphically as Figures 2.2-2.5. In agreement with earlier work, these plots are non-linear for decomposition in formate, acetate and phosphate buffers; there is distinct curvature at high [Buffer-acid] and sometimes a rate maximum, and the intercept is positive and pH dependent. For decomposition in pyridine buffers, however, the plot is reasonably linear and the intercept is consistent with the pH.

2.2.2 Decomposition of *N*-(2-Diazo-3-hydroxybutanoyl)glycine ethyl ester (2.1)

This compound was examined as a typical diazo derivative of a non-glycyl peptide. Similar data for the variation of k_o with [Buffer-acid] is reported in Tables 2.5-2.8 and plotted as Figures 2.6-2.9. As for *N*-(2-diazoacetyl)glycinamide (1.4) above, these plots are curved for decomposition in formate, acetate and phosphate buffers, but linear in pyridine buffers.

2.2.3 Decomposition of *N*-(2-Diazo-3-methylbutanoyl)glycine ethyl ester (2.3)

This compound was examined in acetate buffers at pH 4.28 and 25 °C only. The results are reported in Table 2.9 and the plot in Figure 2.10 is also distinctly curved.

Table 2.1 Variation of *Pseudo* First-Order Rate Coefficient k_o, with [HCO_2H] for the Decomposition of *N*-(2-Diazoacetyl)glycinamide (1.4) in Formate Buffers at pH = 3.48 (± 0.03) and 25 (± 0.1) °C; Initial [(1.4)] *ca.* 10^{-4} M; μ = 1

[HCO_2H] M	[$NaCO_2H$] M	[$NaClO_4$] M	k_o s^{-1}
0	0	1	0.0069*
0.05	0.05	0.95	0.0135
0.1	0.1	0.9	0.0148
0.2	0.2	0.8	0.0174
0.3	0.3	0.7	0.0189
0.5	0.5	0.5	0.0233
0.7	0.7	0.3	0.0236
1.0	1.0	-	0.0221

**Calculated from results in Section 2.4*

Figure 2.2 *Decomposition of N-(2-Diazoacetyl)glycinamide (1.4) in Formate Buffers at pH 3.48 and 25 °C*

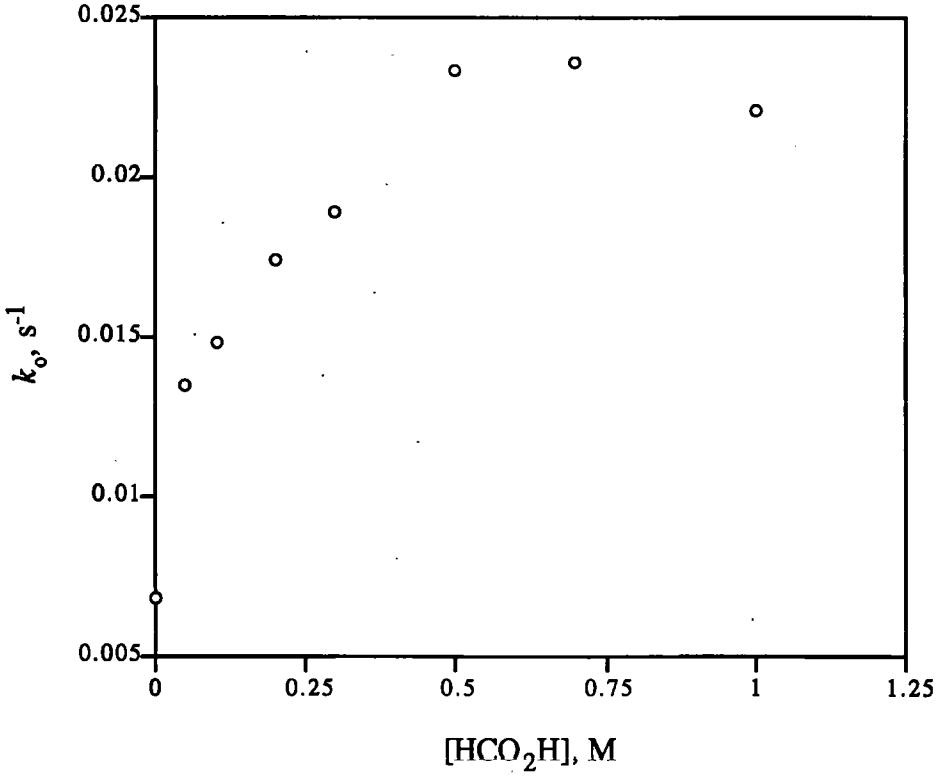

Table 2.2 Variation of *Pseudo* First-Order Rate Coefficient k_o, with [HOAc] for the Decomposition of *N*-(2-Diazoacetyl)glycinamide (1.4) in Acetate Buffers, at pH = 4.22 (± 0.06) and 25 (± 0.1) °C; Initial [(1.4)] *ca.* 10^{-4} M; μ = 1

[HOAc] M	[NaOAc] M	[$NaClO_4$] M	k_o s^{-1}
0	0	1	0.00127*
0.025	0.025	0.975	0.00204
0.05	0.05	0.95	0.00269
0.1	0.1	0.9	0.00293
0.2	0.2	0.8	0.00316
0.3	0.3	0.7	0.00320
0.5	0.5	0.5	0.00313
0.7	0.7	0.3	0.00311
1.0	1.0	-	0.00289

**Calculated from results in Section 2.4*

Figure 2.3 *Decomposition of N-(2-Diazoacetyl)glycinamide (1.4) in Acetate Buffers at pH 4.22 and 25 °C*

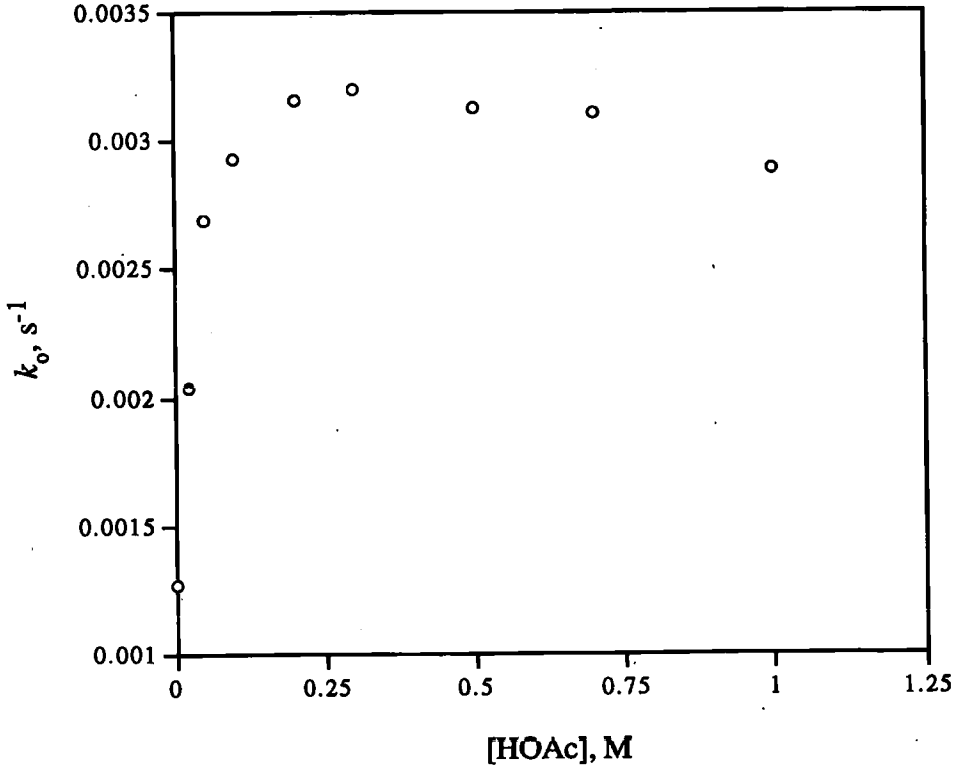

Table 2.3 Variation of *Pseudo* First-Order Rate Coefficient k_o, with [Pyridinium ion] for the Decomposition of *N*-(2-Diazoacetyl)glycinamide (1.4) in Pyridine Buffers at pH = 5.30 (± 0.10), and 25 (± 0.1) °C; Initial [(1.4)] *ca.* 10^{-3} M; $\mu = 1$

[Pyridine] M	[Pyridinium ion] M	[$NaClO_4$] M	k_o s^{-1}
0	0	1	0.000105*
0.05	0.05	0.95	0.000203
0.5	0.5	0.5	0.000379
0.7	0.7	0.3	0.000480
1.0	1.0	-	0.000547

**Calculated from results in Section 2.4*

Figure 2.4 *Decomposition of N-(2-Diazoacetyl)glycinamide (1.4) in Pyridine Buffers at pH 5.3 and 25 °C*

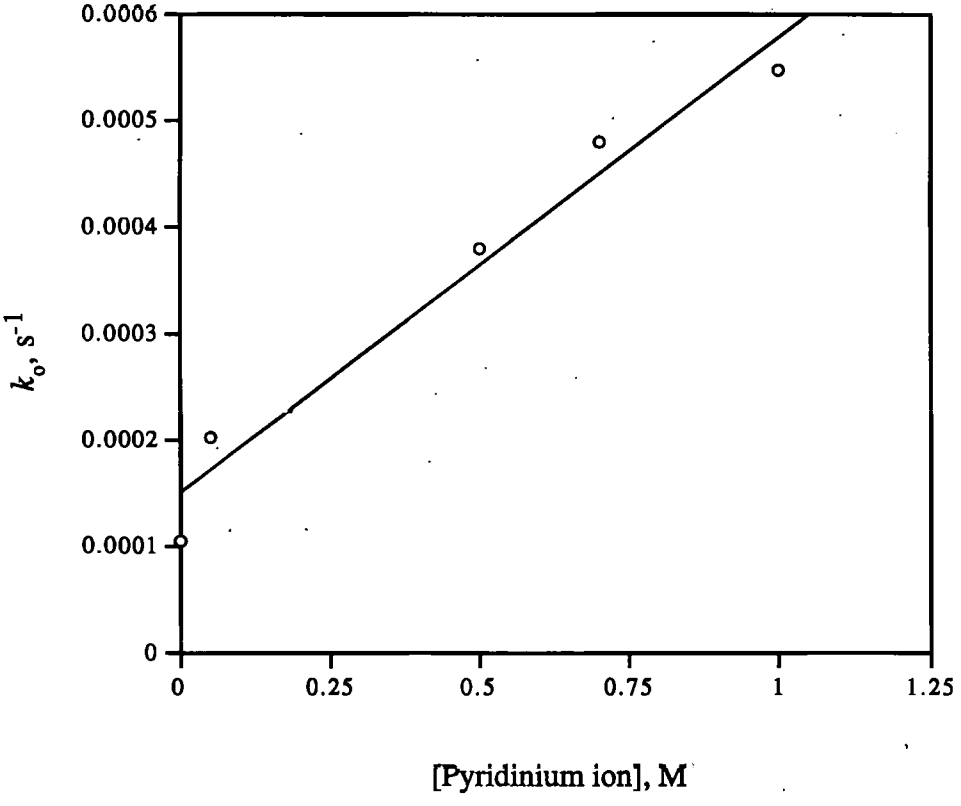

Table 2.4 Variation of *Pseudo* First-Order Rate Coefficient k_o, with $[H_2PO_4^-]$ for the Decomposition of *N*-(2-Diazoacetyl)glycinamide (1.4) in Phosphate Buffers at pH = 6.20 (± 0.20), T = 25 (± 0.1) °C; Initial [(1.4)] *ca.* 10^{-4} M; μ = 1.25

$[NaH_2PO_4]$ M	$[Na_2HPO_4]$ M	$[NaClO_4]$ M	k_o s^{-1}
0	0	1	0.000013*
0.05	0.05	0.95	0.000155
0.1	0.1	0.9	0.000206
0.2	0.2	0.8	0.000213
0.3	0.3	0.7	0.000208
0.5	0.5	0.5	0.000190
0.7	0.7	0.3	0.000183
1.0	1.0	-	0.000169

**Calculated from results in Section 2.4*

Figure 2.5 *Decomposition of N-(2-Diazoacetyl)glycinamide (1.4) in Phosphate Buffers at pH 6.2 and 25 °C*

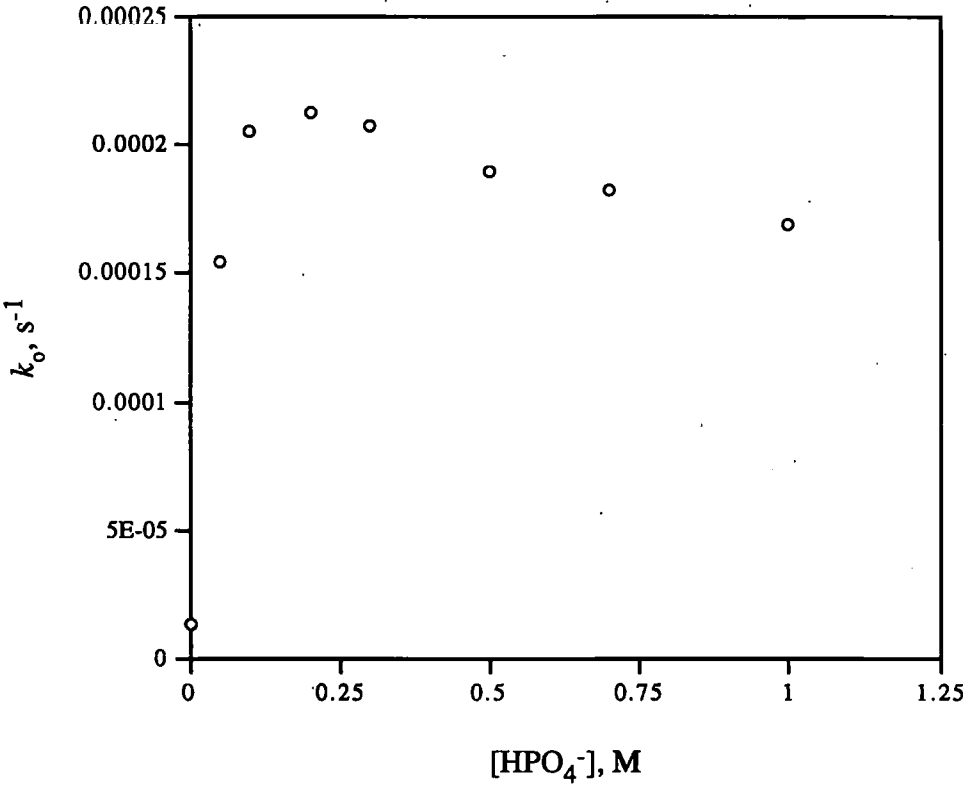

Table 2.5 Variation of *Pseudo* First-Order Rate Coefficient k_o, with [HCO_2H] for the Decomposition of *N*-(2-Diazo-3-hydroxybutanoyl)glycine ethyl ester (2.1) in Formate Buffers at pH = 3.48 (± 0.03) and 25 (± 0.1) °C; Initial (2.1) *ca.* 10^{-4} M; $\mu = 1$

[HCO_2H] M	[$NaCO_2H$] M	[$NaClO_4$] M	k_o s^{-1}
0	0	1	0.005*
0.05	0.05	0.95	0.063
0.1	0.1	0.9	0.11
0.2	0.2	0.8	0.21
0.3	0.3	0.7	0.34
0.5	0.5	0.5	0.39
0.7	0.7	0.3	0.44
1.0	1.0	-	0.49

**Calculated from results in Section 2.4*

Figure 2.6 *Decomposition of N-(2-Diazo-3-Hydroxybutanoyl)glycine ethyl ester (2.1) in Formate Buffers at pH 3.48 and 25 °C*

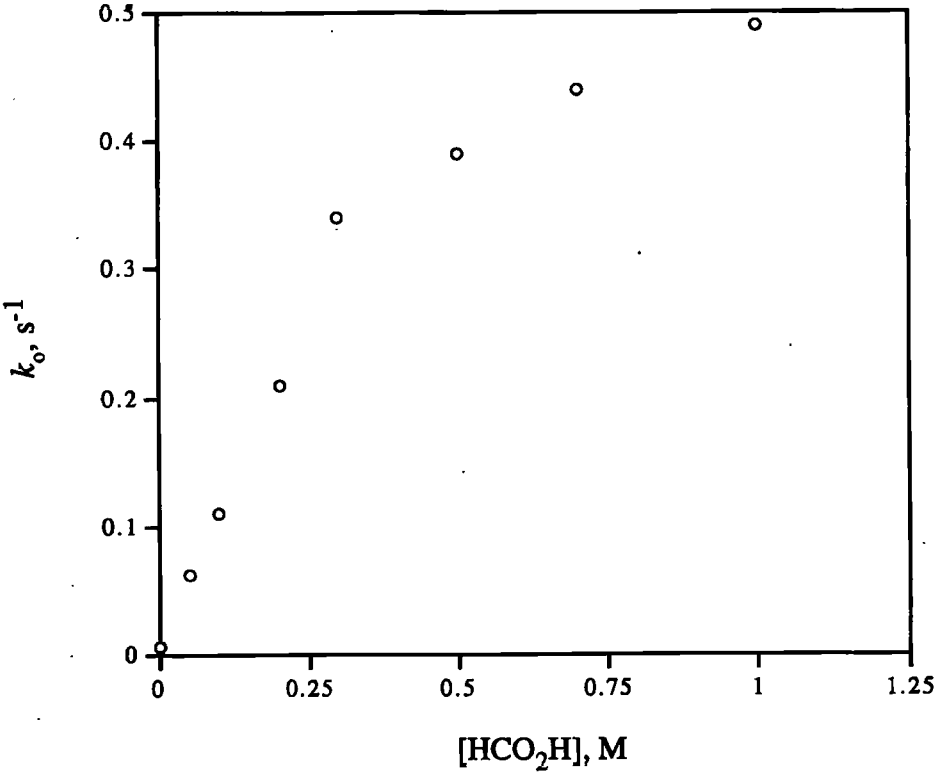

Table 2.6 Variation of *Pseudo* First-Order Rate Coefficient k_o, with [HOAc] for the Decomposition of *N*-(2-Diazo-3-hydroxybutanoyl)glycine ethyl ester (2.1) in Acetate Buffers at pH = 4.25 (± 0.05) and 25 (± 0.1) °C; Initial [(2.1)] *ca.* 10^{-4} M; $\mu = 1$

[HOAc] M	[NaOAc] M	[$NaClO_4$] M	k_o s^{-1}
0	0	1	0.0009*
0.05	0.05	0.95	0.0135
0.1	0.1	0.9	0.0148
0.2	0.2	0.8	0.0174
0.3	0.3	0.7	0.0189
0.5	0.5	0.5	0.0233
0.7	0.7	0.3	0.0236
1.0	1.0	-	0.0221

**Calculated from results in Section 2.4.*

Figure 2.7 *Decomposition of N-(2-Diazo-3-hydroxybutanoyl)glycine ethyl ester (2.1) in Acetate Buffers at pH 4.25 and 25 °C*

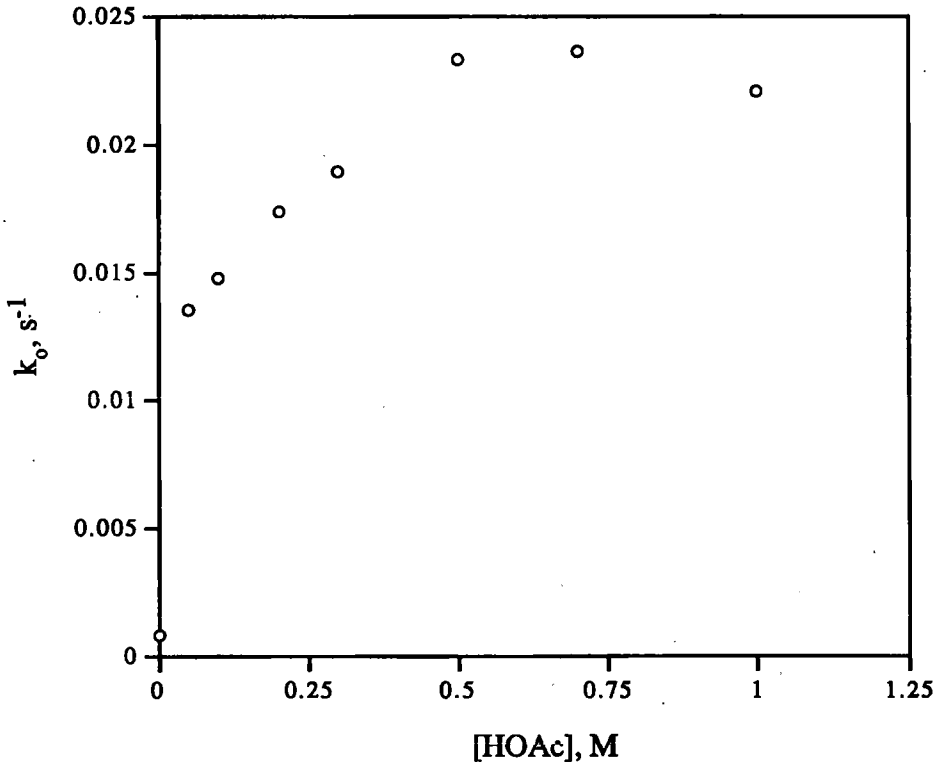

Table 2.7 Variation of *Pseudo* First-Order Rate Coefficient k_o, with [Pyridinium ion] for the Decomposition of *N*-(2-Diazo-3-hydroxybutanoyl)glycine ethyl ester (2.1) in Pyridine Buffers at pH = 5.28 (± 0.11) and 25 (± 0.1) °C; Initial [(2.1)] *ca.* 10^{-3} M; $\mu = 1$

[Pyridine] M	[Pyridinium ion] M	[$NaClO_4$] M	k_o s^{-1}
0	0	1	0.00008*
0.1	0.1	0.9	0.00109
0.3	0.3	0.7	0.00222
0.5	0.5	0.5	0.00410
0.7	0.7	0.3	0.00530
1.0	1.0	-	0.00775

**Calculated from results in Section 2.4*

Figure 2.8 *Decomposition of N-(2-Diazo-3-hydroxybutanoyl)glycine ethyl ester (2.1) in Pyridine Buffers at pH 5.28 and 25 °C*

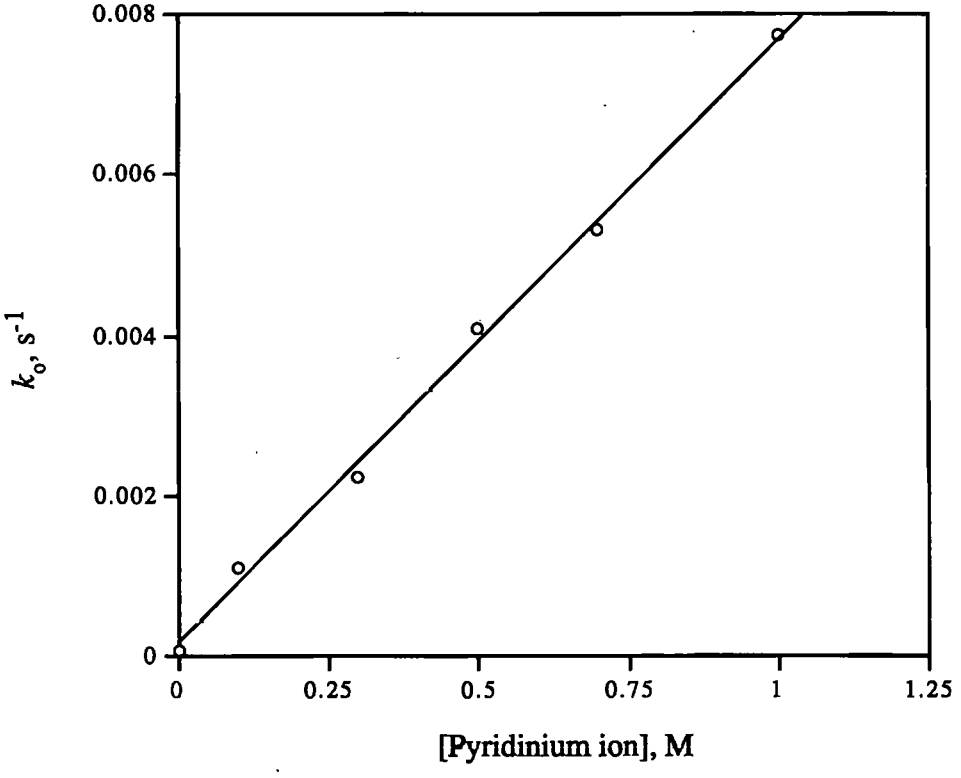

Table 2.8 Variation of *Pseudo* First-Order Rate Coefficient k_o, with $[H_2PO_4^-]$ for the Decomposition of *N*-(2-Diazo-3-hydroxybutanoyl)glycine ethyl ester (2.1) in Phosphate Buffers at pH = 6.18 (± 0.16) and 25 (± 0.1) °C; Initial [(2.1)] *ca.* 10^{-4} M; μ = 1.25

$[NaH_2PO_4]$ M	$[Na_2HPO_4]$ M	$[NaClO_4]$ M	k_o s^{-1}
0	0	1	0.00001*
0.05	0.05	0.95	0.00320
0.1	0.1	0.9	0.00456
0.2	0.2	0.8	0.00656
0.3	0.3	0.7	0.00633
0.5	0.5	0.5	0.00583
0.7	0.7	0.3	0.00560
1.0	1.0	-	0.00321

**Calculated from results in Section 2.4*

Figure 2.9 *Decomposition of N-(2-Diazo-3-hydroxybutanoyl)glycine ethyl ester (2.1) in Phosphate Buffers at pH 6.20 and 25 °C*

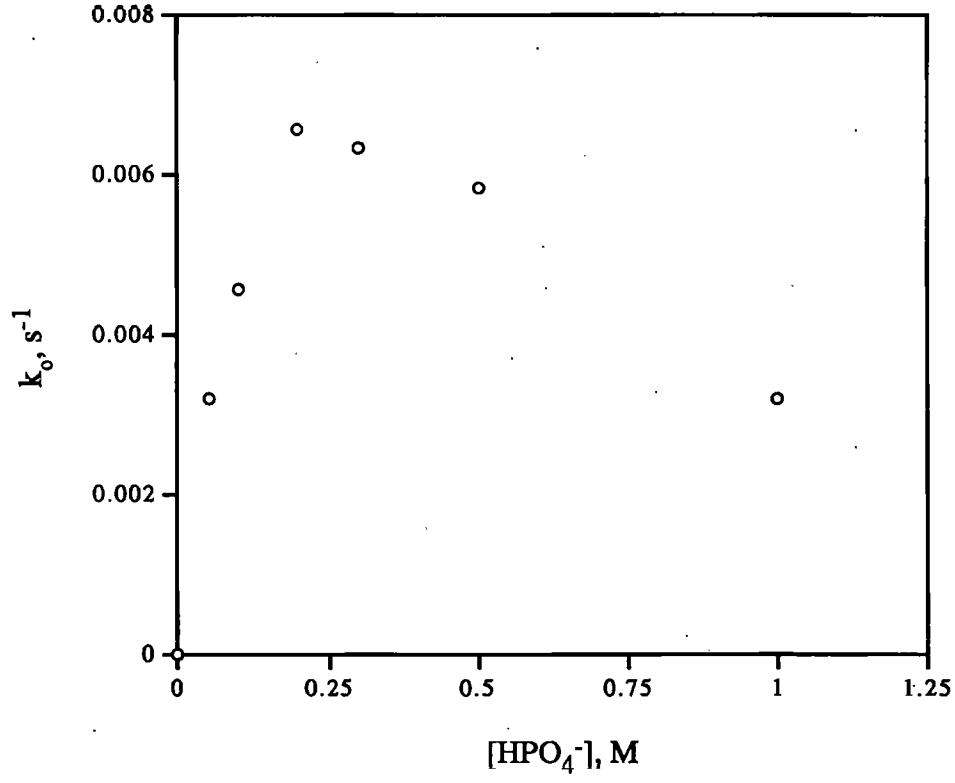

Table 2.9 Variation of *Pseudo* First-Order Rate Coefficient k_o, with [HOAc] for the Decomposition of *N*-(2-Diazo-3-methylbutanoyl)glycine ethyl ester (2.2) in Acetate Buffers at pH = 4.28 (± 0.05) and 25 (± 0.1) °C; Initial [(2.2)] *ca.* 10^{-4} M; $\mu = 1$

[HOAc] M	[NaOAc] M	[$NaClO_4$] M	k_o s^{-1}
0	0	1	0.005*
0.05	0.05	0.95	0.11
0.1	0.1	0.9	0.19
0.2	0.2	0.8	0.34
0.3	0.3	0.7	0.50
0.5	0.5	0.5	0.78
0.7	0.7	0.3	1.02
1.0	1.0	-	1.30

**Calculated from results in Section 2.4*

Figure 2.10 *Decomposition of N-(2-Diazo-3-methylbutanoyl)glycine ethyl ester (2.2) in Acetate Buffers at pH 4.28 and 25 °C*

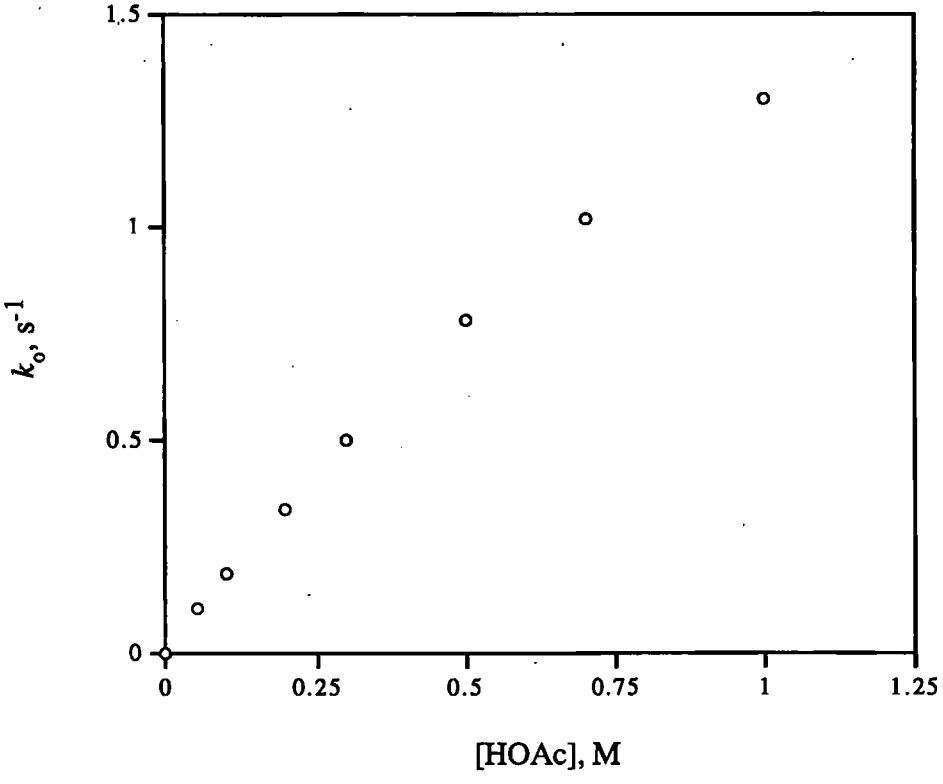

2.3 Extent of General-Acid-Catalysed Decomposition

Although several of the k_o *vs.* [Buffe-acid] plots are complex, it is clear that the decompositions of the diazo derivatives of both glycyl and non-glycyl diazopeptides are catalysed by formic, acetic and phosphoric acids, and by the pyridinium ion. Thus, the reactions are subject to general-acid-catalysis and the reaction rates may be expected to follow Equation 2.2.

$$\text{Rate} = [\text{Diazopeptide}] \{k_{H_3O^+} [H_3O^+] + \sum_{HA_i} k_{HA_i} [HA_i]\} \qquad (2.2)$$

Values of k_{HA_i} evaluated from linear portions of the plots in Figures 2.1-2.10 (*i.e.* at the lower $[HA_i]$) are summarised in Table 2.10.

Table 2.10 Second-Order Rate Coefficients (k_{HA_i}) for the General-Acid-Catalysed Decomposition of Diazopeptides in Various Buffers at 25 °C; Initial [Substrate] *ca.* 10^{-4} M; μ =1

Diazopeptide	Buffer Acid	pH	k_{HA_i}, $M^{-1} s^{-1}$
N-(2-Diazoacetyl) glycinamide (1.4)	Formic	3.48	0.125
	Acetic	4.22	0.028
	Pyridinium ion	5.30	0.00051
	$H_2PO_4^-$	6.20	0.0020
N-(2-Diazo-3-hydroxybutanoyl) glycine ethyl ester (2.1)	Formic	3.48	1.02
	Acetic	4.25	0.22
	Pyridinium ion	5.28	0.0075
	$H_2PO_4^-$	6.18	0.040
N-(2-Diazo-3-methylbutanoyl) glycine ethyl ester (2.2)	Acetic	4.28	1.50

These coefficients show:

1) Decomposition rates increased with the strength of the acid-catalyst.

2) *N*-(2-Diazo-3-hydroxybutanoyl)glycine ethyl ester (2.1) and *N*-(2-diazo-3-methylbutanoyl)glycine ethyl ester (2.2) are less stable than *N*-(2-diazoacetyl)glycinamide (1.4).

The mechanistic significance of these conclusions is discussed further below.

2.4 Decomposition of Diazopeptides in Dilute $HClO_4$

The decomposition of diazopeptides (2.1), (2.2), (2.3) and (2.4) in dilute aqueous $HClO_4$ at 25 °C were measured to obtain an unambiguous value for $k_{H_3O^+}$ and to check earlier work. These reactions were too fast to use a conventional uv/visible spectrophotometer, so a stopped-flow procedure was used as discussed in Section 7.3.1.2. As before, the decomposition of the diazopeptide was monitored by the decrease in the absorbance of the reaction solution at λ = 250-260 nm. These measurements were continued until the absorbance was constant (time infinity). The pH or $HClO_4$ concentration of the reaction solution was then determined by pH meter or titration against standard NaOH using methyl orange as indicator.

Pseudo first-order rate coefficients (Equation 2.3) for decomposition at 25 °C and μ = 1.0 ($NaClO_4$) {initial [substrate] *ca.* 10^{-4} M} were calculated from linear plots of $\ln(\Lambda_t - \Lambda_\infty)$ *vs.* time, where Λ_t = absorbance at time t and Λ_∞ = absorbance at time infinity. Values of k_o were reproducible to ± 10 %. Similarly, plots of k_o *vs.* [$HClO_4$] showed good linearity (as exemplified for the decomposition of *N*-(2-diazo-3-hydroxy-propanoyl)glycine ethyl ester (2.3) in Figure 2.11).

Figure 2.11 *Decomposition of N-(2-Diazo-3-hydroxypropanoyl) glycine ethyl ester (2.3) in $HClO_4$ at 25 °C*

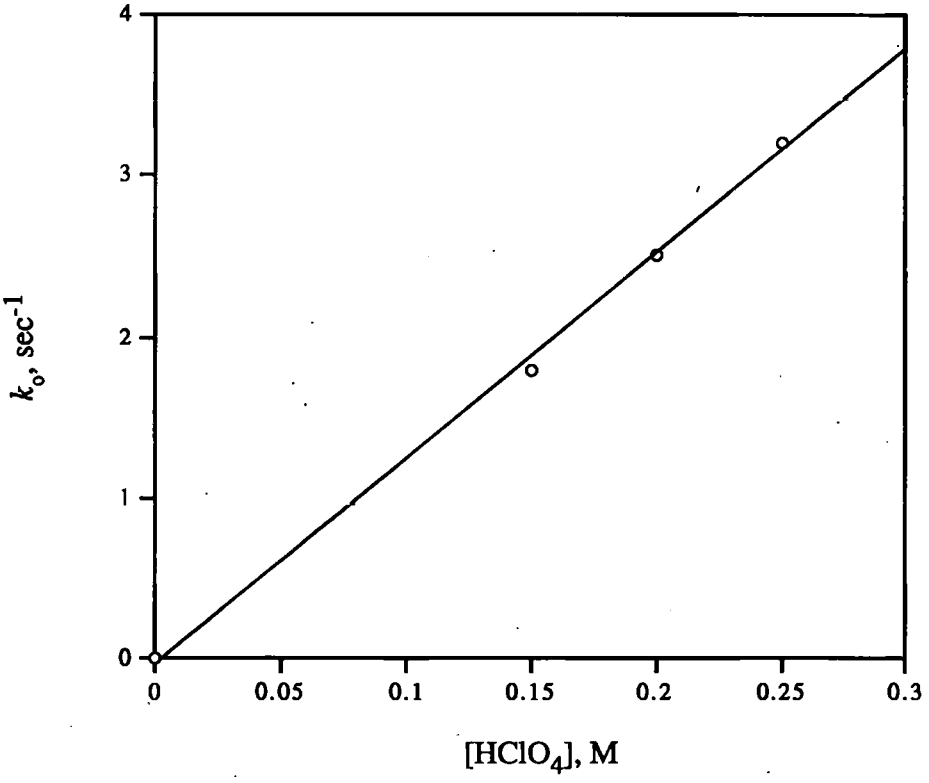

Values of $k_{H_3O^+}$ (Equation 2.3) obtained from the slopes of these plots are summarised in Table 2.11. Values of $k_{H_3O^+}$ obtained earlier by Shuja[18] are also given in Table 2.11 and the agreement between the two sets of data is excellent.

$$\text{Rate} = k_{H_3O^+}\,[\text{Diazopeptide}]\,[HClO_4] \qquad (2.3)$$

The results in Table 2.11 are uncomplicated by the non-linear kinetic dependences found with the buffer-acid-catalysis and show:

1) The substituent (R) adjacent to the diazo group affects the stability of the diazopeptide. Compounds bearing an electron-withdrawing α-side-group {e.g. R = CHOH, $CH(CH_3)OH$} are most stable, presumably because electron withdrawal reduces the basicity of the substrate (which slows the rate-limiting H^+-transfer step). These compounds are *ca.* two fold more stable than *N*-(2-diazoacetyl) -compounds (R = H) where loss of N_2 from the protonated substrate is considered to be

Table 2.11 Values of $k_{H_3O^+}$ (Equation 2.3) for the Decomposition of Diazopeptides in Aqueous 0-0.25 M $HClO_4$ at 25 °C; Initial [Substrate] *ca.* 10^{-4} M; $\mu = 1$

Diazopeptide	$k_{H_3O^+}$, M^{-1} s^{-1}
N-(2-Diazo-3-hydroxybutanoyl) glycine ethyl ester (2.1)	16 (12)
N-(2-Diazo-3-hydroxybutanoyl) sarcosine ethyl ester (2.4)	17 (16)
N-(2-Diazo-3-hydroxypropanoyl) glycine ethyl ester (2.3)	13 (16)
N-(2-Diazo-3-methylbutanoyl) glycine ethyl ester (2.2)	85 (86)
N-(2-Diazoacetyl)glycinamide (1.4)	- (21)

**The values given in parenthesis are those reported by S. Shuja[18]*

rate-limiting and $k_{H_3O^+}$ is typically *ca.* 20-30 M^{-1} s^{-1}.[18] Diazopeptides bearing an electron-donating alkyl α-side chain (e.g. R = CH_3, $CH(CH_3)_2$, $CH_2CH(CH_3)_2$) are less stable, presumably because electron-donation increases the basicity of the substrate (which increases the rate-limiting H^+-transfer step) and stabilises the carbocation intermediate (which increases the rate of N_2 expulsion). Indeed, decomposition of *N*-(2-diazo-3-methylbutanoyl)glycine ethyl ester (2.2) was too fast to be measured accurately by the stopped-flow equipment available and $k_{H_3O^+}$ was estimated as *ca.* 70-100 M^{-1} s^{-1} *i.e. ca.* five fold greater than (2.1) (2.3) and (2.4).

2) Sarcosyl compounds (bearing a peptide -N(CH_3)CHRCO- group) gave similar rates of acid-catalysed decomposition to glycyl compounds (bearing an -N(H)CHRCO- group). Thus, the peptide N-H is probably not involved in a mechanistically significant step.

2.5 Discussion

2.5.1 Kinetics and Mechanism of Acid-Catalysed Decompositions

Rates of decomposition have been measured and reported for several diazopeptides in dilute aqueous acid and buffer solutions at 25 °C. These reactions are clearly subject to general-acid-catalysis although the kinetic form of this catalysis is more complex (e.g. curved plots) than is usually observed.

The general-acid-catalysis and other kinetic dependencies are consistent with decomposition *via* a common pathway (Scheme 2.1) where the rate-limiting step is dependent upon the structure of the α-substituent R to the diazo group.

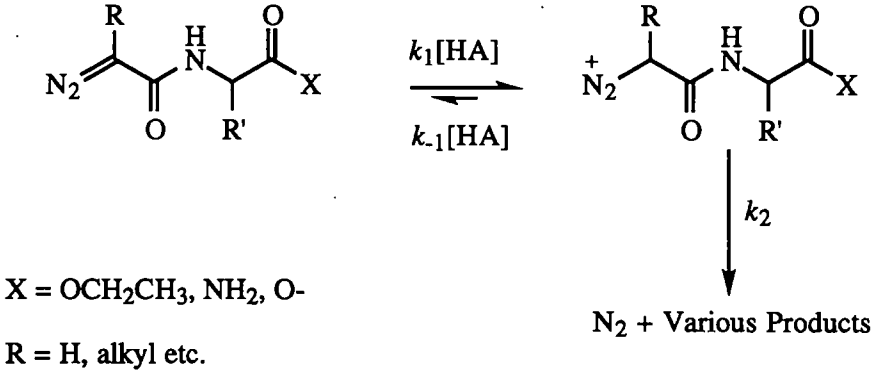

Scheme 2.1

For compounds where R = H (glycyl peptides), inverse solvent deuterium isotope effects ($k_{H_3O^+} / k_{D_3O^+} < 1$) and the nucleophilic-catalysis (e.g. $S_2O_3^- > I^- > Br^- > Cl^-$) suggest that k_2 is rate-limiting.[18] But for compounds where R ≠ H (non-glycyl peptides), normal

solvent deuterium isotope effects ($k_{H_3O^+}$ / $k_{D_3O^+}$ > 1) and the absence of appreciable nucleophilic-catalysis suggest that k_1 (H^+-transfer) is rate-limiting.[18]

The results in Section 2.2 show that non-linear general-acid-catalysis applies to the decomposition of diazopeptides in aqueous buffer solutions *i.e.* catalysis at high buffer-acid concentrations is attenuated giving curved plots of k_o *vs.* [HA]. Further, this unexpected kinetic behaviour applies to both glycyl and non-glycyl diazopeptides, which excludes any explanation based on a change of the rate-limiting step with increasing [HA]. The attenuation of the buffer-acid-catalysis must therefore relate to a pre-equilibrium interaction such as the generation of an alkyl diazonium ion intermediate (2.5) *via* protonation of the peptide O-atom, which is then trapped by the buffer anion (A^-) to form a relatively stable, covalent azo compound (2.6) {Scheme 2.2}.

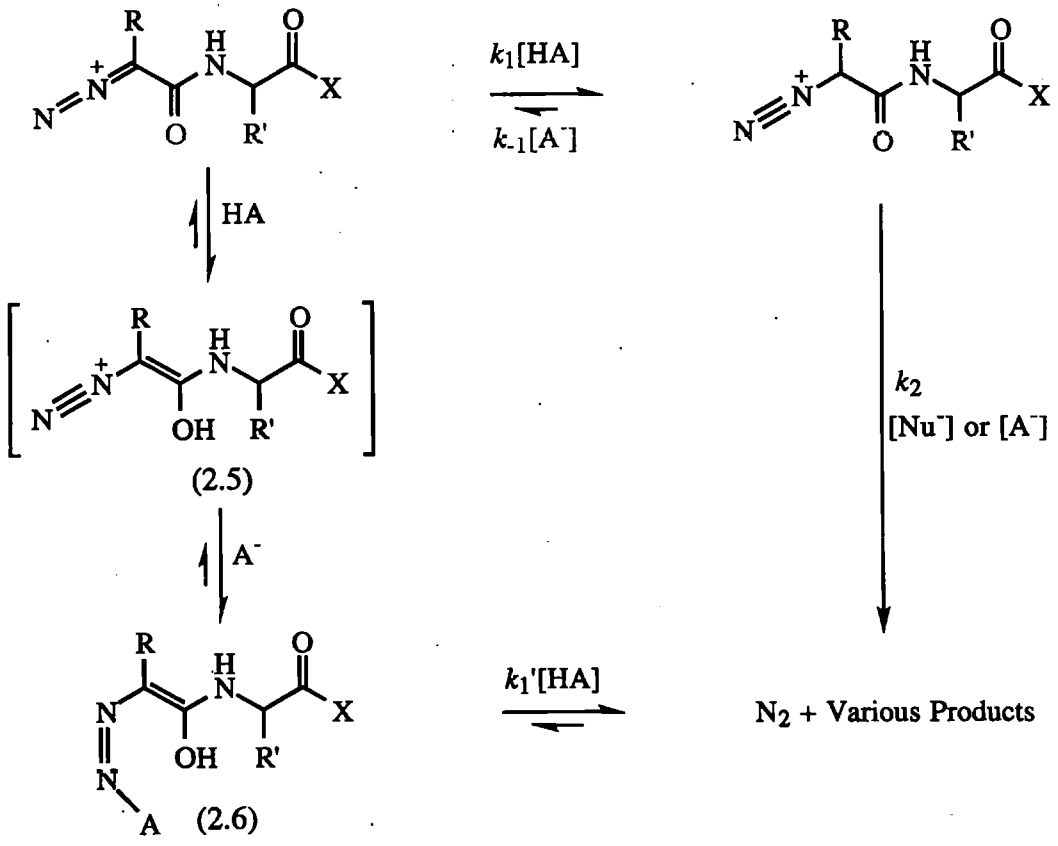

Scheme 2.2

At higher [HA], the equilibrium (2.5) $\rightleftharpoons$ (2.6) is driven towards (2.6) and non-linear general-acid-catalysis would result if (2.6) were either completely stable (*i.e.* $k_1' = 0$) or less reactive than the diazopeptide substrate (*i.e.* $k_1 > k_1'$).

Three other observations support formation of azo intermediates (2.6) as an explanation for the curved general-acid plots. Thus;

1) A similar covalent diazoacetic acid ester (2.7) is reported to form from benzene diazonium ion and acetate ion, although the equilibrium lies well to the left (K_E *ca.* 10^{-5} M^{-1}) {Equation 2.4}.[132]

$$PhN_2^+ + {}^-OAc \underset{}{\overset{k_E}{\rightleftharpoons}} \underset{(2.7)}{PhN{=}N\text{-}OAc} \qquad (2.4)$$

For A^- = acetate ion, the azo compound (2.6) from diazopeptides should be more stable than (2.7), because of the inherent basicity of the peptide O-atom (pK_a *ca.* 0). Further, structure (2.6) would be further stabilised by intramolecular H-bonding.

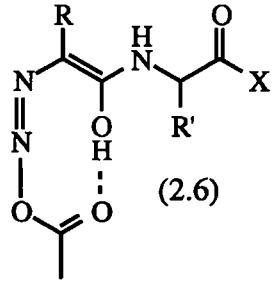

(2.6)

2) Non-linear acid-catalysis is *not* observed for either glycyl or non-glycyl diazopeptides in pyridine buffers at similar pH. This is readily explained by the corresponding charged triazene (2.8) from pyridine being much less stable than (2.6).

3) Diazo derivatives of non-glycyl peptides give rise to decomposition products whose structure and % yield is independent of the acid-catalyst (see Chapter 4). Thus, the acid-catalysis and the non-linear kinetics cannot relate to product forming steps.

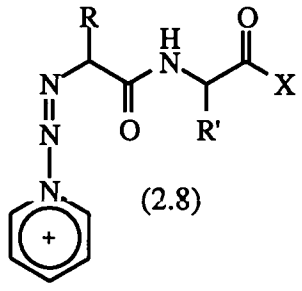

(2.8)

2.5.2 Analysis of the Curved General-Acid-Catalysis Plots

For the pre-equilibrium and decomposition pathways outlined in Scheme 2.3, where DIAZO = diazopeptide substrate and AZO = complex formed by reaction with buffer-acid,

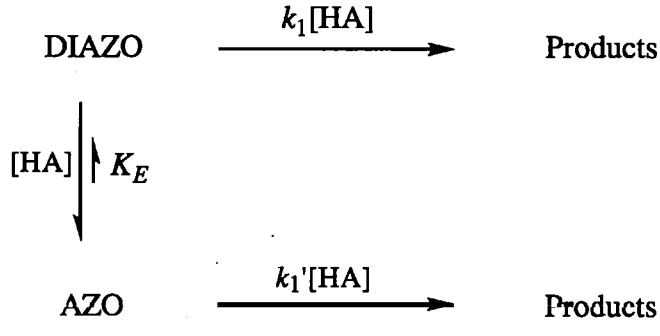

Scheme 2.3

the equilibrium constant K_E can be evaluated from the non-linear kinetic data in the following way:

Rate = k_o {[DIAZO] + [AZO]}

= k_1[DIAZO] [IIA] + k_1'[AZO] [HA] (2.5)

and K_E = [DIAZO] [HA] / [AZO] or [AZO] / [DIAZO] = [HA] / K_E (2.6)

If k_1[HA] > k_1'[HA] or k_1'[HA] = 0 (*i.e.* the azo compound is much less reactive than the diazo substrate), then to a good approximation:

Rate ≈ k_1[DIAZO] [HA]

From Equations (2.5) and (2.6):

$$k_o \{[DIAZO] / [DIAZO] + [AZO] / [DIAZO]\} = k_1[HA] \quad (2.7)$$

and from Equation (2.7):

$$k_o \{1 + [HA] / K_E\} = k_1[HA]$$

Taking reciprocals gives Equation (2.8):

$$1/k_o = 1/k_1[HA] + 1/k_1K_E \quad (2.8)$$

From Equation (2.8), the Line-Weaver Burke plot of $1/k_o$ *vs.* 1/[HA] should be linear, with slope = $1/k_1$ and intercept = $1/k_1K_E$. Indeed, Line-Weaver Burke plots of $1/k_o$ *vs.* 1/[HA] show good linearity for both glycyl and non-glycyl diazopeptides in formate acetate and phosphate buffer solutions, as exemplified for the reactions of *N*-(2-diazo-3-hydroxybutanoyl)glycine ethyl ester (2.1) in formate buffers, *N*-(2-diazoacetyl)glycinamide (1.4) in acetate buffers and *N*-(2-diazo-3-methylbutanoyl)glycine ethyl ester (2.2) in acetate buffers, shown as Figures 2.13, 2.14 and 2.15, respectively. These support the existence of pre-equilibrium azo product (2.6) formation in the acid-catalysed decomposition of diazopeptides. Values of the equilibrium constants (K_E) and rate coefficients (k_1) calculated *via* Equation (2.8) for various buffer-acid/diazopeptide combinations are summarised in Table 2.12.

From Equation (2.6), the value of the K_E decreases for increased stability of the azo compound (2.6). It follows from the data in Table 2.12, that the reaction of *N*-(2-diazoacetyl)glycinamide (1.4) with acetic acid to form azo compound (2.9) should be most extensive.

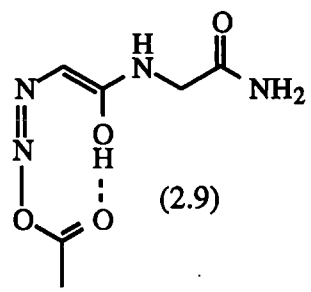

(2.9)

Table 2.12 Rate Coefficients (k_1) and Equilibrium Constants (K_E) for the Decomposition of Diazopeptides in Aqueous Buffers at 25 °C

Diazopeptide	Buffer-acid	k_1, s^{-1}	K_E, M^{-1}
N-(2-Diazoacetyl)	Formate	0.36	0.068
glycinamide (1.4)	Acetate	0.20	0.017
	Phosphate	0.0081	0.032
N-(2-Diazo-3-hydroxybutanoyl)	Formate	1.35	0.62
glycine ethyl ester (2.1)	Acetate	0.36	0.068
	Phosphate	0.095	0.099
N-(2-Diazo-3-methylbutanoyl)	Acetate	1.98	1.72
glycine ethyl ester (2.2)			

Figure 2.12 *Line-Weaver Burke Plot for the Decomposition of N-(2-Diazo-3-hydroxybutanoyl)glycine ethyl ester (2.1) in Formate Buffers*

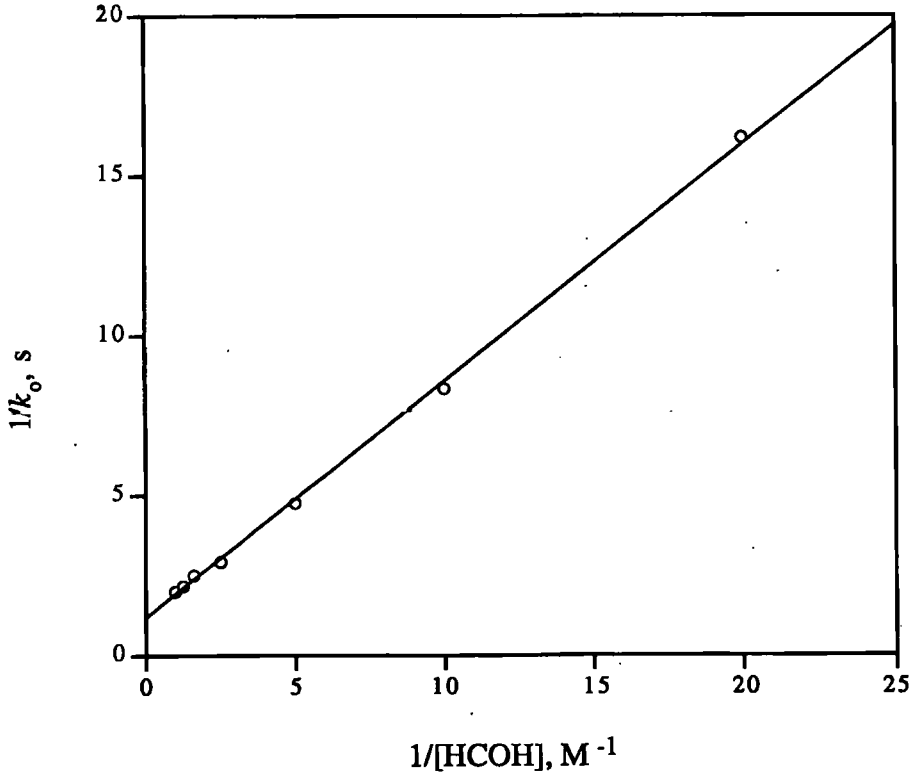

Figure 2.13 *Line-Weaver Burke Plot for the Decomposition of N-(2-Diazoacetyl)glycinamide (1.4) in Acetate Buffers*

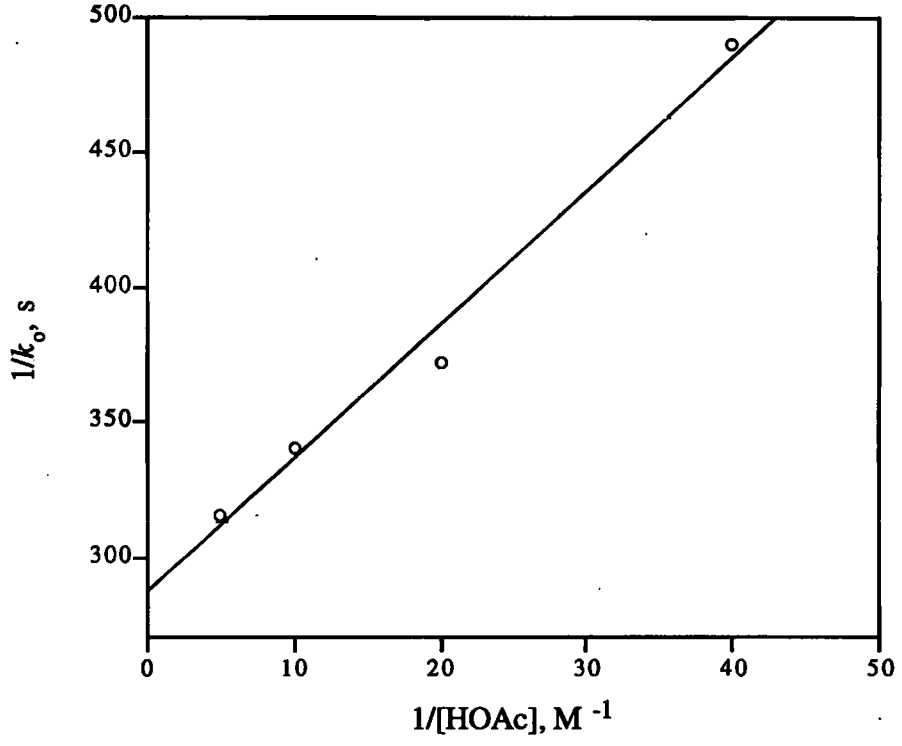

Figure 2.14 *Line-Weaver Burke Plot for the Decomposition of N-(2-Diazo -3-methylbutanoyl)glycine ethyl ester (2.2) in Acetate Buffers*

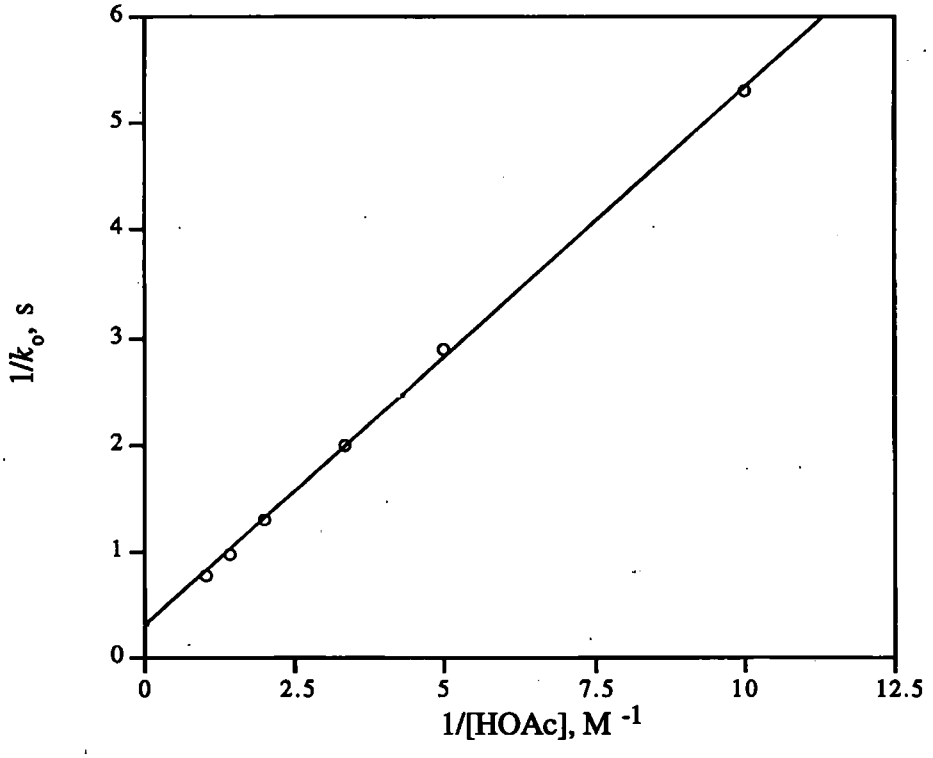

Attempts to observe compound (2.9) from the reaction of (1.4) in neat glacial acetic acid by uv/visible spectrophotometry were unsuccessful. These experiments showed loss of the diazo group absorptions at λ_{max} *ca.* 250 and 390 nm, but no new peaks corresponding to the formation of the azo compound with n->π^* and π->π^* transitions at λ_{max} *ca.* 350 and 265 nm, respectively. Separate experiments showed, that addition of crystalline *N*-(2-diazoacetyl)glycinamide (1.4) to glacial acetic acid produced an immediate effervescence. It was therefore concluded that the decomposition of the diazopeptide (with expulsion of N_2 gas) proceeded faster than azo compound (2.9) formation in glacial acetic acid.

The formation of a relatively stable covalent azo compound (2.6) appears to be the best explanation for the unusual kinetic dependencies observed for the general-acid-catalysed decomposition of diazopeptides in carboxylic and phosphoric acid buffers. Thus far, independent confirmatory evidence for the existence of these azo compounds has proven elusive and further work such as ^{15}N-nmr experiments in glacial acetic acid may be necessary.

3. Reactions of Diazopeptides with Amines

3.1 Introduction

The results in Chapter 2 suggest that diazopeptides may react with buffer components in two ways:

1) H^+-transfer from the buffer-acid to the α-C-atom which leads to loss of N_2 and decomposition.

2) Addition of the buffer-acid to form a metastable diazotate intermediate which retards the rate of decomposition of the diazopeptide.

To obtain further evidence of 2), the interaction of diazoglycylpeptides with amines was investigated. As reported in Chapter 1, there is much evidence for the formation of triazenes from the reactions of diazo compounds (especially aryl diazonium ions) with primary and secondary amines. These reactions have not been previously reported for diazopeptides, but they should lead to relatively stable triazenes (Scheme 3.1) structurally analogous to the proposed diazotate complexes with carboxylic and phosphoric acids (see Chapter 2).

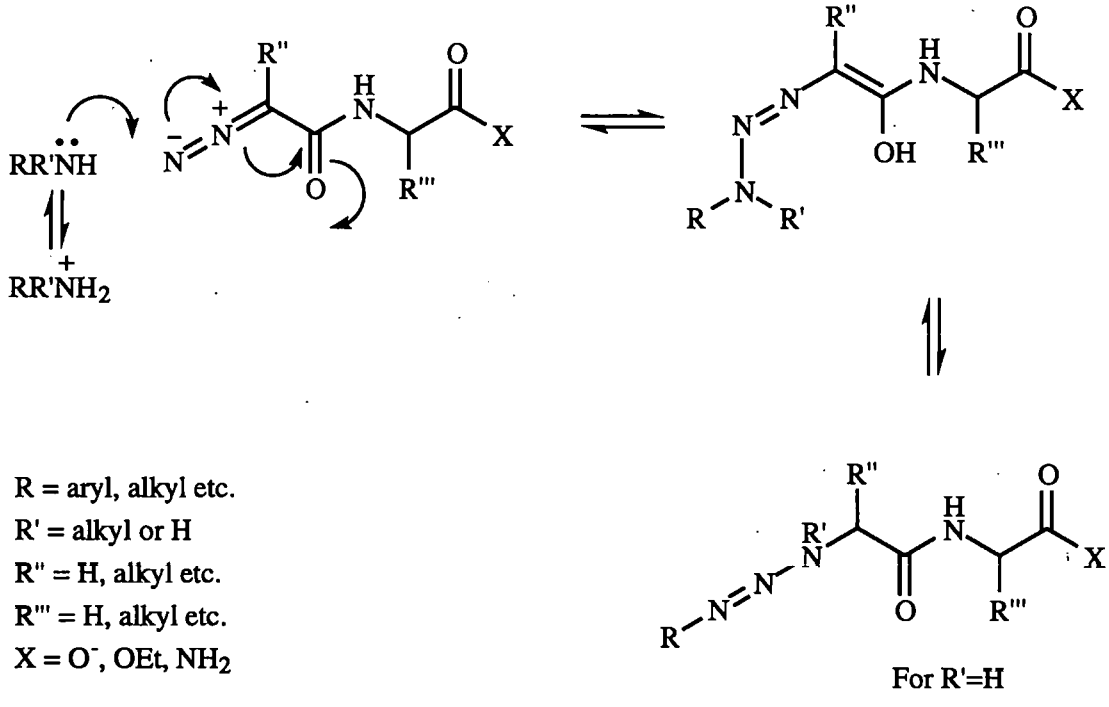

Scheme 3.1

The present studies centred on aromatic amines able to act as acidic-buffers, but reactions with morpholine in $CDCl_3$ were also briefly examined.

3.2 Decomposition of *N*-(2-Diazoacetyl)glycine ethyl ester (1.3) in Aniline/$HClO_4$ Buffers

Evidence that anilinium ions catalyse the decomposition of diazopeptides was sought using *N*-(2-diazoacetyl)glycine ethyl ester (1.3) in aniline/$HClO_4$ buffers at pH 4.4, 25°C and constant ionic strength (μ) = 1.0 adjusted with $NaClO_4$. These reactions were monitored at λ = 380 nm, beyond the absorption of the aniline component. The decomposition reactions followed *pseudo* first-order kinetics and as before, k_o was obtained from the slopes of $\ln(A_t-A_\infty)$ *vs.* time, where A_t and A_∞ are absorbances at time t and infinity, respectively. These plots showed good linearity, as exemplified for the decomposition of (1.3) in 0.2 M aniline buffer in Figure 3.1. Average values of k_o from triplicate reactions (reproducible to ± 5%) are reported in Table 3.1.

Figure 3.1 *First-Order Plot for the Decomposition of N-(2-Diazoacetyl) glycine ethyl ester (1.3) in 0.2 M Aniline/$HClO_4$ Buffers at pH 4.4 and 25 °C; Initial [(1.3)] ca. 10^{-3} M; μ =1*

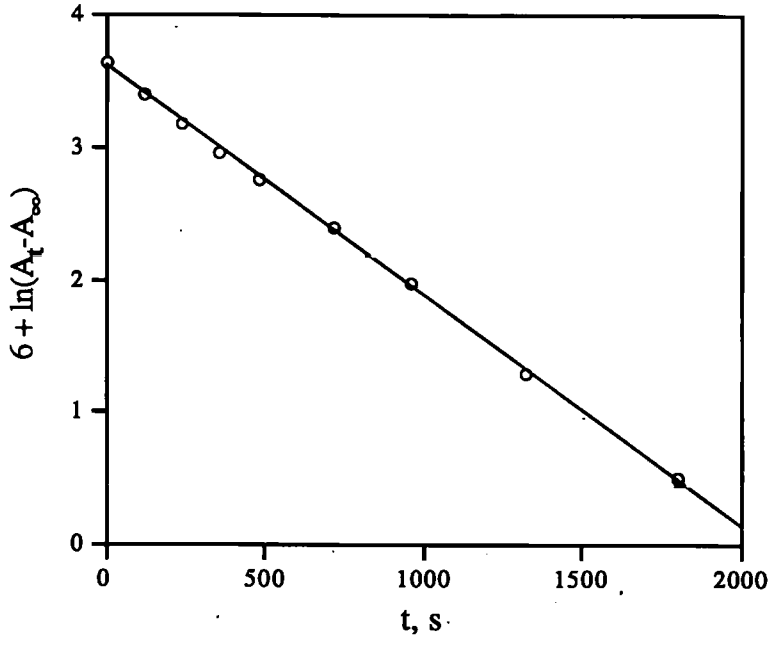

Table 3.1 Variation of the *Pseudo* First-Order Rate Coefficient (k_o) with [$PhNH_3^+$] for the Decomposition of *N*-(2-Diazoacetyl)glycine ethyl ester (1.3) in Aniline/$HClO_4$ Buffers at pH = 4.4 (± 0.20) and 25 (± 0.1) °C; Initial [(1.3)] *ca.* 10^{-3} M; μ = 1

[$PhNH_2$] M	[$PhNH_3^+$] M	[$NaClO_4$] M	$10^3 k_o$ s^{-1}
0.05	0.05	0.95	0.99
0.1	0.1	0.9	1.27
0.2	0.2	0.8	1.73
0.5	0.5	0.5	2.84
0.7	0.7	0.3	3.55
1.0	1.0	-	4.73

Figure 3.2 *Decomposition of N-(2-Diazoacetyl) glycine ethyl ester (1.3) in Aniline/$HClO_4$ Buffers at 25 °C*

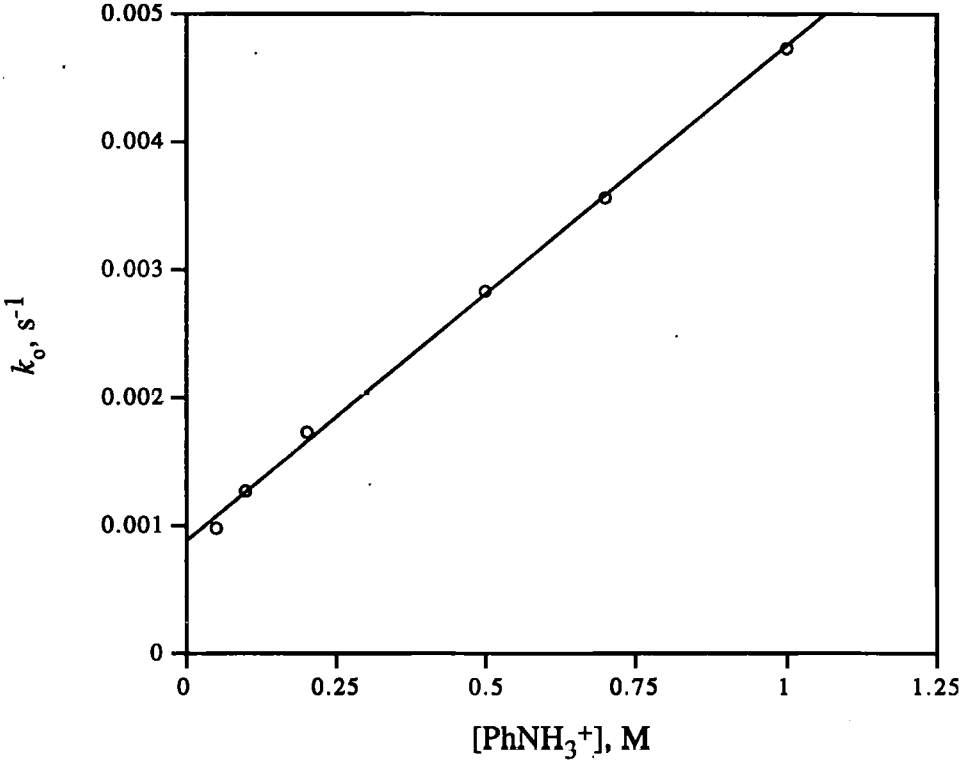

The plot of k_o *vs.* [$PhNH_3^+$] (Figure 3.2) is linear, and values of kHA and $k_{H_3O^+}$ (Equation 2.1) obtained from the slope and intercept, respectively, are reported in Table 3.2. The intercept value of $k_{H_3O^+}$ is in excellent agreement with $k_{H_3O^+}$ for the decomposition of (1.3) in aqueous $HClO_4$ measured by Shuja,[18] and reported in parenthesis in Table 3.2. More importantly, Figure 3.2 shows no curvature or rate attenuation at high [$PhNH_3^+$], which suggests that extensive triazene formation (Scheme 3.1) does not compete with the acid-catalysed decomposition of the diazopeptide. Figure 3.2 does confirm, however, that anilinium ions act as general-acid-catalysts for diazopeptide decomposition.

Table 3.2 Values of kHA and $k_{H_3O^+}$ for the Decomposition of (1.3) in Aniline/$HClO_4$ Buffers at pH 4.4 (± 0.2) and 25 (± 0.1) °C; Initial [(1.3)] *ca.* 10^{-3} M; $\mu = 1$

kHA, $M^{-1}s^{-1}$	$k_{H_3O^+}$, $M^{-1}s^{-1}$
3.9×10^{-2}	9.2×10^{-4} (8.4×10^{-4})

3.2.2 Decomposition of *N*-(2-Diazoacetyl)glycine ethyl ester (1.3) in 0.25 M Phosphate Buffers Plus Aniline at 25 °C

The unexpected linearity of Figure 3.2 may reflect a high lability of the triazene intermediate due to protonation at pH 4.4. The effect of aniline on the decomposition of (1.3) in aqueous phosphate buffers (0.25 M) at pH 6.8 and 25 °C was therefore examined. The 0.25 M phosphate buffers were prepared using 20% (v/v) ethanol in water to solubilise the aniline, and the reactions were monitored at $\lambda = 380$ nm to avoid the aniline absorption. These decomposition reactions also followed *pseudo* first-order kinetics and as before, k_o was obtained from the slopes of $\ln(A_t - A_\infty)$ *vs.* time, where A_t and A_∞ are absorbances at time t and infinity, respectively. These plots showed good linearity, as exemplified for the reaction of (1.3) in 0.05 M $PhNH_2$ plus 0.25 M

phosphate buffers in Figure 3.3. Average values of k_o from triplicate reactions (reproducible to ± 5%) are reported in Table 3.3.

Figure 3.3 *First-Order Plot for the Decomposition of N-(2-Diazoacetyl)glycine ethyl ester (1.3) in 0.25 M Phosphate Buffers Plus 0.05 M Aniline at pH = 6.80 and 25 °C: Initial [(1.3)] ca. 10^{-3} M*

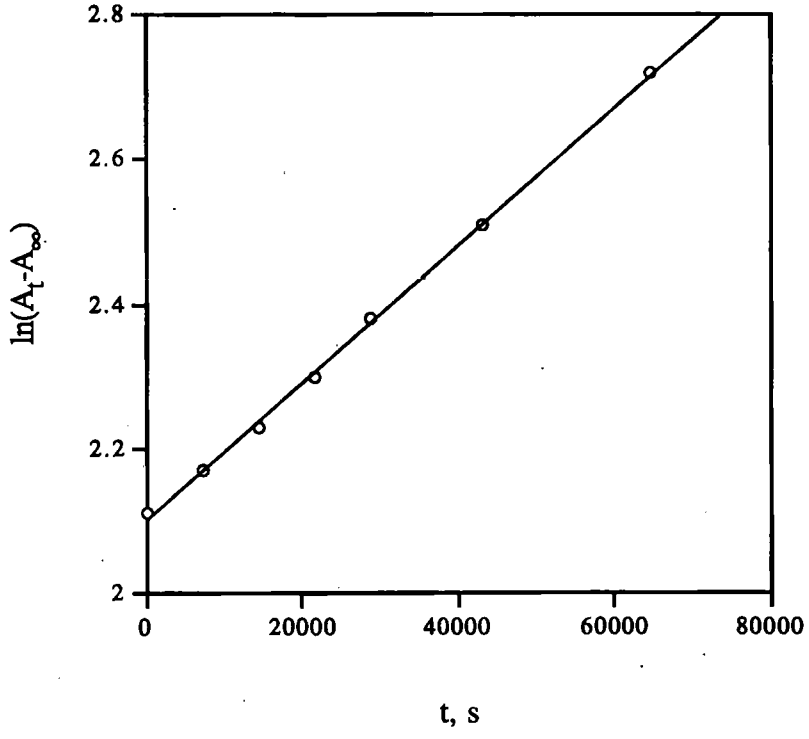

Table 3.3 Variation of the *Pseudo* First-Order Rate Coefficient (k_o) with [$PhNH_2$] for the Decomposition of *N*-(2-Diazoacetyl)glycine ethyl ester (1.3) in 0.25 M Phosphate Buffers at pH = 6.80 (± 0.1) and 25 (± 0.1) °C; Initial [(1.3)] *ca.* 10^{-3} M

[$PhNH_2$] M	[NaH_2PO_4] M	[Na_2HPO_4] M	$10^5 k_o$ s^{-1}
0	0.25	0.25	1.276
0.025	0.25	0.25	1.165
0.05	0.25	0.25	0.958
0.10	0.25	0.25	0.740
0.15	0.25	0.25	0.700
0.20	0.25	0.25	0.647
0.30	0.25	0.25	0.603

Figure 3.4 *Decomposition of N-(2-Diazoacetyl)glycine ethyl ester (1.3) in 0.25 M Phosphate Buffers plus Aniline at pH 6.80 and 25 °C*

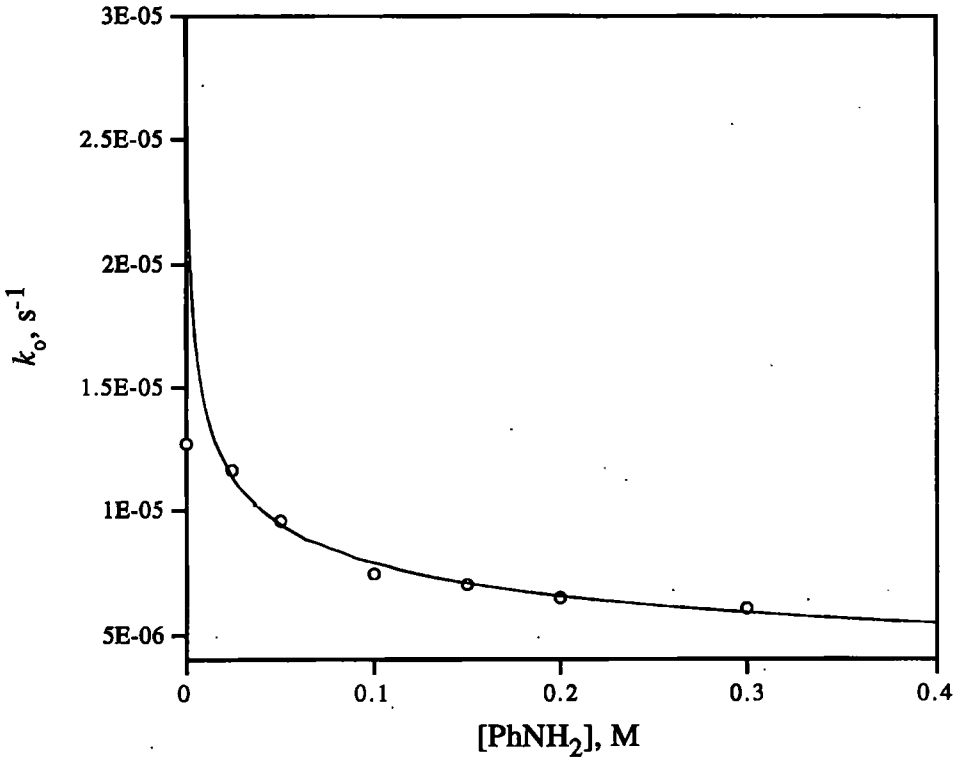

The plot of k_o *vs.* [$PhNH_2$] in Figure 3.4 shows negative curvature indicating that aniline decreases the rate of decomposition of (1.3). This is consistent with triazene (3.1) formation with aniline in a reversible pre-equilibrium competing with $H_2PO_4^-$ -catalysed decomposition of the diazopeptide. The intercept value shows good agreement with k_o from the decomposition of (1.4) in 0.25 M phosphate buffers at 25 °C (Section 2.2.3).

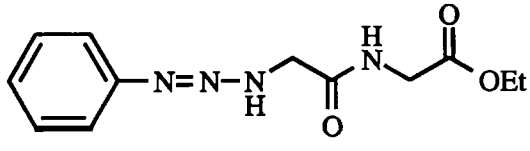

(3.1)

3.4 Decomposition of *N*-(2-Diazoacetyl)glycine ethyl ester (1.3) by Sulphanilic Acid in 1.0 M Phosphate Buffers at 25 °C and pH 6.2

The results in 3.1.2 prompted a brief investigation of diazopepetide (1.3) with sulphanilic acid in phosphate buffer. Sulphanilic acid was chosen because it is an

aromatic amine with high aqueous solubility. The decomposition of (1.3) was examined in 1.0 M phosphate buffers containing 0.25 M sulphanilic acid at 25 °C and pH 6.20 following the reaction spectroscopically at $\lambda = 380$ nm. The results, summarised in Table 3.4, show that the absorbance of the reaction solution increases slowly with time over 45 h. A full uv/visible scan of the reaction solution after 48 h. (Figure 3.5) shows this relates to formation of a product with an absorption maximum at $\lambda_{max} = 356$ nm. On addition of a few drops of conc. HCl to the cuvette, this absorbance disappeared immediately, as shown in Figure 3.5.

Table 3.4 Time-dependent Absorbance at $\lambda = 380$ nm for the Reaction of *N*-(2-Diazoacetyl)glycine ethyl ester (1.3) with Sulphanilic Acid (0.25 M) in Phosphate Buffers (1.0 M) at pH = 6.20 and 25 (± 0.1) °C; Initial [(1.3)] *ca.* x 10^{-3} M

Time, h.	Absorbance, $\lambda = 380$ nm	Time, h.	Absorbance, $\lambda = 380$ nm
0	0.086	25	0.342
5	0.137	30	0.375
10	0.200	35	0.403
15	0.255	40	0.427
20	0.302	45	0.448

At first sight the results with sulphanilic acid seem contrary to those with aniline. It is consistent, however, with slow formation of triazene (3.2) which has a strong absorbance at $\lambda_{max} = 356$ nm (Section 3.7.2) and is relatively stable at pH 6.2, but is labile at lower pH where decomposition (probably with loss of nitrogen) occurs rapidly on treatment with acid.

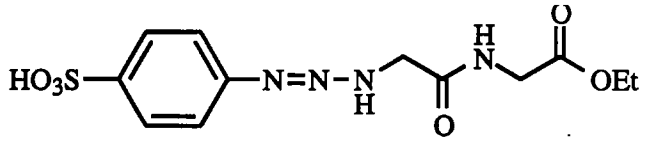

(3.2)

Figure 3.5 *uv Scan of (1.3) in 1.0 M Phosphate Buffers Plus 0.25 M Sulphanilic acid*

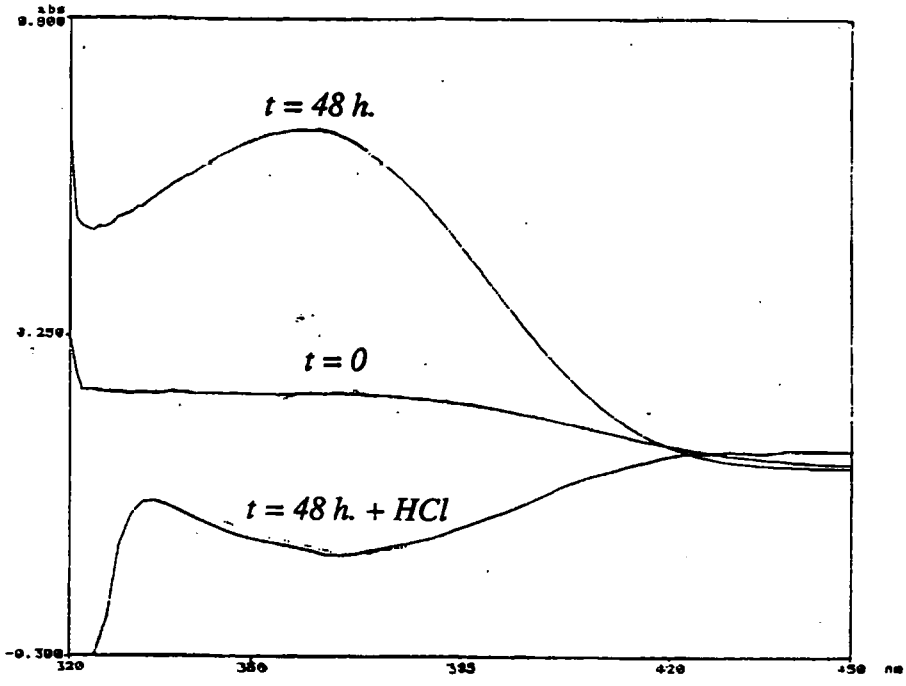

The absence of an isobestic point for the reaction of (1.3) with sulphanilic acid relates to the similar wavelengths of their absorption maxima (diazopeptide (1.3); λ_{max} = 374 nm, ε =17 $dm^3cm^{-1}mol^{-1}$: and triazene (3.2); λ_{max} = 356 nm, ε *ca.* 20,000 $dm^3cm^{-1}mol^{-1}$) and a much higher molar extinction coefficient for the triazene. Thus, by spectrophotometry only the triazene is observed in an equilibrium mixture of the two compounds. This conclusion is supported by the physical properties of triazene (3.3) and silver-triazene (3.3a), synthesised independently as reported in Section 3.7.1. Triazene (3.3) shows similar uv/visible properties {λ_{max} (EtOH) = 356 nm, ε = 20,827 $dm^3cm^{-1}mol^{-1}$} to the sulphanilic acid reaction solution. Further, addition of conc. HCl to an aqueous EtOH solution of triazene (3.3) causes rapid loss of the peak at λ_{max} = 356 nm (Figure 3.6) as observed for the sulphanilic acid reaction solutions in Figure 3.5.

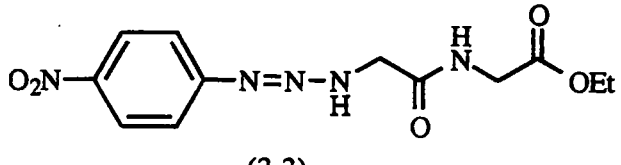

(3.3)

Figure 3.6 *uv Scan of N-(4-Nitrophenylazo) glycylglycine ethyl ester (3.3) in EtOH.*

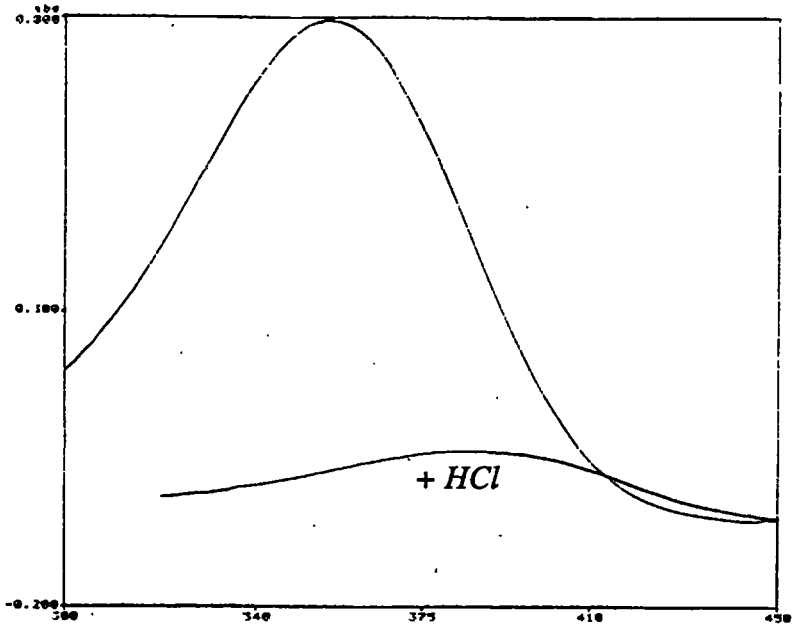

Unfortunately, insufficient time was available to examine the time dependent reactions of diazopeptide (1.3) with aromatic amines in more detail. In retrospect, it would be particularly helpful to compare the reactions of (1.3) with aniline and sulphanilic acid under exactly similar reaction conditions *i.e.* same solvent and pH.

3.5 Reaction of *N*-(2-Diazoacetyl)glycine ethyl ester (1.3) with Morpholine

The potential for forming triazenes from aliphatic amines was examined for the reaction of *N*-(2-diazoacetyl)glycine ethyl ester (1.3) {0.3 mmol} with a 10-fold excess of morpholine (3 mmol) in $CDCl_3$. The reaction was followed by monitoring the peak due to the C=N=N stretch of the diazopeptide at $\nu_{max} = 2112\ cm^{-1}$ by FTIR. After stirring at ambient temperature for one week, no reaction was observed. After heating at 60 °C for a further 48 h., loss of some diazopeptide was apparent by FTIR and the 400 MHz ^{1}H-nmr spectrum showed formation of a product containing a morpholine substituent by the appearance of two new triplets at $\delta = 2.60$ and 3.75 ppm (Figure 3.7b). The reaction solution, however, contained much unreacted diazopeptide and morpholine, as shown by comparison with Figures 3.7a.

Figure 3.7a *400 MHz ^1H-nmr Spectrum of (1.3) Plus Morpholine (10 equiv.) in $CDCl_3$ at 60 °C At t = 0*

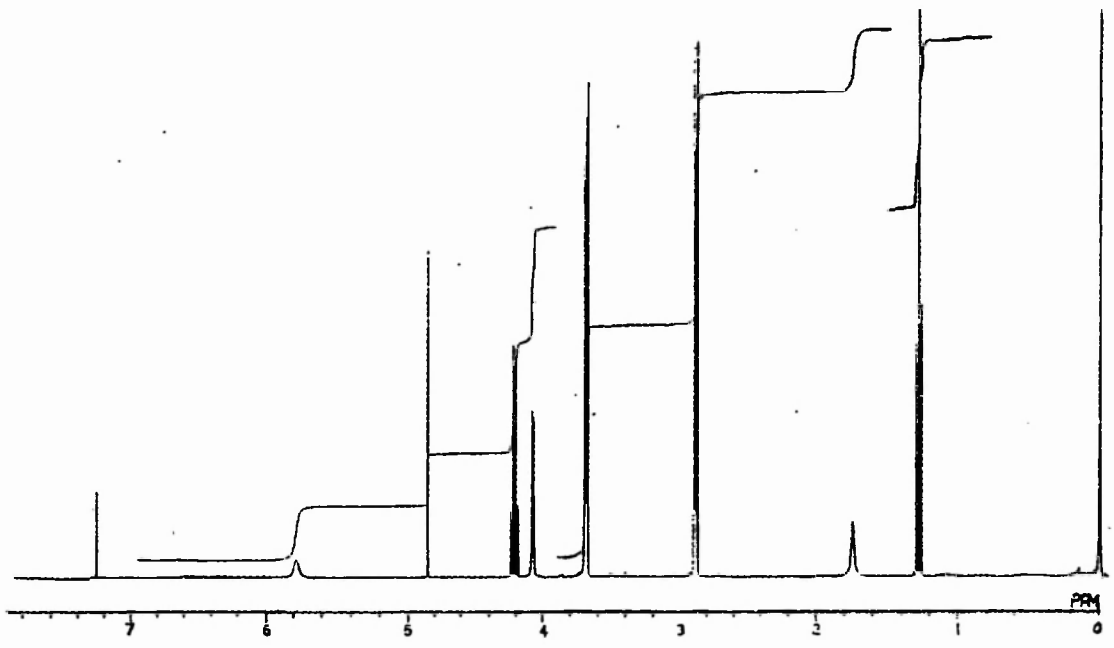

Figure 3.7b *After 2 d.*

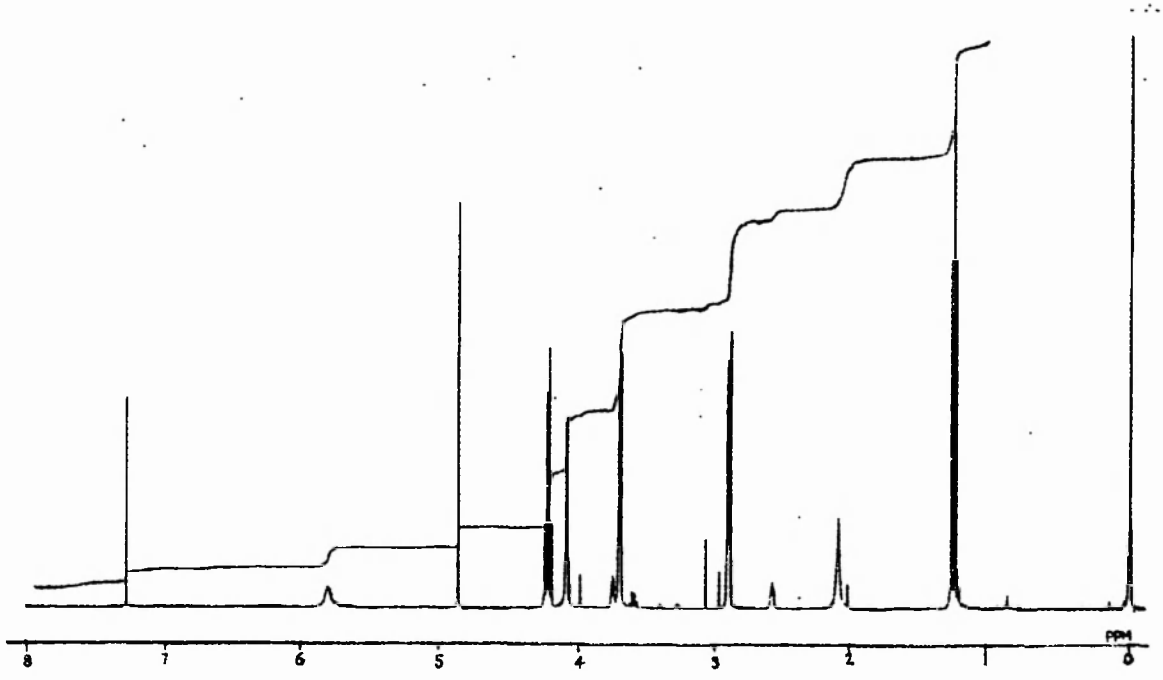

The mixture was heated at 60 °C for a further 10 d. until complete loss of (1.3) was apparent by FTIR. Following removal of $CDCl_3$ and excess morpholine under vacuum, the white solid residue was examined by 400 MHz ^{1}H-nmr and FAB mass spectrometry. The ^{1}H-nmr spectrum (Figure 3.8) indicated two products in the residue bearing morpholine substituents by the presence of two pairs of triplets attributed to morpholine -NC*H*$_2$- and -OC*H*$_2$- methylene groups. The chemical shifts for these two products and their relative yields from the integrated signals are summarised in Table 3.5. These show that the major product A contains a morpholino residue shielded relative to morpholine itself, whereas the minor product B contains a deshielded morpholino residue.

Table 3.5 400 MHz ^{1}H-nmr Data for Products A and B in $CDCl_3$

Compound	δ; Morpholino triplet, ppm		Relative Yield
	-C*H*$_2$NC*H*$_2$-	-C*H*$_2$OC*H*$_2$-	,%
Product A	2.58	3.75	80
Product B	3.17	3.93	20
Morpholine	2.80	3.69	-

The positive mode FAB mass spectrum of the white residue (Figure 3.9) gave m/z = 231 as the m/z = 100 {probably 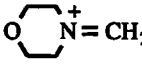 } as the base peak. The negative mode FAB mass spectrum gave m/z = 229 as the M-H$^+$ with fragmentations at m/z = 201 and 183 corresponding to loss of ethene and ethanol, respectively, and characteristic of compounds bearing ethyl ester groups.

These data are consistent with *N*-(2-morpholinoacetyl)glycine ethyl ester (3.4) as the major product A from the reaction of (1.3) with morpholine in $CDCl_3$.

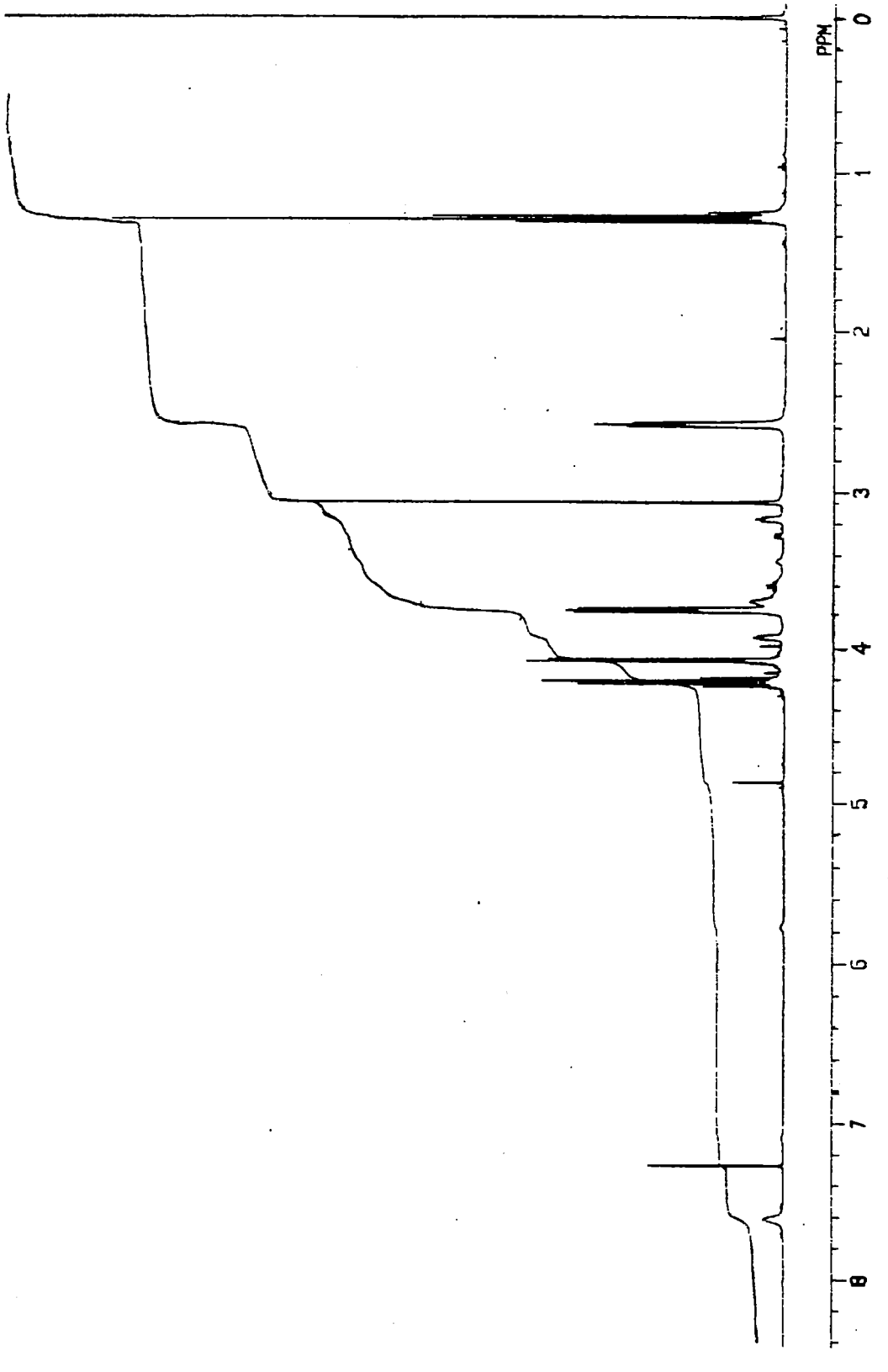

Figure 3.8 *400 MHz ^1H-nmr Spectrum of Products from the Reaction of (1.3) with Morpholine in $CDCl_3$ at 60 °C After 12 d.*

Figure 3.9 *FAB Mass Spectrum of Products from the Reaction of (1.3) with Morpholine in $CHCl_3$ at 60 °C After 12 d.*

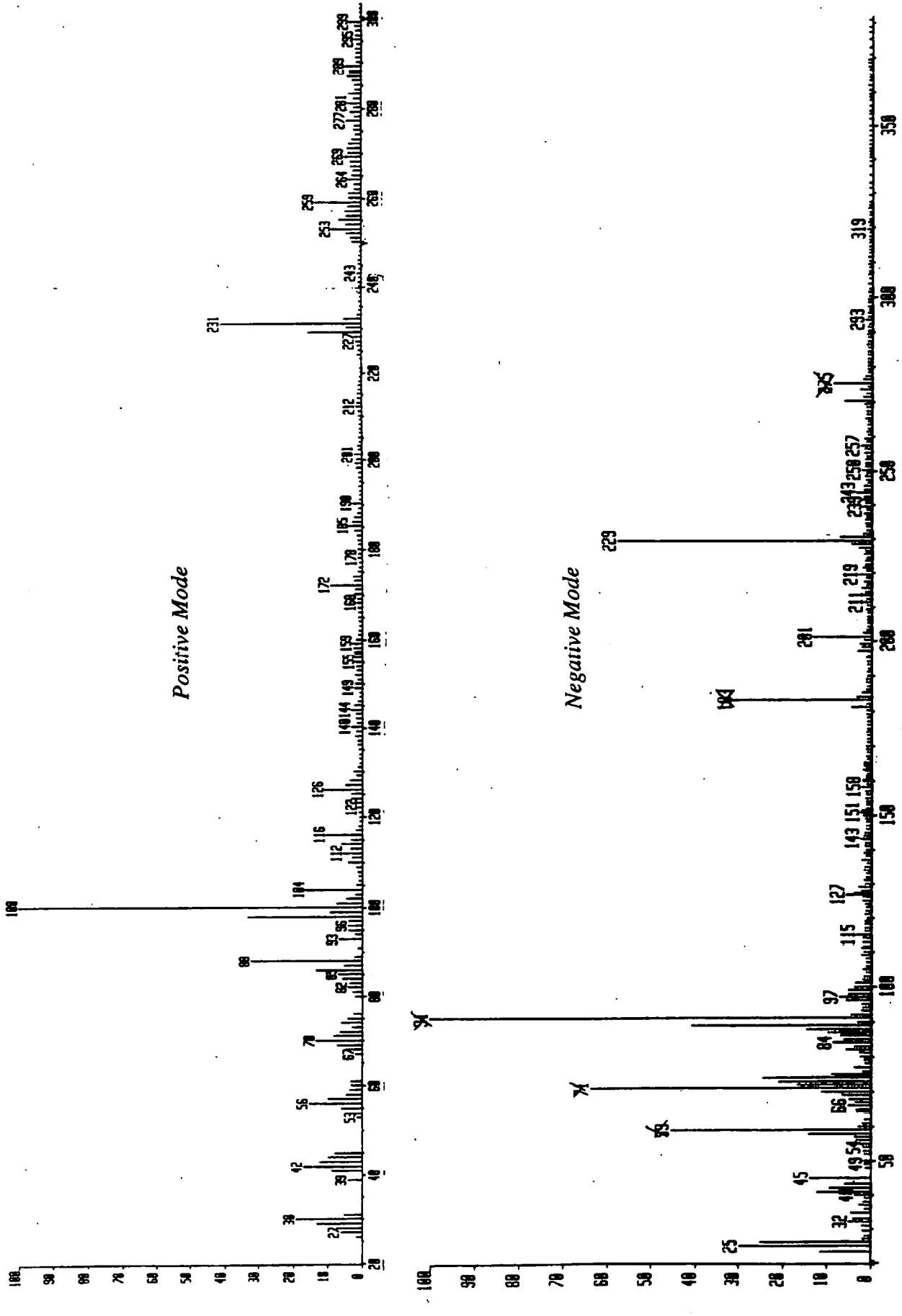

Compound (3.4) probably forms *via* a triazene intermediate (3.5) {Scheme 3.2}, although nucleophilic displacement of N_2 by morpholine from the conjugate acid of the diazopeptide cannot be discounted, but is unlikely. The structure of the minor product B is more conjectural. Close scrutiny of the FAB mass spectrum reveals weak ions at m/z = 257 in the negative mode and m/z = 259 in the positive mode *i.e.* both 28 amu greater than MH^+ and $M\text{-}H^+$ ions of the major product A. This suggests that the minor product may be the intermediate triazene (3.5) which loses N_2 to the major product (3.4) as postulated in Scheme 3.2.

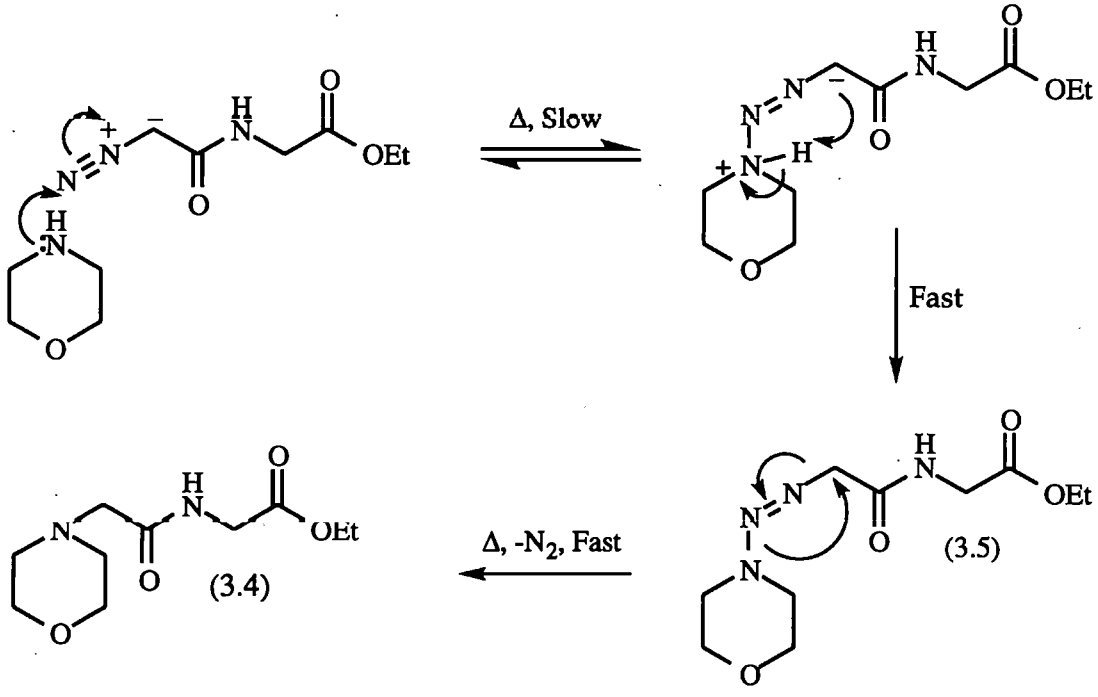

Scheme 3.2

An alternative for the minor product B is the isomeric iminodialkanoic acid derivative (3.6) formed *via* the Wolff rearrangement (Scheme 3.3).[28, 123, 124] The reaction involves thermal generation of a singlet carbene, rearrangement *via* an oxirene to form ketene (3.7) which then undergoes nucleophilic substitution by morpholine to give product (3.6) {Scheme 3.3}. Products arising from the Wolff rearrangement are well documented for azo esters and ketones.[28, 123, 124] Compounds (3.5) and (3.6) are consistent with the ^{1}H-nmr data for product B, the morpholino -CH_2NCH_2- protons being more deshielded than those of product A. The mass spectrum of (3.6) would be very similar, if not identical, to major product A (3.4).

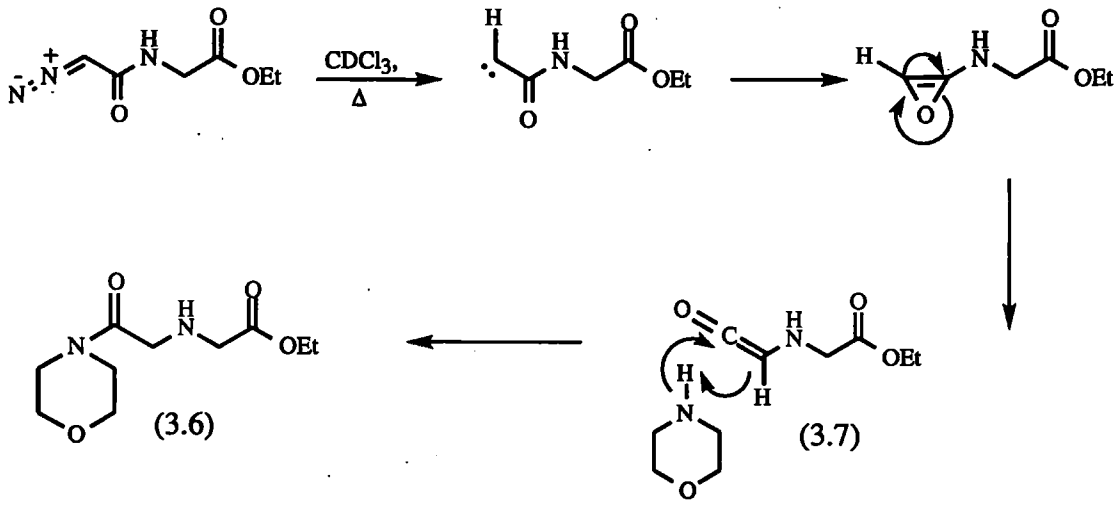

Scheme 3.3

3.6 Independent Synthesis of *N*-(2-Morpholinoacetyl)glycine ethyl ester (3.4)

The identity of the major product A was confirmed *via* an independent synthesis of (3.4) in two simple, high yielding steps from 2-chloroacetic acid (Scheme 3.4). The chloroacetic acid was heated under reflux with two equivalent of morpholine in ethanol to give the morpholine salt (3.8) as a white crystalline solid. The authentic *N*-(2-morpholinoacetyl)glycine ethyl ester (3.4) was prepared directly by DECP mediated coupling of (3.8) with glycine ethyl ester hydrochloride.

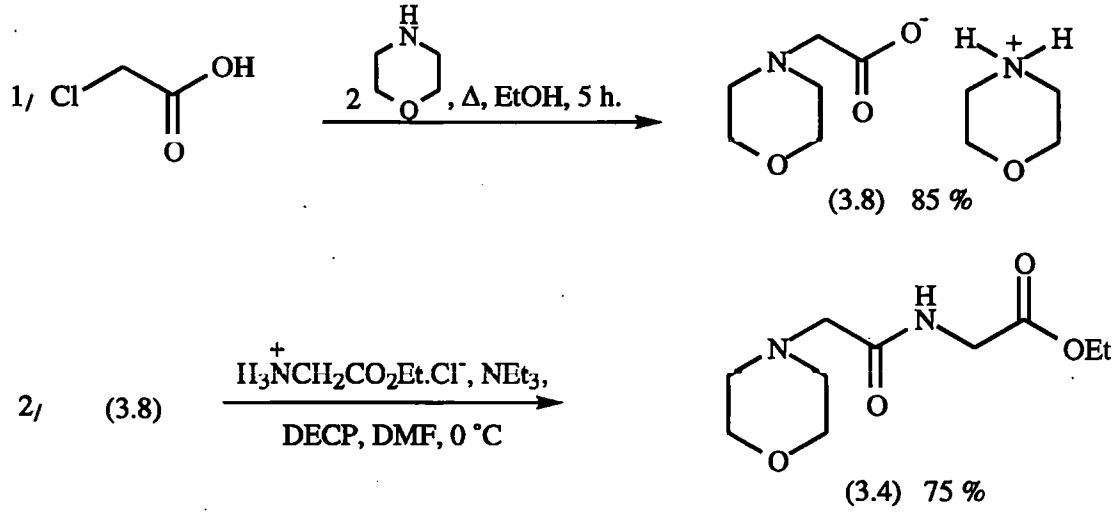

Scheme 3.4

The major product A compared favourably with authentic (3.4) by 400 MHz ^{1}H-nmr (Figure 3.10) and FAB mass spectroscopy (Figure 3.11).

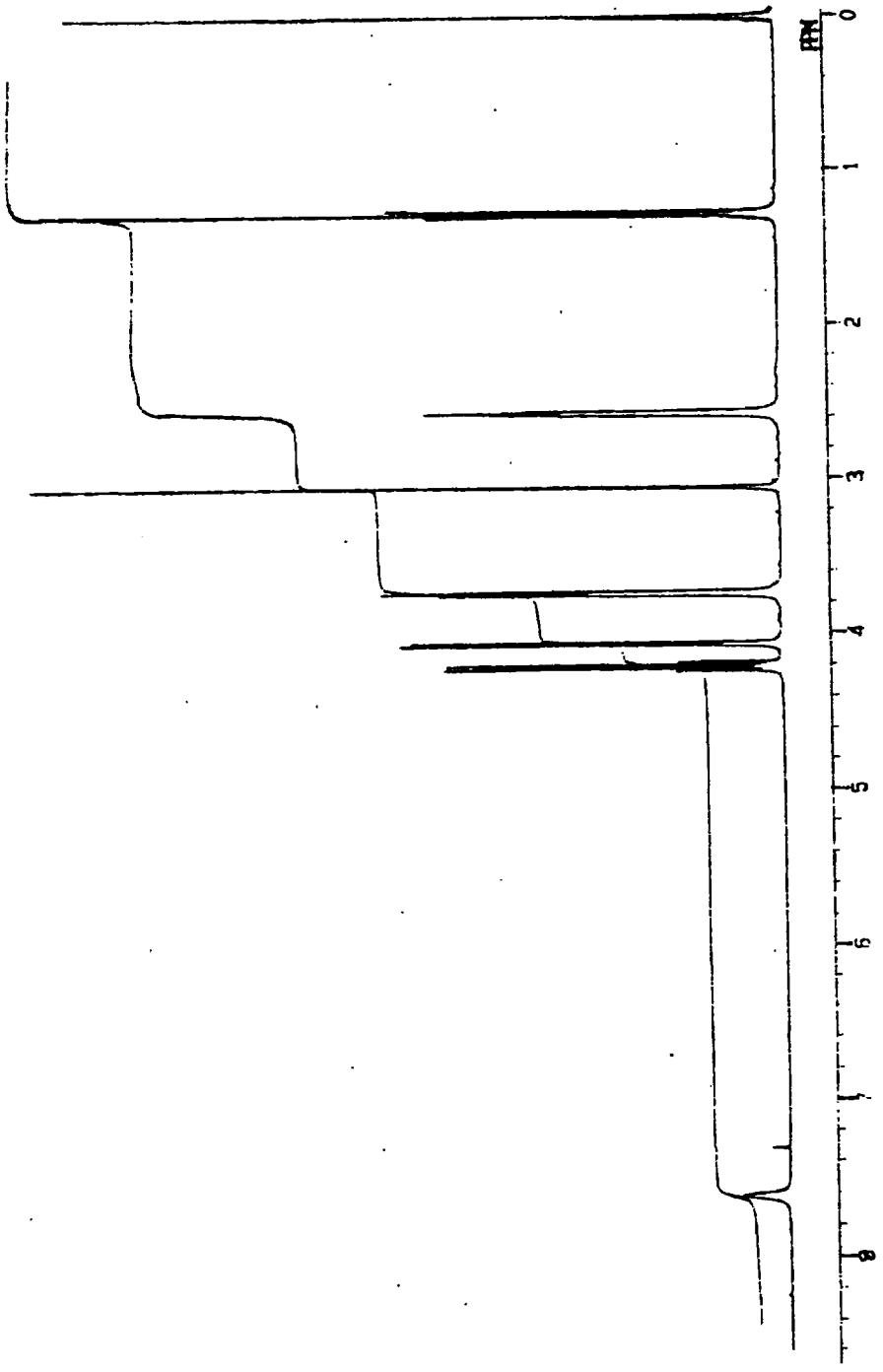

Figure 3.10 *400 MHz ^{1}H-nmr Spectrum of N-(2-Morpholinoacetyl)glycine ethyl ester (3.4) in $CDCl_3$*

Figure 3.11 *FAB Mass Spectrum of N-(2-Morpholinoacetyl)glycine ethyl ester (3.4)*

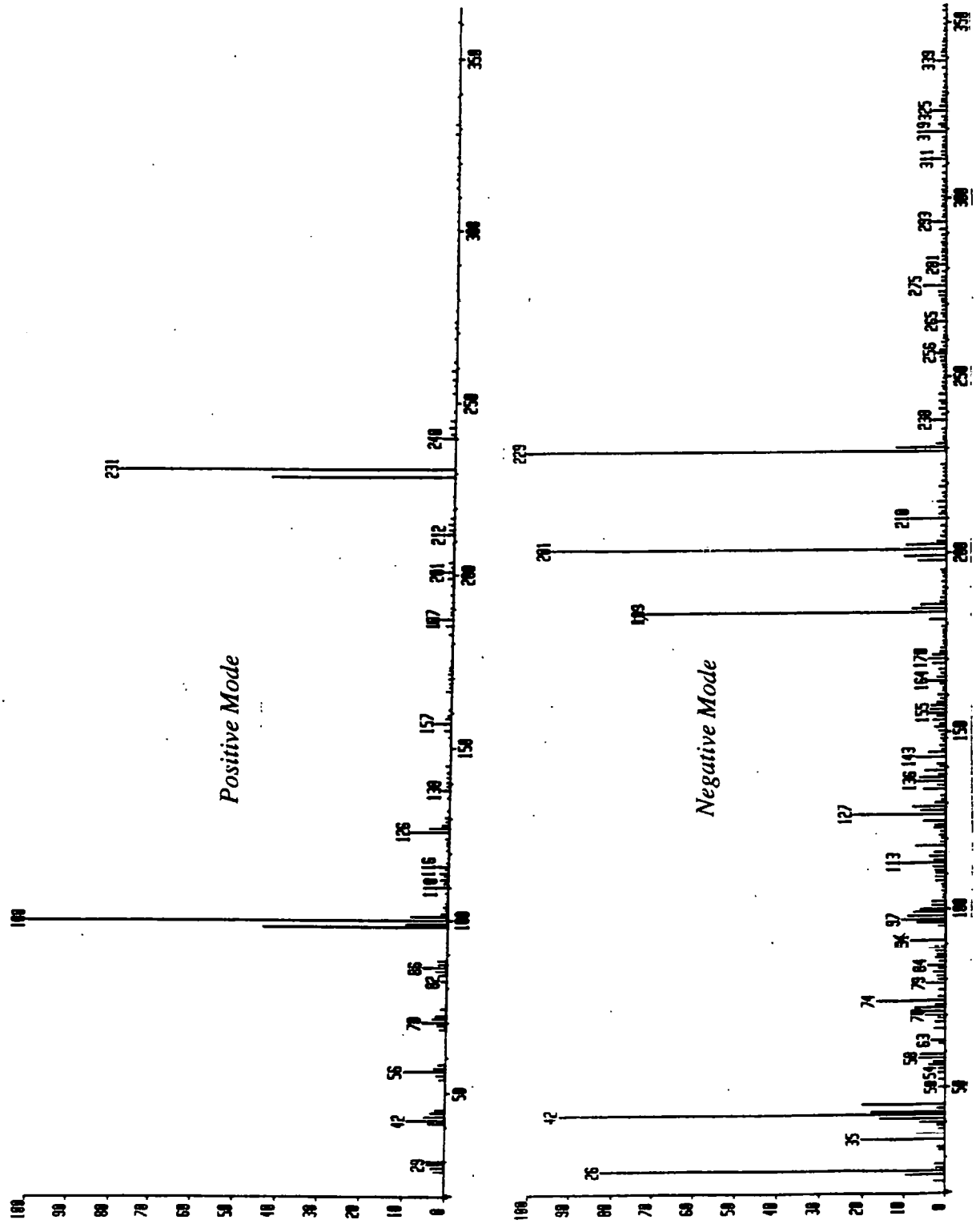

3.7 Independent Syntheses of Alkylaryltriazenes (ArN=N-NHR)

As discussed in Chapter 1, primary amino compounds form triazenes only on reaction with diazonium ions bearing strong, electron-withdrawing substituents.[47] Comparable reactions with the phenyl diazonium ion lead to penta-azadienes, because the triazene reacts readily with a second phenyl diazonium ion. These observations are consistent with the results in Sections 3.3 and 3.4. Triazene (3.1) was not detected by uv/visible spectrophotometry from the reaction of *N*-(2-diazoacetyl)glycine ethyl ester (1.3) with aniline in aqueous media, although attenuation of the rate of acid-catalysed decomposition of (1.3) with increasing [$PhNH_2$] was apparent. This behaviour is consistent with either reversible pre-equilibrium triazene (3.1) formation competing with acid-catalysed decomposition of the diazopeptide, or further reaction of the transient triazene (3.1) with a second diazopeptide to give a penta-azadiene.

Triazene (3.2) was detected by uv/visible spectrophotometry, however, from the reaction of (1.3) with sulphanilic acid. Here, triazene (3.2) contains the strong electron-withdrawing -SO_3H aryl substituent which renders it stable to further coupling.

Several alkylaryltriazenes have been synthesised in good yield by coupling of glycine ethyl ester with aryl diazonium ions in aqueous sodium acetate, where electron-withdrawing groups (e.g. 4-NO_2, 4-CN, 4-Cl) are present in the aryl ring.[46] It seemed feasible that these reactions could be extended to the synthesis of the novel alkylaryltriazenes (3.2) and (3.3) *via* the coupling of glycylglycine ethyl ester with the aryl diazonium ions of sulphanilic acid and 4-nitroaniline, respectively. Authentic (3.2) was required to confirm and quantitate the formation of (3.2) from the reaction of *N*-(2-diazoacetyl)glycine ethyl ester (1.3) with sulphanilic acid (Section 3.4). As triazenes derived from the sulphanilic acid diazonium ion have never been isolated

(probably due to their high aqueous solubility), the more isolable triazene (3.3) was first prepared as a pilot for (3.2).

3.7.1 Synthesis and Characterisation of *N*-(4-Nitrophenylazo)glycylglycine ethyl ester (3.3)

Triazene (3.3) was synthesised in good yield (68 %) *via* the method outlined in Scheme 3.5. The product readily precipitated from the reaction mixture due to the low aqueous solubility inferred by the presence of the 4-nitro group (Section 7.5.2.1).

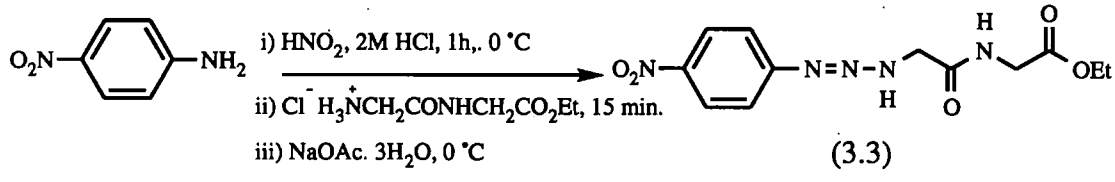

Scheme 3.5

Following isolation, triazene (3.3) was converted into silver-triazene (3.3a) by the addition of a five-fold excess of aqueous silver nitrate to a solution of (3.3) in ethanol. This gave an immediate, luminous yellow precipitate and subsequently a fine yellow powder (Section 7.5.2.2). The solid was micro-analytically pure for $AgC_{12}H_{14}N_5O_5$ (structure 3.3a) and probably exists as the silver salt rather than a metal-ligand complex.

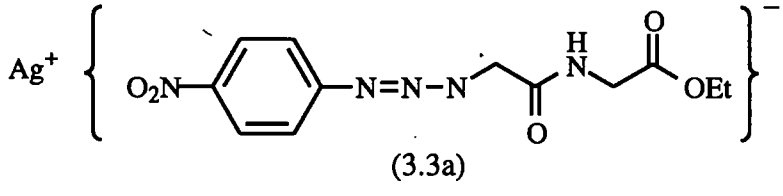

The solubility of the silver-triazene (3.3a) is much less than the free triazene (3.3), and it is only sparingly soluble in DMSO and completely insoluble in alcohol and water. Both

triazene (3.3) and silver-triazene (3.3a) are thermally unstable and decompose explosively with loss of nitrogen. Triazene (3.3) and silver-triazene (3.3a) were examined by ^{1}H-nmr, m/s, FTIR and uv procedures, as reported in Section 3.8.

3.7.2 Synthesis and Characterisation of *N*-(4-Sulphonylphenylazo)glycylglycine ethyl ester (3.2)

Triazene (3.2) could not be isolated from the aqueous reaction mixture using the method for (3.3), because of its higher aqueous solubility. Attempts were therefore made to isolate (3.2) from the reaction mixture as the less soluble silver-triazene (3.2a). It was necessary, however, to modify the method of silver-triazene formation as summarised in Scheme 3.6 and described in more detail in 7.5.2.1.

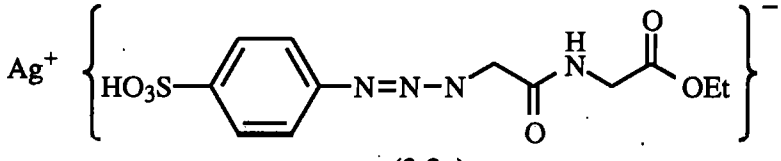

(3.2a)

In particular, because of the need to add excess $AgNO_3$ to precipitate the complex derived from sulphanilic acid, both chloride and acetate ions had to be absent from the reaction mixture to avoid concurrent precipitation of insoluble silver chloride and acetate salts. Hence;

1) $HClO_4$ was used instead of HCl with sodium nitrite to effect diazotisation of the sulphanilic acid.

2) The nitrate salt of glycylglycine ethyl ester was prepared *in situ* from an aqueous solution of the hydrochloride salt and silver nitrate. The aqueous solution of the peptide salt was decanted after centrifuging from precipitated silver chloride.

3) Dilute sodium hydroxide was added to give pH 7 and a bright orange precipitate of triazene (3.2).

4) Addition of excess aqueous silver nitrate to the orange solution gave a luminous yellow solution, and precipitation of a yellow solid was effected by the addition of acetone at 0 °C, which was immediately filtered and dried.

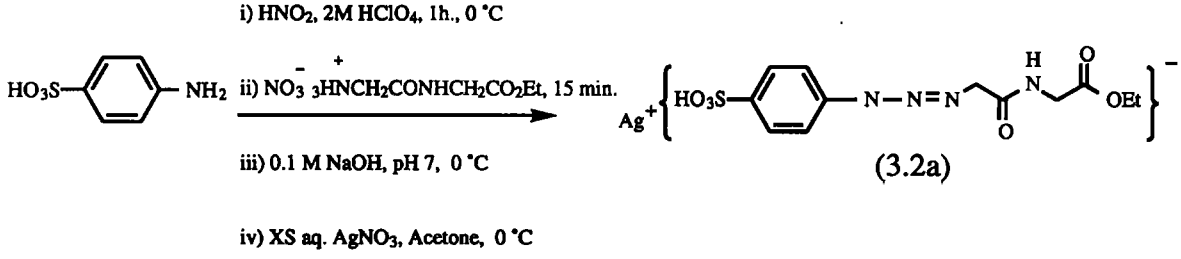

(3.2a)

Scheme 3.6

On exposure to air, moisture or light, the yellow solid blackened within a few hours indicating decomposition. The solid was therefore stored in darkness under nitrogen at low temperature. Addition of dilute HCl to an aqueous solution of the solid resulted in an immediate discharge of its yellow colour with effervescence (expulsion of N_2).

The micro-analytical data for the yellow solid is summarised in Table 3.6. This shows that it contains a considerable impurity which could not be removed by usual procedures. The assays for all three elements are consistently low indicating that *ca.* 40 % of the yellow solid is the silver-triazene (3.2a), $AgC_{12}H_{15(16)}N_4O_6S$. The agreement between C, H and N assays indicates that the impurity is inorganic, (probably silver nitrate) which would account for the blackening observed on exposure to light. Due to lack of time, further purification of the yellow solid and alternative methods for the extraction of (3.2a) from the reaction solution were not investigated. The yellow solid was examined further by ^{1}H-nmr, m/s, FTIR and uv procedures (Section 3.8), and the results broadly confirm the conclusions made above.

Table 3.6 Summary of Micro-Analytical Data for Silver-triazene (3.2a) {$AgC_{12}H_{16(15)}N_4O_6S$}

Element	Theory, %	Found, %	% of Theory
C	31.87 (31.93)	13.03	40.9 (40.9)
H	3.57 (3.33)	1.45	40.6 (43.5)
N	12.39 (12.42)	4.76	38.4 (38.3)

*The figures in parenthesis represent theoretical % and actual % atom values of theory for the deprotonated triazene ligand *i.e.* silver-triazene salt (3.2a)

3.8 Spectroscopic Characterisation of Triazene (3.3) and Silver-triazenes (3.3a) and (3.2a)

3.8.1 ^{1}H-nmr Spectroscopy

The 400 MHz ^{1}H-nmr spectrum of triazene (3.3) in $CDCl_3$ is shown as Figure 3.12 and summarised in Table 3.7. The data are entirely consistent with the proposed structure. Thus, the two methylene groups of the glycylglycine moiety are observed at $\delta = 4.12$ and 4.46 ppm, the ethyl ester at $\delta = 1.28$ and 4.23 ppm and the aromatic resonances appear at $\delta = 7.26$, 7.52 and 8.24 ppm. Both the coupling constants and relative integrals are consistent with these assignments.

An interesting detail of Figure 3.12 is the broadening of both the *N*-methylene ($-CH_{2\ b}$ & $-CH_{2\ b'}$, $\delta = 4.46$ ppm) and the aromatic signals (H_a, $\delta = 7.52$ ppm and $H_{a'}$, $\delta = 6.84$ ppm), which suggests that triazene (3.3) undergoes rapid tautomerism at room temperature (Scheme 3.7).

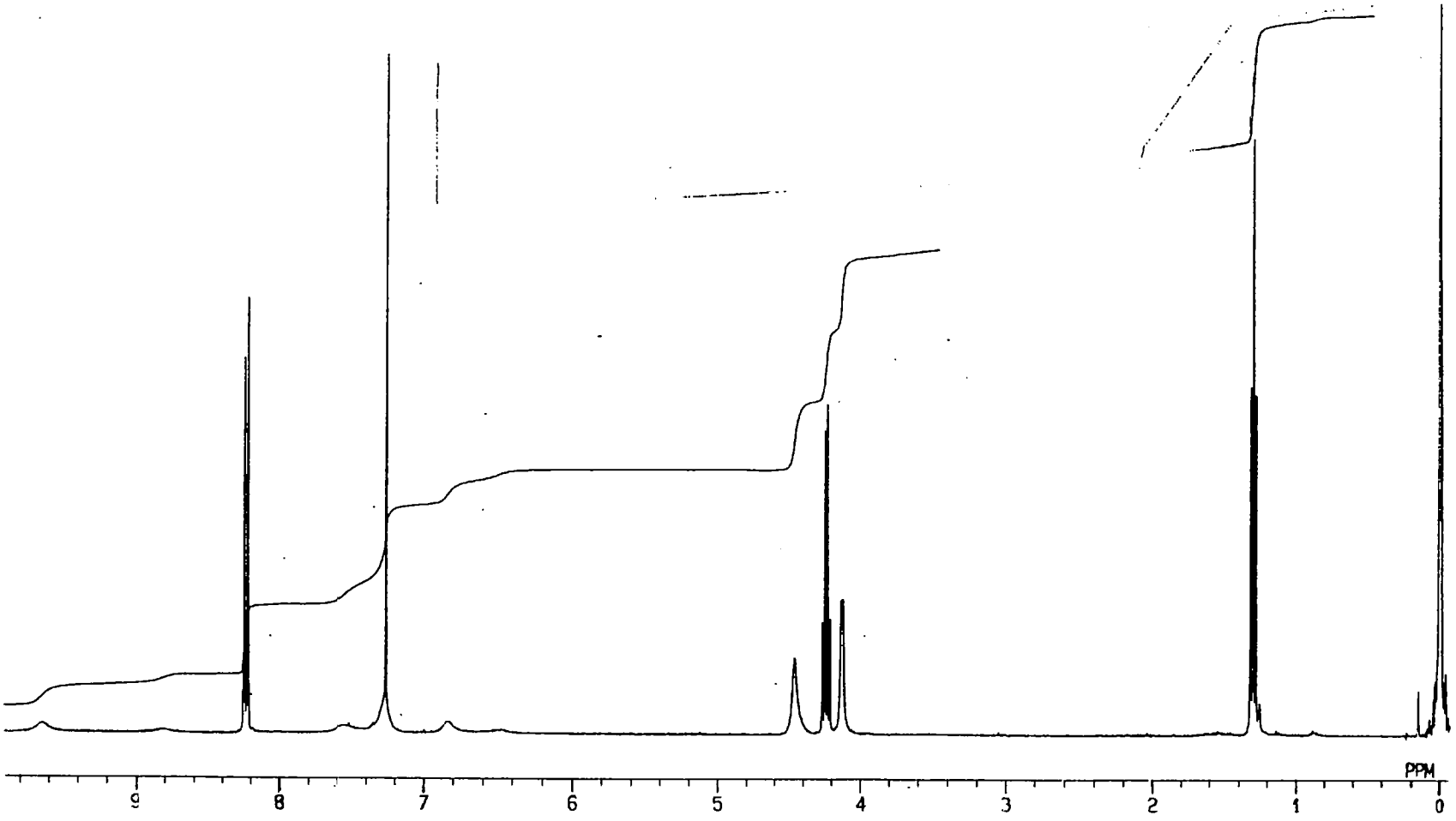

Figure 3.12 *400 MHz ^{1}H-nmr Spectrum of N-(4-Nitrophenylazo)glycylglycine ethyl ester (3.3) in $CDCl_3$*

Table 3.7 ^{1}H-nmr Assignments for Triazene (3.3) in $CDCl_3$

δ, ppm	Assignment	m	J, Hz	Relative Integral
1.28	CH_2CH_3	t	7.2	3
4.12	-NHCH_2CO-	d	4.8	2
4.23	-CH_2CH$_3$	q	7.2	2
4.46	=N-NH-CH_2CO-	s (br.)		2
6.84, 7.52	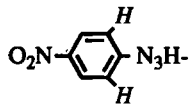	2 x s (br.)		2
8.24	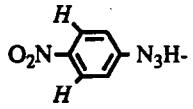	d	9.2	2

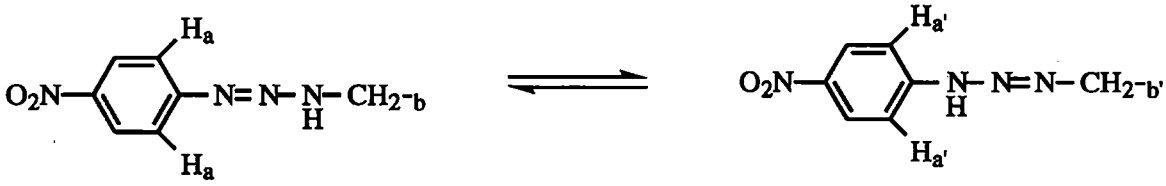

(X) (Y)

Scheme 3.7

As the rate of interchange in $CDCl_3$ lies within the nmr time-scale, both tautomers can be identified. The downfield H_a (δ = 7.52 ppm) and upfield $H_{a'}$ (δ = 6.48 ppm) aromatic

protons are assigned to tautomers (X) and (Y), respectively. Further, the tautomeric interchange is sufficiently rapid for collapse of both doublets expected for the H_a and $H_{a'}$ protons to baseline singlets.

Nmr-studies of alkylaryltriazenes have shown that tautomerism is temperature and solvent dependent and influenced by the aryl substituent.[68-71] The solvent dependence for the tautomerism of triazene (3.3) was therefore briefly investigated. The 400 MHz ^{1}H-nmr data for *N*-methylene and aromatic proton resonances adjacent to the triazene group for triazene (3.3) in various solvents at room temperature are summarised in Table 3.8.

Table 3.8 ^{1}H-nmr Data for Tautomers of Triazene (3.3) in Various Solvents

Solvent	Tautomer (δ, ppm)			
	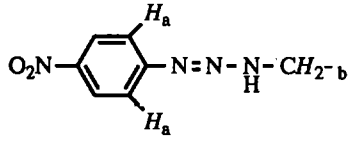		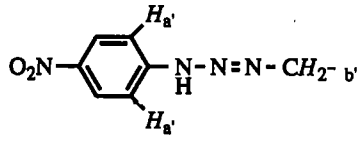	
	H_a	H_b	$H_{a'}$	$H_{b'}$
$CDCl_3$	7.52 (s, br.)	4.46 (s, br.)	6.84 (s, br.)	4.46 (s, br.)
d_6 acetone	7.61 (d)	4.42 (s)	7.46 (d)	4.47 (s)
d_6 DMSO	-	-	6.59 (d)	6.75 (s)

The 400 MHz ^{1}H-nmr spectrum of triazene (3.3) in d_6 acetone is shown as Figure 3.13. The main difference from the spectrum in $CDCl_3$ (Figure 3.12) concerns the *N*-methylene ($-CH_{2\,b}$ and $-CH_{2\,b'}$) and the aromatic (H_a and $H_{a'}$) resonances, which appear as two sharp singlets and two sharp doublets, respectively. The methylene singlet

at $\delta = 4.47$ ppm assigned to the $-CH_{2\ b}$ protons of tautomer (Y) is adjacent to the double bonded N-atom of the triazene group, hence it is slightly more deshielded than the methylene singlet at $\delta = 4.42$ ppm assigned to the $-CH_{2\ b'}$ protons of tautomer (X). Conversely, the aromatic doublet $\delta = 7.61$ ppm assigned to the H_a protons of tautomer (X) is adjacent to the double bonded N-atom of the triazene group, hence it is more deshielded than the aromatic doublet at $\delta = 7.47$ ppm assigned to the $H_{a'}$ protons of tautomer (Y). The sharpness of these signals in d_6 acetone shows that the rate of tautomeric interchange is less rapid compared with solvent $CDCl_3$, and within the nmr time-scale.

The 400 MHz ^{1}H-nmr spectrum of triazene (3.3) in d_6 DMSO (Figure 3.14) differs considerably from those in Figures 3.12 and 3.13 for $CDCl_3$ and d_6 acetone solvents, respectively. Thus, no signals are broadened and only one signal is observed for the *N*-methylene and aromatic protons adjacent to the triazene group implying that triazene (3.3) exists in one tautomeric form only. The *N*-methylene protons at $\delta = 6.75$ are significantly more deshielded (suggesting they are adjacent to the double-bonded triazene N-atom) and the doublet at $\delta = 6.59$ for the aromatic protons is significantly more shielded, (suggesting they are adjacent to the triazene NH-atoms) than in solvents $CDCl_3$ and d_6 acetone. The chemical shifts in d_6 DMSO for triazene (3.3) favour tautomer (Y), but the large differences in δ for these signals compared with tautomers in solvents $CDCl_3$ and d_6 acetone may indicate that d_6 DMSO complexes with triazene (3.3) and prevents tautomerism.

Figure 3.13 *400 MHz ^{1}H-nmr Spectrum of N-(4-Nitrophenylazo)glycylglycine ethyl ester (3.3) in d_6 Acetone*

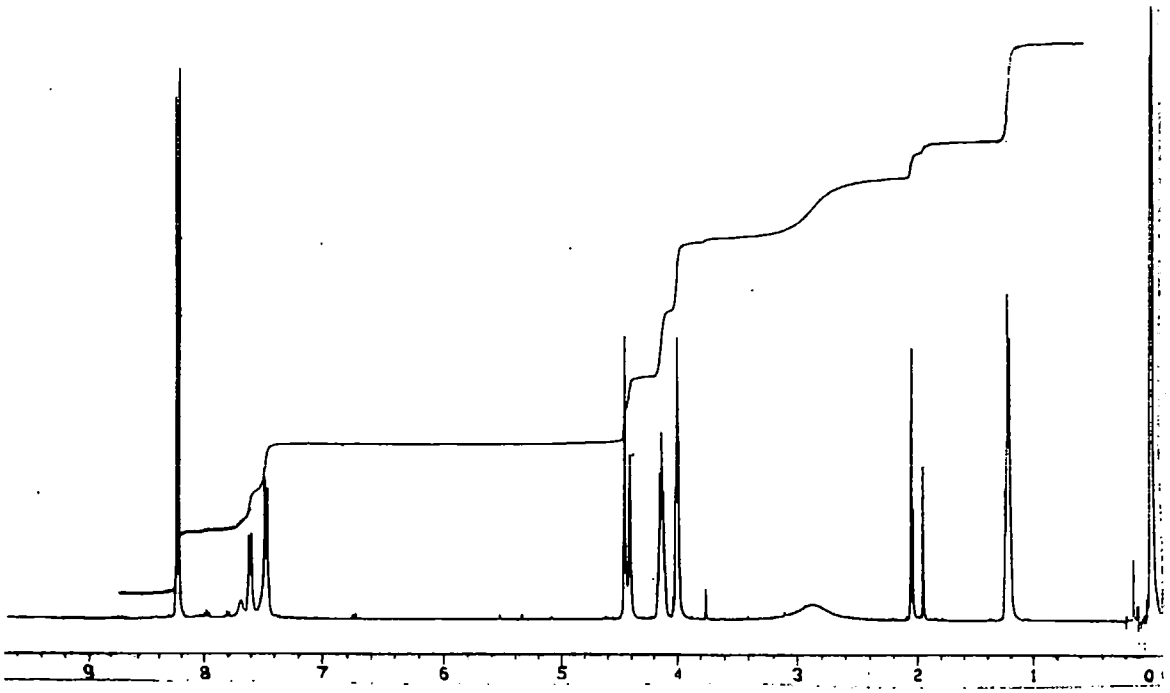

Figure 3.14 *400 MHz ^{1}H-nmr Spectrum of N-(4-Nitrophenylazo)glycylglycine ethyl ester (3.3) in d_6 DMSO*

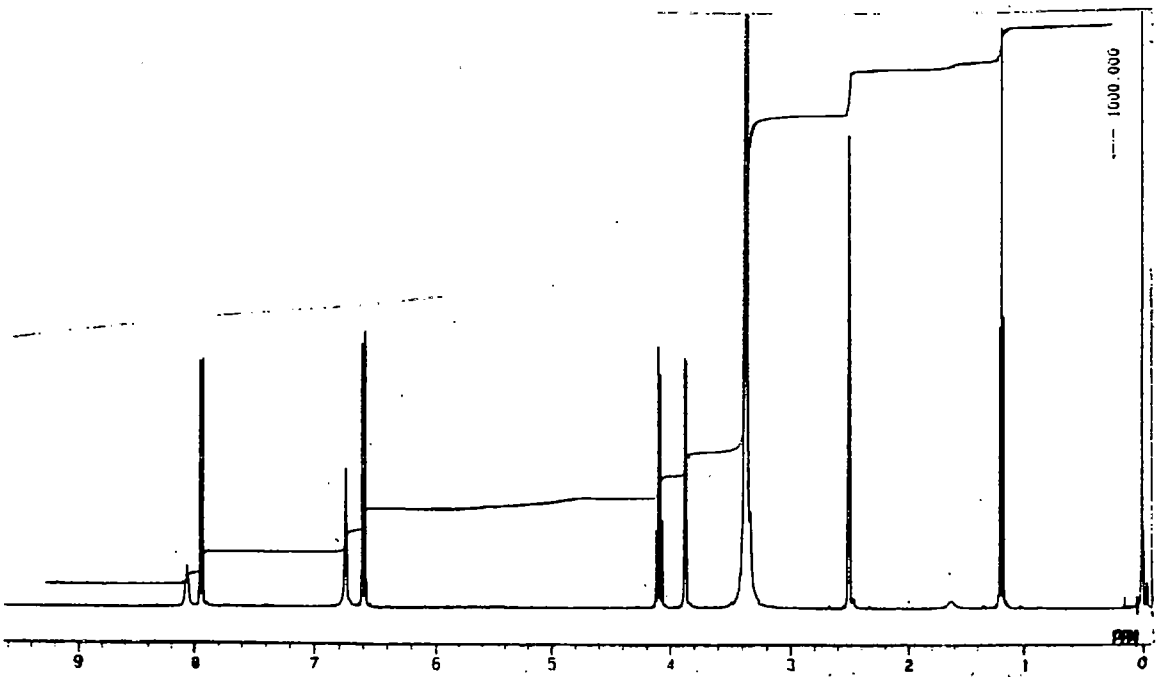

The 400 MHz ^{1}H-nmr spectrum of silver-triazenes (3.3a) and (3.2a) in d_6 DMSO are shown as Figures 3.15 and 3.16, respectively, and summarised in Table 3.9. Although the spectra are weak due to low solubility of the complexes in d_6 DMSO, these data are consistent with the structures assigned to (3.3a) and (3.2a).

Table 3.9 ^{1}H-nmr Data for Silver-triazenes (3.3a) and (3.2a) in d_6 DMSO

Assignment	(3.3a)		(3.2a)	
	δ, ppm	J, Hz	δ, ppm	J, Hz
-CH_2CH_3	1.21 (t)	7.2	1.21 (t)	7.2
-HNCH_2CO-	4.04 (d)	5.6	4.00 (d)	-
-CH_2CH_3	4.10 (q)	7.2	4.12 (q)	7.2
-N=N-NHCH_2CO-	4.61 (s)	-	4.54 (s)	-
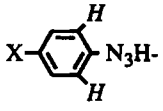	7.60 (d)	8.6	7.49 (s, br.)	-
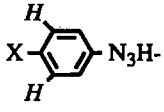	8.10 (d)	8.6	7.36 (d)	8.0
-CONH-CH_2	8.94 (t, br.)	-	8.79 (s, br.)	-

As expected, both metal complexes show similar chemical shifts for equivalent protons and both compounds appear to exist in one isomeric form with single, sharp resonances for both the *N*-methylene and aromatic protons adjacent to the triazene group (although the aromatic protons for (3.2a) show some broadening, which might result from

Figure 3.15 *400 MHz ^{1}H-nmr Spectrum of N-(4-Nitrophenylazo)glycylglycine ethyl ester silver salt (3.3a) in d_6 DMSO*

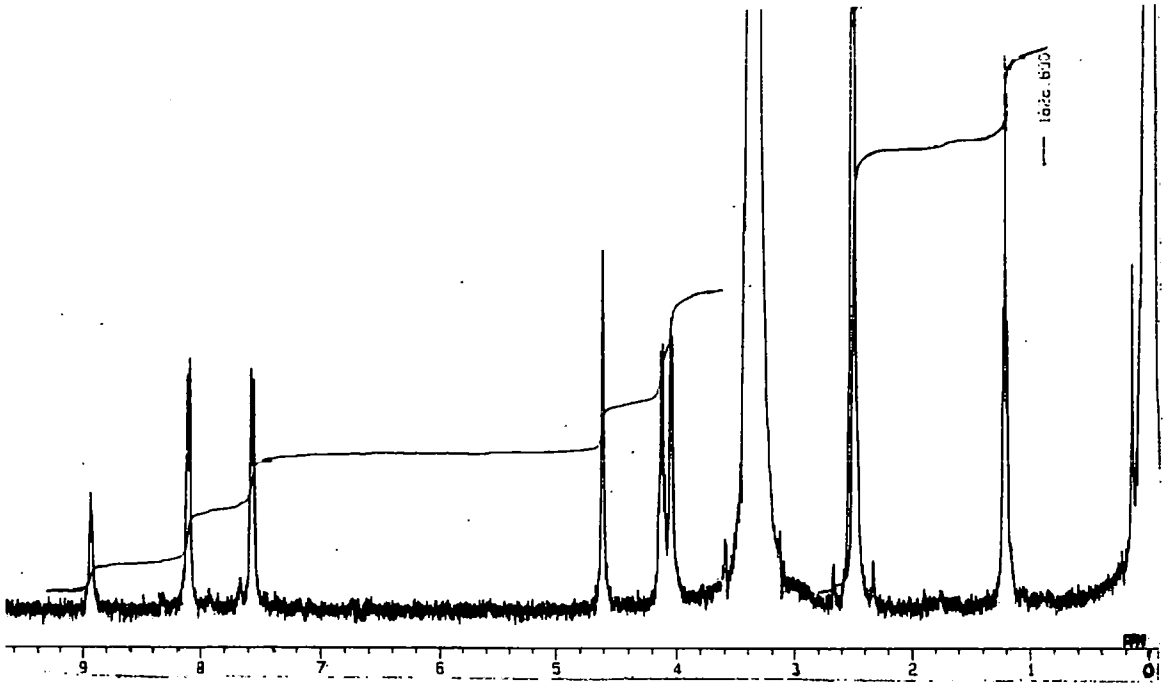

Figure 3.16 *400 MHz ^{1}H-nmr Spectrum of N-(4-Sulphonylphenylazo)glycylglycine ethyl ester silver salt (3.2a) in d_6 DMSO*

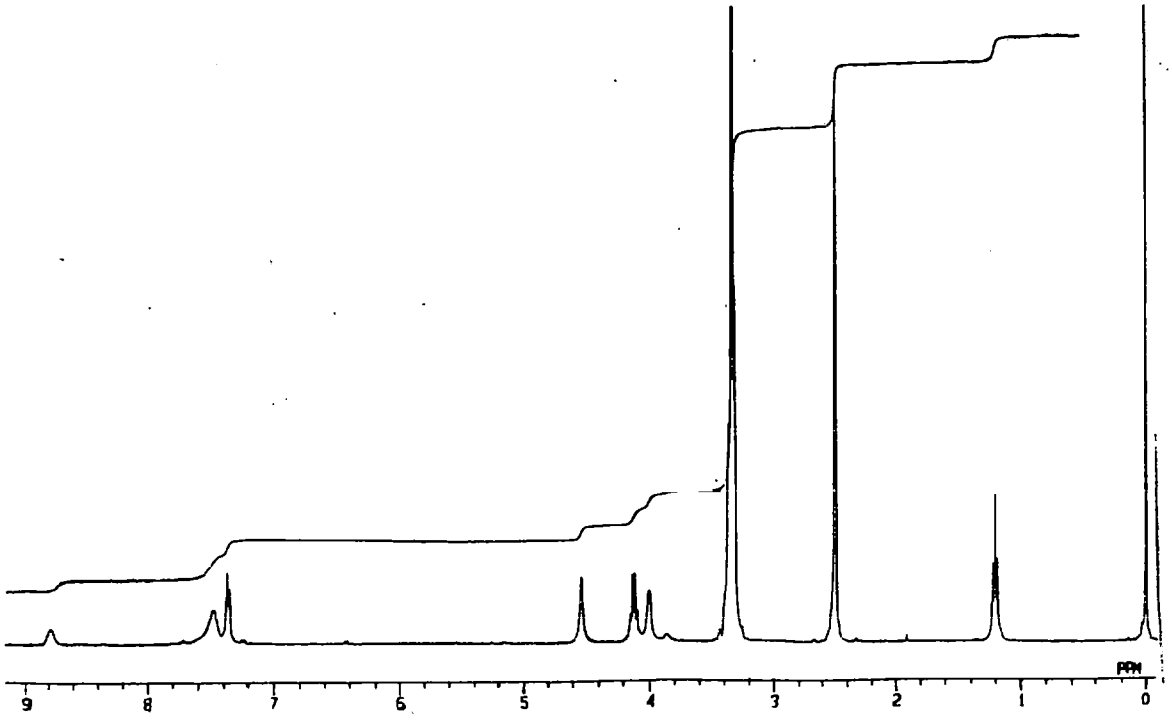

impurities and a poorly resolved spectrum). This may indicate that silver-triazene compounds (3.3a) and (3.2a) are in fact silver salts which have lost the tautomeric NH proton on reaction with Ag^+.

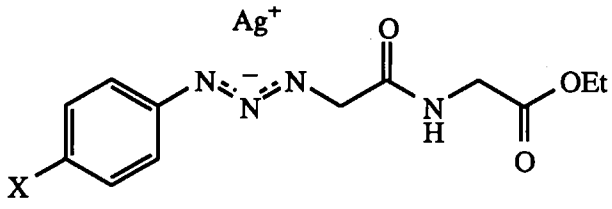

3.2.7.2 FAB Mass Spectrometry

The FAB positive mode mass spectrum of triazene (3.3) {Figure 3.17} is entirely consistent with the proposed structure. The MH^+ and corresponding MNa^+ cluster ions are apparent at m/z = 310 and 332, respectively. Fragment ions at m/z = 161, 150 and 122 are consistent with decomposition of the protonated triazene to form either aryl diazonium ion (m/z = 150) or glycylglycine ethyl ester (m/z = 161). Subsequently, the diazonium ion decomposes with loss of nitrogen to form nitrobenzene cation (m/z = 122) {Scheme 3.8}.

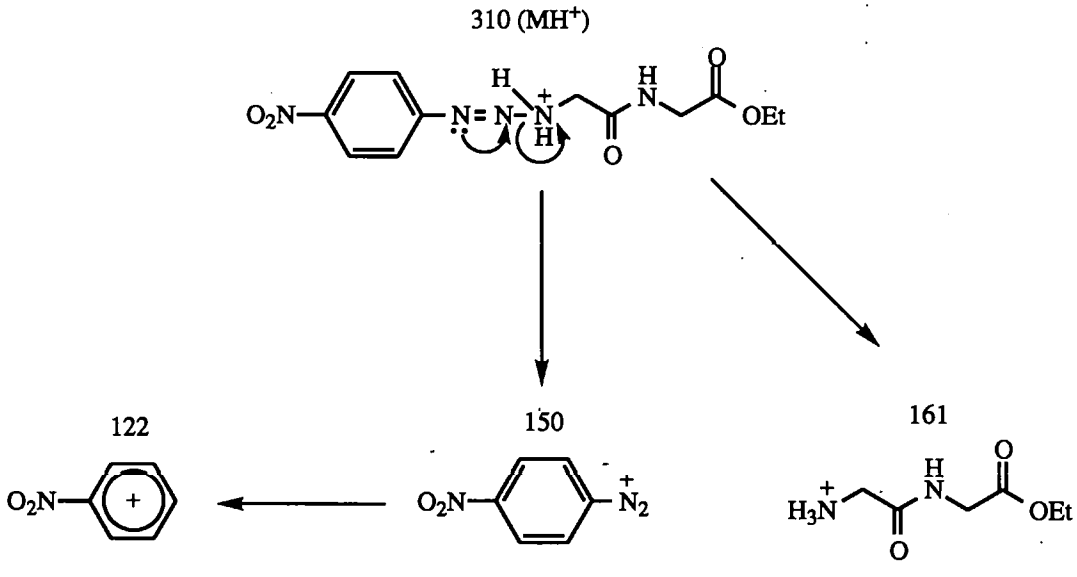

Scheme 3.8

Figure 3.17 *FAB Mass Spectrum of N-(4-Nitrophenylazo)glycylglycine ethyl ester (3.3)*

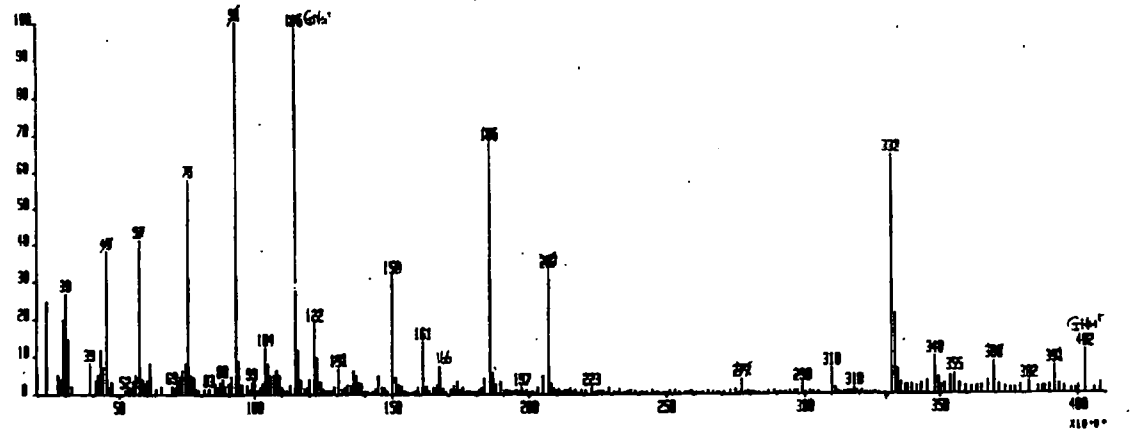

Positive Mode

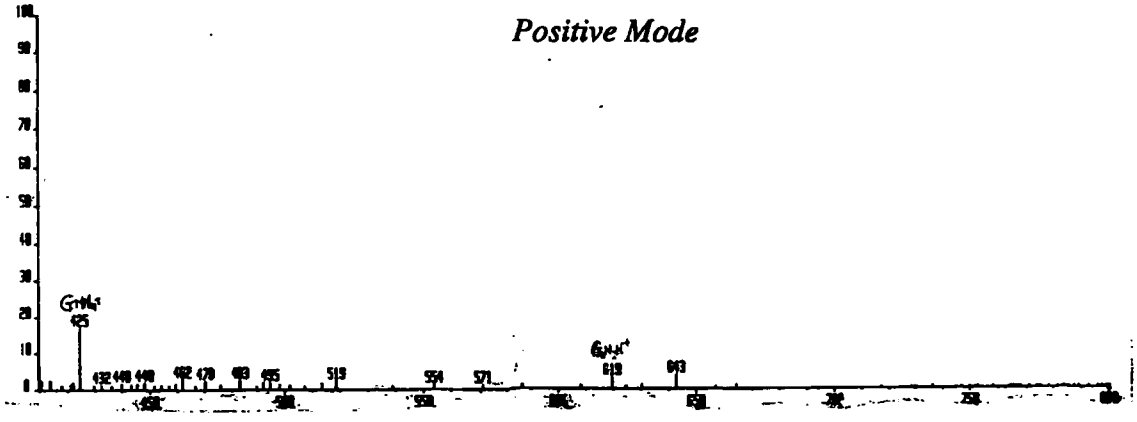

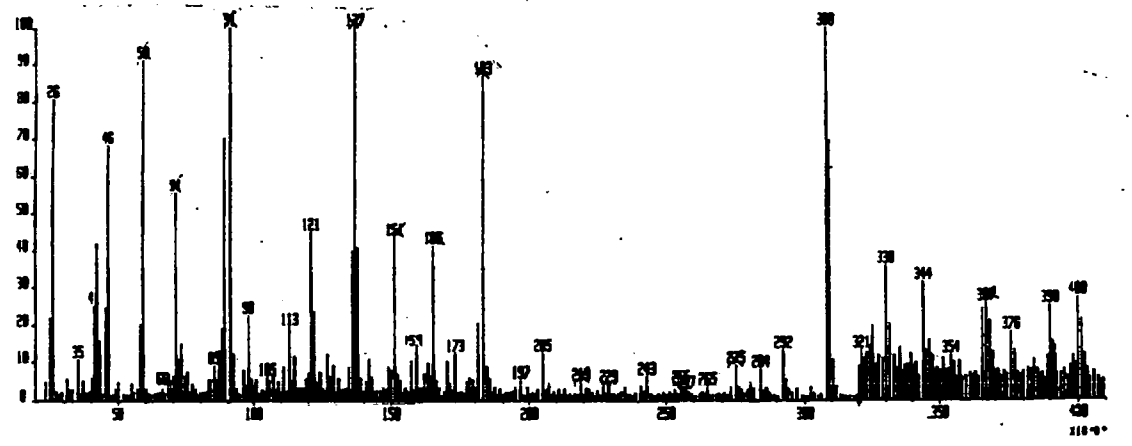

Negative Mode

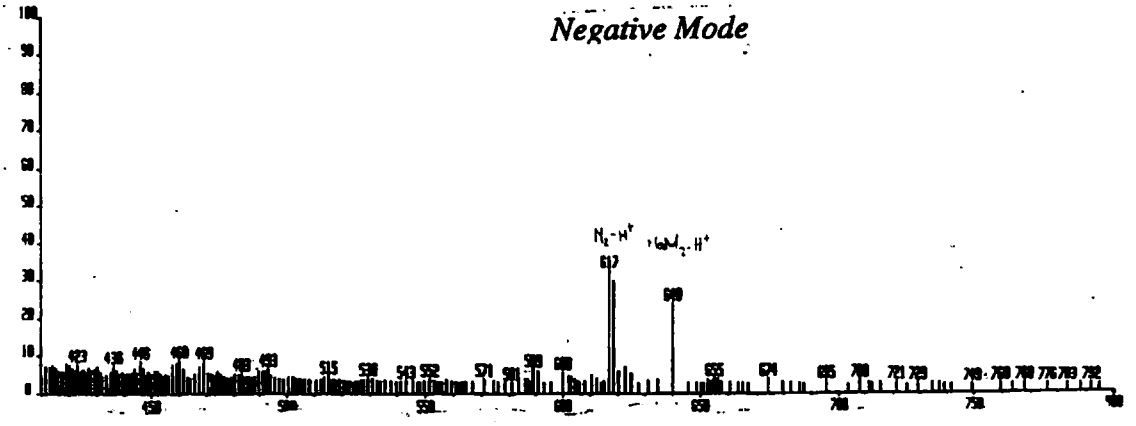

As expected, the negative mode mass spectrum of triazene (3.3) gives a strong parent ion M-H^+ at m/z = 308, which is the base peak. Fragment ions corresponding to loss of M- $H_3N^+CH_2CO_2Et$ and M- $O_2NPhN_2^+$ are also observed at m/z = 205 (12 %) and 159 (14 %), respectively. Further, (3.3) is observed in dimeric form *i.e.* M_2-H^+ at m/z = 617 (3 %).

The mass spectral data for the silver-triazenes (3.3a) and (3.2a) were less clear-cut because of their instability and low solubility in the FAB matrices, and because of the presence of impurities in complex (3.2a).

Nonetheless, for complex (3.3a), the MAg^+ cluster ion at m/z = 418 is clearly evident in the FAB positive mode mass spectrum (Figure 3.18). Further the FAB negative mode mass spectrum of (3.3a) shows an identical pattern of fragmentation to its parent triazene (3.3) described above, although the spectrum is fairly weak because of low solubility of (3.3a) in DMSO (Figure 3.18).

Silver-triazene (3.2a) was both insoluble and unstable in most FAB matrices. For example, a solution of impure (3.2a) in DMSO quickly blackened with effervescence on addition to thioglycerol, a slightly acidic matrix. The best results were obtained from a solution of impure (3.2a) in a thiodiethanol matrix (Figure 3.19). The FAB negative mode mass spectrum shows the M-Ag-H^+ parent ion at m/z = 343 and fragmentations at m/z = 315, corresponding to elimination of nitrogen, and 291, corresponding to M-H -N_2 -CH_2=CH_2. After elimination of matrix ions from the FAB mass spectrum, fragment ions at m/z = 171, 157 and 80 remain above the background signals. These are difficult to assign and probably arise from impurities.

Figure 3.18 *FAB Mass Spectrum of N-(4-Nitrophenylazo)glycylglycine ethyl ester silver salt (3.3a)*

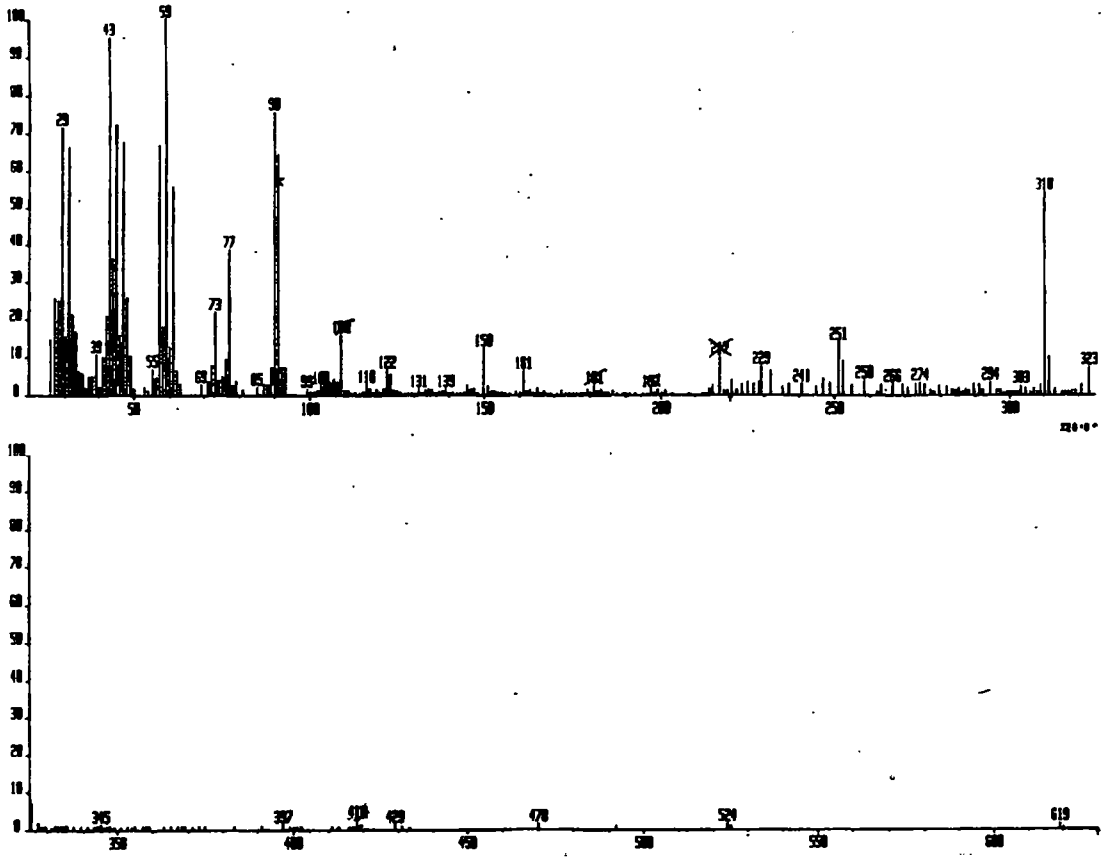

Figure 3.19 *FAB Negative Mode Mass Spectrum of N-(4-Sulphonylphenylazo)-glycylglycine ethyl ester silver salt (3.2a)*

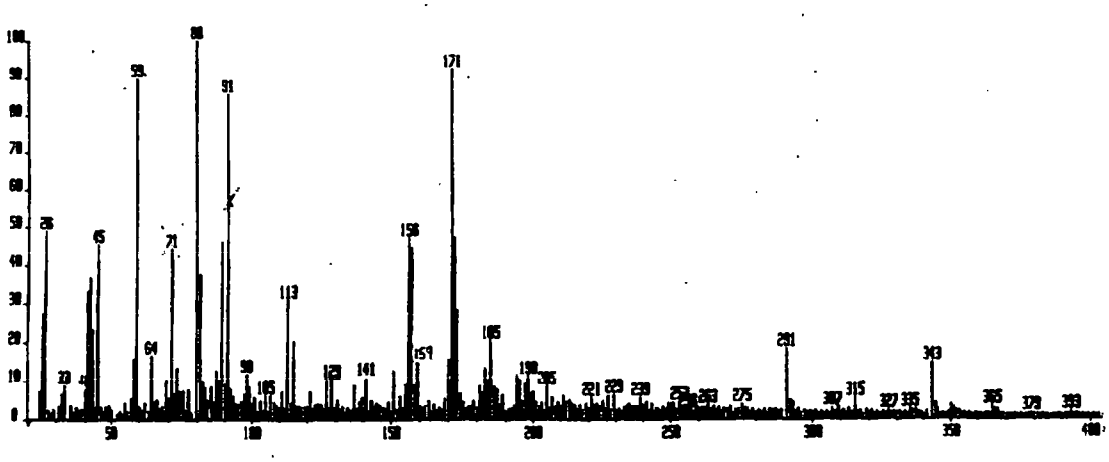

3.8.3 FTIR Spectroscopy

The FTIR spectra of triazene (3.3) and silver-triazenes (3.3a) and (3.2a) are shown as Figures 3.20, 3.21 and 3.22, respectively, and summarised in Table 3.9. Figure 3.20 shows an NH absorption at ν_{max} = 3285 cm^{-1}, which disappears on reaction with Ag^+ (see Figures 3.21 and 3.22). All three spectra, however, show an NH amide absorption at 3400-3500 cm^{-1}. The absence of the low frequency NH band in Figures 3.21 and 3.22 is as expected for formation of a silver salt on reacting the neutral triazene with $AgNO_3$. Triazene (3.3) and silver-triazene (3.3a) show common ester and amide absorptions at ν_{max} *ca.* 1740 and 1650 cm^{-1}, respectively, exhibit common nitro group bands at ν_{max} *ca.* 1510 and 1335 cm^{-1} and an azo N=N stretching absorption at ν_{max} *ca.* 1540 cm^{-1}. Although impure, silver-triazene (3.2a) exhibits similar absorptions to silver-triazene (3.2a), plus additional sulphonyl S=O bands at ν_{max} = 1381 and 1122 cm^{-1} in place of the nitro group absorptions. The FTIR spectra of compounds (3.3), (3.3a), and (3.2a) are consistent with the assignment of a triazene structure.

Figure 3.20 *FTIR Spectrum of N-(4-Nitrophenylazo)glycylglycine ethyl ester (3.3)*

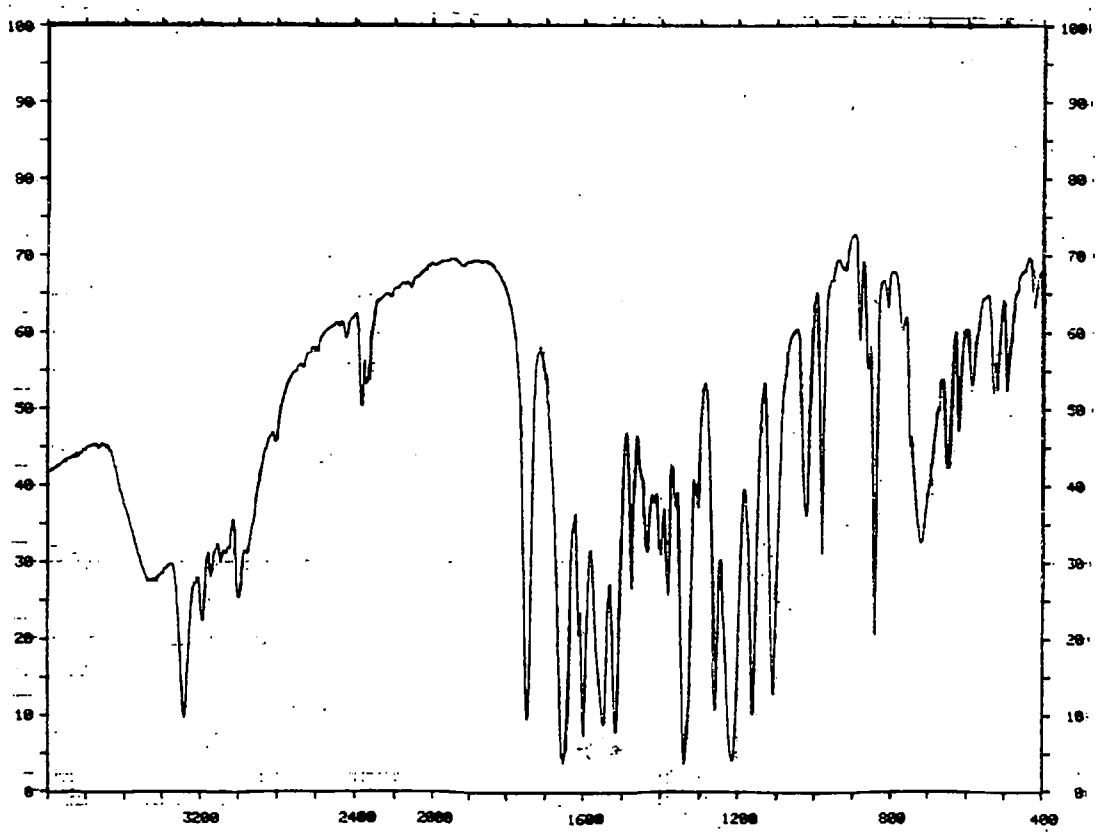

Figure 3.21 *FTIR Spectrum of N-(4-Nitrophenylazo)glycylglycine ethyl ester silver salt (3.3a)*

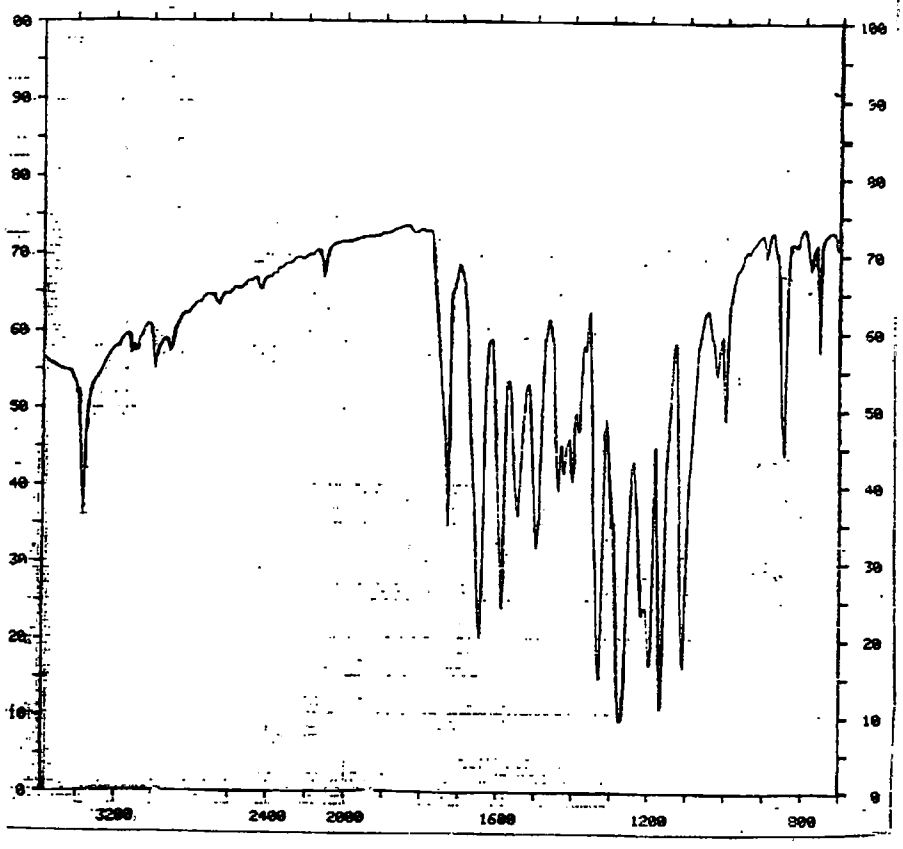

Figure 3.22 *FTIR Spectrum of N-(4-Sulphonylphenylazo)glycylglycine ethyl ester silver salt (3.2a)*

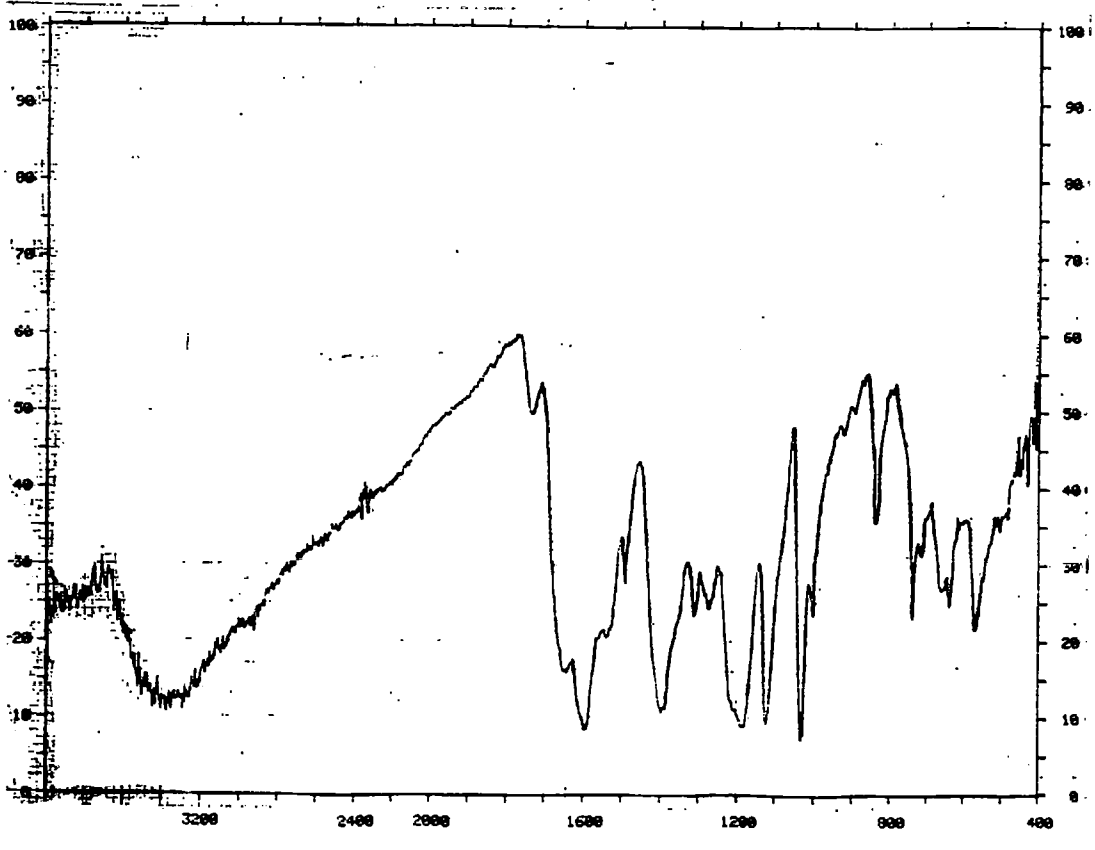

Table 3.9 FTIR Data for Triazene (3.3) and Silver-triazenes (3.3a) and (3.2a)

Triazene	ν_{max}, cm^{-1}	Assignment
N-(4-Nitrophenyl-azo)glycylglycine ethyl ester (3.3)	3468 (br.)	NH amide
	3285	NH triazene
	1740	C=O ester
	1652	C=O amide
	1599	C-C aromatic
	1548	N=N azo
	1516	NO (antisymm.)
	1338	NO (symm.)
	1214	C-O ester
N-(4-Nitrophenyl-azo)glycylglycine ethyl ester silver salt (3.3a)	3422 (br.)	NH amide
	1728	C=O ester
	1645	C=O amide
	1586	C-C aromatic
	1545	N=N azo
	1500	NO (antisymm.)
	1330	NO (symm.)
	1218	C-O ester
N-(4-Sulphonylphenyl-azo)glycylglycine ethyl ester silver salt (3.2a)	3465 (br.)	NH amide
	1749	C=O ester
	1655	C=O amide
	1548	N=N azo
	1591	C-C aromatic
	1381	S=O (antisymm.)
	1209	C-O ester
	1122	S=O (symm.)

3.8.4 uv Spectroscopy

Triazene (3.3) and silver-triazenes (3.3a) and (3.2a) in DMSO all exhibit a single absorption in the uv/visible spectrum at λ_{max} = 356 nm, probably associated with n->π^* electronic transitions. Micro-analytically pure (3.3) and (3.3a) give similar molar extinction coefficients of ε = 20,827 and 21,254 $dm^3mol^{-1}cm^{-1}$, respectively. Hence, on reaction with $AgNO_3$, triazene (3.3) gives the silver-triazene (3.3a) with identical visible absorption properties. Similar properties were also observed for independently synthesised triazene (3.2) and silver-triazene (3.2a), where aqueous solutions of the crude reaction mixture of (3.2) before and after the addition of $AgNO_3$ showed identical visible spectra. Further, impure silver-triazene (3.2a) gave a molar extinction coefficient in DMSO of ε = 8,156 $dm^3mol^{-1}cm^{-1}$. From the micro-analysis results for silver-triazene (3.2a) {Section 3.2.6.2}, this complex is *ca.* 40 % pure, hence, 100 % pure (3.2a) would give ε *ca.* 20,390 $dm^3mol^{-1}cm^{-1}$, in excellent agreement with micro-analytically pure triazenes (3.3) and (3.3a). The uv/visible spectrum of (3.2) and (3.2a) is very similar to that observed for the reaction of *N*-(2-diazoacetyl)glycine ethyl ester (1.3) with sulphanilic acid in aqueous solution (Section 3.7.2), which supports the formation of triazene (3.2) in these reactions.

3.9 Summary

The results show that triazenes form readily from the reaction of aryl diazonium ions with peptide substrates. These triazenes have very characteristic ^{1}H-nmr, mass spectral, FTIR and uv/visible spectral properties. Key questions are whether similar triazene compounds form in the reactions of amines with diazopeptides, and play a role in the decomposition reactions of diazopeptides. This reaction is clearly demonstrated for morpholine with *N*-(2-diazoacetyl)glycine ethyl ester (1.3) in $CDCl_3$. Many of the results imply the occurrence of this reaction when diazopeptides decompose in the presence of aromatic amines.

4. Diazopeptide Decomposition Products

4. Products of Diazopeptide Decomposition

4.1 Introduction

Kinetic studies (reported in Chapter 2) show that the acid-catalysed decompositions of diazopeptides involves H^+-transfer followed by product forming steps involving the expulsion of nitrogen. Further, the rate-determining step depends upon the structure of the diazopeptide.

Products of substitution, elimination and rearrangement reactions involving either unimolecular or bimolecular pathways may be generated from the carbocation intermediate generated by the loss of nitrogen from the conjugate acid of the diazopeptide. The plethora of pathways is the same as those found, of course, for the deamination of primary amino compounds, as discussed in Chapter 1.

Previous product studies have mostly concerned diazo-derivatives of either glycyl peptides, or more highly functionalised aspartyl, glutamyl, cysteinyl and seryl peptides. For *N*-(2-diazoacetyl) compounds derived from glycyl peptides substitution products formed *via* S_N2 pathways predominate for obvious reasons. For the more highly functionalised diazopeptides, intramolecular substitution reactions (either S_N1 or S_N2) to give cyclic products appear to be pre-eminent. The decomposition of non-glycyl diazopeptides in aqueous media at ambient temperature is characterised by a strong pH dependence, general-acid-catalysis, a normal solvent deuterium isotope effect and the absence of appreciable catalysis by added nucleophiles. All these factors are consistent with decomposition *via* an acid-catalysed pathway in which the H^+-transfer step is rate-limiting, hence kinetic studies reveal nothing about the mechanism(s) of subsequent product forming reactions of the diazonium ions, and therefore, the role of potential

neighbouring group interactions. These questions were therefore addressed by product studies. To advance understanding, both the products formed by acid-catalysed decomposition and their pH dependence was investigated.

The investigations concerned three different non-glycyl diazopeptides, *N*-(2-diazo-3-methylbutanoyl)glycine ethyl ester (2.2), *N*-(2-diazo-3-hydroxybutanoyl)glycine ethyl ester (2.1), *N*-(2-diazo-3-carbamoylpropanoyl)glycine benzyl ester (4.1) obtained from *L*-valylglycine ethyl ester (4.2), *L*-threonylglycine ethyl ester (4.3) and *L*-asparaginylglycine benzyl ester (4.4), respectively.

4.2 *N*-(2-Diazo-3-methylbutanoyl)glycine ethyl ester (2.2)

4.2.1 Decomposition in 0.1 M Perchloric Acid

Addition of *N*-(2-diazo-3-methylbutanoyl)glycine ethyl ester (2.2) {*ca.* 50 mg} to aq. 0.1 M $HClO_4$ (25 cm^3) at ambient temperature produced an immediate discharge of the yellow diazopeptide with effervescence. After neutralisation with solid sodium bicarbonate (pH 7-8), aliquots (20 µl) of the reaction mixture were analysed by reverse-phase, analytical hplc (see Section 7.4.1.1) with uv detection at $\lambda = 210$ nm. Authentic (2.2) {*ca.* 50 mg} was also decomposed in 0.1 M $DClO_4$ (5 cm^3), and the mixture examined by 400 MHz ^{1}H-nmr spectroscopy.

4.2.1.1 Hplc Studies

Examination of the reaction mixture by reverse-phase hplc suggested the formation of only one major product eluting at $R_f = 12.6$ min. A typical hplc chromatogram is shown as Figure 4.1 and the results are summarised in Table 4.1. This product was identified by spectroscopic examination as *N*-(3-methylbut-2-enoyl)glycine ethyl ester (4.5) and subsequently confirmed by independent synthesis (see Section 7.5.1.1).

Figure 4.1 *Hplc Chromatogram of Products from the Decomposition of (2.2) in $HClO_4$*

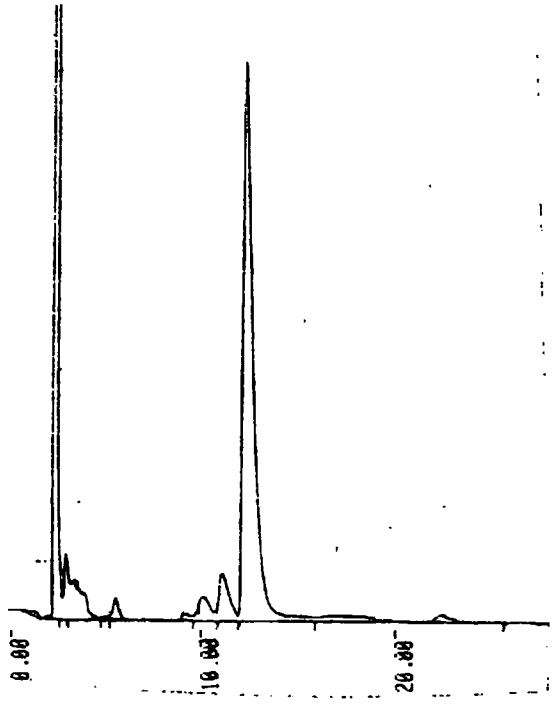

Table 4.1

Peak	R_f, min.	Product
1	12.6	*N*-(3-methylbut-2-enoyl) glycine ethyl ester (4.5)

4.2.1.2 Nmr Studies

Figure 4.2 shows the 400 MHz ^{1}H-nmr spectra of (2.2) before (Spectrum A) and after (Spectrum B) the addition of $DClO_4$. Attention is drawn to the disappearance of the methyl doublet of the isopropyl group in the valyl residue of (2.2) at δ = 1.6 ppm with J = 6.8 Hz, and the appearance of two uncoupled, more deshielded methyl singlets at δ = 1.86 and 2.16 ppm.

Figure 4.2 *Spectrum A: 400 MHz ^{1}H-nmr Spectrum of N-(2-Diazo-3-methylbutanoyl)-glycine ethyl ester (2.2) in $CDCl_3$*

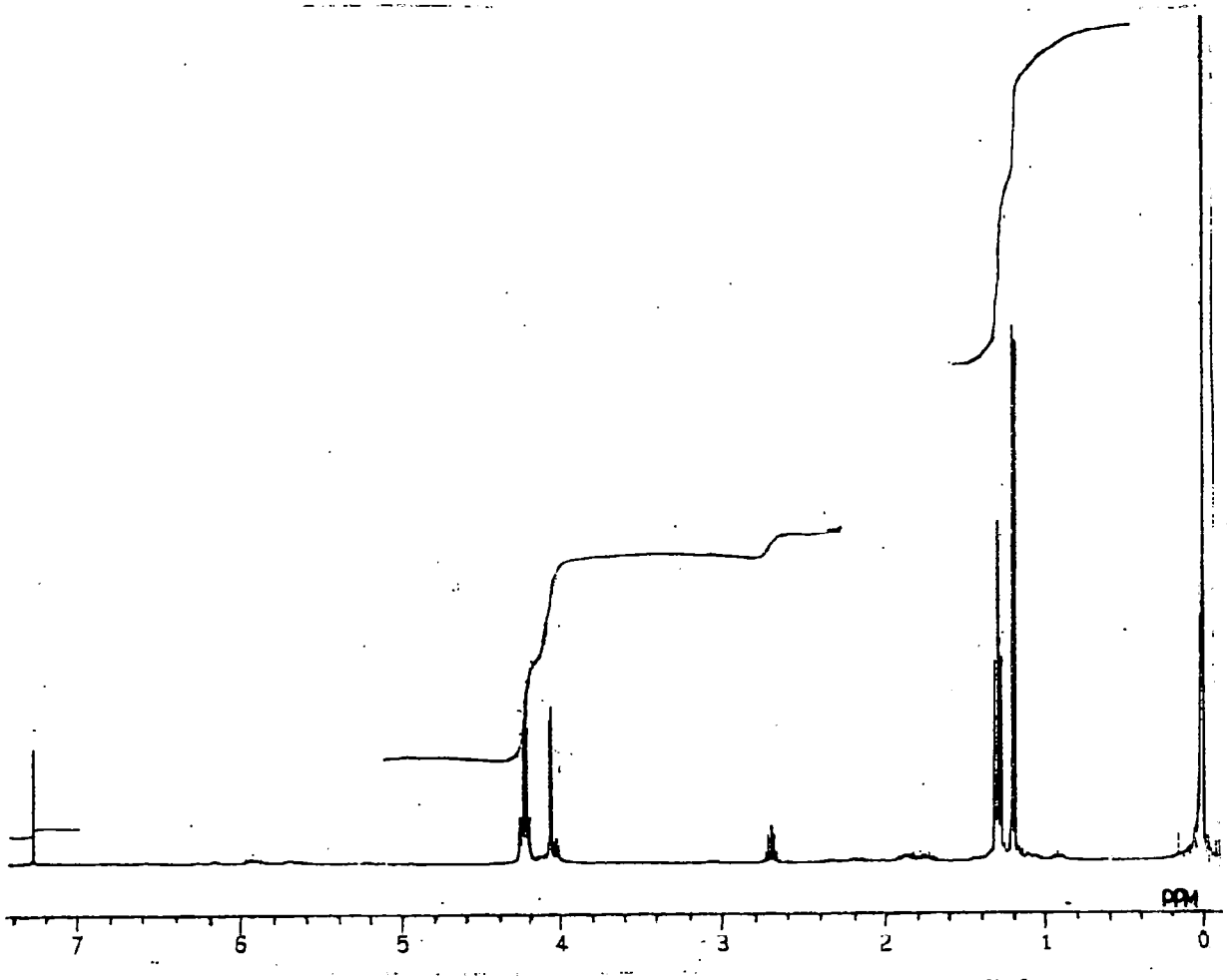

Spectrum B: 400 MHz ^{1}H-nmr Spectrum of N-(2-Diazo-3-methylbutanoyl)glycine ethyl ester (2.2) in $DClO_4$

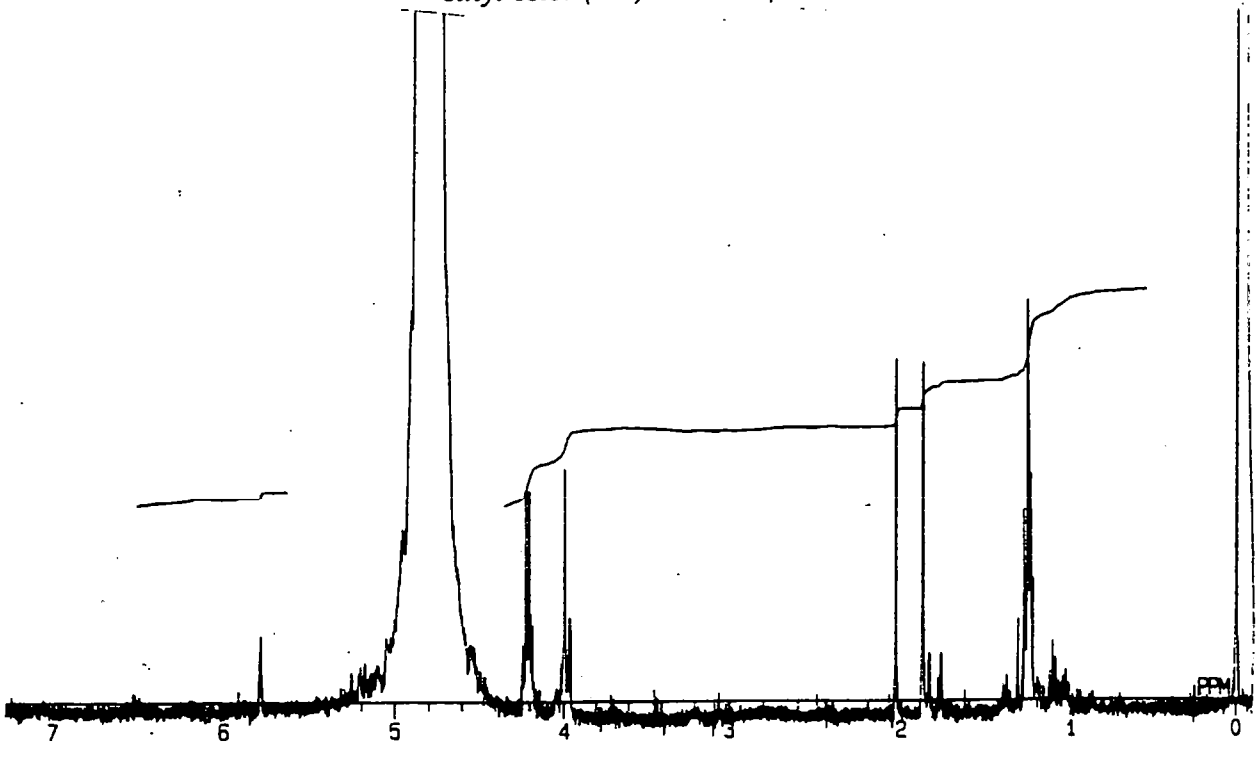

4.2.2 Product Isolation

Larger amounts (*ca.* 200 mg) of (2.2) decomposed in 0.1 M $HClO_4$ (10 cm^3) were neutralised with solid sodium bicarbonate to pH 7-8. The product at R_f = 12.6 min. was extracted by semi-preparative, reverse-phase hplc with uv detection at λ = 210 nm. Fractions from repeat injections (1-2 cm^3) were combined, and the methanol and water solvents removed by vacuum evaporation and freeze-drying, respectively (see Section 7.4.1.1). The solid residue was examined by 400 MHz ^{1}H-nmr and FAB mass spectrometry as described below.

4.2.3 Characterisation of Product (4.5) with R_f = 12.6 min.

The FAB mass spectrum of this product (Figure 4.3) indicates m/z = 186 for the MH^+ ion in the positive mode (with subsequent loss of ethanol to give the fragment ion with m/z = 140) and m/z = 184 for the $M\text{-}H^+$ ion in the negative mode (with loss of ethene and ethanol to give the fragment ions with m/z = 156 and 138, respectively, both characteristic fragmentations of ethyl esters by McLafferty rearrangements). The FAB positive mode mass spectrum shows the ion m/z = 83 as the base peak, which probably relates to the relatively stable $[(CH_3)_2C{=}CHCO]^+$ fragment.

These data are consistent with *N*-(3-methylbut-2-enoyl)glycine ethyl ester (4.5) as the product with R_f = 12.6 min.

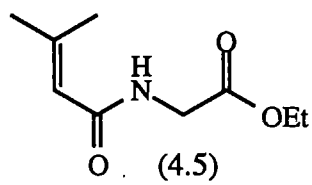

(4.5)

Figure 4.3 *FAB Mass Spectrum of Product with Rf = 12.6 min.*

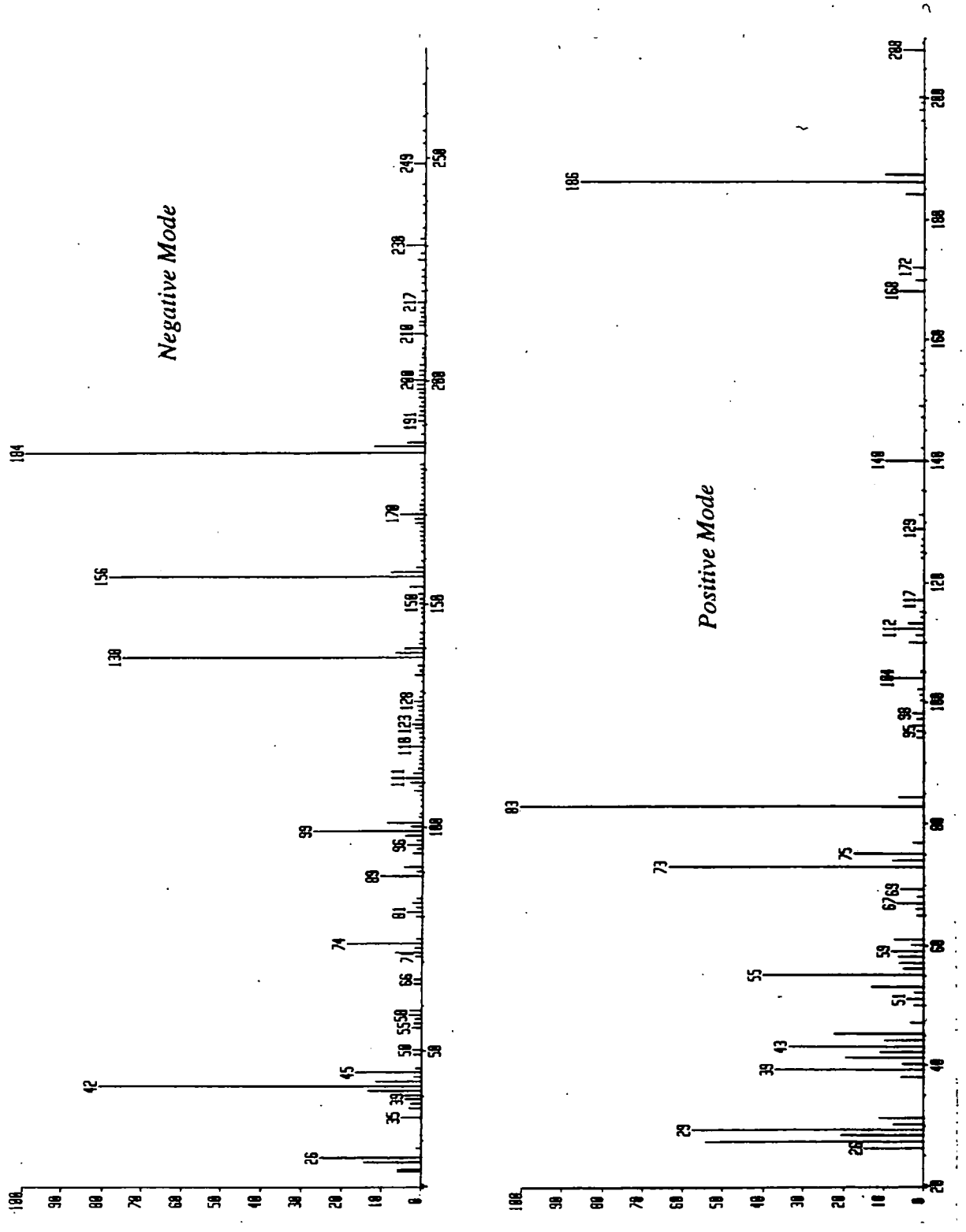

4.2.4 Independent Synthesis of (4.5)

To confirm its identity and enable quantitative analysis (see Section 7.4.1.1), compound (4.5) was synthesised by an independent route (see Section 7.5.3.1). The synthesis involved the diphenylphosphoryl azide (DPPA) mediated coupling of 3,3-dimethyl-acrylic acid with glycine ethyl ester (Scheme 4.1) to give (4.5) in 30 % yield.

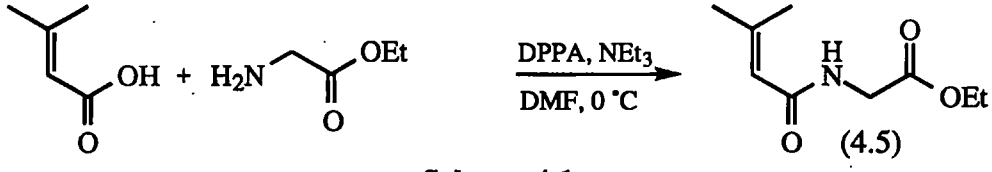

Scheme 4.1

The mass spectra, the 400 MHz ^{1}H-nmr spectrum (Figures 4.4 and 4.5, respectively) and the hplc retention time of the authentic *N*-(3-methylbut-2-enoyl)glycine ethyl ester (4.5) compare favourably with the product at R_f = 12.6 min. generated by the acid-catalysed decomposition of *N*-(2-diazo-3-methylbutanoyl)glycine ethyl ester (2.2).

The 400 MHz ^{1}H-nmr spectrum of (4.5) {Figure 4.5} shows two non-equivalent, deshielded methyl singlets (attached to an sp^2 carbon atom) at δ = 1.86 and 2.16 ppm and a single olefinic proton at δ = 5.63 ppm, identical to those observed in Spectrum A of Figure 4.2.

4.2.5 Quantitation of (4.5) from the Decomposition of *N*-(2-Diazo-3-methylbutanoyl)glycine ethyl ester (2.2) Under Various Conditions

Product (4.5) was quantitated by both hplc assay and 400 MHz ^{1}H-nmr spectroscopy. For the hplc assay, a calibration curve showing the integrated area of the peak R_f = 12.6 min. *vs.* concentration of authentic (4.5), was linear (Figure 4.6). The yield of (4.5) from the decomposition of *N*-(2-diazo-3-methylbutanoyl)glycine ethyl ester (2.2)

Figure 4.4 *FAB Mass Spectrum of N-(3-Methylbut-2-enoyl)glycine ethyl ester (4.5)*

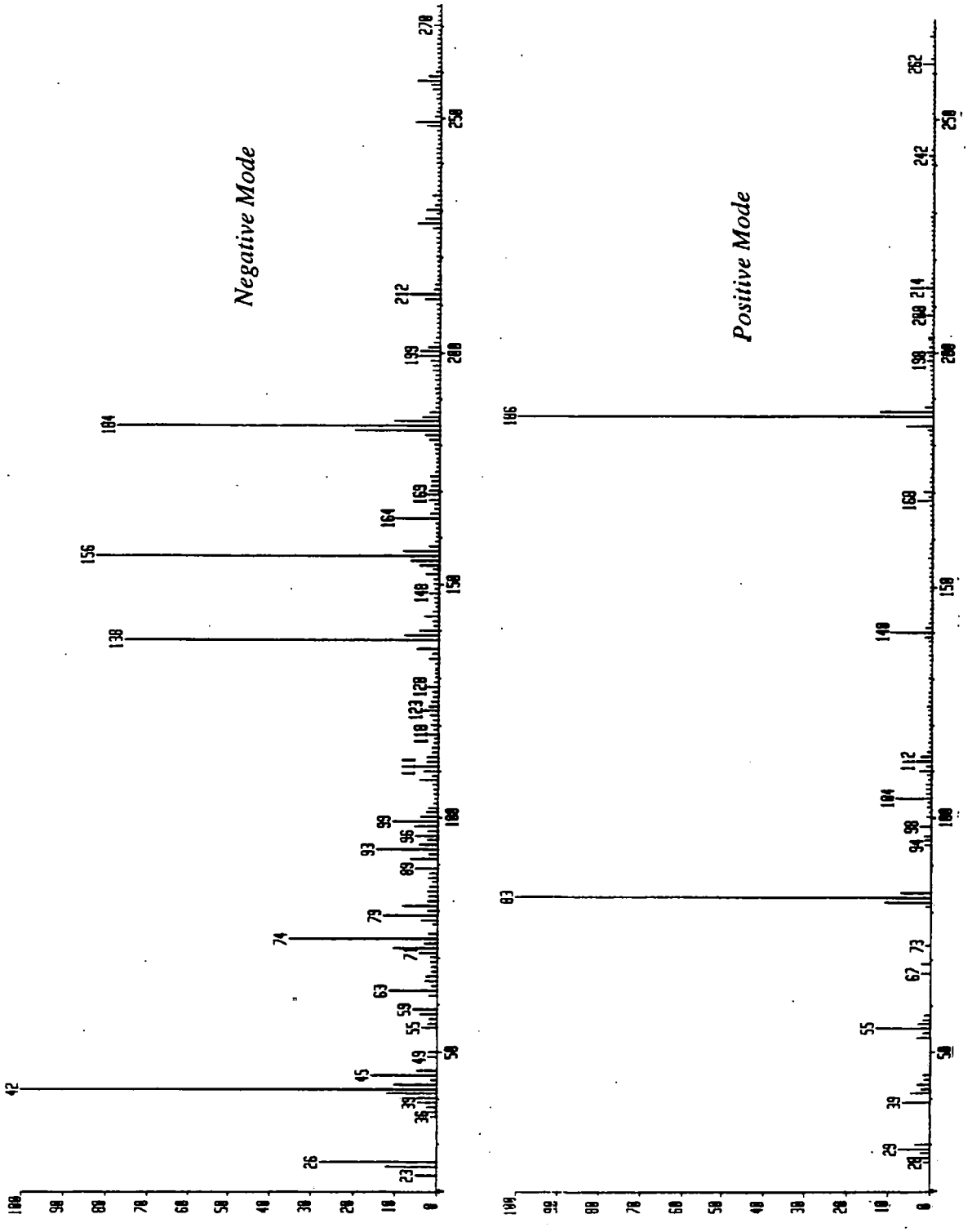

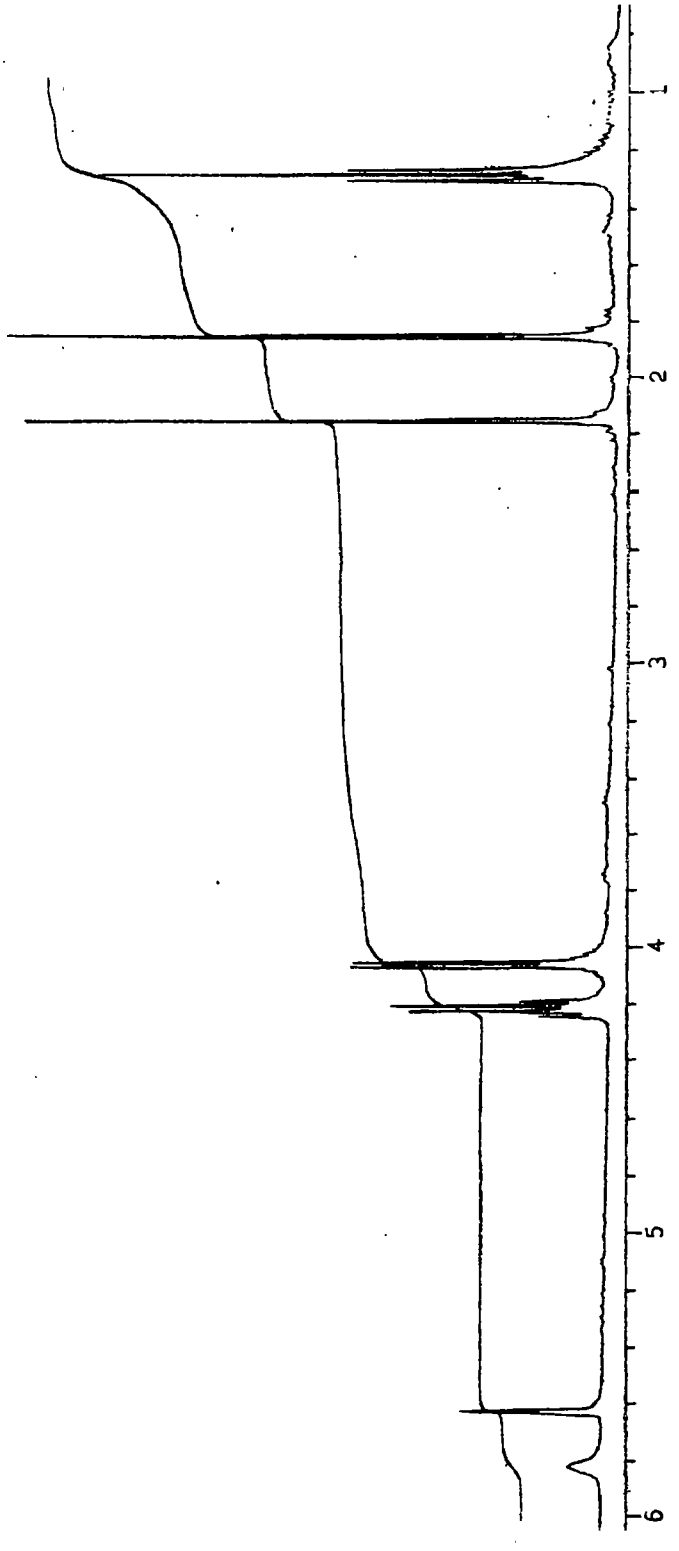

Figure 4.5 *400 MHz ^{1}H-nmr Spectrum of N-(3-Methylbut-2-enoyl)glycine ethyl ester (4.5) in $CDCl_3$*

under various conditions was determined from the calibration curve by interpolation, as described in more detail in Section 7.4.1.1. The error in these assays was estimated as ± 5 %.

Figure 4.6 *Calibration Curve for N-(3-methylbut-2-enoyl)glycine ethyl ester (4.5) by Hplc Assay*

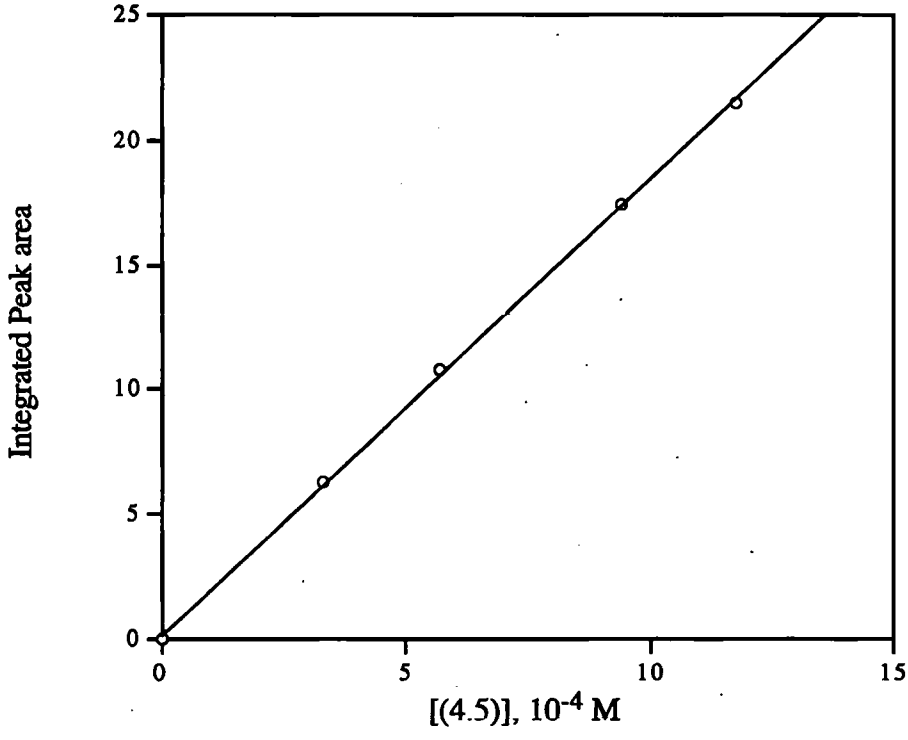

The yield of (4.5) from the decomposition of (2.2) in 0.1 M $DClO_4$ was also estimated from ^{1}H-nmr spectra of the reaction mixture. Specifically, the integrals of the three singlets at δ = 1.87 {=C(C*H*$_3$)CH$_3$}, 2.03 {=C(CH$_3$)C*H*$_3$} and 5.63 ppm {(CH$_3$)$_2$C=C*H*CO-} were compared with those for the peptide ethyl ester at δ = 1.26 (-CH$_2$C*H*$_3$), 4.02 (-HNC*H*$_2$CO$_2$Et) and 4.23 ppm (-C*H*$_2$CH$_3$), and then converted into a % yield. The error in this assay was estimated as ± 10 %. The yields of (4.4) from the decomposition of (2.2) in various media summarised in Table 4.2 show good agreement between the hplc and the ^{1}H-nmr methods. Further, the yield of (4.5) is *ca.* 60 %, irrespective of the composition (pH and buffer) of the reaction mixture. It is clear that other product (s) must form to achieve a mass balance. Although these product(s) were not apparent by analytical hplc (Figure 4.1), they were from the *in situ* 400 MHz ^{1}H-nmr of reactions in $DClO_4$ (see Figure 4.2, Spectrum B). To identify these

other product(s), the crude mixture from reaction in 0.1 M $HClO_4$ was neutralised with sodium bicarbonate (pH 7-8), freeze-dried to remove water, then extracted with ethyl acetate. After vacuum evaporation of the solvent, the residue was analysed by FAB mass spectrometry.

Table 4.2 Yield of (4.5) from the Decomposition of *N*-(2-Diazo-3-methylbutanoyl)glycine ethyl ester (2.2) Under Various Conditions at Ambient Temperature

Reaction Solution	pH	% Yield (4.5)
0.1 M $HClO_4$	<2	60 (55)
0.1 M $HClO_4$ + 0.9 M NaCl	<2	55
0.1 M Formate Buffers	3.5	57
0.1 M Acetate Buffers	4.2	58
0.1 M Phosphate Buffers	6.2	61

**The figure in parenthesis is % yield estimated by ^{1}H-nmr assay.*

The FAB positive mode mass spectrum of this residue (Figure 4.7) showed the presence of two products with molecular (*i.e.* MH^+) ions at m/z = 186 and 204, both of which gave fragment ions corresponding to the loss of ethanol (characteristic of ethyl esters) at m/z = 158 and 140, respectively. As discussed above, the product with MH^+ at m/z = 186 is (4.5), whereas that with MH^+ at m/z = 204 is consistent with either the hydroxy substituted compound (4.6), the isomeric product (4.7) or possibly a mixture of both. The yield of (4.6) plus (4.7) must be *ca.* 40 % in the absence of other products.

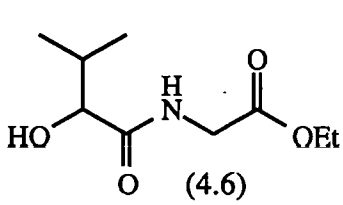

(4.6)

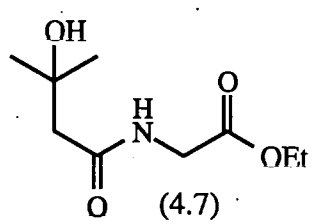

(4.7)

Figure 4.7 *FAB Positive Mode Mass Spectrum of Products from the Decomposition of (2.2) in $HClO_4$*

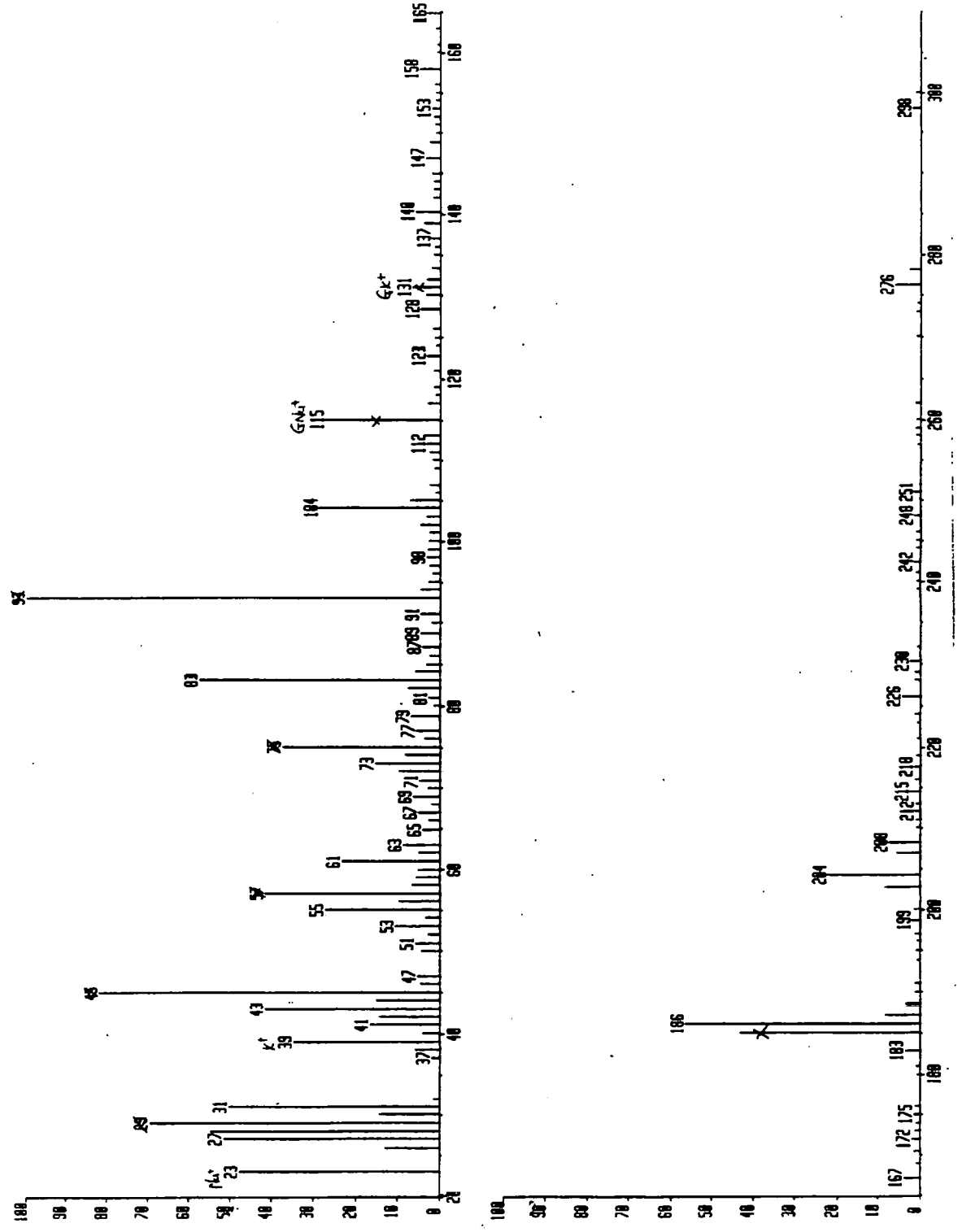

Clearly, compounds (4.6) and (4.7) were not observed by analytical hplc of reaction mixtures because either they eluted rapidly with the solvent front or they co-eluted with the product (4.5). For the latter, the much larger molar extinction coefficient for (4.5) due to conjugation of the double bond with the carbonyl group would make the detection of (4.6) and (4.7) difficult.

4.3 *N*-(2-Diazo-3-hydroxybutanoyl)glycine ethyl ester (2.1)

4.3.1 Decomposition in 0.1 M Perchloric Acid

Addition of *N*-(2-diazo-3-hydroxybutanoyl)glycine ethyl ester (2.1) {*ca.* 50 mg} to aq. 0.1 M $HClO_4$ (25 cm^3) at ambient temperature also produced an immediate discharge of the yellow colour with effervescence. After *ca.* 10 min., the solution was neutralised with solid sodium bicarbonate (pH 7-8) and aliquots (20 μl) on examination by reverse-phase, analytical hplc (see Section 7.4.1.2) with uv detection at $\lambda = 210$ nm, showed the formation of five major products eluting at $R_f = 6.2$, 7.9, 8.9, 12.7 and 13.5 min. (Figure 4.8 and Table 4.3).

Figure 4.8 *Hplc Chromatogram of Products from the Decomposition of (2.1) in $HClO_4$*

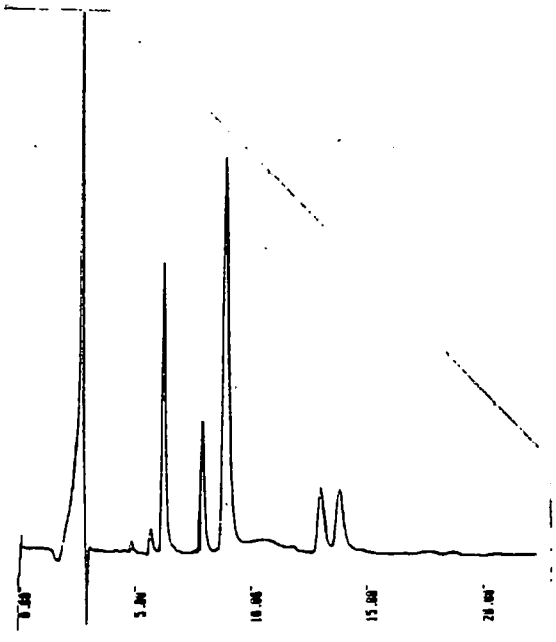

Table 4.3

Peak	R_f (min.)	Product
1 & 2	6.2 & 7.9	*N*-(2(*S*),3(*R*)-Dihydroxybutanoyl) glycine ethyl ester (4.8) and *N*-(2(*R*),3(*R*)-Dihydroxybutanoyl) glycine ethyl ester (4.8), respectively.
3	8.9	*N*-(3-Ketobutanoyl)glycine ethyl ester (4.9).
4 & 5	12.7 & 13.5	*N*-(2,3-Epoxybutanoyl) glycine ethyl ester (4.10), *cis* and *trans*-geometrical isomers, respectively.

The products 2(*S*),3(*R*)-(4.8), (4.9) and *cis*-(4.10) were subsequently identified as peaks 1, 3 and 4 respectively, by independent synthesis of authentic compounds (see Section 7.5.1).

4.3.2 Product Isolation and Characterisation

Larger samples of (2.1) {*ca.* 200 mg} were decomposed in 0.1 M $HClO_4$ (10 cm^3) and neutralised with solid sodium bicarbonate (pH 7-8). The products eluting at R_f = 6.2, 7.9 and 8.9 min. were separated by semi-preparative, reverse-phase hplc with uv detection at λ = 210 nm. After repeat injections (1-2 cm^3), fractions were combined and the methanol and water removed by vacuum evaporation and freeze-drying, respectively (see Section 7.4.1.2). The residues were examined by 400 MHz ^{1}H-nmr and FAB mass spectral analysis. The hplc chromatograms (Figure 4.9) of the combined fractions of purified products with R_f = 6.2, 7.9 and 8.9 min. show the separation was very successful.

Figure 4.9

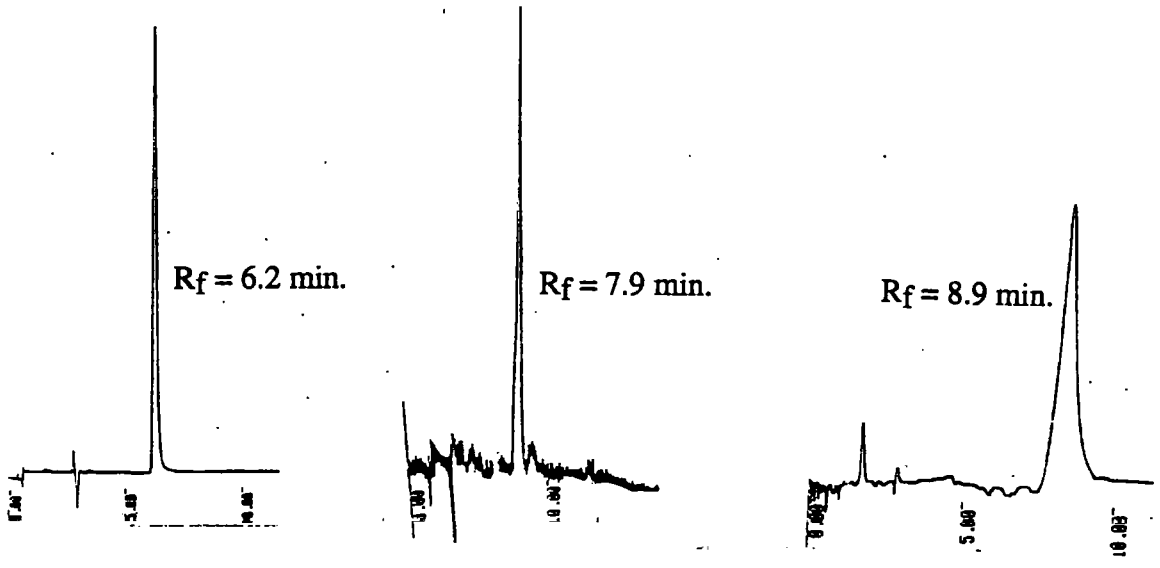

4.3.2.1 Characterisation of Product with Rf = 6.2 min.

The FAB mass spectrum of this product (Figure 4.10) indicated m/z = 208 for the MH^+ ion in the positive mode and m/z = 206 for the $M\text{-}H^+$ in the negative mode. Comparison of the 400 MHz ^{1}H-nmr spectrum of the authentic diazopeptide (2.1) in $CDCl_3$ (Figure 4.11a) with product with Rf = 6.2 min. in CD_3OD (Figure 4.11b) reveals an upfield shift in the signal due to the -C*H*(OH)CH_3 proton of the threonyl residue (δ = 4.05 ppm, J = 2.8 Hz) and the appearance of a new CH adjacent to the threonyl residue *i.e.* $CH_3CH(OH)CH(X)CO$- (δ = 3.89 ppm, J = 2.8 Hz). The remaining ^{1}H-nmr signals are largely unchanged, suggesting that the remainder of the original diazopeptide structure and its configuration are unaltered. The FAB mass spectrum is consistent with *N*-(2,3-dihydroxybutanoyl)glycine ethyl ester (4.8) as the product with Rf = 6.2 min., formed *via* hydrolysis of the diazopeptide.

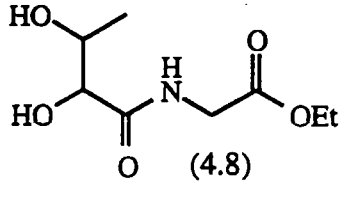

(4.8)

Figure 4.10 *FAB Mass Spectrum of Product with Rf = 6.2 min.*

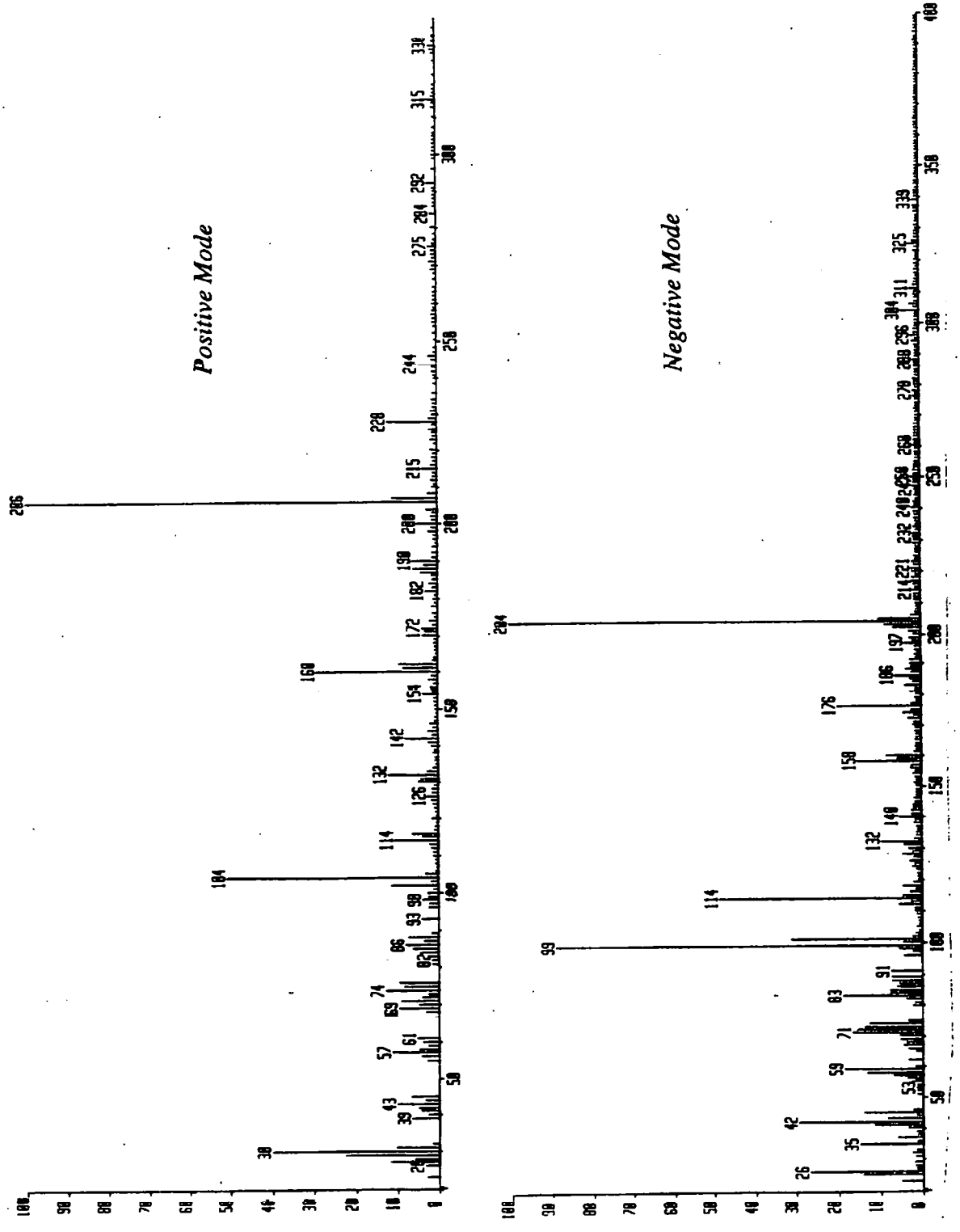

Figure 4.11a *400 MHz ^{1}H-nmr Spectrum of N-(2-Diazo-3-hydroxybutanoyl)glycine ethyl ester (2.1) in $CDCl_3$*

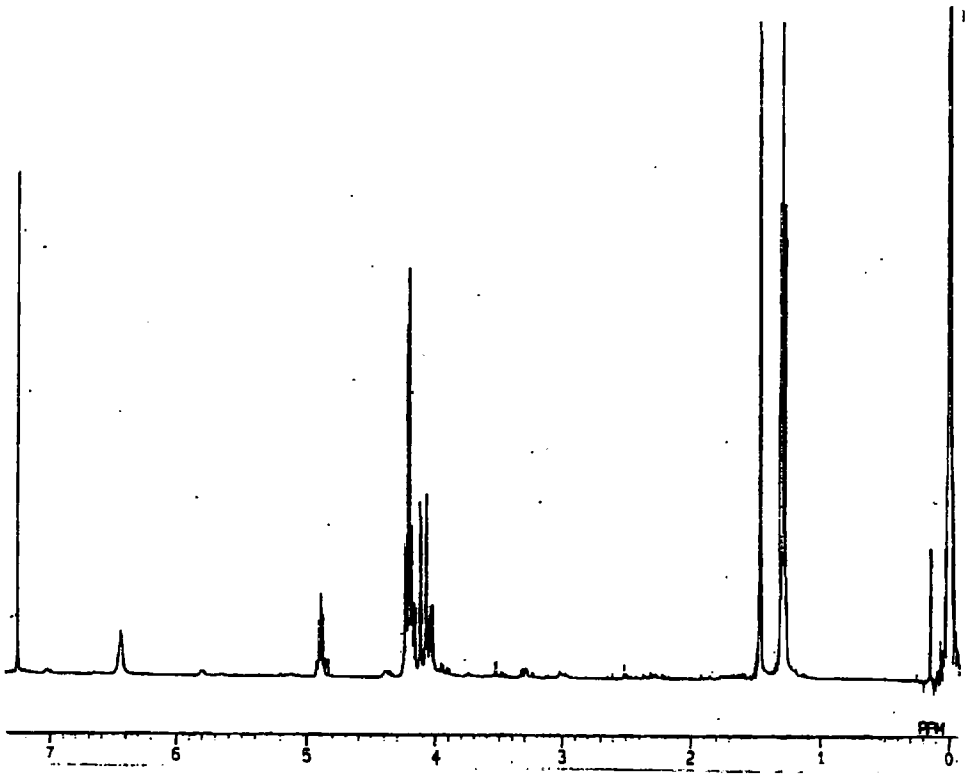

Figure 4.11b *400 MHz ^{1}H-nmr Spectrum of Product with R_f = 6.2 min. in CD_3OD*

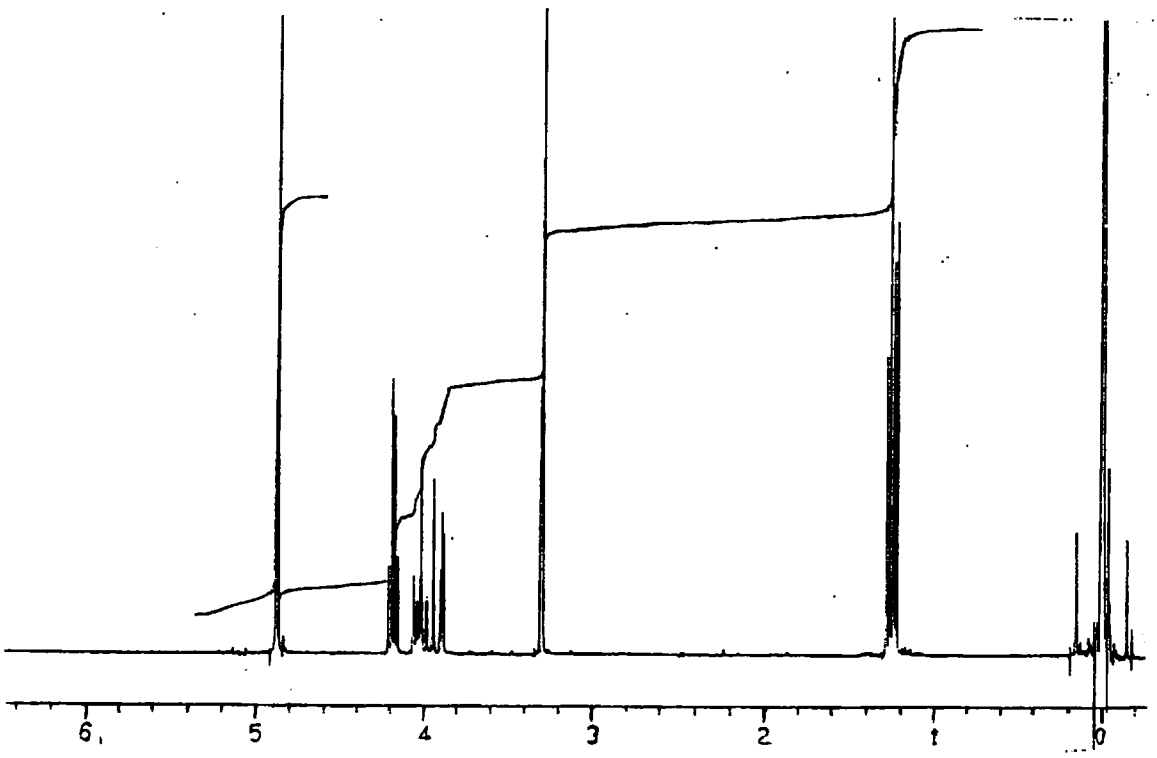

4.3.2.2 Characterisation of Product with R_f = 7.9 min.

The mass recovery of this product was very low (< 5 mg) and relatively poor spectra were therefore obtained. The FAB mass spectrum in the positive mode indicated m/z = 206 for the MH^+ and in the negative mode m/z = 204 for the $M\text{-}H^+$ (Figure 4.12). These values are indicative of a diol product similar to (4.8) above and indeed, the mass spectra for both products were similar. Thus, fragment ions at m/z = 160 (MH^+ -EtOH) and 104 ($[H_3NCH_2OEt]^+$) in the positive mode, and 176 ($M\text{-}H^+$ -CH_2=CH_2) and 158 ($M\text{-}H^+$ -EtOH) in the negative mode are apparent in both sets of spectra (compare Figures 4.10 and 4.12).

However, the 400 MHz ^{1}H-nmr spectrum for product R_f = 7.9 min. in CD_3OD (Figure 4.13) is considerably different to that for product R_f = 6.2 min. (Figure 4.11b). The ^{1}H-nmr assignments in CD_3OD for both products are compared and summarised in Table 4.4. The main differences concern the methyl doublet of the threonyl residue, which is more deshielded in product R_f = 6.2 min. than in product R_f = 7.9 min. The methylene protons of the glycyl residue (-NHC*H*$_2$CO$_2$Et) are diastereotopic and are seen as a widely split AB quartet for product R_f = 6.2 min. For product R_f = 7.9 min., however, the corresponding protons are equivalent and apparently coupled to the peptide N*H* to form a doublet. Further, the two C*H*- resonances {-C*H*(OH)CH$_3$, m, and -C*H*(OH)CONH-, d} are strikingly different. For product R_f = 6.2 min. the multiplet is more deshielded than the doublet, whereas the opposite is observed for product R_f = 7.9 min.

An alternative structure considered for the product at R_f = 7.9 min. was the isomeric iminodialkanoic acid derivative (4.11) derived *via* a Wolff type rearrangement[91, 109-111] of the diazopeptide (2.1) {see Section 1.6}. Structure (4.11) would be consistent with the molecular ions in the FAB mass spectrum

Figure 4.12 *FAB Mass Spectrum of Product with R_f = 7.9 min.*

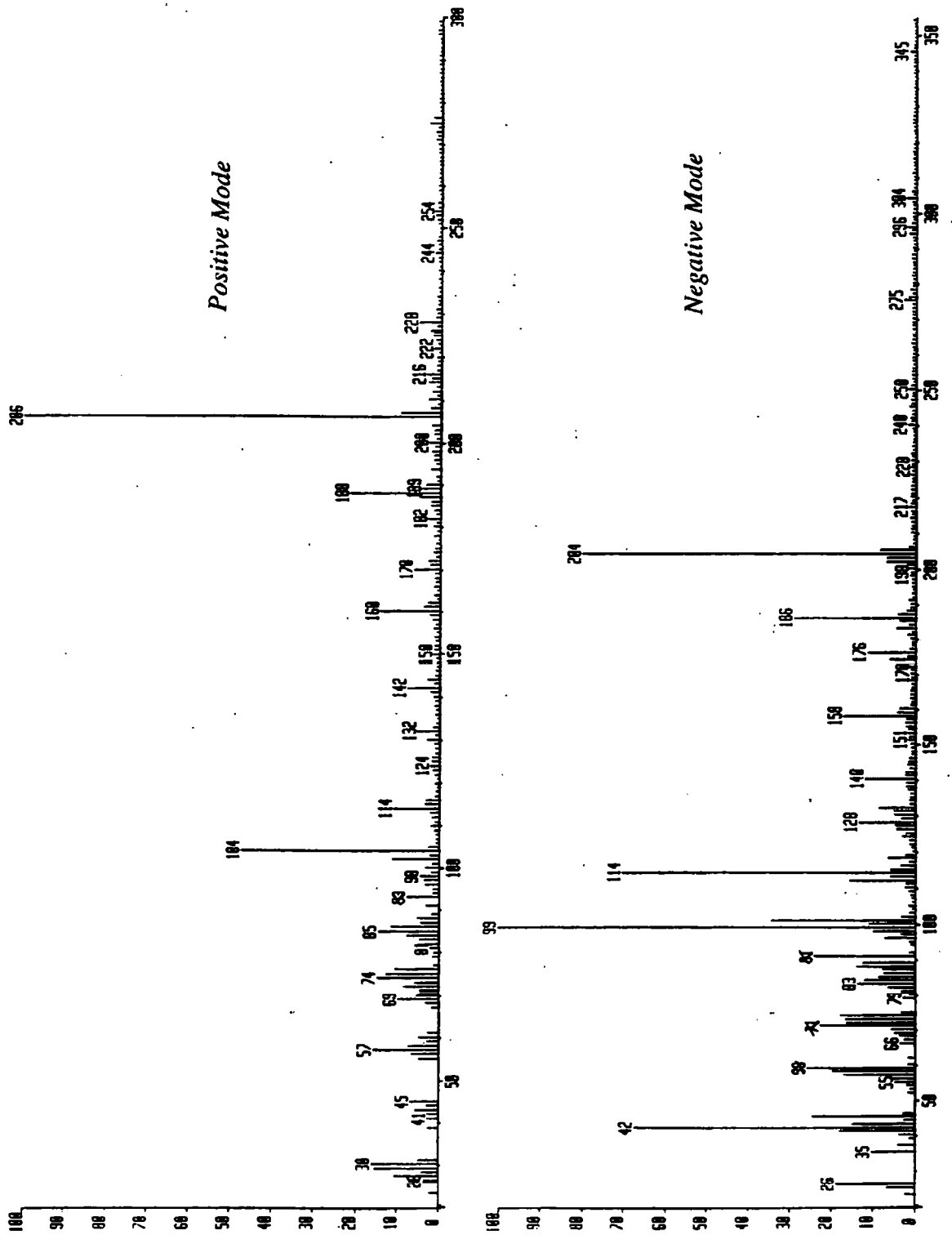

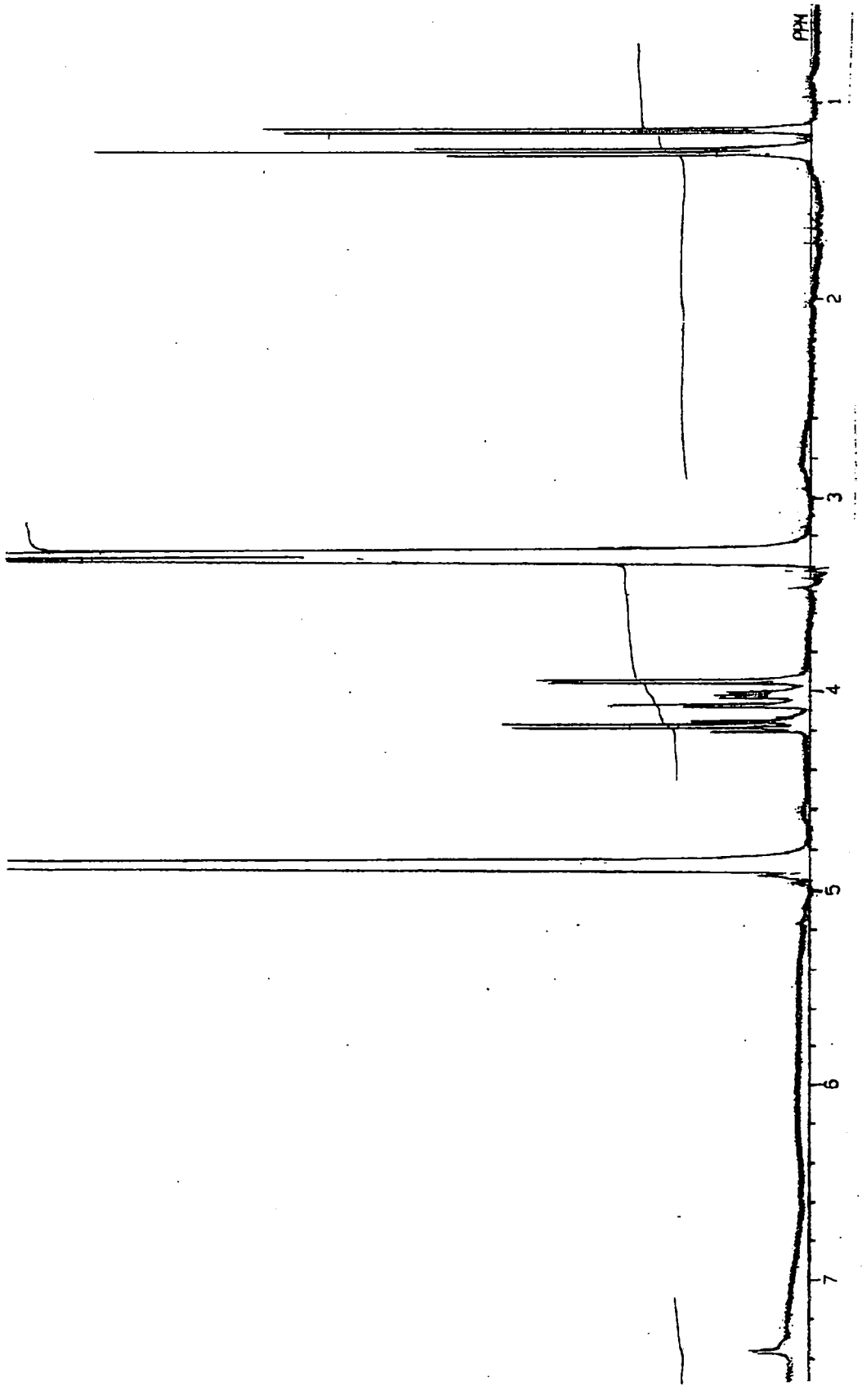

Figure 4.13 *400 MHz ^1H-nmr Spectrum of Product with Rf = 7.9 min. in CD_3OD*

and should give a very similar ^{1}H-nmr spectrum to that observed. Because of the carboxylic acid group, however, the iminodialkalonic acid derivative should give a much stronger M-H$^+$ at m/z = 204 than that observed in Figure 4.12 and in the ^{1}H-nmr spectrum, the HO_2C-C*H*-NH- doublet for (4.11) should be upfield of the -C*H*(OH)CONH doublet observed for (4.8) contrary to the actual shifts observed for the product at R_f = 7.9 min. (Figure 4.13).

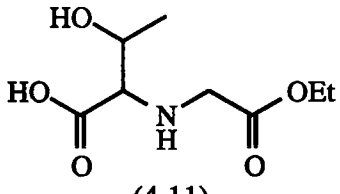

(4.11)

Table 4.4 Comparison of 400 MHz ^{1}H-nmr Assignments in CD_3OD for Products with R_f = 6.2 and 7.9 min

Assignment	Product R_f = 6.2 min.			Product R_f = 7.9 min.		
	δ, ppm	m	J, Hz	δ, ppm	m	J, Hz
-CH_2CH_3	1.27	t	7.2	1.25	t	7.2
-CH(OH)CH_3	1.24	d	6.4	1.15	d	6.4
-NHCH_2CO_2Et	3.92-4.03	AB q	-	3.95	d	6.8
-C*H*(OH)CH_3	4.03	m	-	4.05	m	-
-C*H*(OH)CONH-	3.88	d	2.8	4.09	d	4.0
-CH_2CH_3	4.19	q	7.2	4.18	q	7.2

The spectroscopic data are therefore more consistent with a second diastereoisomer *N*-(2,3-dihydroxybutanoyl)glycine ethyl ester structure (4.8) for the product at R_f = 7.9 min. than the iminodialkalonic acid derivative (4.11).

4.3.2.3 Characterisation of Product with R_f = 8.9 min.

In the positive mode, the FAB mass spectrum of this product indicated m/z = 188 for the MH^+ ion and in the negative mode, m/z = 186 for the $M\text{-}H^+$ ion (Figure 4.14). The 400 MHz ^{1}H-nmr spectrum of the product in $CDCl_3$ (Figure 4.15), differed considerably from that of the parent diazopeptide (Figure 4.11a). In particular, both the methyl doublet due to CH_3CH(OH)- at δ = 1.45 and the quartet due to CH_3CH(OH)- at δ = 4.91 ppm of the threonyl residue are missing and replaced by methyl and methylene singlets at δ = 2.3 (3H) and 3.5 ppm (2H), respectively.

The 100 MHz ^{13}C-nmr spectrum of this product (Figure 4.16) showed the presence of a third carbonyl at δ = 204 ppm, downfield to both ester and amide carbonyl signals. These comparisons strongly suggest that the product at R_f = 8.3 min. is *N*-(3-ketobutanoyl)glycine ethyl ester (4.9). The ^{1}H and ^{13}C-nmr spectral assignments are summarised in Table 4.5. This structure is also consistent with the presence of three C=O absorptions in the FTIR spectrum at 1730, 1710, and 1665 cm^{-1}.

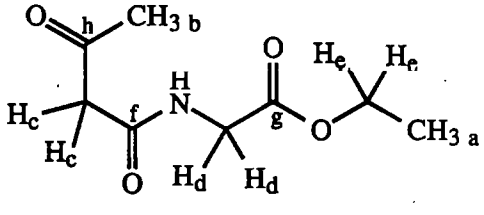

(4.9)

Figure 4.14 *FAB Mass Spectrum of Product with Rf = 8.9 min.*

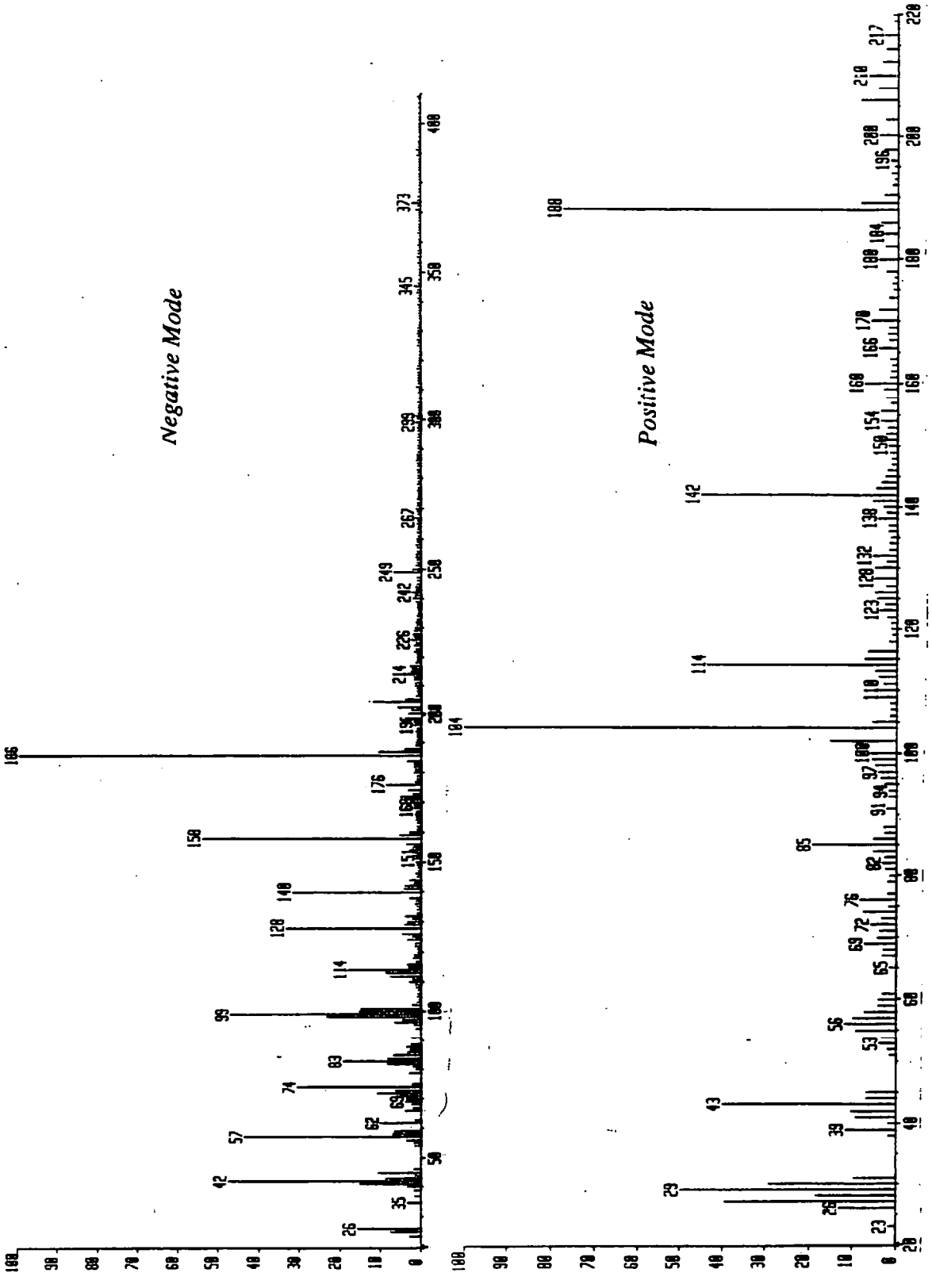

Figure 4.15 *400 MHz ^{1}H-nmr Spectrum of Product with R_f = 8.9 min. in $CDCl_3$*

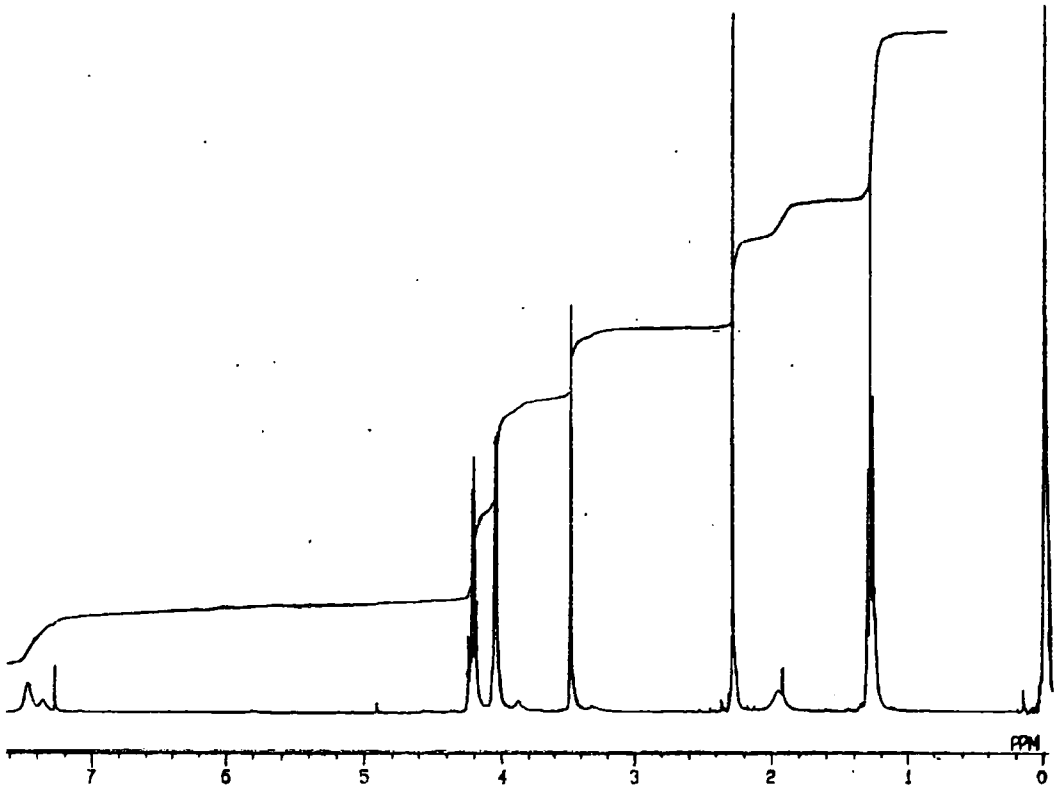

Figure 4.16 *100 MHz ^{13}C-nmr Spectrum of Product with R_f = 8.9 min. in $CDCl_3$*

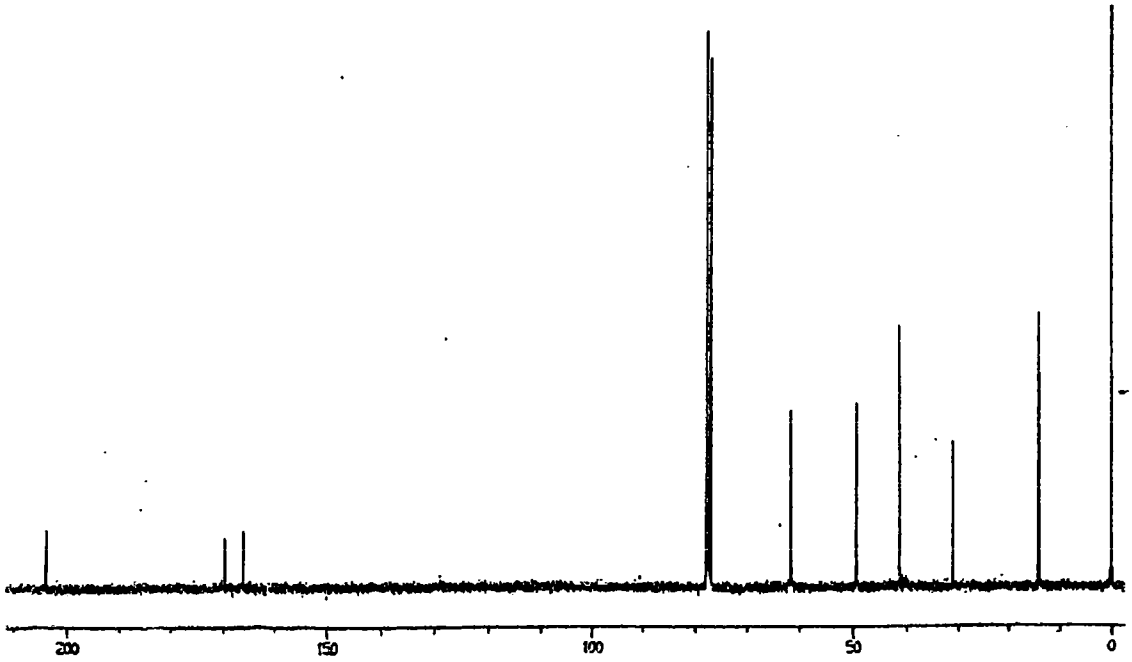

Table 4.5 400 MHz ^{1}H and ^{13}C-Nmr Data for Product R_f = 8.9 min. in $CDCl_3$

Assignment	δ, ppm	
	^{1}H	^{13}C
a	1.26 (3H, t)	14.1
b	2.29 (3H, s)	30.9
c	3.49 (2H, s)	41.1
d	4.04 (2H, d)	49.9
e	4.22 (2H, q)	61.6
f	-	165.9
g	-	169.6
h	-	204.6

4.3.3 Independent Synthesis of Authentic Products

To confirm their identity, decomposition products (4.8) and (4.9) were synthesised by independent routes. Further, the proposed identities of the two other products at R_f = 12.7 and 13.5 min. were confirmed *via* the retention times of independently synthesised compounds (see Section 7.5.3).

4.3.3.1 *N*-(2(*S*),3(*R*)-Dihydroxybutanoyl)glycine ethyl ester (4.8)

The most convenient route to *trans-N*-(but-2-enoyl)glycine ethyl ester (4.12), in 69 % yield was *via* reaction of *trans*-crotonic acid with glycine ethyl ester hydrochloride using diethylcyanophosphonate (DECP) as the coupling reagent. *cis*-Hydroxylation of the *trans*-alkene using osmium tetroxide as a catalyst then gave the diol 2(*S*),3(*R*)-(4.8) in a satisfactory 30 % yield (Scheme 4.2).

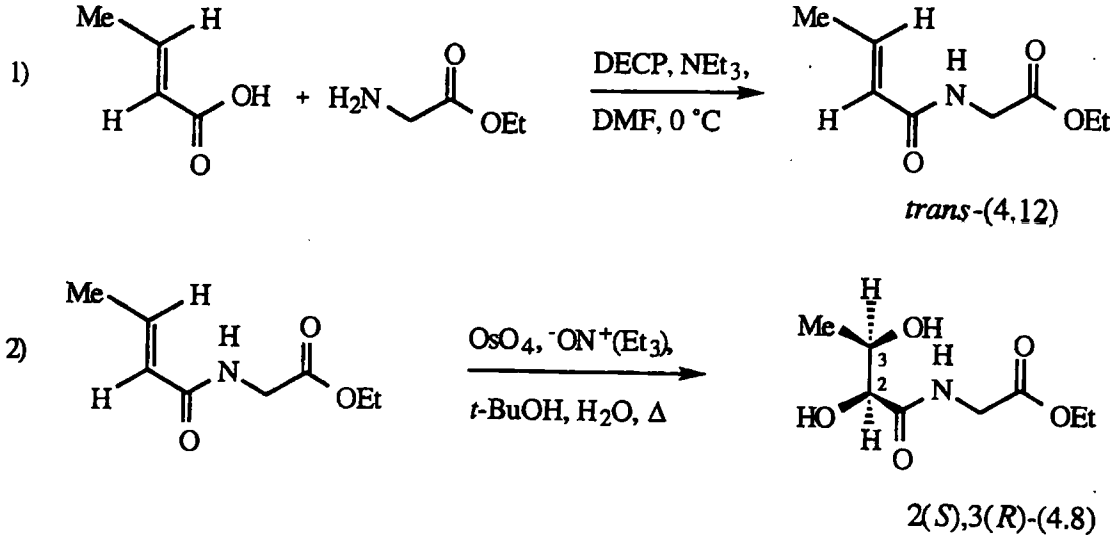

Scheme 4.2

The authentic 2(*S*),3(*R*)-(4.8) {plus the 2(*R*),3(*S*)-(4.8) enantiomer} gave an identical hplc retention time, 400 MHz ^{1}H-nmr (Figure 4.17) and FAB mass spectrum (Figure 4.18) to the product with R_f = 6.2 min.

Figure 4.17 *400 MHz ^{1}H-nmr Spectrum of N-(2(S),3(R)-Dihydroxybutanoyl)glycine ethyl ester (4.8) in CD_3OD*

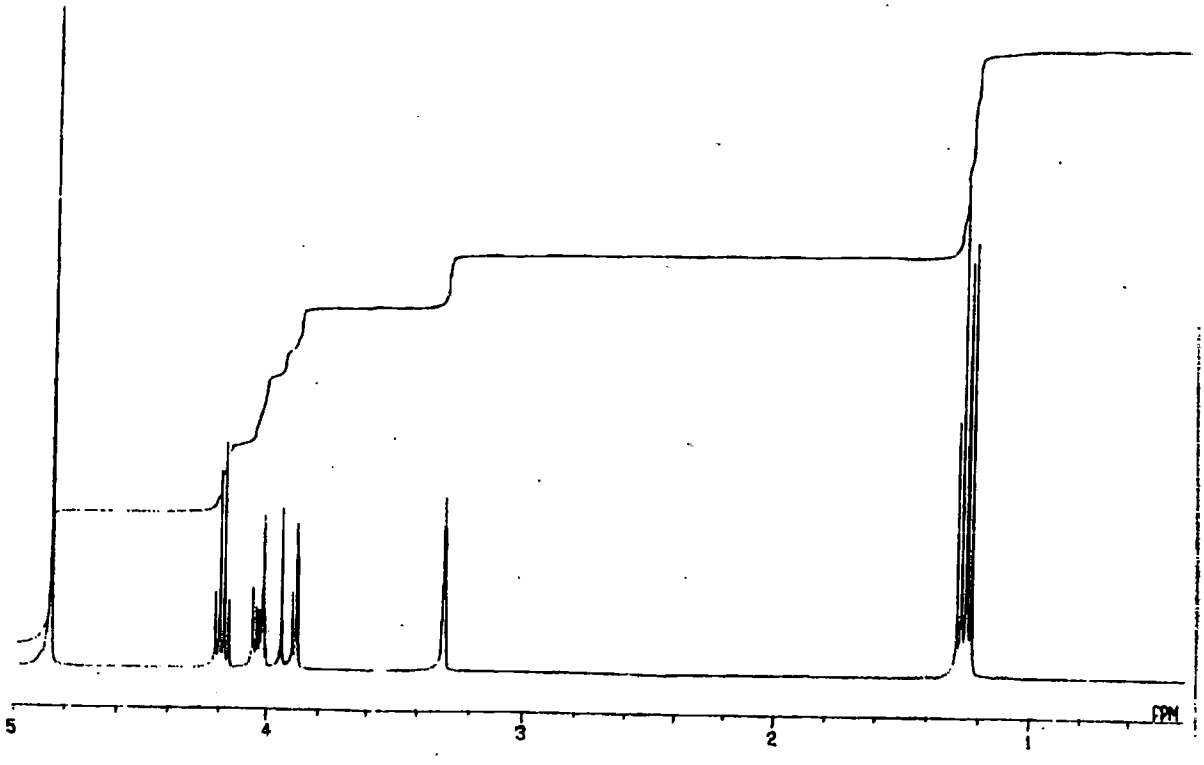

Figure 4.18 *FAB Mass Spectrum of N-(2(S),3(R)-Dihydroxybutanoyl)glycine ethyl ester (4.8)*

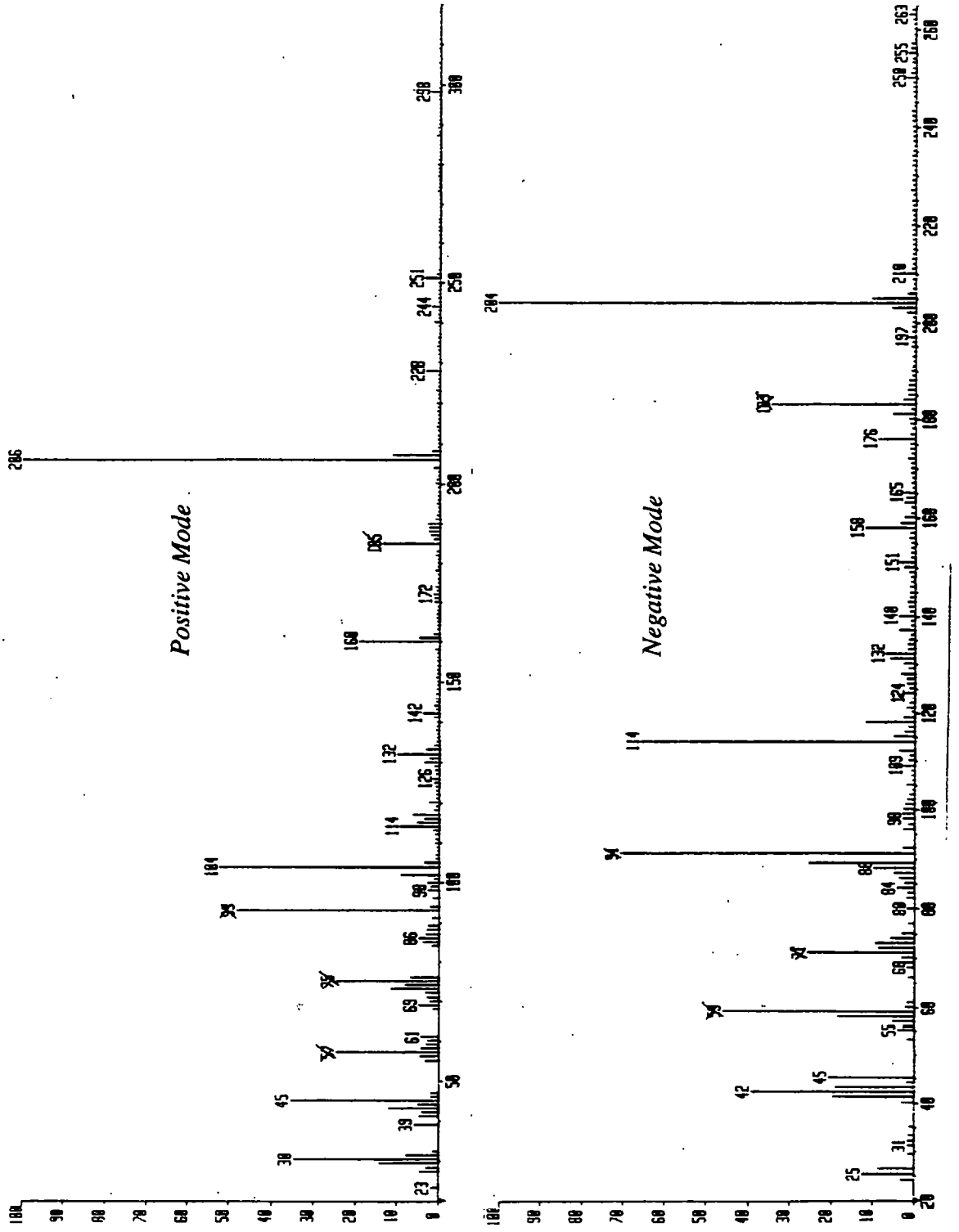

4.3.3.2 *N*-(3-Ketobutanoyl)glycine ethyl ester (4.9)

Product (4.9) was synthesised by coupling 3-hydroxybutyric acid with glycine ethyl ester using DECP as the coupling reagent to give the β-hydroxyamide derivative (4.13), followed by a Collin's oxidation[125] to give the ketone (4.9) in a satisfactory 40 % yield (Scheme 4.3). The versatile pyridium chlorochromate oxidant was initially tried to affect this oxidation, but it led to destruction of the starting material without formation of the required product (4.9). The synthesis of 1,3 diketones and β-ketoesters in good yield from β-hydroxyketones has been reported using both the Collin's oxidation method and the Swern procedure using oxalyl chloride.[126]

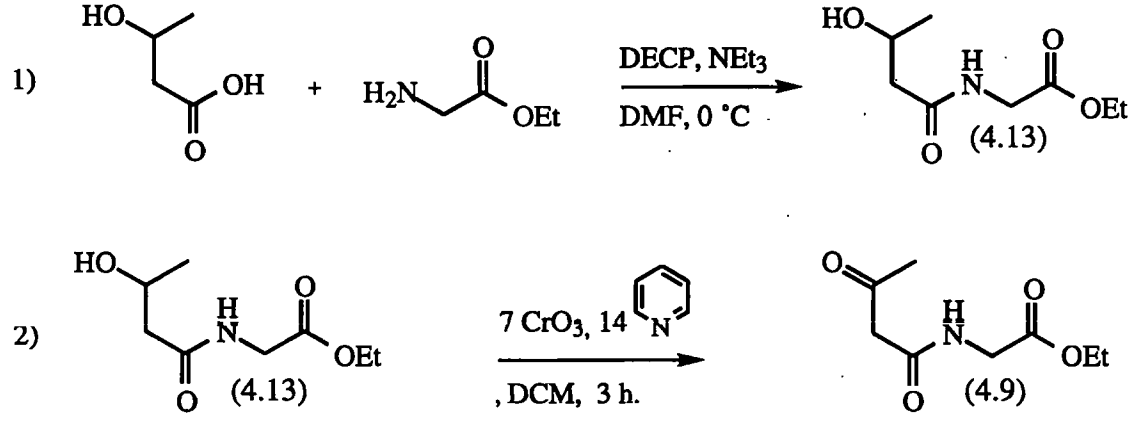

Scheme 4.3

Compound (4.9) gave the same hplc retention time as the product with R_f = 8.9 min., and compared favourably by FAB mass spectrometry (Figure 4.19) and 400 MHz ^{1}H-nmr (Figure 4.20).

4.3.3.3 cis-*N*-(2,3-Epoxybutanoyl)glycine ethyl ester (4.10)

Because the diazonium ion intermediate from (2.1) is chiral, two stereoisomers result from reaction with nucleophiles, which should be separable by analytical, reverse-phase

Figure 4.19 *FAB Mass Spectrum of N-(3-Ketobutanoyl)glycine ethyl ester (4.9)*

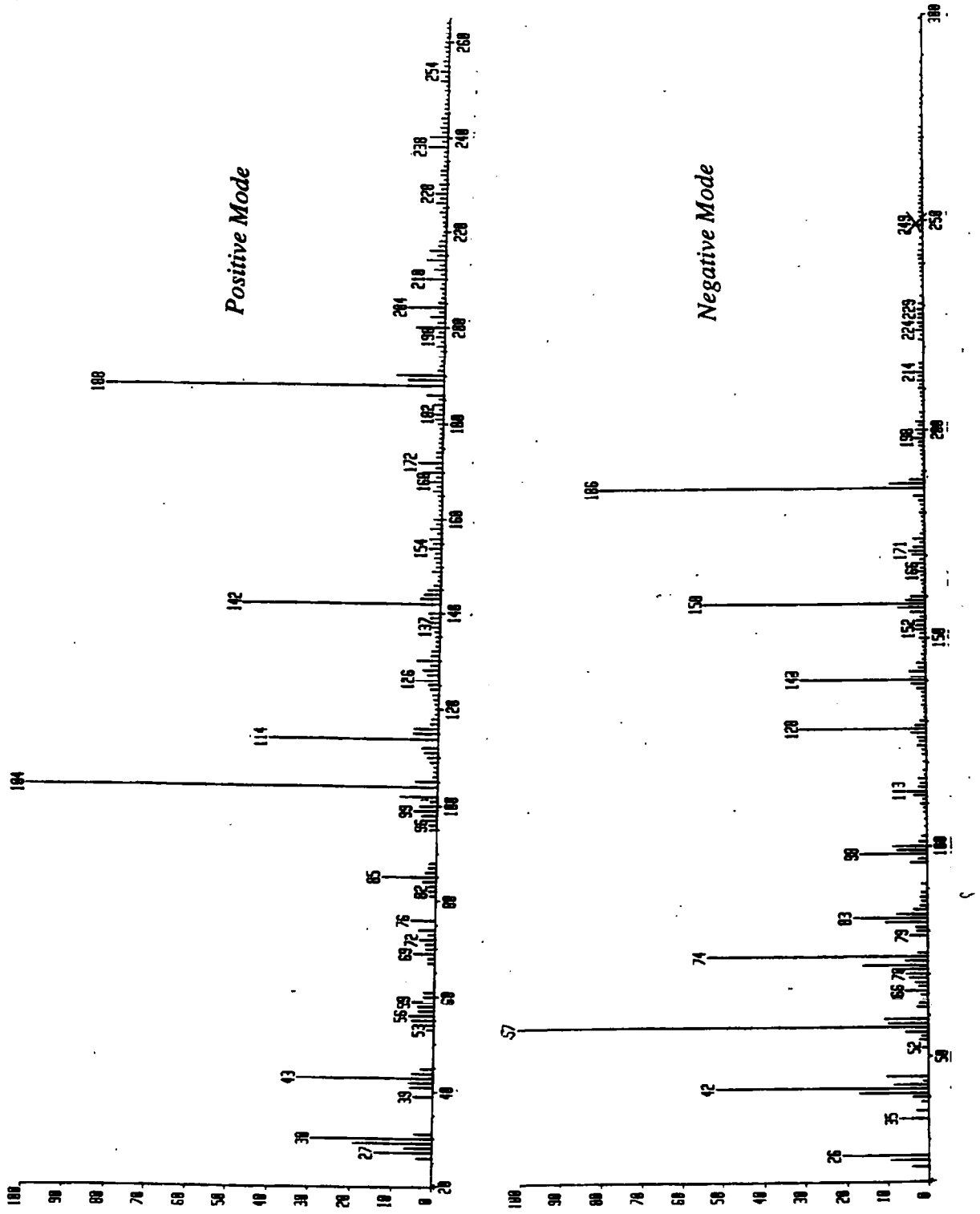

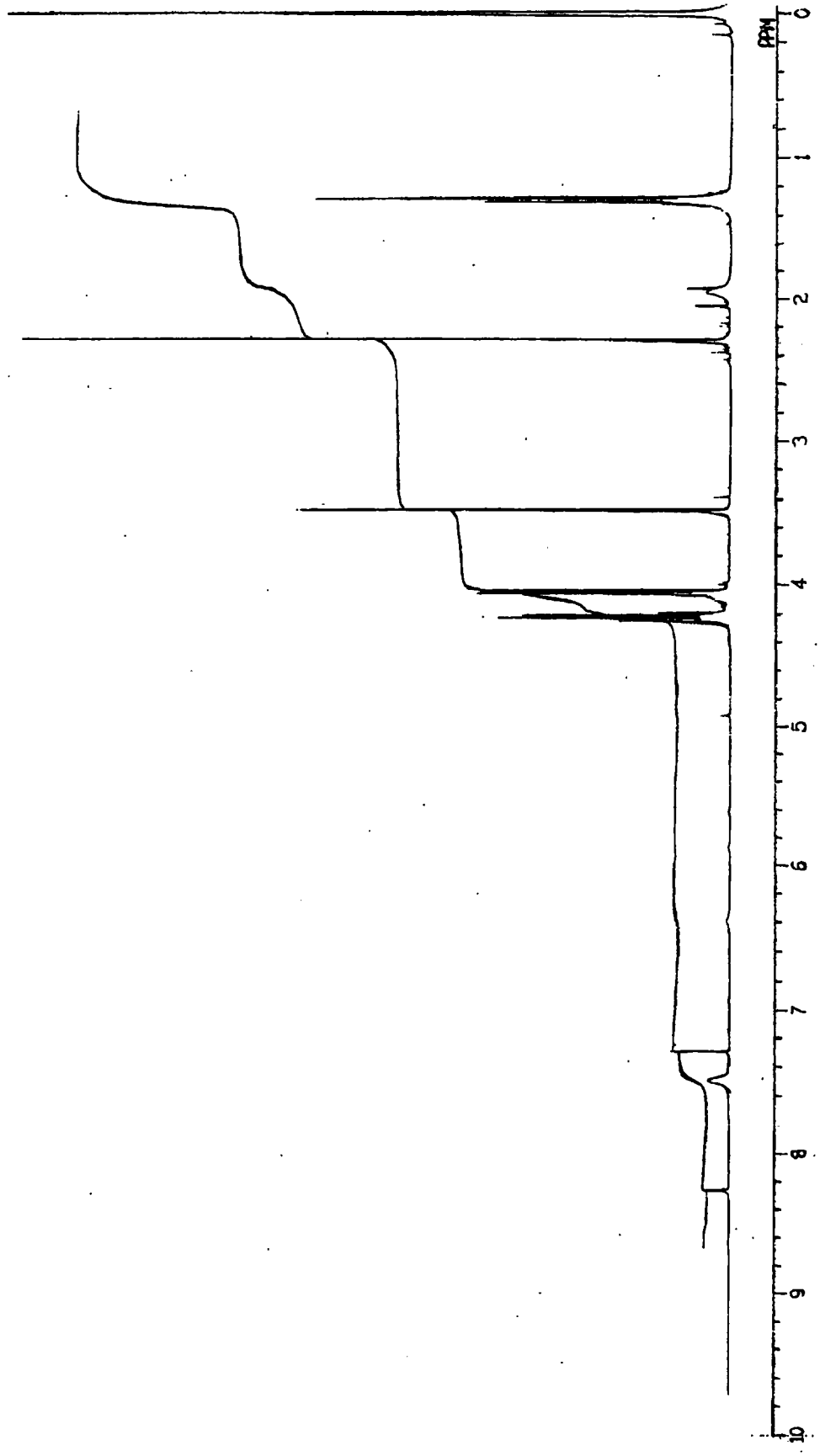

Figure 4.20 *400 MHz ^{1}H-nmr Spectrum of N-(3-Ketobutanoyl)glycine ethyl ester (4.9) in $CDCl_3$*

hplc. The two products with R_f = 12.7 and 13.5 min. were thought to be the *cis*- and *trans*-isomers of the epoxide (4.10), on the basis that a similar epoxide {*N*-(2,3-epoxypropanoyl)glycine ethyl ester (4.14)} was obtained from the acid-catalysed decomposition of *N*-(2-diazo-3-hydroxypropanoyl)glycine ethyl ester (2.3) {see Section 1.6}[18] probably *via* an intramolecular interaction of the diazonium ion with the 3-hydroxy substituent.

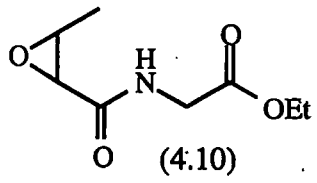

(4.10)

The successful route to *cis*-(4.10) involved coupling of *cis*-2,3-epoxybutanamide (4.15) with ethylbromoacetate in the presence of LDA, to generate the epoxyamide anion which readily displaces Br^- from the ethylbromoacetate (Scheme 4.4). This gave the epoxide *cis*-(4.10) in 68 % yield by hplc (see Section 7.5.3.4).

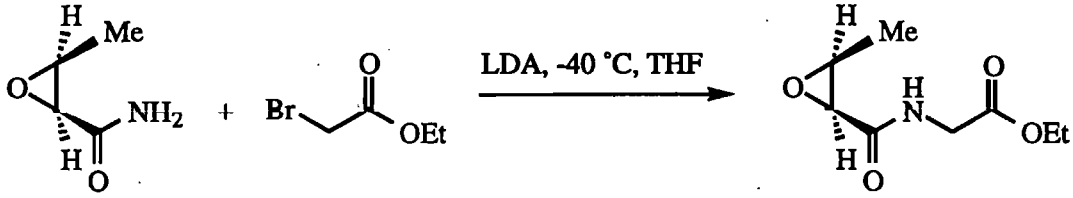

cis -(4.15) *cis* -(4.10)

Scheme 4.4

2,3-Epoxybutanamide (4.15) itself was synthesised *via* a literature procedure (Section 7.5.3.4) involving the alkaline epoxidation of crotononitrile with hydrogen peroxide.[127] Reaction of equimolar quantities of crotononitrile and hydrogen peroxide at pH 7.0-7.5 gave (4.15) in 28 % yield (Scheme 4.5).

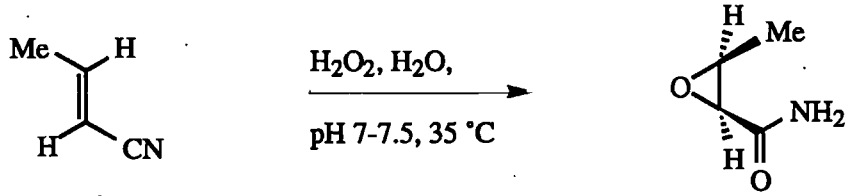

cis and *trans* *cis*-(4.15)

Scheme 4.5

The epoxidation is thought to involve an intramolecular rearrangement of the initial peroxycrotonimidic acid intermediate (4.16): the double bond of (4.16) {no longer polarised by electron-withdrawal by the cyano group} is more susceptible to electrophilic attack than the double bond of crotononitrile, itself, especially if the electrophilic attack is intramolecular (Scheme 4.6).

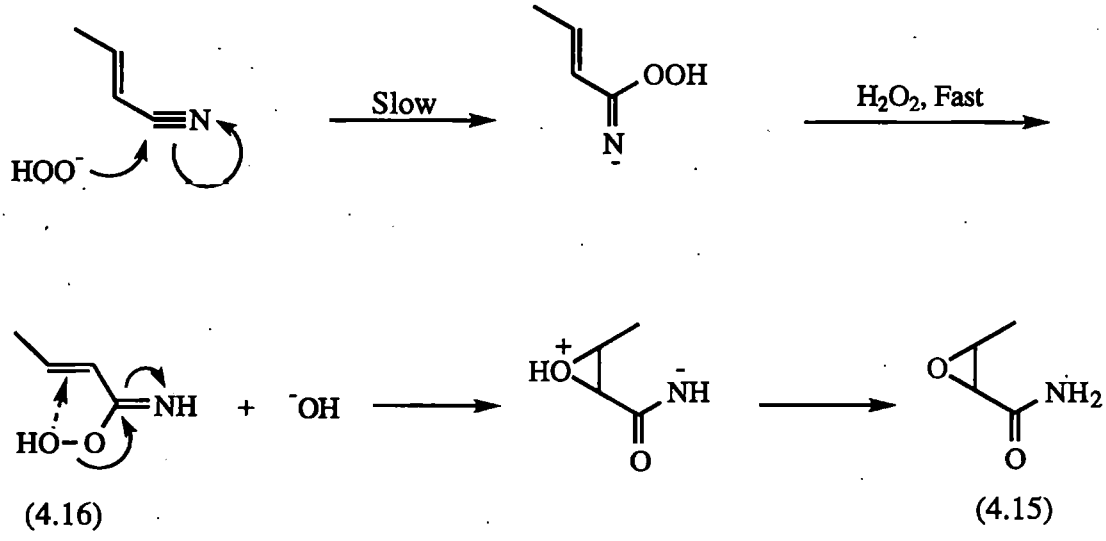

Scheme 4.6

On isolation, the 400 MHz ^{1}H-nmr spectrum of (4.15) indicated predominant formation of a single epoxide geometrical isomer, even from a 50:50 mixture of the *cis*- and *trans*-isomers of the crotononitrile starting material (Figure 4.21). The coupling constant (J = 4.8 Hz) for the ring proton at δ = 3.64 ppm is typical of *cis*-epoxides. Close scrutiny of the ^{1}H-nmr spectrum of the reaction product, however, indicates the presence of a small amount of the *trans*-epoxide. Thus, there is a second pair of epoxide ring protons at δ = 3.12 and 3.18 ppm with a coupling constant (J = 2.4 Hz) typical of the *trans*-epoxide. The ratio of *trans*:*cis* epoxide stereoisomers from the synthesis is *ca.* 9:1 estimated from the two pairs of the epoxide ring ^{1}H-nmr integrals. The ^{1}H-nmr assignments and product ratios for (4.15) are summarised in Table 4.6.

Analytical, reverse-phase hplc of the reaction mixture from the synthesis of epoxide *cis*-(4.10) indicated a major peak at 12.7 min. and a minor peak at 13.5 min., identical to the

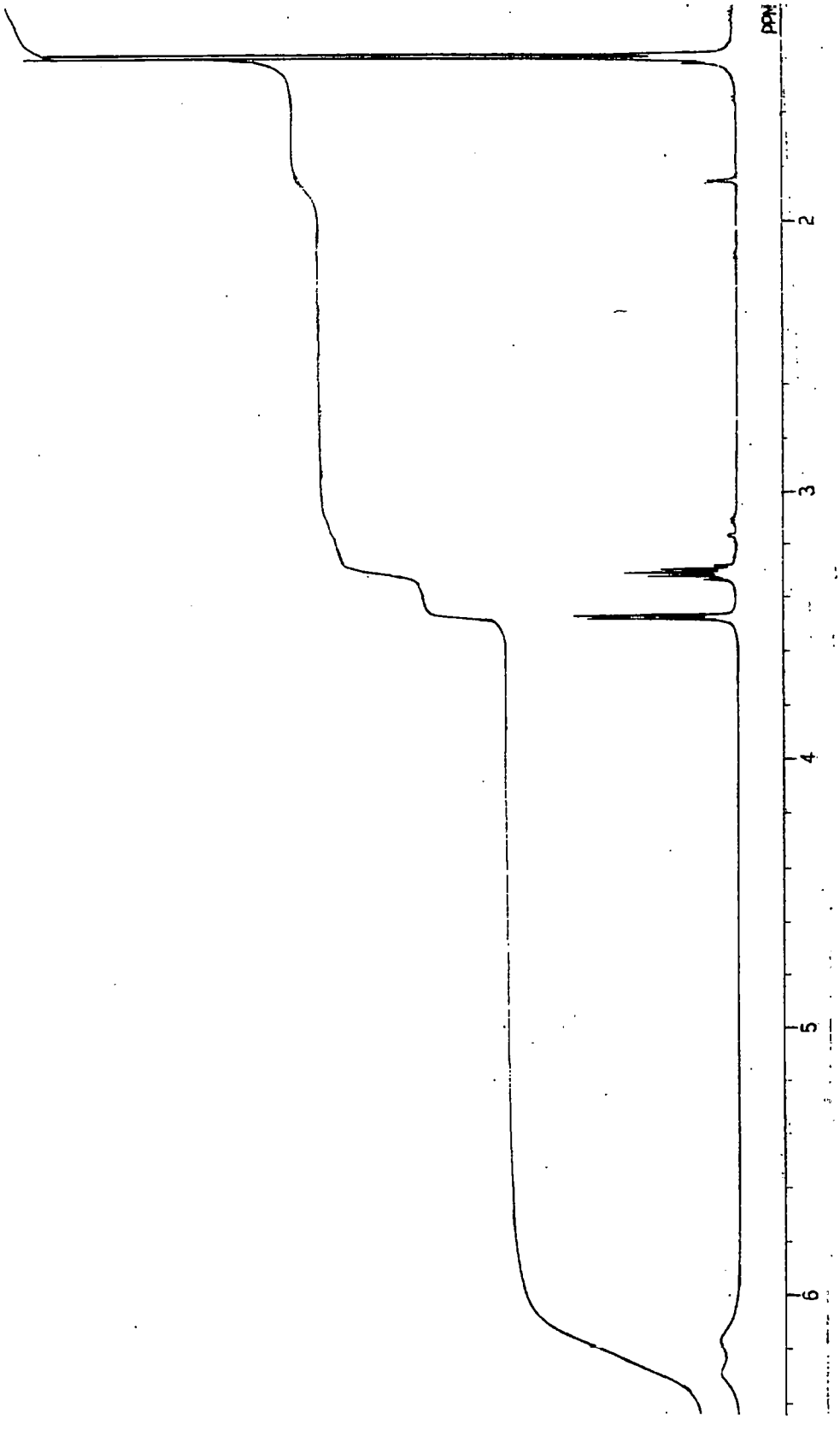

Figure 4.21 *400 MHz ^{1}H-nmr Spectrum of cis-2,3-Epoxybutanamide (4.15) in $CDCl_3$*

retention times observed for the unknown products from the decomposition of diazopeptide (2.1) in 0.1 M perchloric acid (see Figure 4.8).

Table 4.6 Comparison of *cis*- and *trans*- 2,3-Epoxybutanamide (4.15) 400 MHz ^{1}H-nmr Assignments in $CDCl_3$

Signal	*cis*-2,3-Epoxybutanamide				*trans*-2,3-Epoxybutanamide			
	δ, ppm	m	J, Hz	Ratio, %	δ, ppm	m	J, Hz	Ratio, %
-CH(CH_3)	1.41	d	5.6	90	1.88	d	5.6	10
-C*H*(CH_3)	3.31	m	-	90	3.12	m	-	10
-C*H*$CONH_2$	3.48	d	4.8	90	3.18	m	2.4	10

The product at R_f = 12.7 min. was purified by semi-preparative, reverse-phase hplc with uv detection at λ = 210 nm (see Section 7.5.3.4) and the chromatogram of the combined isolated fractions is shown in Figure 4.22. The yield of *cis*-(4.10) was 68 % by hplc assay, and the isolated yield was a reasonable 21 %. It was further examined by 400 MHz ^{1}H-nmr and FAB mass spectrometry.

Figure 4.22 *Hplc Chromatogram of (4.10)*

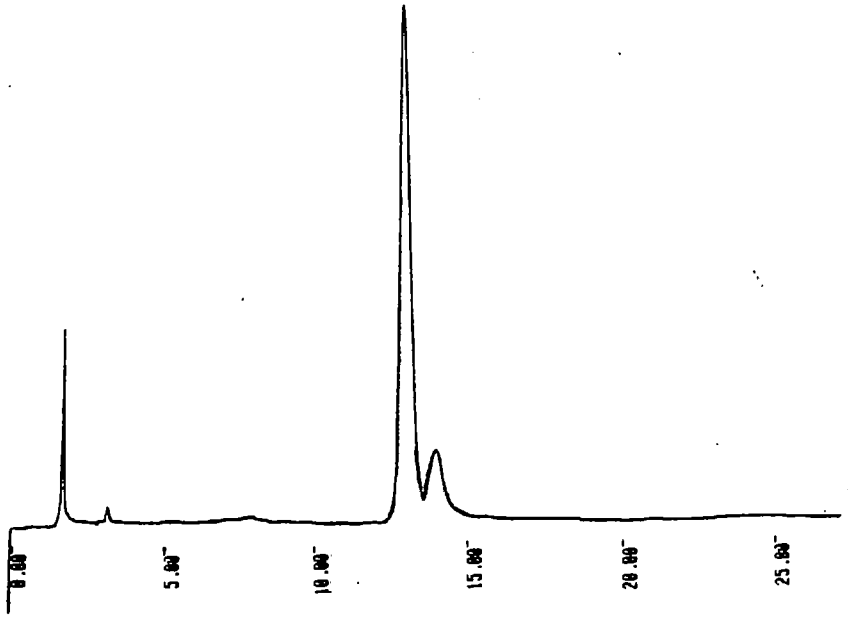

The FAB mass spectrum gave m/z = 188 as the MH^+ ion in the positive mode, and 186 as the $M\text{-}H^+$ ion in the negative mode (Figure 4.23). The FAB (+ve) mass spectrum shows a very similar fragmentation pattern to that of the isomeric ketone product (4.9) {Figure 4.20}, but the base peak is m/z = 104 ($[H_3NCH_2CO_2Et]^+$) for the ketone, and m/z = 188 (MH^+) for the epoxide. Both spectra show the presence of a dimeric product at m/z = 375 (M_2H^+).

The 400 MHz ^{1}H-nmr spectrum of (4.10) in $CDCl_3$ (Figure. 4.24) indicates the presence of a single epoxide stereoisomer. This was expected as *ca.* 90 % *cis*-(4.15) starting material has been used for the synthesis of this product sample. The main features of the ^{1}H-nmr spectrum are the two characteristic epoxide ring protons at δ = 3.32 and δ = 3.54 ppm with J = 4.8 Hz. As mentioned above, this coupling constant is typical of *cis* geometrical epoxide isomers. The glycyl -$HNCH_2$COEt protons are diastereotopic and are seen widely split at δ = 3.9 and 4.2 ppm (partial overlap with the ethyl ester -$CO_2CH_2CH_3$ quartet).

Spiking the crude reaction mixture of (2.1) in perchloric acid with authentic *cis*-(4.10) {after purification} gave a single, shoulderless peak by hplc of increased magnitude at R_f = 12.7 min. The peaks from authentic *cis*-(4.10) and the product R_f = 12.7 min. from the decomposition of diazopeptide (2.1) in perchloric acid also gave identical purity parameter values from hplc diode-array analysis, indicating they are identical compounds.

All of the data are consistent with products at R_f = 12.7 and 13.5 min. being the *cis* and *trans* geometrical isomers of epoxide (4.10), respectively, from the decomposition of diazopeptide (2.1) in 0.1 M $HClO_4$. For the authentic synthesis none of the *trans*-(4.10) was apparent by ^{1}H-nmr, but a small amount (< 5% by peak height) was observable at R_f= 13.5 min. by analytical hplc of the reaction mixture (see Figure 4.22).

Figure 4.23 *FAB Mass Spectrum of cis-N-(2,3-Epoxybutanoyl)glycine ethyl ester (4.10)*

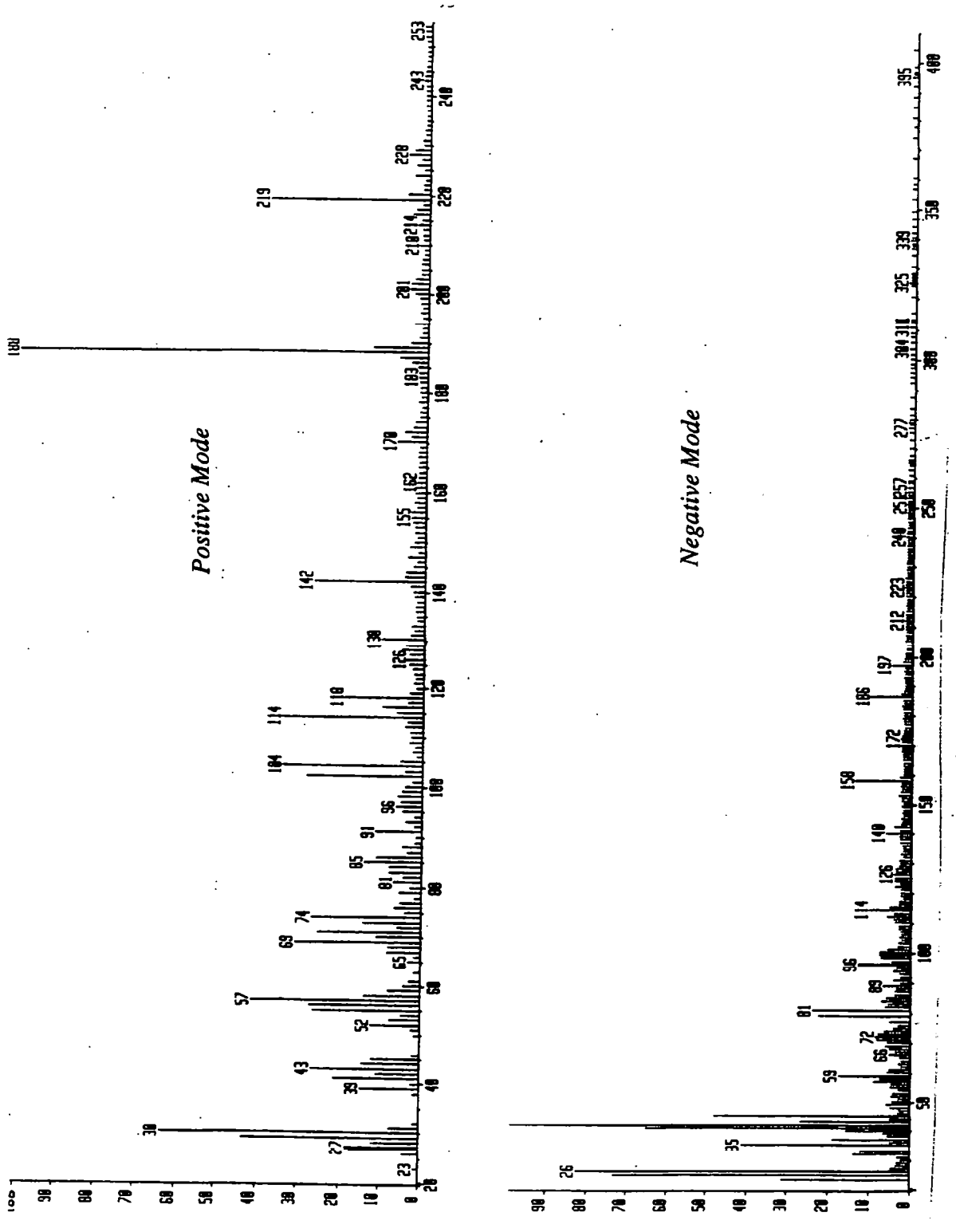

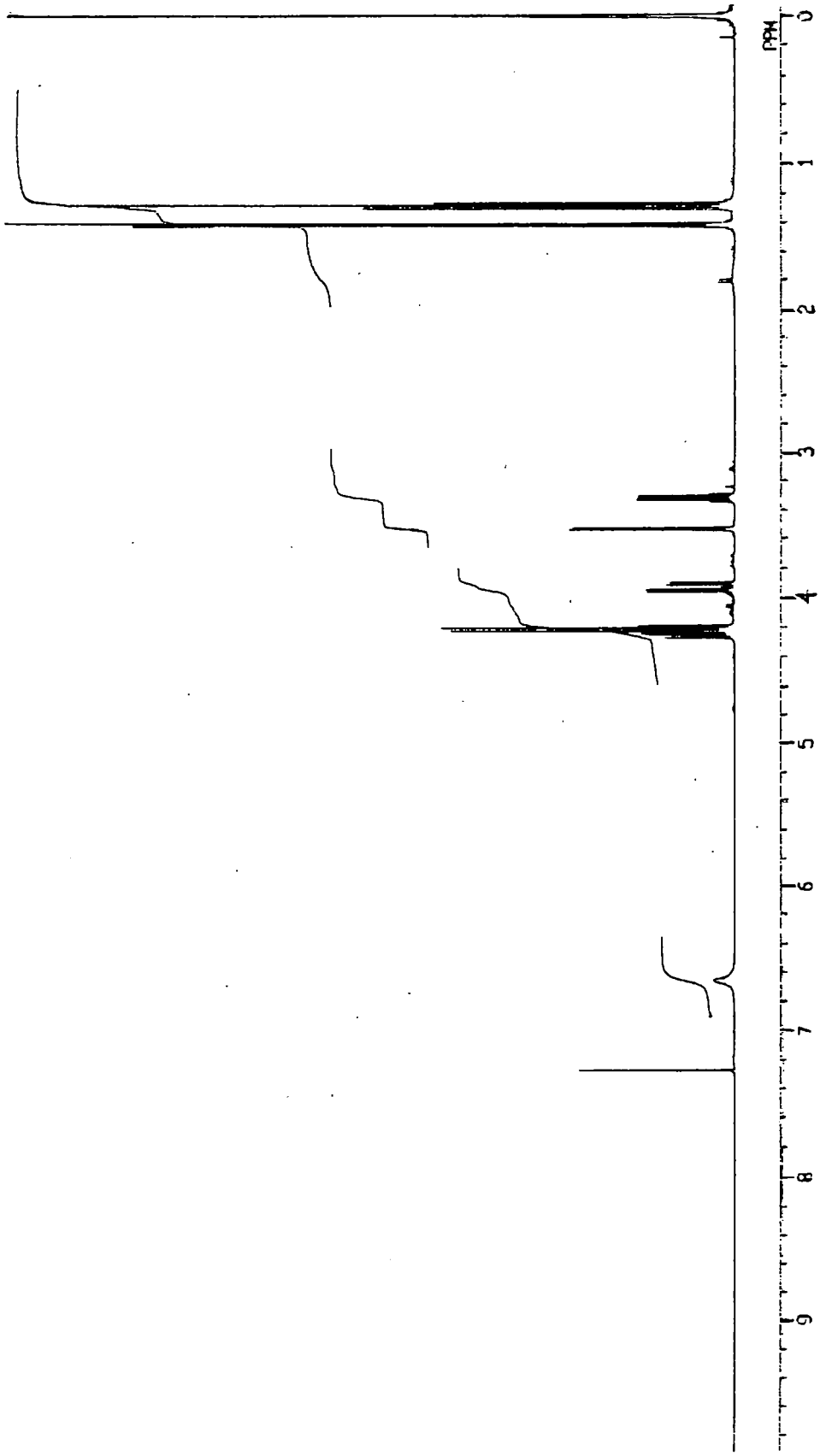

Figure 4.24 *400 MHz ^{1}H-nmr Spectrum of cis-N-(2,3-Epoxybutanoyl)glycine ethyl ester (4.10) in $CDCl_3$*

4.3.4 Quantitation of Products from the Decomposition of (2.1) in Perchloric acid and Buffer Solutions

The three reaction products at R_f = 6.2, 8.9 and 12.7 min., {*i.e.* compounds 2(*S*),3(*R*)-(4.8), (4.9), and *cis*-(4.10), respectively} were quantitated by analytical hplc assay (see Section 7.4.1.2). Calibration curves showing integrated peak areas *vs.* concentration were generated for authentic 2(*S*),3(*R*)-(4.8), (4.9) and *cis*-(4.10): all were linear, as exemplified for 2(*S*),3(*R*)-(4.8) in Figure 4.25.

Figure 4.25 *Calibration Curve for N-(2(S),3(R)-Dihydroxybutanoyl) glycine ethyl ester (4.8) by Hplc Assay*

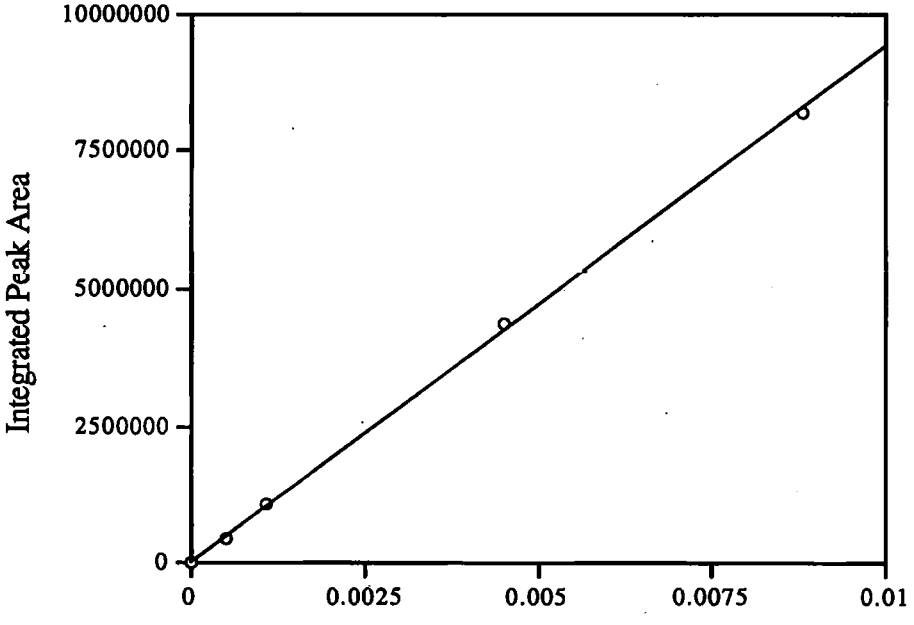

The hplc chromatograms for the decomposition of *N*-(2-diazo-3-hydroxybutanoyl)glycine ethyl ester (2.1) in various media are shown in Figure 4.26 and the yields of the products 2(*S*),3(*R*)-(4.8), (4.9) and *cis*-(4.10), estimated by interpolation from the calibration curves, are summarised in Table 4.7. The error in these assays is

estimated as ± 5%. The relative yields (%) of each product for decomposition under various conditions are summarised in Table 4.7.

Table 4.7 Product Yields (%) by Hplc Assay for the Decomposition of *N*-(2-Diazo-3-hydroxybutanoyl)glycine ethyl ester (2.1) in Various Aqueous Solutions at Various pH and at Ambient Temperature.

Reaction Solution	pH	% Yields of Products by Hplc Assay					Total inc. isomers
		R_f = 6.2 2(*S*),3(*R*)- (4.8)	7.9 2(*R*),3(*R*)- (4.8)	8.9 (4.9)	12.7 *cis*- (4.10)	13.5 min. *trans*- (4.10)	
0.1 M $HClO_4$	<2	19	(19)	46	8	(8)	100
0.1M $HClO_4$ + 0.9 M NaCl	<2	14	(14)	50	10	(10)	98
0.1 M Formate	3.5	17	(17)	39	8	(8)	89
0.1 M Acetate	4.2	16	(16)	34	8	(8)	82
0.1 M Phosphate	6.2	8	(8)	35	12	(12)	75

*Authentics 2,(*R*),3(*R*)-(4.8) and *trans*-(4.10) were not available for quantitative assay. Their yields (given in parenthesis) were assumed to be similar to 2(*S*),3(*R*)-(4.8) and *cis*-(4.10), respectively, on the basis of comparison by hplc peak height (see Figures 4.8 and 4.26).

Although the products are not strongly influenced by the reaction conditions, the yield of isomeric diols decrease with increasing pH. This may reflect reaction of the protonated diazopeptide and/or carbocation with nucleophilic buffer components, other than H_2O, and a reduced rate of epoxide hydrolysis to diol products at higher pH (reflected in the slight increase in epoxide yield in phosphate buffers).

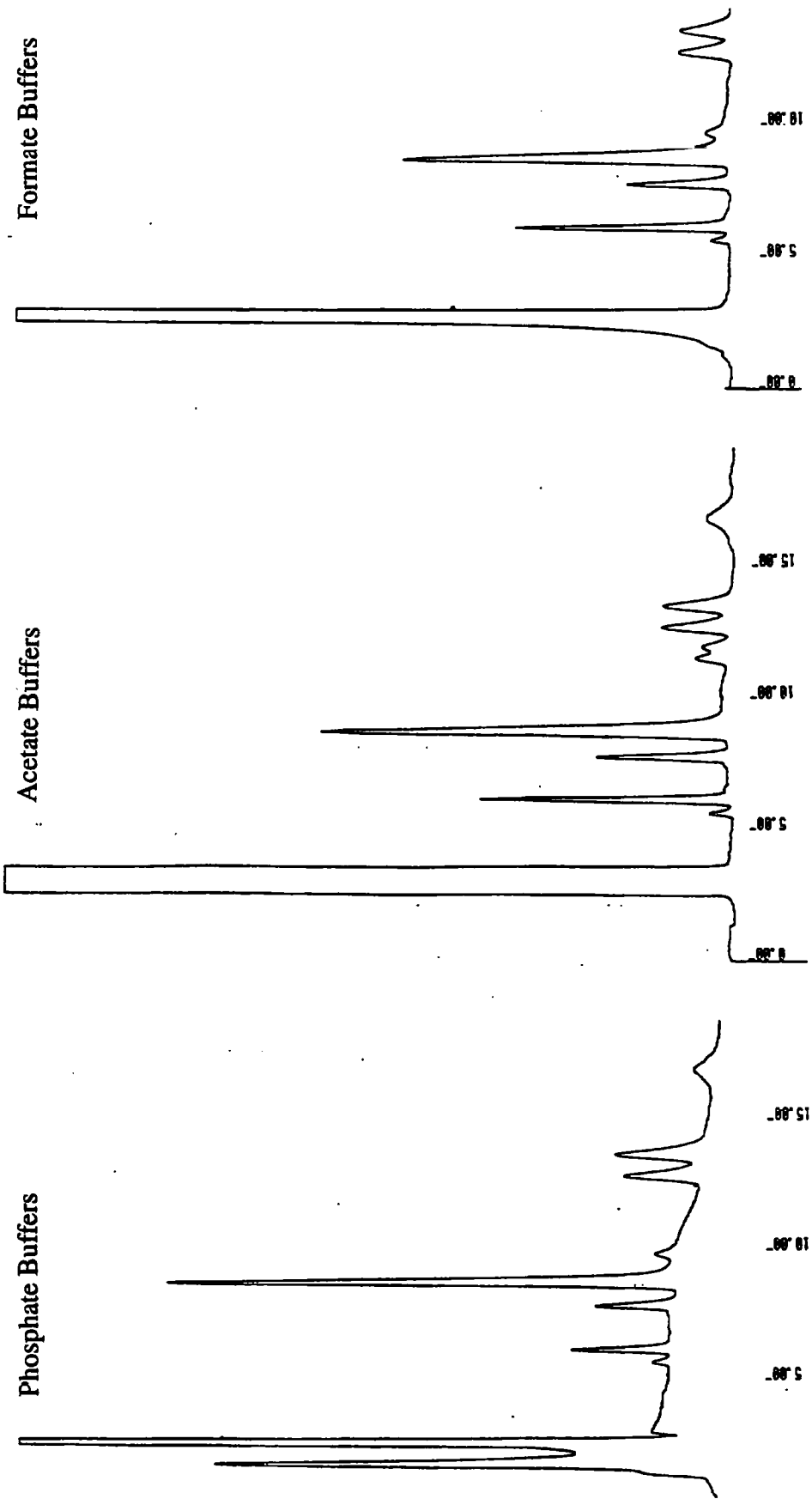

Figure 4.26 *Hplc Chromatograms of Products from the Decomposition of (2.1) in Buffer Solutions*

4.4 *N*-(2-Diazo-3-carbamoylpropanoyl)glycine benzyl ester (4.1) and *N*-(2-Diazo-3-carbamoylpropanoyl)glycine ethyl ester (4.17)

4.4.1 Decomposition of *N*-(2-Diazo-3-carbamoylpropanoyl)glycine benzyl ester (4.1) and *N*-(2-Diazo-3-carbamoylpropanoyl)glycine ethyl ester (4.17)

N-(2-Diazo-3-carbamoylpropanoyl)glycine benzyl ester (4.1) and *N*-(2-diazo-3-carbamoylpropanoyl)glycine ethyl ester (4.17) could not be isolated, hence they were generated *in situ* by the nitrosation of *L*-asparaginylglycine benzyl ester (4.4) and *L*-asparaginylglycine ethyl ester (4.18), respectively, using liquid dinitrogen tetroxide. Diazopeptides (4.1) and (4.17) were then allowed to decompose to products in the reaction vessel by warming to room temperature (see Section 7.4.1.3).

4.4.1.1 Hplc Studies.

Only the decomposition reactions of (4.1) were examined in detail by analytical hplc at $\lambda = 258$ nm. This facilitated the identification of products from impurities as only compounds bearing benzyl ester groups {from (4.1)} absorb strongly at 258 nm, whereas those bearing ethyl ester groups {from (4.17)} absorb at λ *ca.* 210 nm and are less easily distinguished from impurities. Hence, after aqueous washing the reaction mixture from the decomposed *N*-(2-diazo-3-carbamoylpropanoyl)glycine benzyl ester (4.1) gave an oily residue (*ca.* 5 mg). This was dissolved in 40 % (v/v) methanol in water (25 cm^3), and aliquots (20 μl) were then analysed by reverse-phase, analytical hplc with uv detection at $\lambda = 258$ nm. This indicated formation of only two products eluting at $R_f = 6.3$, and 16.3 min. (Table 4.8 and Figure 4.27). The additional peak eluting at 13.3 min. was later found to be an unidentified impurity and not a product from the decomposition of (4.1).

Table 4.8

Peak	R_f, min.	Product
1	6.3	*N*-(2-Hydroxy-3-carbamoylpropanoyl) glycine benzyl ester (4.19) or *L*-Aspartylglycine benzyl ester (4.20)
2	16.3	β-lactam (4.21)

Figure 4.27 *Hplc Chromatogram of Products from the Decomposition of (4.1) in $HClO_4$*

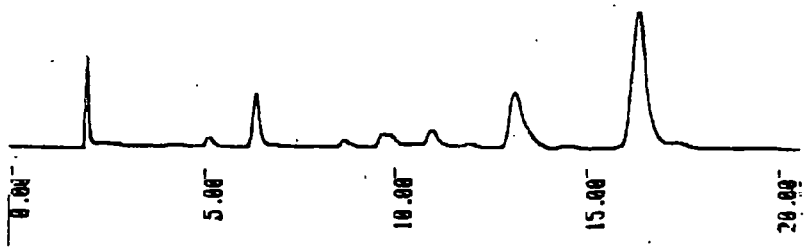

4.4.2 Product Isolation and Characterisation.

Larger amounts (0.5 g) of the oily residue from the reaction mixture dissolved in 40 % (v/v) methanol in water (10 cm^3) were purified by semi-preparative, reverse-phase hplc with uv detection at λ = 258 nm, and the products eluting at 6.3 and 16.3 min. separated. From repeat injections (1-2 cm^3), product fractions were combined, and the methanol and water removed by vacuum evaporation and freeze-drying, respectively (see Section 7.4.1.3). These residues were then examined by 400 MHz ^{1}H-nmr and FAB mass spectral analyses.

4.4.2.1 Characterisation of Product with R_f = 6.3 min.

The FAB mass spectrum of this product (Figure 4.28) indicated m/z = 281 for the MH^+ and m/z = 303 for the MNa^+ ions in the positive mode (with losses of ammonia and water to give fragment ions at m/z = 264 and 246, respectively) and m/z = 279 for the $M\text{-}H^+$ ion in the negative mode (with loss of water to give a fragment ion at m/z = 261 and loss of the stable tropylium ion {*i.e.* M- $[C_7H_7]^+$} to give a fragment ion at m/z = 189). The FAB positive mode mass spectrum also shows fragment ions at m/z = 91 (100 %), which relates to the stable tropylium ion $[C_7H7]^+$, and m/z = 166, which relates to the $[H_3NCH_2CO_2CH_2Ph]^+$ ion. These data are consistent with either (4.19) or the isomeric (4.20) structure for the product with R_f = 6.3 min. Structure (4.20), however, contains a carboxylic acid group, so an intense signal for the $M\text{-}H^+$ ion would be expected. As this is not the case, the FAB -ve mass spectrum is more supportive of structure (4.19).

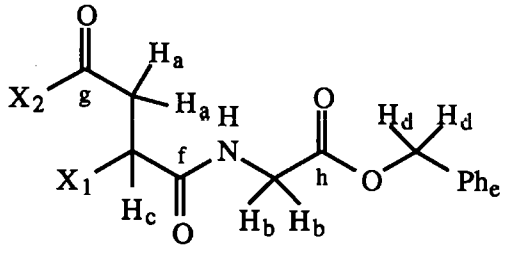

For (4.19) X_1 = OH, X_2 = NH_2
For (4.20) X_1 = $\overset{+}{N}H_3$, X_2 = O^-
For (4.4) X_1 = $\overset{+}{N}H_3$, X_2 = NH_2

The 400 MHz ^{1}H-nmr spectrum of the isolated product with R_f = 6.3 min. in CD_3OD (Figure 4.29) is very similar to the 400 MHz ^{1}H-nmr spectrum of the parent *L*-asparaginylglycine benzyl ester (4.4) in CD_3OD (Figure 4.30). The only significant difference concerns the double doublet (due to coupling with each of the adjacent diastereotopic methylene protons H_a) at δ = 4.46 ppm assigned to H_c of either structure (4.19) or (4.20) compared to δ = 4.04 ppm assigned to H_c of the parent (4.4), as summarised in Table 4.9.

The X_1 substituent of both stucture (4.20) the TFA salt of the parent peptide (4.4) should be protonated in CD_3OD {*i.e.* the aspartic acid side-group of stucture (4.20) should

Figure 4.28 *FAB Mass Spectrum of Product with Rf = 6.3 min.*

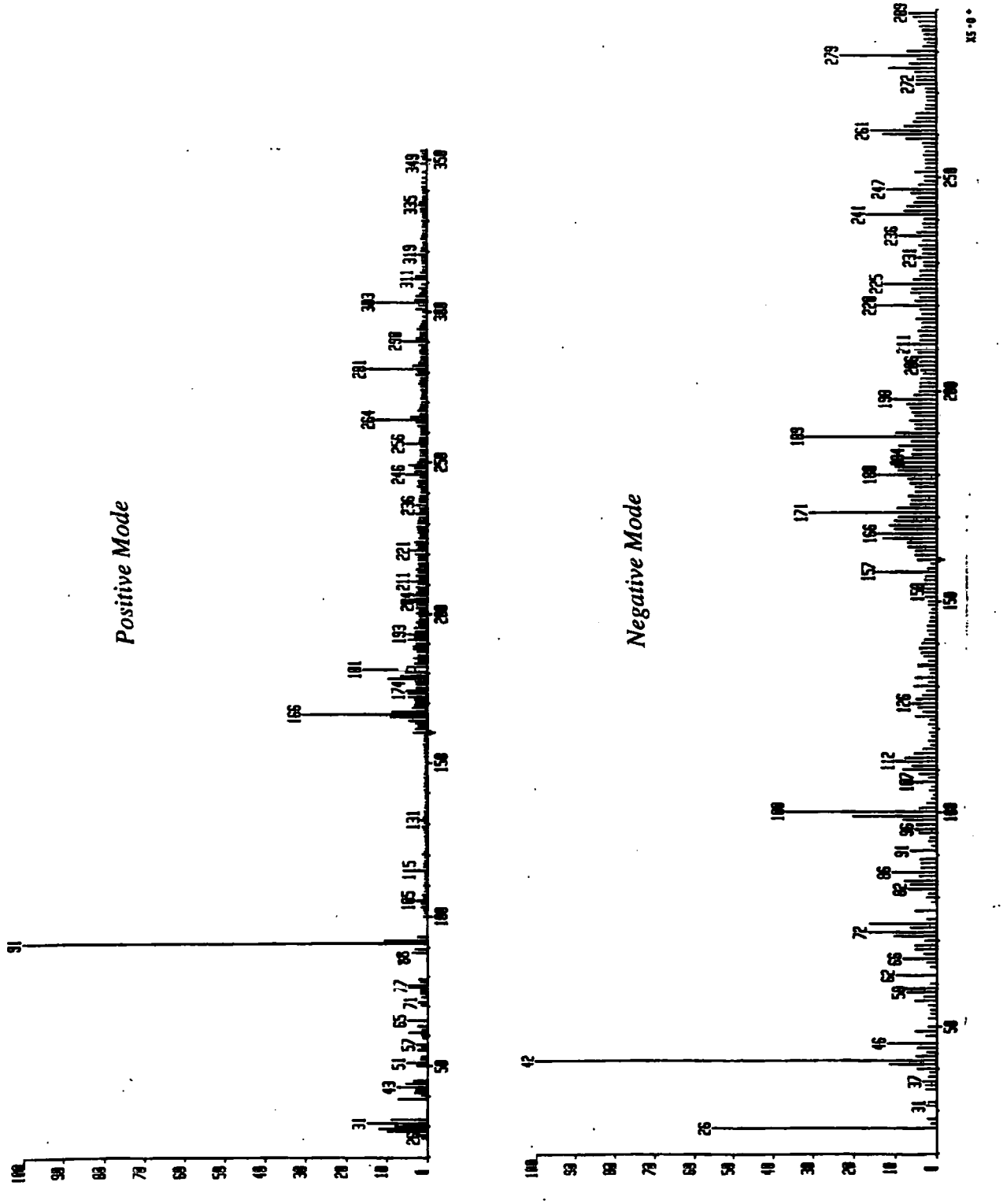

Figure 4.29 *400 MHz ^{1}H-nmr Spectrum of Product with Rf = 6.3 min. in CD_3OD*

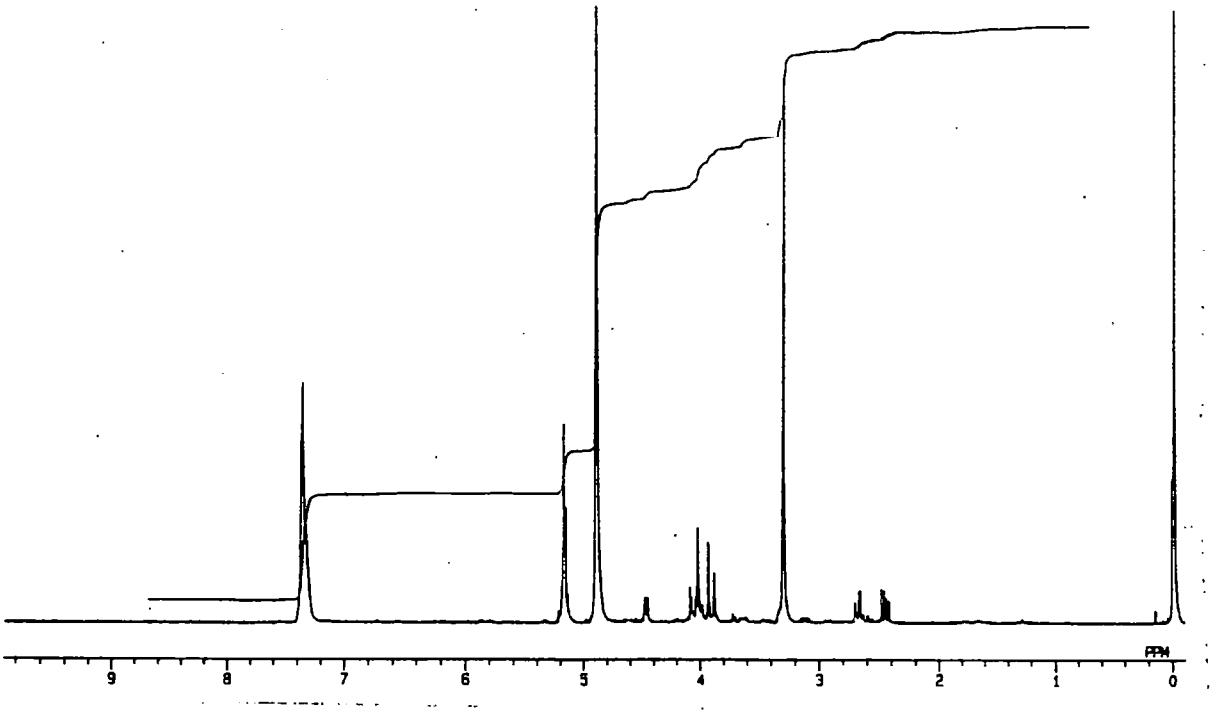

Figure 4.30 *400 MHz ^{1}H-nmr Spectrum of L-Asparaginylglycine benzyl ester trifluoroacetate (4.4) in CD_3OD*

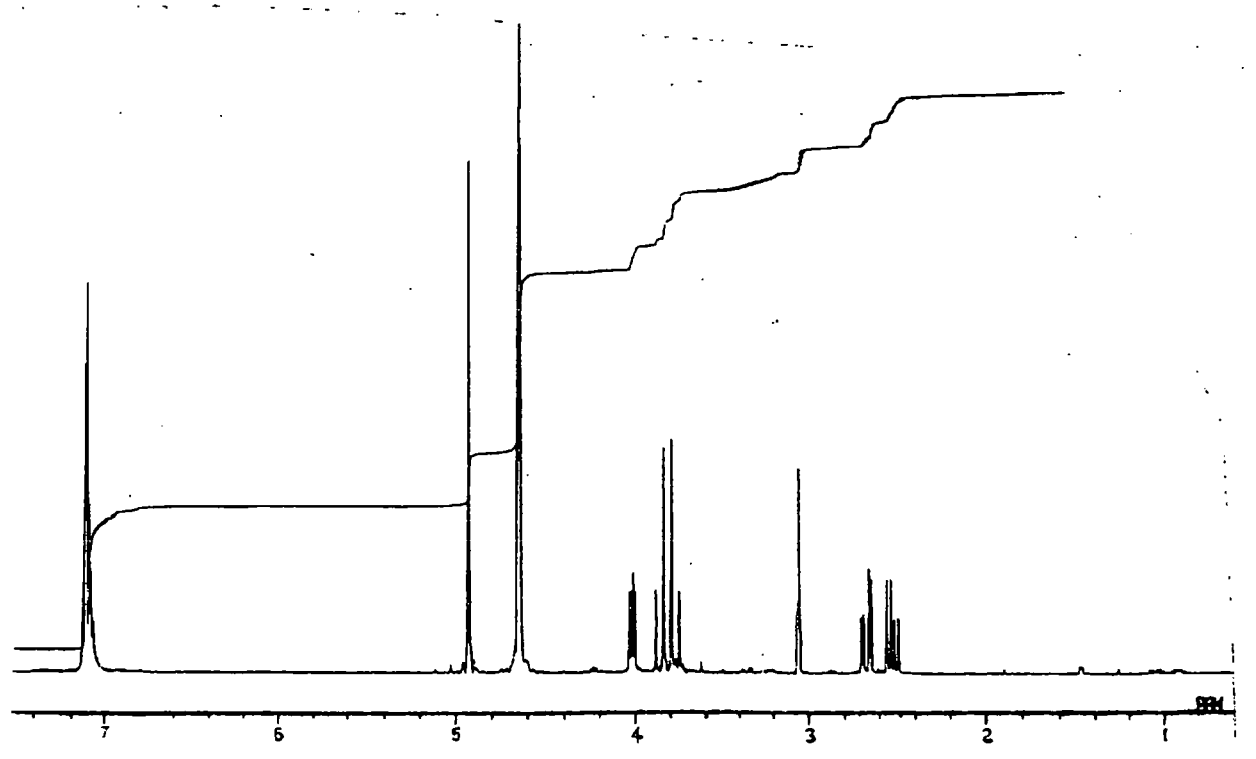

exist in the zwitterionic form}. Hence, δH_c for structure (4.20) and salt (4.4) should be similar at *ca.* 4.0 ppm. Conversely, δH_c of (4.19) should be more shielded than (4.4) and structure (4.20) because it is adjacent to a hydroxyl group rather than a protonated amino group, as observed for authentic *N*-(2(*S*),3(*R*)-dihydroxybutanoyl)glycine ethyl ester (4.8) where δH_c = 3.88 ppm (see Section 4.3.2.1).

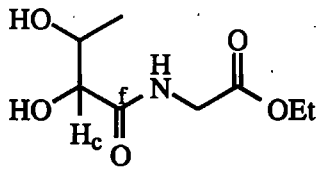

2(*S*),3(*R*)-(4.8)

Table 4.9 Comparison of 400 MHz ^{1}H and 100 MHz ^{13}C-Nmr Assignments in CD_3OD for Product with R_f = 6.3 min. and *L*-Asparaginylglycine benzyl ester trifluroacetate (4.4)

Signal δ, ppm	Product with R_f = 6.3 min. {Structure (4.19) or (4.20)}		*L*-Asparaginylglycine benzyl ester trifluroacetate (4.4)	
	^{1}H	^{13}C	^{1}H	^{13}C
a	2.45-2.67 (2H, dd)	38.7	2.50-2.70 (2H, dd)	36.1
b	3.88-4.08 (2H, ABq)	41.0	3.70-3.90 (2H, ABq)	42.2
c	4.46 (1H, dd)	67.4	4.04 (1H, dd)	51.2
d	5.15 (2H, s)	67.2	5.01 (2H, s)	68.0
e	7.32 (5H, s)	128.5	7.28 (5H, s)	129.3
f	-	174.6	-	170.8
g	-	169.7	-	170.2
h	-	173.6	-	173.6

Thus, neither structure (4.19) nor (4.20) agrees satisfactorily with the assignment for H_c at δ = 4.46 ppm. It is possible that the signal at δ = 4.46 ppm relates to an impurity and the H_c signal for the product with R_f = 6.3 min. is hidden beneath the AB quartet signal for the -NHCH_2CO$_2$Bz moeity at δ = 3.9-4.1 ppm. Indeed, the ratio of this integral to the -CH_2CHCONH- methylene protons is *ca.* 3:2. Hence, the product with R_f = 6.3 min. can not be identified as either compound (4.19) or (4.20) by ^{1}H-nmr.

The 100 MHz ^{13}C-nmr spectra of the product with R_f = 6.3 min. and *L*-asparaginylglycine ethyl ester (4.4) are shown as Figures 4.31 and 4.32, respectively, and are summarised in Table 4.9. For the parent (4.4), the two amide carbonyl signals C_g and C_f at δ = 170.2 and 170.8 ppm, respectively, appear upfield relative to the ester carbonyl signal C_h at δ = 173.6 ppm. By comparison, the ^{13}C-nmr spectrum for the product with R_f = 6.3 min. shows two similar carbonyl signals at δ = 169.7 and 173.6 ppm corresponding to amide C_g and ester C_h, respectively, with a third carbonyl signal downfield at δ = 174.6 ppm. These data are consistent with structure (4.19) for the product with R_f = 6.3 min. with the signal at δ = 174.6 ppm corresponding to amide carbonyl C_f, presumably deshielded by the α-hydroxy substituent. This interpretation is supported by the δ = 176.1 ppm (see Section 7.5.3.3) for the corresponding amide carbonyl signal C_f of 2(*S*),3(*R*)-(4.8), which has a similar chemical environment and is also deshielded, presumably by an α-hydroxy effect. Further, signal C_c (-*C*HCONH-) of authentic 2(*S*),3(*R*)-(4.8) at δ = 69.6 ppm is in excellent agreement with the corresponding signal C_c of the product with R_f = 6.3 min. at δ = 67.4 ppm, whereas signal C_c at δ = 51.2 ppm for the parent (4.4) {analogous to structure (4.20)} is significantly more shielded.

Thus, the ^{13}C-nmr data are more supportive of structure (4.19) for the product with R_f = 6.3 min. with an unaltered α-asparaginyl side group and an α-hydroxyl substituent rather than an α-aspartic acid side group and a protonated α-primary amino substituent.

Figure 4.31 *100 MHz ^{13}C-nmr Spectrum of Product with R_f = 6.3 min. in CD_3OD*

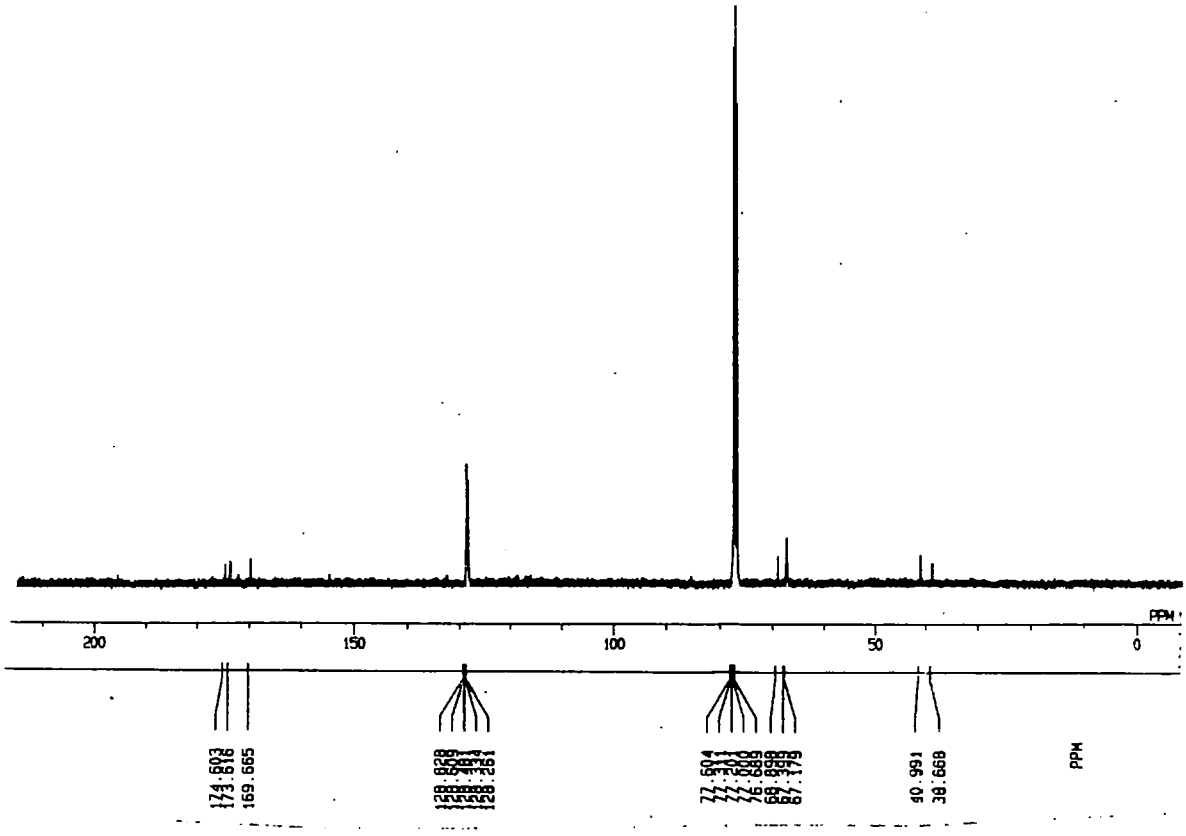

Figure 4.32 *100 MHz ^{13}C-nmr Spectrum of L-Asparaginylglycine benzyl ester trifluoroacetate (4.4) in CD_3OD*

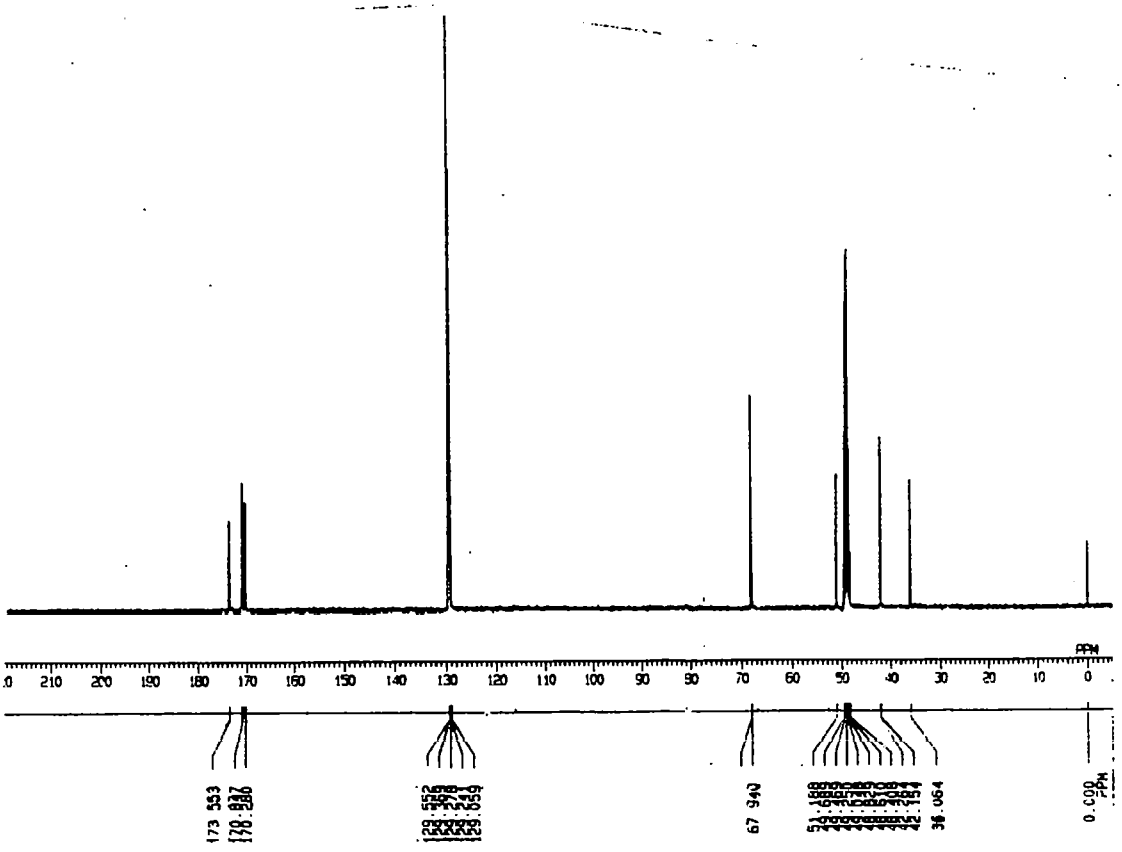

4.4.2.2 Characterisation of Product with R_f = 16.3 min.

The FAB mass spectrum of this product (Figure 4.33) suggests that m/z = 263 could be the MH^+ ion in the positive mode and m/z = 261 the $M\text{-}H^+$ ion in the negative mode. Further, the positive mode mass spectrum shows a peak at m/z = 115 and the negative mode mass spectrum peaks at m/z = 127 and 113. All of these probably relate to fragment ions derived from the β-lactam structure (4.21), as assigned in Table 4.10. Furthermore, the ion observed at m/z = 171 in the negative mode probably represents the negatively charged fragment derived from the loss of the stable tropylium ion from the neutral molecule, *i.e.* $M\text{-}[C_7H_7]^+$. This is characteristic of compounds bearing benzyl ester groups and is supportive of the product with R_f = 16.3 min. having structure (4.21).

Table 4.10 FAB Mass Spectral Assignments for Product with R_f = 16.3 min.

Positive Mode			Negative Mode		
m/z	Fragment Ion	Relative Abundance, %	m/z	Fragment Ion	Relative Abundance, %
263	MH^+	1	261	$M\text{-}H^+$	38
166	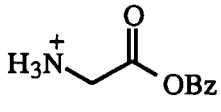	48	171	M - 	22
135	$\overset{+}{O}\equiv COBz$	24	127	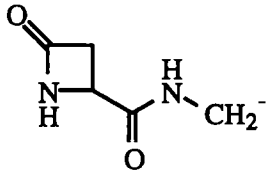	8
115	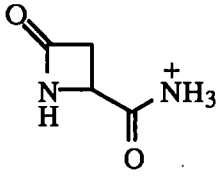	21	11	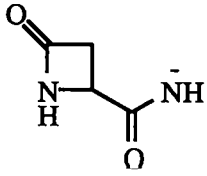	96
91		69			

Figure 4.33 *FAB Mass Spectrum of Product with Rf = 16.3 min.*

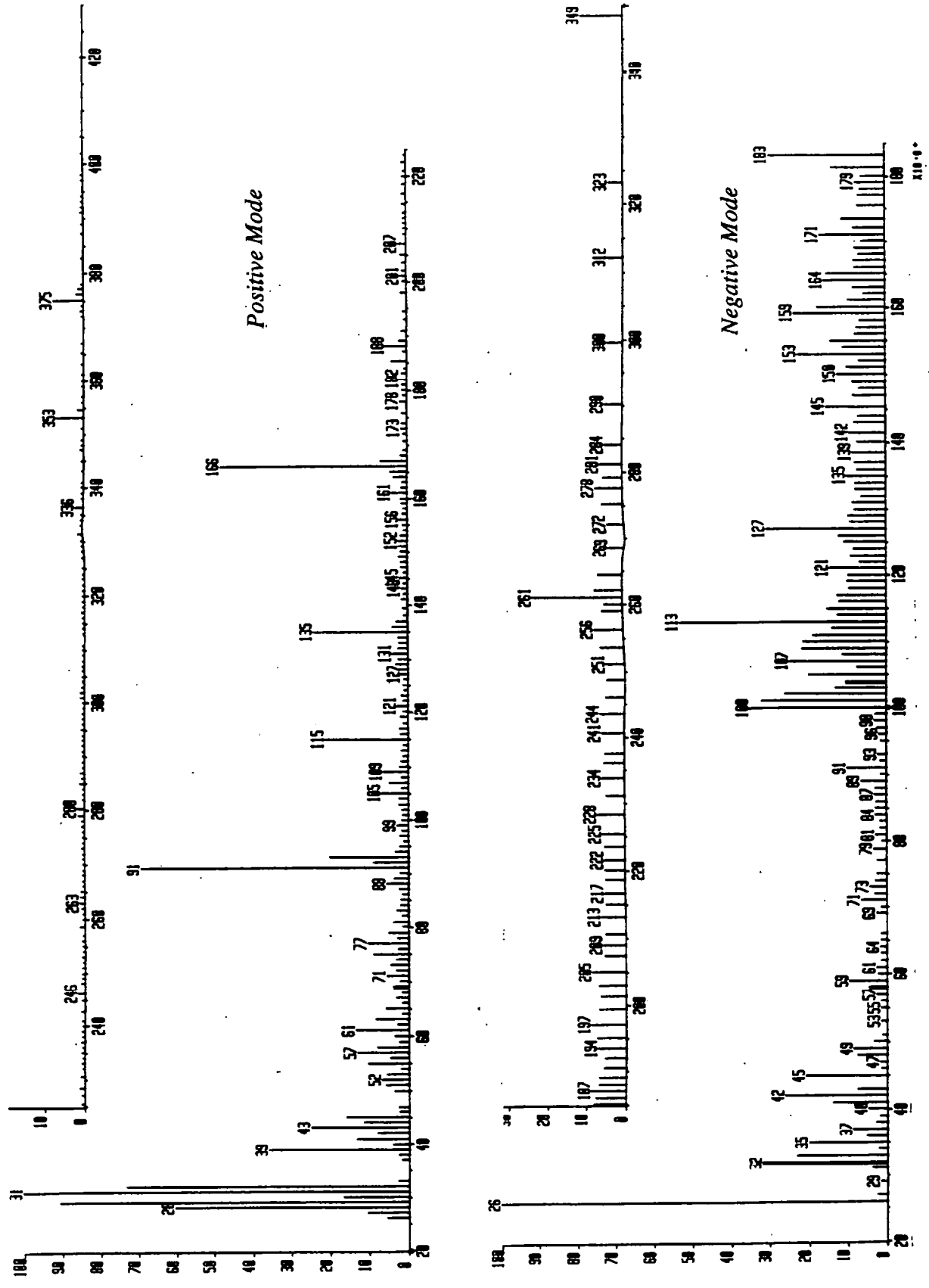

The 400 MHz ^{1}H-nmr spectrum of the product with R_f =16.3 min. in CD_3OD is shown as Figure 4.34. Its most characteristic features compared to the 400 MHz ^{1}H-nmr spectrum of the parent (4.4) {Figure 4.30} are the appearance of two new signals at δ = 3.45 (H_a, dd) and 3.62 (H_b, dd) and the disappearance of the methylene diastereotopic protons (H_2NCOCH_2-) of the asparaginyl α-amino side group at δ = 2.50-2.70 ppm. The rest of the signals are largely unchanged relative to (4.4). The new signals are indicative of a ring-strained cyclic product. Indeed, the δ values of the three ring protons of proposed β-lactam structure (4.21) compare favourably with those for the model compound, methyl 4(*S*)-azetidin-2-one-4-carboxylate (4.22), reported previously by Carmen[107] and given in Table 4.11.

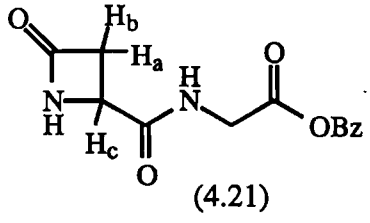

(4.21)

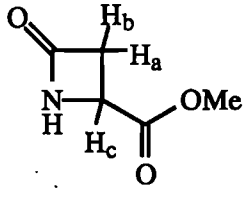

(4.22)

Table 4.11 Comparison of ^{1}H-Nmr δ Values for β-Lactam (4.21) and Methyl 4(*S*)-azetidin-2-one-4-carboxylate (4.22)

Signal	(4.21)	δ, ppm	(4.22)
H_a	3.45 (dd)		3.10 (dd)
H_b	3.62 (dd)		3.30 (dd)
H_c	4.20 (dd)		4.20 (dd)

Thus, both mass spectral and ^{1}H-nmr data are consistent with the product with R_f = 16.3 min. having structure (4.21).

Because only small amounts of products were available from the *in situ* decomposition after the hplc purification procedure, it was not possible to carry out accurate mass balances for the reactions of *L*-asparaginylglycine benzyl ester (4.4). Further, the identities of the products with R_f = 6.3 and 16.3 min. were not confirmed by independent synthesis of authentic compounds due to a lack of time. Hence, the identity of the two products inferred from the spectroscopic information awaits confirmation.

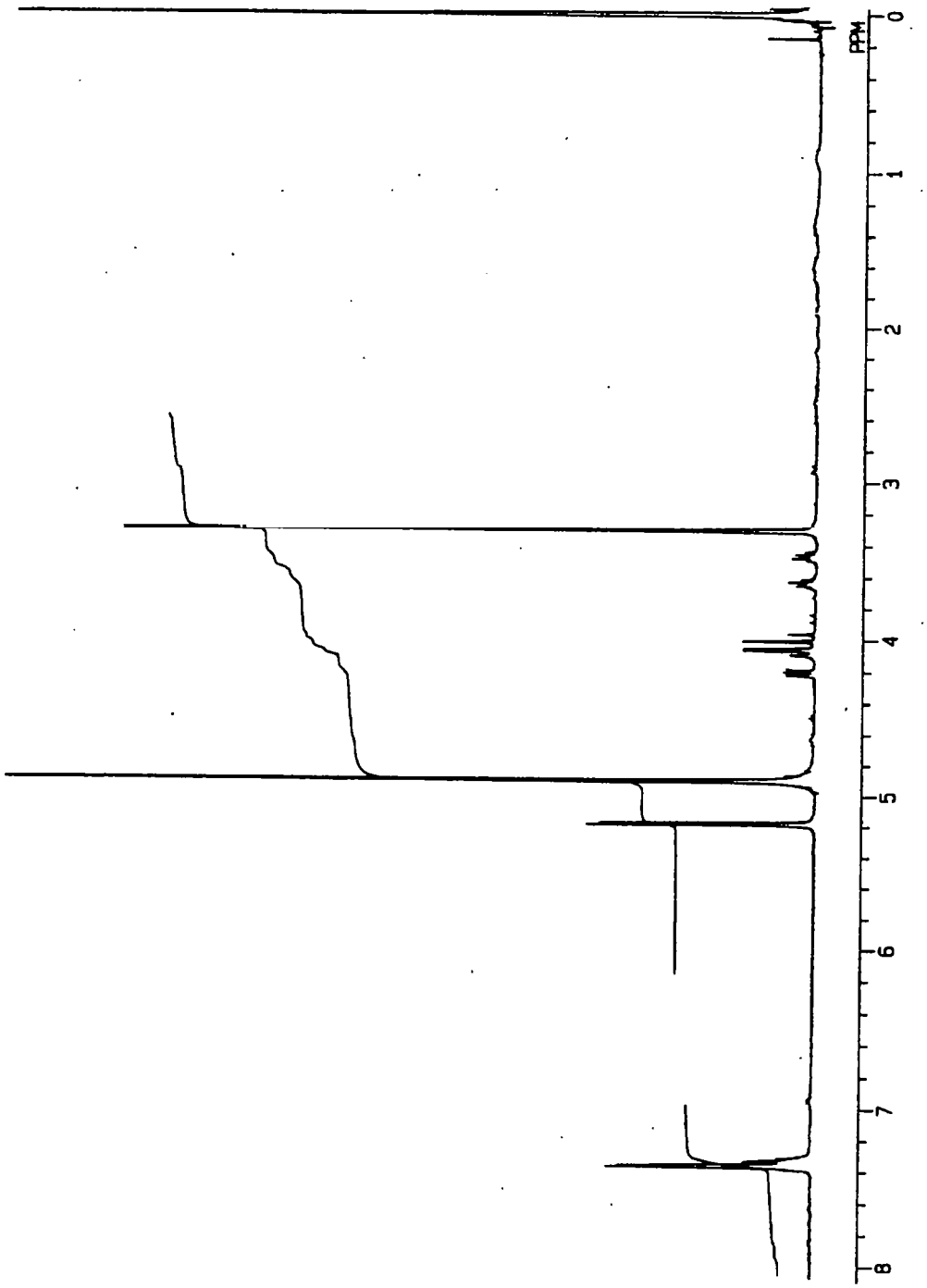

Figure 4.34 *400 MHz ^{1}H-nmr Spectrum of Product with Rf = 16.3 min.*

4.5 Summary and Discussion

The major products were identified and their yields determined for the acid-catalysed decomposition of the diazo derivatives of three non-glycyl peptides: *L*-valylglycine ethyl ester (4.2), *L*-threonylglycine ethyl ester (4.3) and *L*-asparaginylglycine benzyl ester (4.4). The reactions of all three compounds show two common characteristics:

1) Neither the structures nor yields of the major decomposition products are very dependent on the nature of the acid-catalyst or pH.

2) Iminodialkanoic acids (formed by Wolff rearrangement pathways[91, 109-111]) are not major decomposition products.

4.5.1 *N*-(2-Diazo-3-methylbutanoyl)glycine ethyl ester (2.2)

Compound (4.5) is the major (60 %) product from the acid-catalysed decomposition of *N*-(2-diazo-3-methylbutanoyl)glycine ethyl ester (2.2). The concurrent formation of isomeric products (4.6) and/or (4.7) is only revealed by spectral analysis of reaction mixtures and their combined yield is estimated as 40 %, in the absence of other products. The pathways for their formation are summarised in Scheme 4.7.

Products (4.5) and (4.6) are the expected β-elimination (*E*) and substitution (S_N) products, respectively, for decomposition with N_2 elimination of the diazonium ion (4.23). Product (4.7) probably forms *via* a 1,2 hydride shift to generate a tertiary carbocation intermediate, which then undergoes an S_N reaction with H_2O. It could also form *via* acid-catalysed addition of H_2O to (4.5), but this seemed unlikely because the yield of (4.5) is largely independent of pH. An analogous product (4.24) was previously

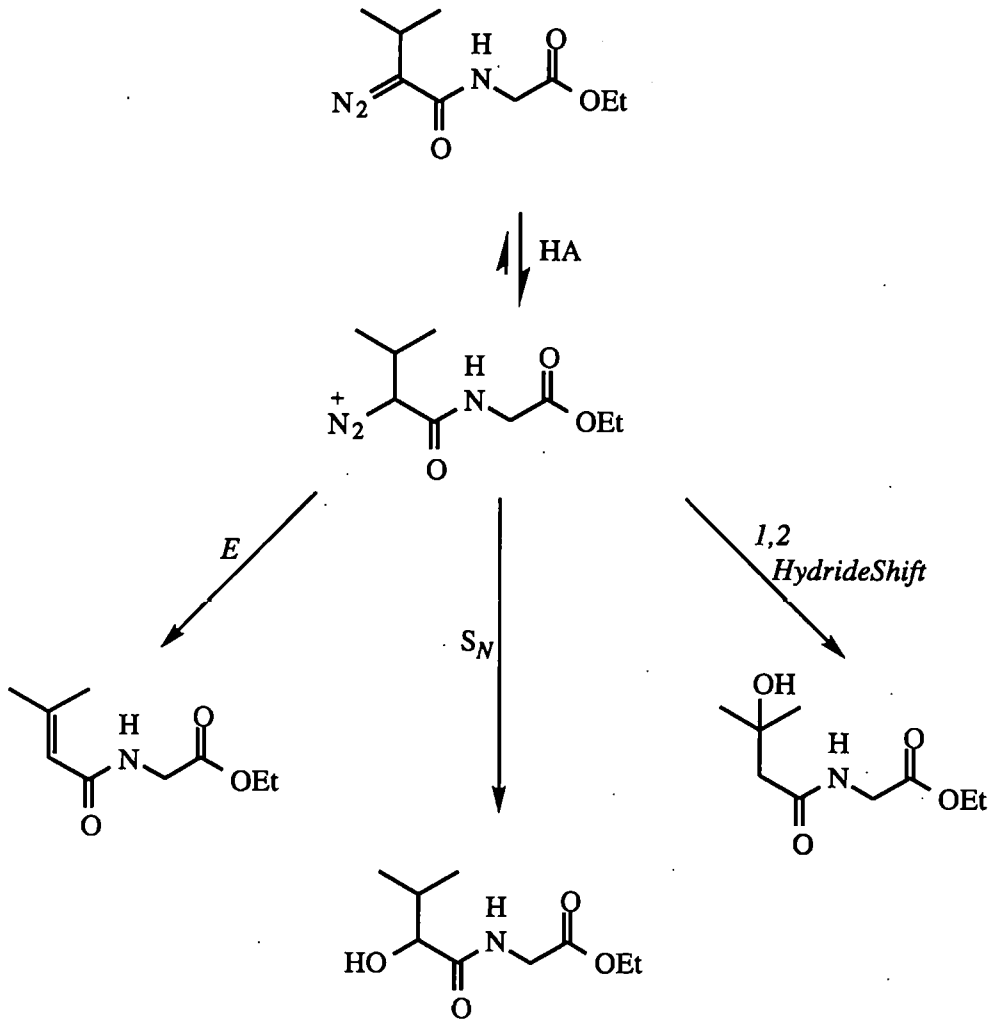

Scheme 4.7 *Major Decomposition Pathways for N-(2-Diazo-3-methylbutanoyl) glycine ethyl ester (2.2) in aq. $HClO_4$ at Ambient Temperature*

reported for the acid-catalysed decomposition of *N*-(2-diazo-4-methylpentanoyl)glycine ethyl ester.[18]

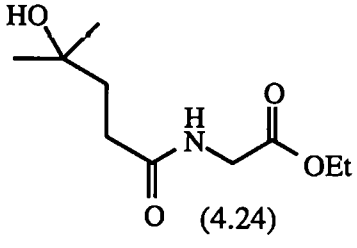

(4.24)

In principal, the isomeric products (4.6) and (4.7) could be distinguished by ^{1}H-nmr, but spectra of reaction mixtures showed the presence of (4.5) only with minor amounts of other, indistinguishable product(s) probably either (4.6) and/or (4.7). Products (4.6) and (4.7) could not be isolated by hplc, hence their concurrent formation is only inferred from the mass spectra of the reaction mixtures.

4.5.2 *N*-(2-Diazo-3-hydroxybutanoyl)glycine ethyl ester (2.1)

Compounds (4.8), (4.9) and (4.10) are unambiguously identified as the three major products from the acid-catalysed decomposition of *N*-(2-diazo-3-hydroxy-butanoyl)glycine ethyl ester (2.1), in yields of 46, 38 and 16 %, respectively. The decomposition pathways for their formation in perchloric acid at ambient temperature are summarised in Scheme 4.8.

The diazonium ion intermediate (4.25) has two chiral centres and is enantiomerically pure (the peptide was originally synthesised using the natural amino acid *L*-threonine *i.e.* 2(*S*)-amino-3(*R*)-hydroxybutanoic acid) and nucleophilic substitution by water gives rise to two pairs of diol diastereoisomers *i.e.* 2(*S*),3(*R*)-(4.8) and 2(*R*),3(*R*)-(4.8) identified by hplc and ^{1}H-nmr as the products eluting at R_f = 6.2 and 7.9 min., respectively. Hence, nucleophilic substitution of the diazonium ion (4.25) by water is non-stereoselective, resulting in an almost even distribution of stereo products (Section 4.3.4) and suggests decomposition *via* a carbocation intermediate (S_N1 like).

Compound (4.10) can form only *via* a neighbouring group interaction (*NGP*) by the HO-substituent, and is also observed in two stereoisomeric forms (*i.e. cis*- and *trans*- epoxide geometrical isomers) by hplc and ^{1}H-nmr, presumably due to the same reasons as above. The diol diastereoisomers 2(*R*),3(*S*)-(4.8) and 2(*S*),3(*S*)-(4.8) *i.e.* enantiomers of the above diols (and therefore identical by hplc and ^{1}H-nmr spectroscopy), may also form

via the acid-catalysed hydrolysis of epoxides *cis*-(4.10) and *trans*-(4.10), respectively (Scheme 4.8). Indeed, epoxide *cis*-(4.10) is shown to hydrolyse to diol 2(*R*),3(*S*)-(4.8) {Rf = 6.3 min.} in aq. $HClO_4$ by hplc (see Section 5.2.1).

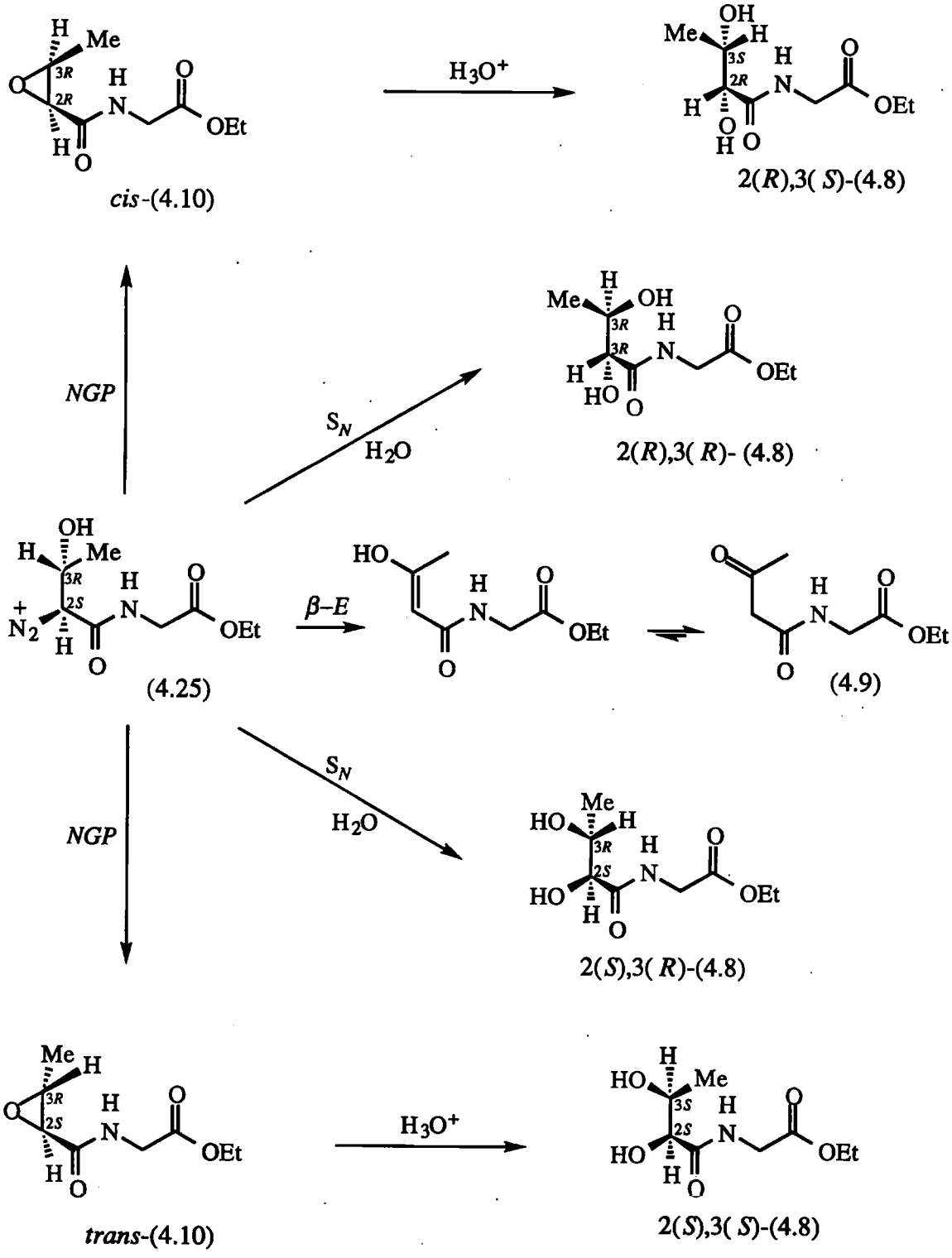

Scheme 4.8 *Major Decomposition Pathways for N-(2-Diazo-3-hydroxybutanoyl) glycine ethyl ester (2.2) in aq. $HClO_4$ at Ambient Temperature*

The major product (4.9) is achiral and therefore observed as a single isomer. Two alternative pathways for its formation seem feasible; either tautomerism of the enol β-elimination product (*PATH 1*) or a neighbouring group interaction (*NGP*) to give the epoxide (4.10) followed by a 1,2 hydride shift (*PATH 2*) {Scheme 4.9}.

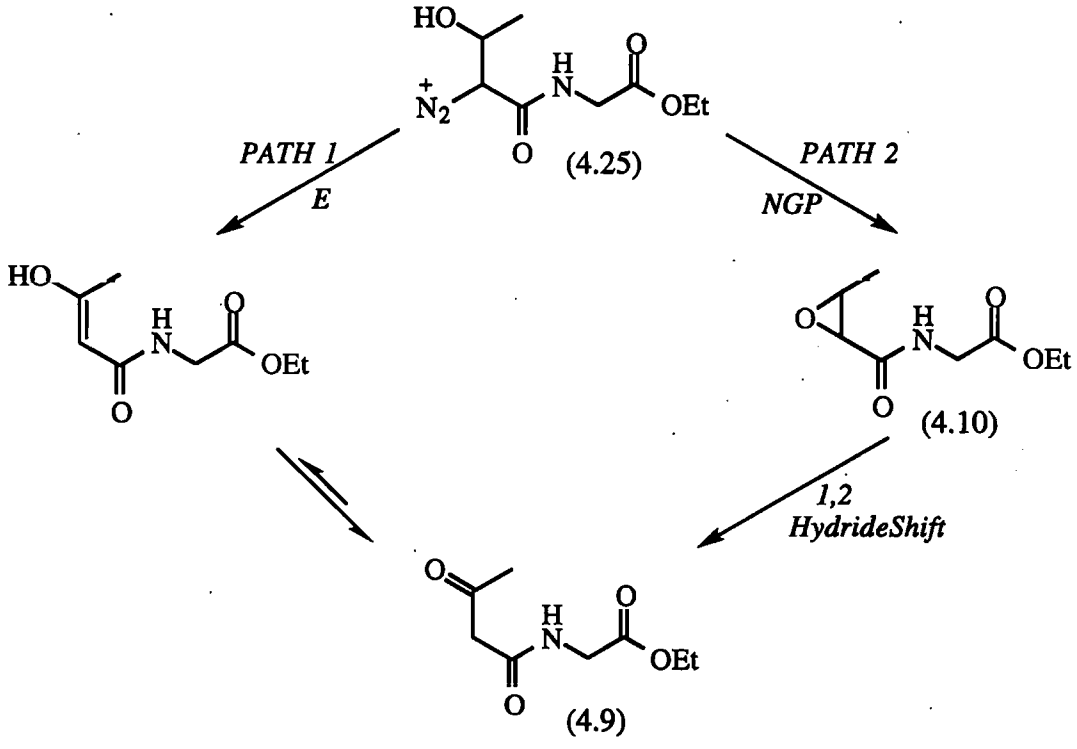

Scheme 4.9 *Possible Pathways for the formation of (4.9) via the Acid-catalysed Decomposition of (2.1)*

PATH 2 is considered unlikely, however, since decomposition of authentic *cis*-(4.10) in dilute $HClO_4$ gives only diol 2(*S*),3(*R*)-(4.8) and no ketone (4.9) {see Section 5.2.1}. Most of the diol products must arrive *via* hydrolysis of the diazopeptide rather than the epoxides. Although the latter reaction may occur in principle, independent measurements show that the hydrolysis of authentic *cis*-(4.10) in $HClO_4$ to form diol 2(*R*),3(*S*)-(4.8) is relatively slow (*i.e.* k_1 *ca.* $4 \times 10^{-4}\ M^{-1}s^{-1}$) at 37 °C (see Section 5.2.1). This conclusion is supported by the relatively constant amount of epoxide products (*ca.* 20 %), irrespective of the pH of the reaction solution (Table 4.7).

4.5.3 *N*-(2-Diazo-3-carbamoylpropanoyl)glycine benzyl ester (4.1)

Compounds (4.19) and (4.21) are identified as products from the *in situ* decomposition of *N*-(2-diazo-3-carbamoylpropanoyl)glycine benzyl ester (4.1) in organic solvent.

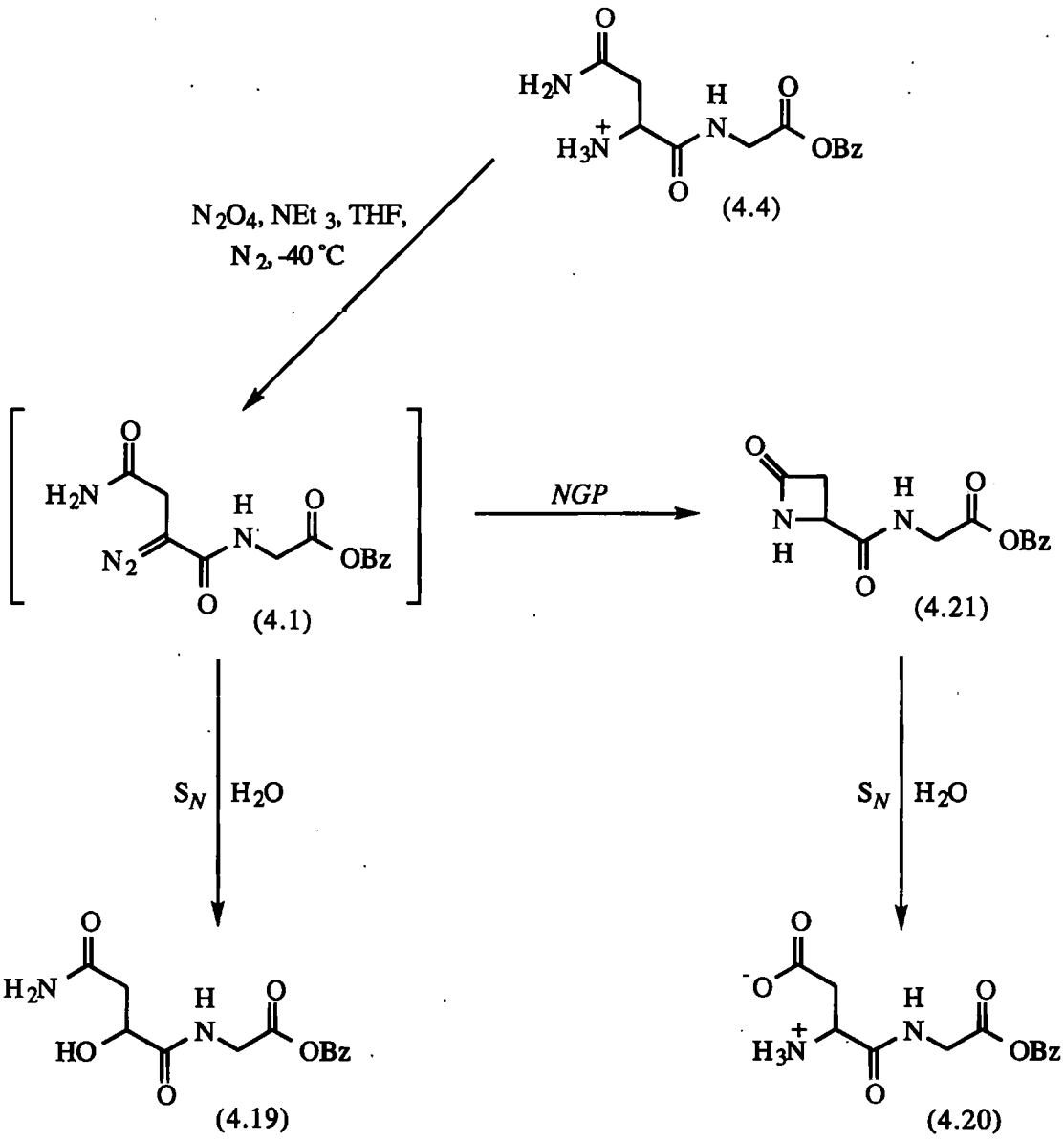

Scheme 4.10 *Decomposition Pathways for N-(2-Diazo-3-carbamoylpropanoyl)glycine benzyl ester (4.1) in Non-Aqueous Solvent at Ambient Temperature*

The major product appears to be the β-lactam (4.21) formed by an *NGP* interaction of the amide side-chain with the diazo reactant. Products resulting from β-elimination of the

diazo substrate are either not formed or not observed by the hplc assay. The other product with R_f = 6.3 min. can be explained by either intermolecular nucleophilic trapping of the diazonium ion by water to form compound (4.19), or the subsequent hydrolysis of the β-lactam (4.21) to form the aspartic acid derivative (4.20). The spectroscopic data is more consistent with the first of these pathways. The products and potential formation pathways are summarised in Scheme 4.10.

As the *in situ* decomposition of the diazopeptide proceeds in what is believed to be non-acidic aprotic media, intramolecular H^+-transfer from the carboxamide substituent may generate an amide anion and the diazonium cation, with subsequent ring-closure to form the β-lactam (4.21) as shown in Scheme 4.11.

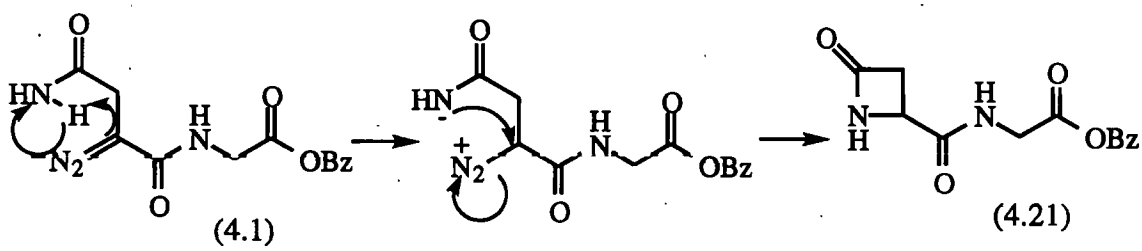

Scheme 4.11

The major product from the *in situ* decomposition of *N*-(2-diazo-3-carbamoylpropanoyl)glycine benzyl ester (4.1) appears to be the β-lactam (4.21) from the hplc peak height and mass recovery, although no mass balance is available from the present work. β-Lactam (4.21) may form in quantitative yield bearing in mind that the only other product detected {either (4.19) or (4.20)} requires reaction with water. This side reaction could be avoided by better exclusion of water, and further investigation into this potentially useful method of obtaining β-lactams from peptide precursors is desirable.

In summary, the decomposition products from the diazo derivatives of non-glycyl peptides are characteristic ones involving substitution (S_N), β-elimination (*E*) and neighbouring group (*NGP*) transformations of a carbocation (diazonium ion) intermediate. Neither the type of products formed nor their yields vary significantly with the reaction conditions (e.g. pH, Cl^-, AcO^-, $HCOO^-$) in aqueous buffer solutions. Hence, the products are largely independent of the type and concentration of the acid used and the pH, which is more consistent with decomposition *via* unimolecular pathways. Because product formation is post rate-limiting, little can be deduced about the mechanism(s) of these steps. The variety of products, however, suggests that the diazonium ion intermediates are very reactive.

5. Reactions of *cis*-*N*-(2,3-Epoxybutanoyl)glycine ethyl ester (4.10) and *cis*-2,3-Epoxybutanamide (4.15)

5.1 Introduction

As reported in Chapter 4, epoxides (4.10) and (4.14) are produced by the acid-catalysed decomposition of *N*-(2-diazo-3-hydroxybutanoyl)glycine ethyl ester (2.1) and *N*-(2-diazo-3-hydroxypropanoyl)glycine ethyl ester (2.3), respectively.

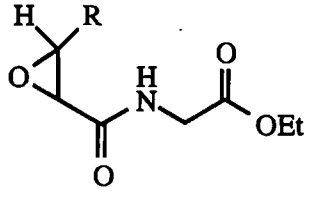

For (4.10) R = CH_3

For (4.14) R = H

It follows that similar epoxides may form when dietary peptides containing terminal primary α-amino threonine and serine residues are nitrosated under gastric conditions (Scheme 5.1). Since some epoxides are cytotoxic, carcinogenic and mutagenic,[129-131] their formation as decomposition products may be relevant to the cytotoxicity of diazopeptides.

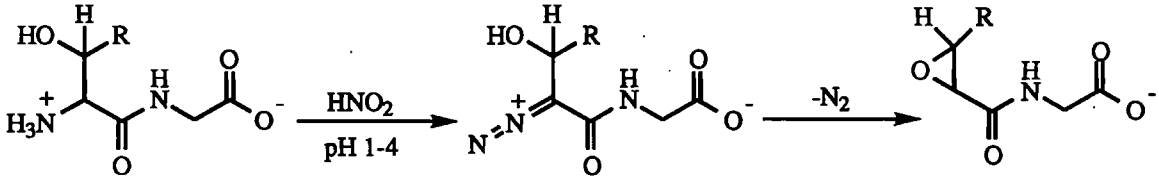

Scheme 5.1

The work below was directed towards the stability of epoxide *cis*-(4.10) and its behaviour as an alkylating agent.

5.2 Hydrolysis of Epoxides *cis*-*N*-(2,3-Epoxybutanoyl)glycine ethyl ester (4.10) and *cis*-2,3-Epoxybutanamide (4.15)

The decomposition kinetics of epoxide *cis*-(4.10), was briefly examined in aqueous $HClO_4$ at 37 °C to assess its stability and potential survival in the gastric tract for

subsequent absorption into the bloodstream. In basic media (pH > 8), however, hydrolysis of the epoxide ring of *cis*-(4.10) was complicated by the much faster competing hydrolysis of the ester moiety (k_2 *ca.* 4.4 M^{-1} s^{-1} at 37 °C[107]) {Scheme 5.2}. Hence, *cis*-2,3 epoxybutanamide (4.15) was examined as a model for (4.10) where competing hydrolysis should be less significant than epoxide hydrolysis.

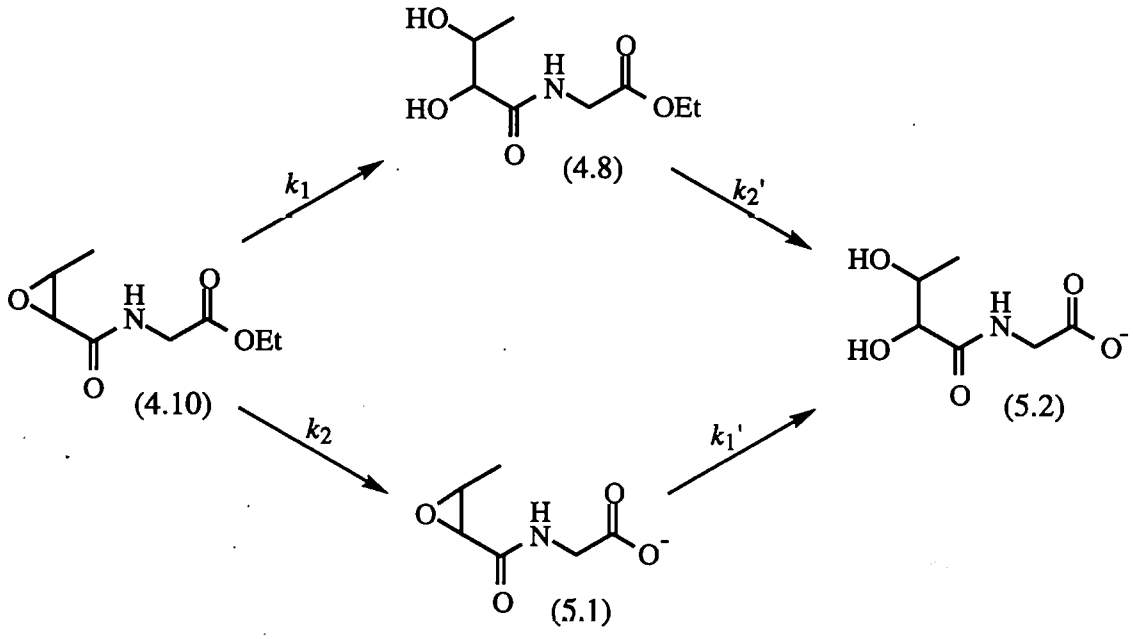

Scheme 5.2 *Alternative Pathways for the Hydrolysis of (4.10)*

Preliminary studies with epoxide *cis*-(4.10) indicated that pathway k_2 was much slower than k_1 in acidic media because diol 2(*R*),3(*S*)-(4.8) was the only product detected from the decomposition of *cis*-(4.10) in dilute $HClO_4$ at 37 °C by analytical hplc and 400 MHz ^{1}H-nmr, with no evidence for formation of (5.1) or (5.2) after complete loss of epoxide *cis*-(4.10). Hence, the hydrolysis kinetics of epoxide *cis*-(4.10) was examined in acidic media. Product studies were carried out for epoxide *cis*-(4.15) in acidic and basic media, and both kinetic and product studies were carried out for the decomposition of epoxide *cis*-(4.15) in aqueous morpholine to assess its alkylating ability towards N-bases.

The decomposition of *cis*-(4.10) and *cis*-(4.15) in all media followed *pseudo* first-order kinetics (Equation 5.1).

Rate = k_o [(4.10) or (4.15)] (5.1)

5.2.1 Hydrolysis of *cis*-(4.10) and (4.14) in Dilute $HClO_4$

Pseudo first-order rate coefficients k_o were determined from the loss of *cis*-(4.10) using the analytical hplc procedure described in Section 7.3.2. Plots of ln (H) *vs.* time {where H is the peak height of *cis*-(4.10)} showed good linearity, as exemplified by Figure 5.1 for the hydrolysis of epoxide *cis*-(4.10) {R_f = 12.7 min.} to diol 2(*S*),3(*R*)-(4.8) {R_f = 6.2 min.} in 0.1 M $HClO_4$ at 37 °C. A typical hplc chromatogram is shown as Figure 5.2. The first-order plots were linear over at least 3 half-lives and several reactions were monitored to *ca.* 10 half-lives (infinity) by which time *cis*-(4.10) was undetectable by hplc. As shown in Table 5.1, values of k_o increase with increasing acidity.

Figure 5.1 *First-Order Plot for the Decomposition of cis-N-(2,3-Epoxybutanoyl) glycine ethyl ester (4.10) in 0.1 M $HClO_4$ at 37 °C*

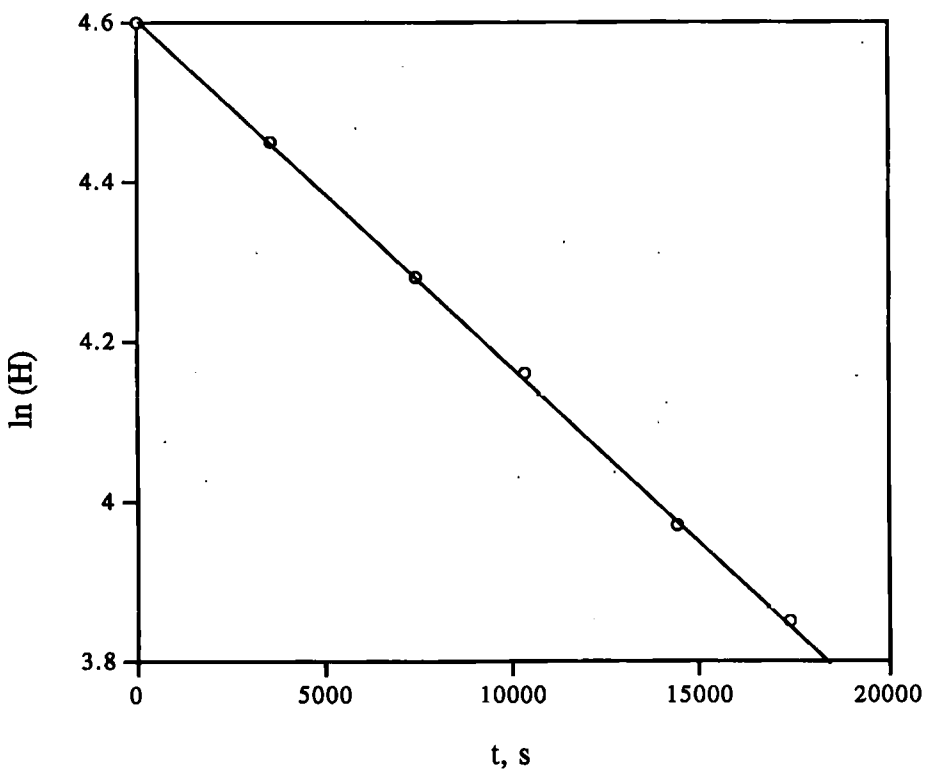

Figure 5.2

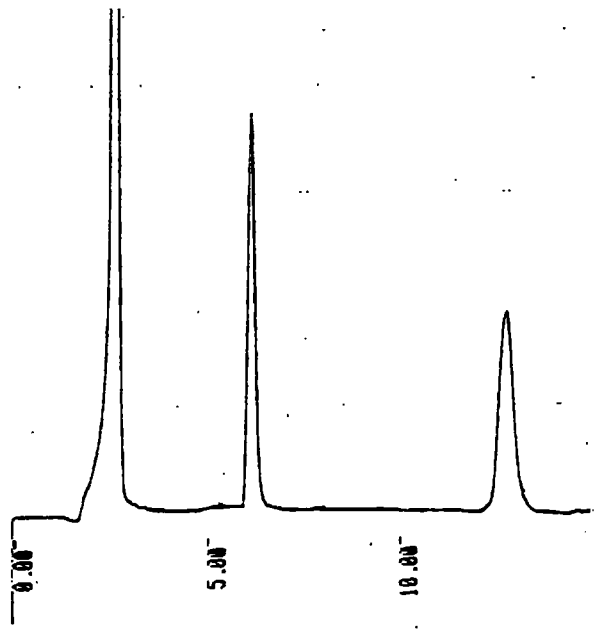

Table 5.1 Variation of the *Pseudo* First-Order Rate Coefficient k_o with [$HClO_4$] for the Hydrolysis of *cis*-*N*-(2,3-Epoxybutanoyl)glycine ethyl ester (4.10) in aqueous Perchloric acid at 37 (± 0.1) °C; Initial [(4.10)] *ca.* 10^{-4} M

[$HClO_4$], M	k_o, 10^{-5}, s^{-1}
0.05	2.45
0.10	4.05
0.15	6.20
0.20	7.58
0.30	12.85
0.50	19.33

The plot of k_o *vs.* [$HClO_4$] showed good linearity (Figure 5.3) and its slope gives a value of $k_1 = 4.02 \times 10^{-4}\ M^{-1}s^{-1}$ at 37 °C.

Figure 5.3 *Second-Order Plot for the Decomposition of cis-N-(2,3-Epoxybutanoyl)glycine ethyl ester (4.10) in $HClO_4$ at 37 °C*

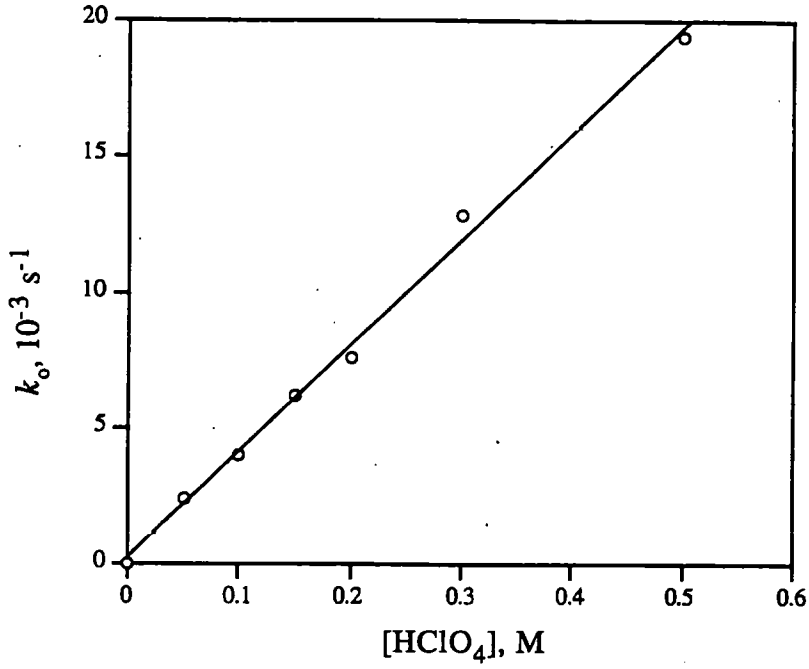

The rate of hydrolysis of epoxide (4.14) was briefly examined for comparative purposes using the method described above. A typical hplc chromatogram for the hydrolysis of epoxide (4.14) {R_f = 8.0 min.} to diol (1.32) {R_f = 5.1 min.} in 0.1 M $HClO_4$ is shown as Figure 5.4. The hydrolysis of epoxide (4.14) in 0.1 M $HClO_4$ at 37 °C gave a linear plot of ln (H) *vs*. time {where H is the peak height of (4.14)}, a value for $k_o = 1.27 \times 10^{-5}\ s^{-1}$ and hence a value for $k_1 = 1.27 \times 10^{-4}\ M^{-1}\ s^{-1}$ at 37 °C. Thus, the hydrolysis of epoxide (4.14) is *ca*. 3-fold faster than epoxide *cis*-(4.10).

Figure 5.4

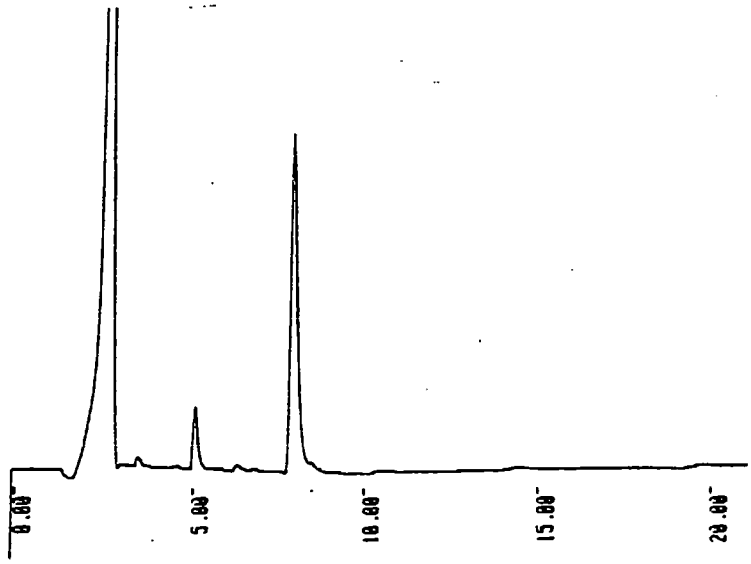

5.2.2 Hydrolysis of Epoxide *cis*-(4.15) in Dilute NaOD

The *pseudo* first-order rate coefficients (k_o) were determined from the loss of epoxide *cis*-(4.15) using the ^{1}H-nmr procedure described in Section 7.3.3.1. Plots of ln (I) *vs.* time {where I is the nmr integral of *cis*-(4.15)} showed good linearity, as exemplified in Figure 5.5 for the reaction of *cis*-(4.15) in 0.3 M NaOD at 37 °C. A typical 400 MHz ^{1}H-nmr spectrum for the reaction after 7 h., showing loss of *cis*-(4.15) and the formation of a product with signals at δ = 1.28, 3.35 and 3.54 ppm, is shown as Figure 5.6.

Figure 5.5 *First-Order Plot for the Decomposition of cis-2,3-Epoxybutanamide (4.15) in 0.3 M NaOD in D_2O at 37 °C*

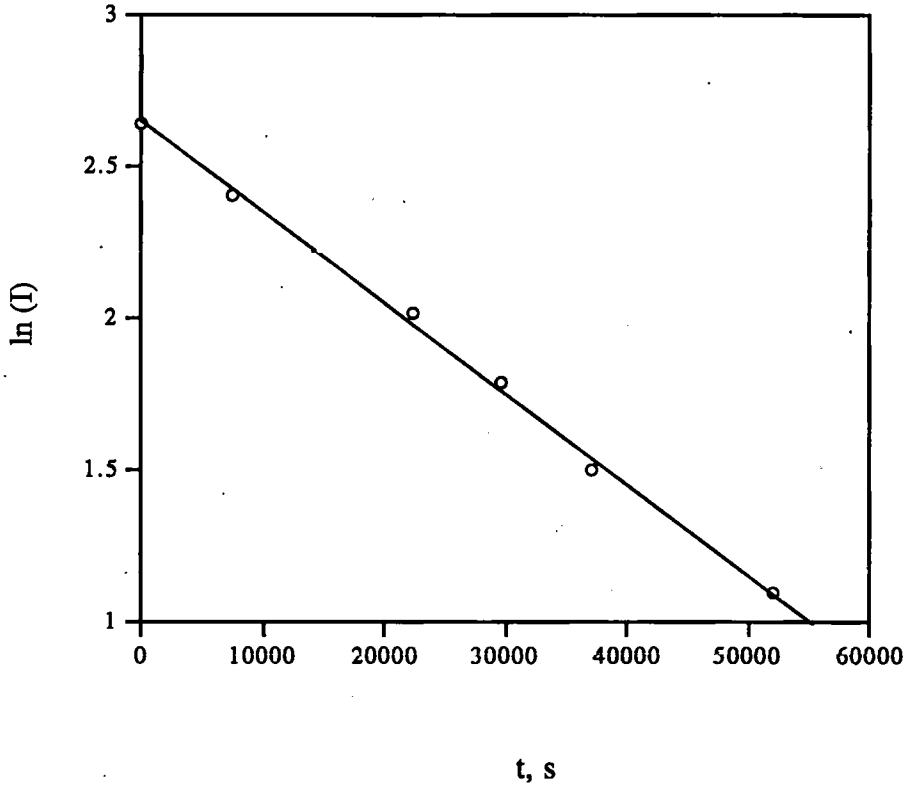

The first-order plots were linear over at least 3 half-lives, and several reactions were monitored to *ca.* 10 half-lives by which time *cis*-(4.15) was unobservable by ^{1}H-nmr. Values of k_o in Table 5.2 increase with increasing [NaOD].

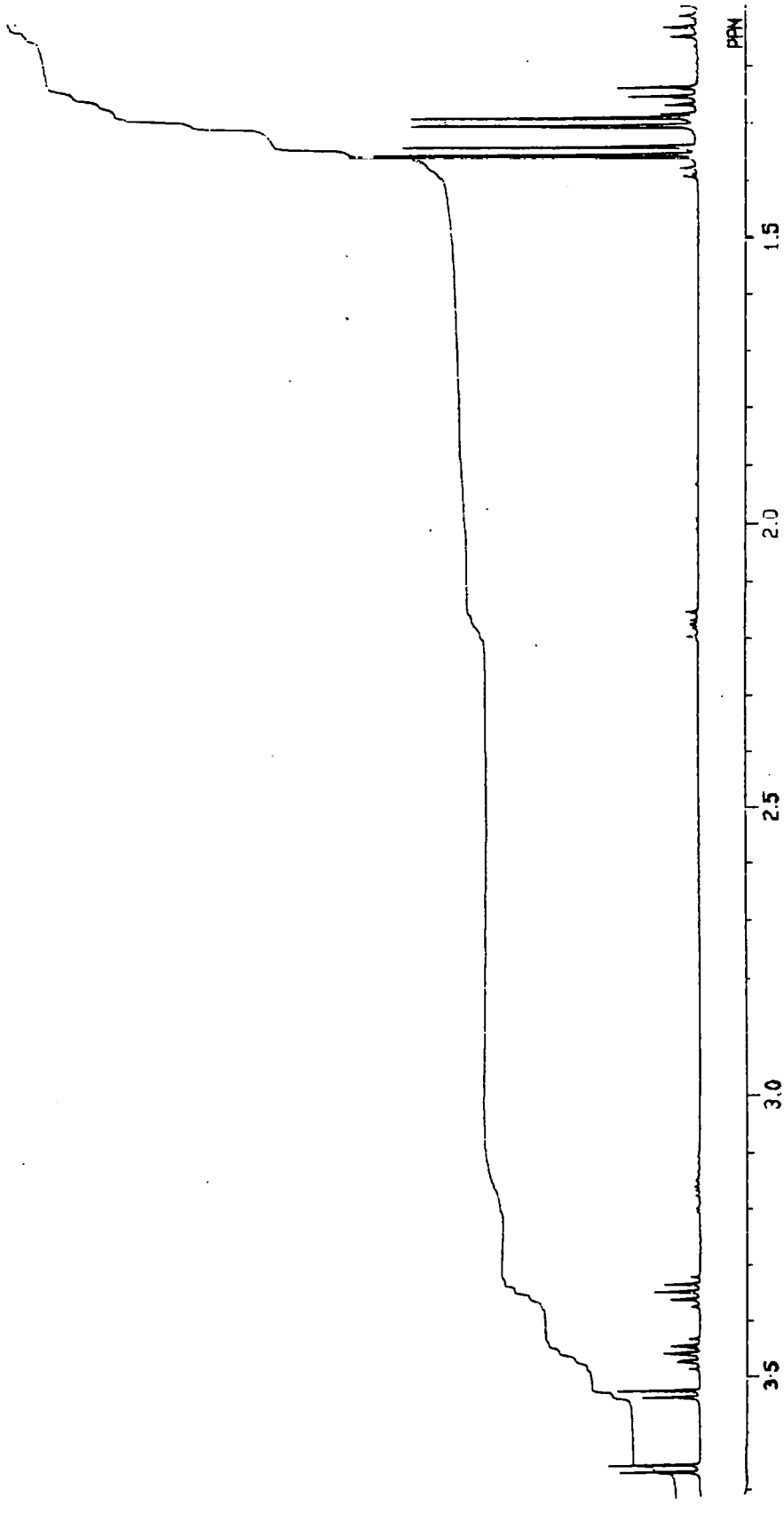

Figure 5.6 *400 MHz ^{1}H-nmr Spectrum of cis-(4.10) in 0.3 M NaOD After 7 h. at 37 °C in D_2O*

Table 5.2 Variation of the *Pseudo* First-Order Rate Coefficient k_o with [NaOD] for the Hydrolysis of *cis*-2,3-Epoxybutanamide (4.15) in D_2O at 37 (± 0.1) °C; Initial [(4.15)] *ca.* 10^{-3} M

[NaOD], M	k_o, 10^{-5} s^{-1}
0.05	0.50
0.30	2.70
0.50	5.50
0.80	9.30

The plot of k_o *vs.* [NaOD] is linear (Figure 5.7) and its slope gives a value of 1.13×10^{-4} $M^{-1}s^{-1}$ for the second-order rate coefficient.

Figure 5.7 *Second-Order Plot for the Decomposition of cis-2,3-Epoxybutanamide (4.15) in NaOD in D_2O at 37 °C*

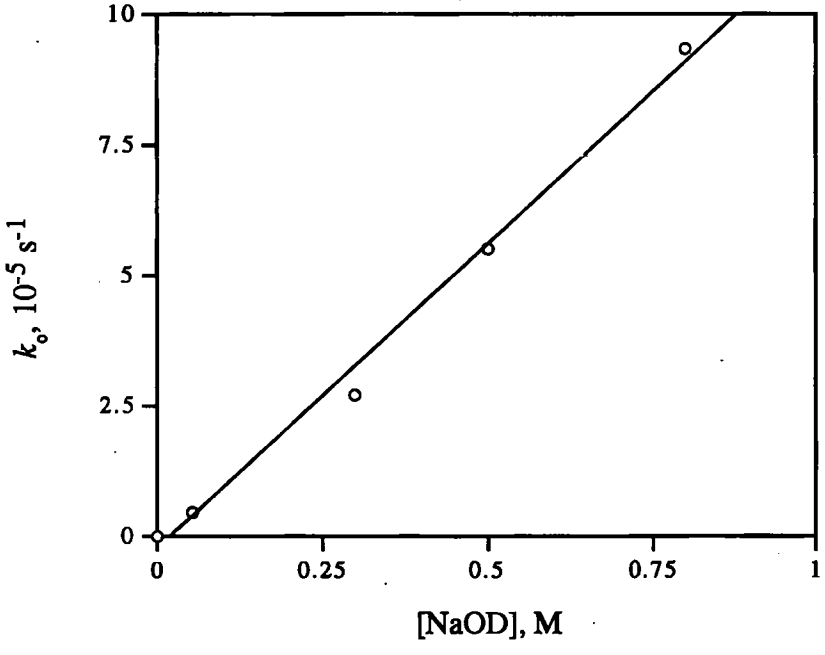

5.2.3 Reaction of Epoxide *cis*-(4.15) in Aqueous Morpholine

Values of k_o were determined from the loss of *cis*-(4.15) {R_f = 4.8 min.} using the analytical hplc procedure described in Section 7.3.3.2. First-order plots of ln (H) *vs.* time

{where H is the peak height of *cis*-(4.15)} showed good linearity as exemplified by Figure 5.8 for the reaction of *cis*-(4.15) in 0.2 M morpholine at pH 10.9 (± 0.2) and 37 °C. A typical hplc chromatogram for the reaction is shown as Figure 5.9. The first-order plots were linear over at least 3 half-lives and several reactions were monitored to *ca.* 10 half-lives by which time *cis*-(4.15) was undetectable by hplc. Values of k_o in Table 5.3 increase with increasing [morpholine].

Figure 5.8 *First-Order Plot for the Decomposition of cis-2,3-Epoxybutanamide in 0.2 M Aqueous Morpholine at pH 10.9 and 37 °C; Initial [cis-(4.15)] ca. 10^{-4} M*

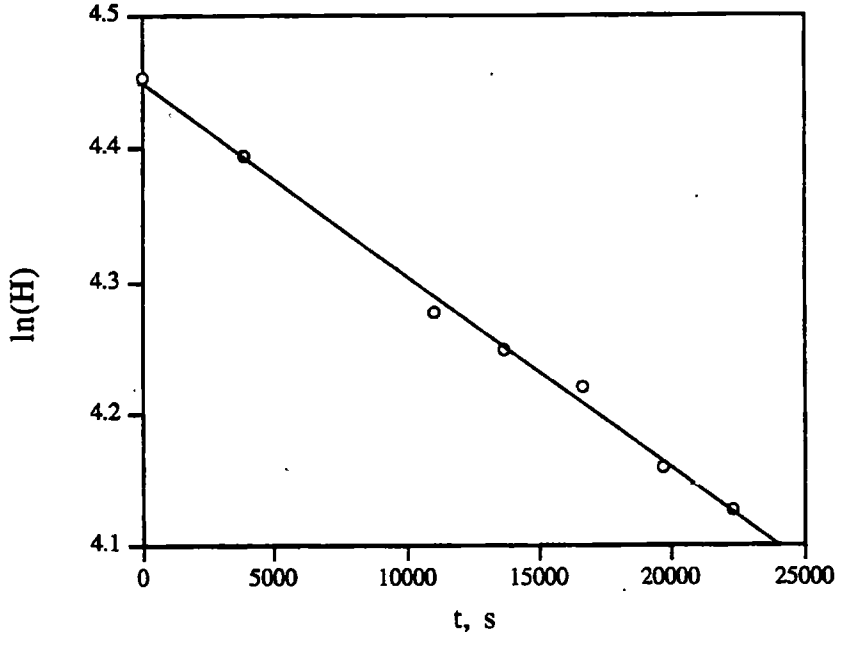

Figure 5.9

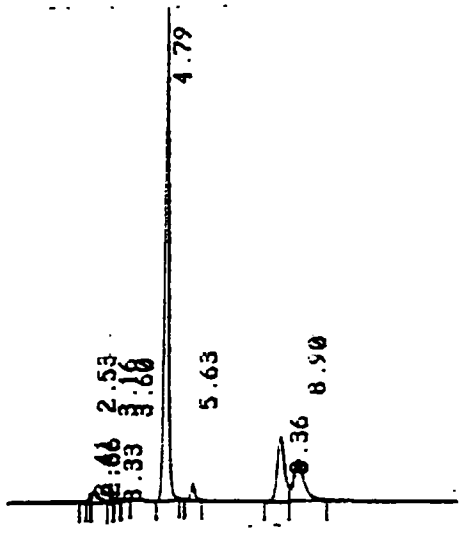

Table 5.3 Variation of the *Pseudo* First-Order Rate Coefficient k_o with [Morpholine] for reaction with *cis*-2,3-Epoxybutanamide (4.15) at pH 10.9 (± 0.25) and 37 (± 0.1) °C; Initial [(4.15)] *ca.* 10^{-4} M

[Morpholine], M	k_o, 10^{-5} s^{-1}
0.05	0.54
0.20	1.46
0.25	2.00
0.30	2.50
0.40	3.27
0.50	4.10

The plot of k_o *vs.* [morpholine] shows good linearity (Figure 5.10) and gives a value for the second-order rate coefficient $k_2 = 8.30 \times 10^{-5}$ $M^{-1}s^{-1}$.

Figure 5.10 *Second-Order Plot for the Decomposition of cis 2,3 Epoxybutanamide(4.15) in aqueous Morpholine at pH 10.9 and 37 °C*

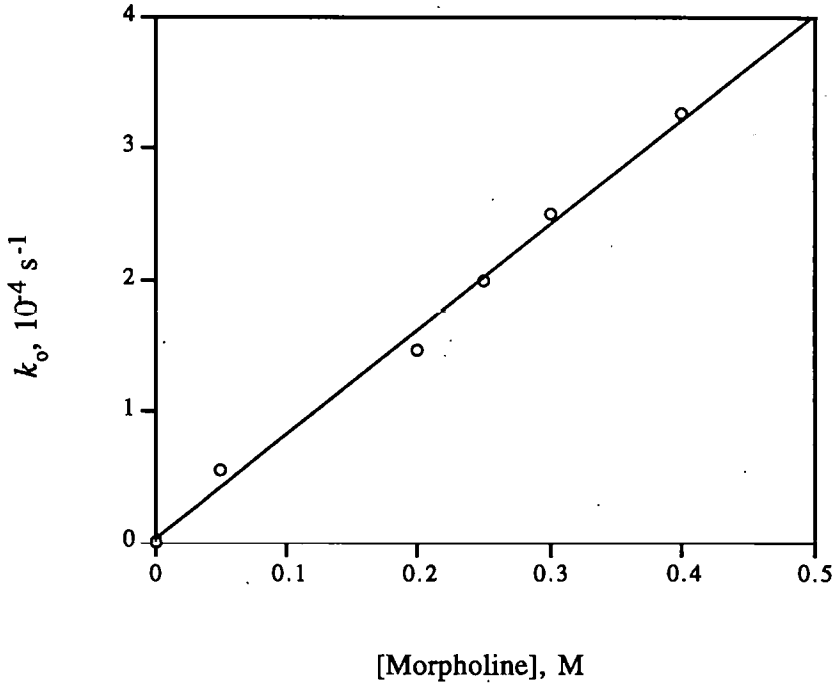

5.3 Product Studies

The products from the decomposition of *cis*-2,3-epoxybutanamide (4.15) in 0.1 M $HClO_4$, 1.0 M NaOD and 0.1 M aq. morpholine were examined by FAB m/s and 400 MHz ^{1}H-nmr spectroscopy (see Section 7.4.2). This work was carried out first because the structural simplicity of *cis*-(4.15) facilitated the ^{1}H-nmr interpretation. Unfortunately insufficient time was available to complete a similar study on *cis*-(4.10) although analogous products may be expected.

5.3.1 Decomposition of *cis*-(4.15) in Dilute $HClO_4$

As described in Section 5.2.1, *cis*-(4.15) was decomposed in 0.1M $HClO_4$ at 37 °C for 5 h. After neutralisation and freeze-drying, the white solid residue (mainly sodium perchlorate) was extracted with ethyl acetate. After evaporation of the solvent, the white solid residue was examined by FAB m/s. The FAB mass spectrum (shown as Figure 5.11) shows intense ions at m/z = 102 and m/z = 120 in the positive mode. These correspond to the MH^+ ions of (4.15) and diol product (5.3), respectively. Further the $M\text{-}H^+$ ions of (4.15) and (5.3) at m/z = 100 and 118, respectively, are the strongest signals in the negative mode mass spectrum.

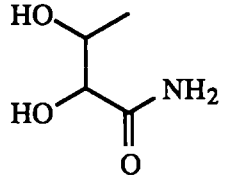

(5.3)

The decomposition of *cis*-(4.15) in 0.1M $DClO_4$ at 37 °C was monitored by 400 MHz ^{1}H-nmr and the spectra at t = 0, 2h., and 2 d. are shown as Figures 5.12a-c, respectively. These spectra clearly show the disappearance of the epoxide reactant with concurrent

Figure 5.11 *FAB Mass Spectrum of Products from the Reaction of cis-(4.15) in 0.1 M $HClO_4$ After 5 h.*

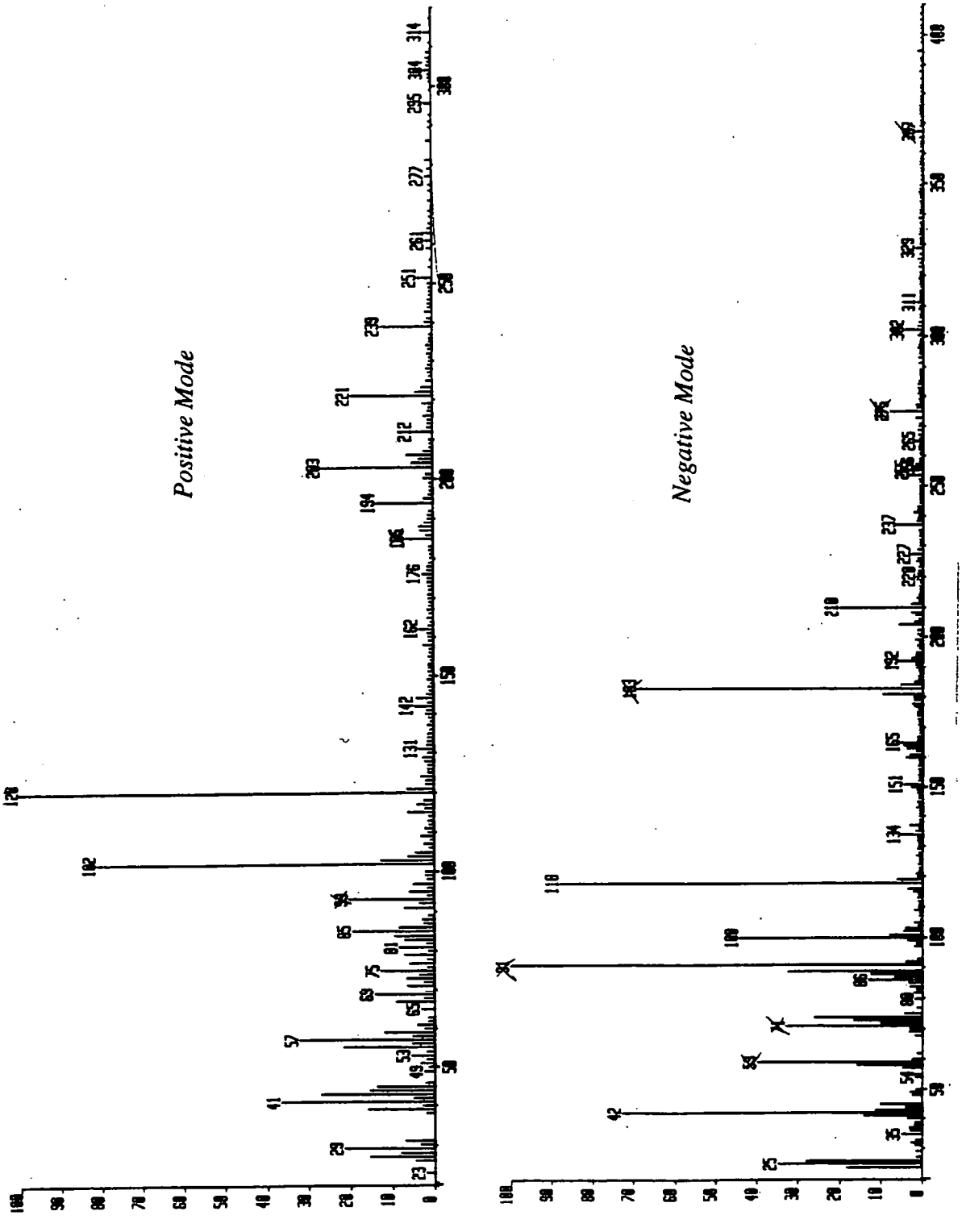

Figure 5.12a *400 MHz ^{1}H-nmr Spectrum of cis-(4.15) in 0.1 M $DClO_4$ in D_2O at 37 °C: At t = 0*

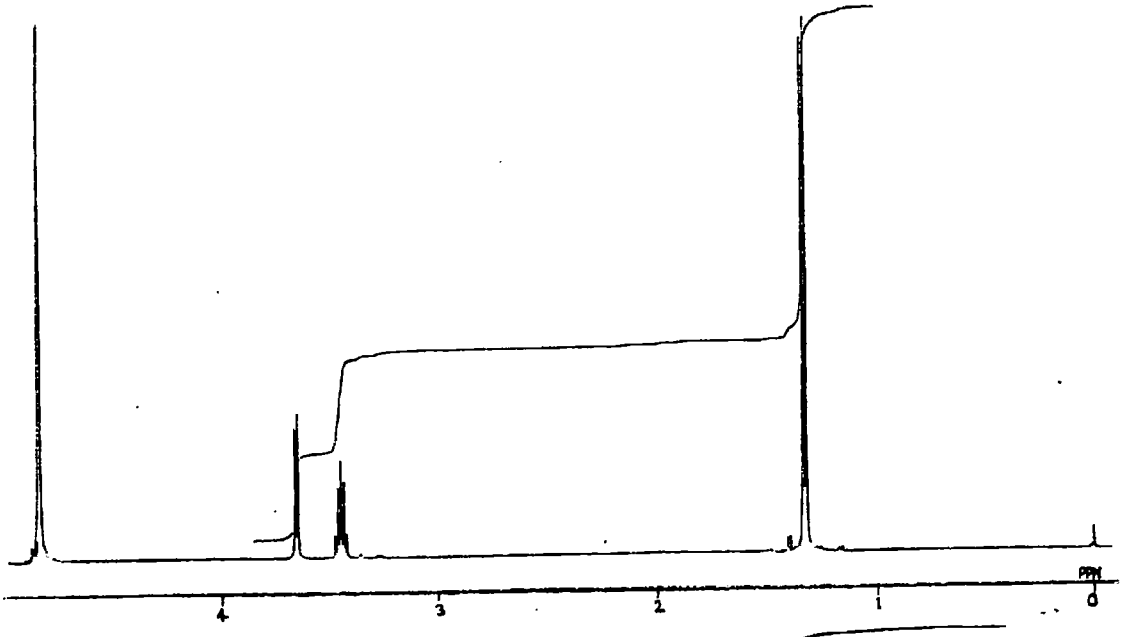

Figure 5.12b *After 2 h.*

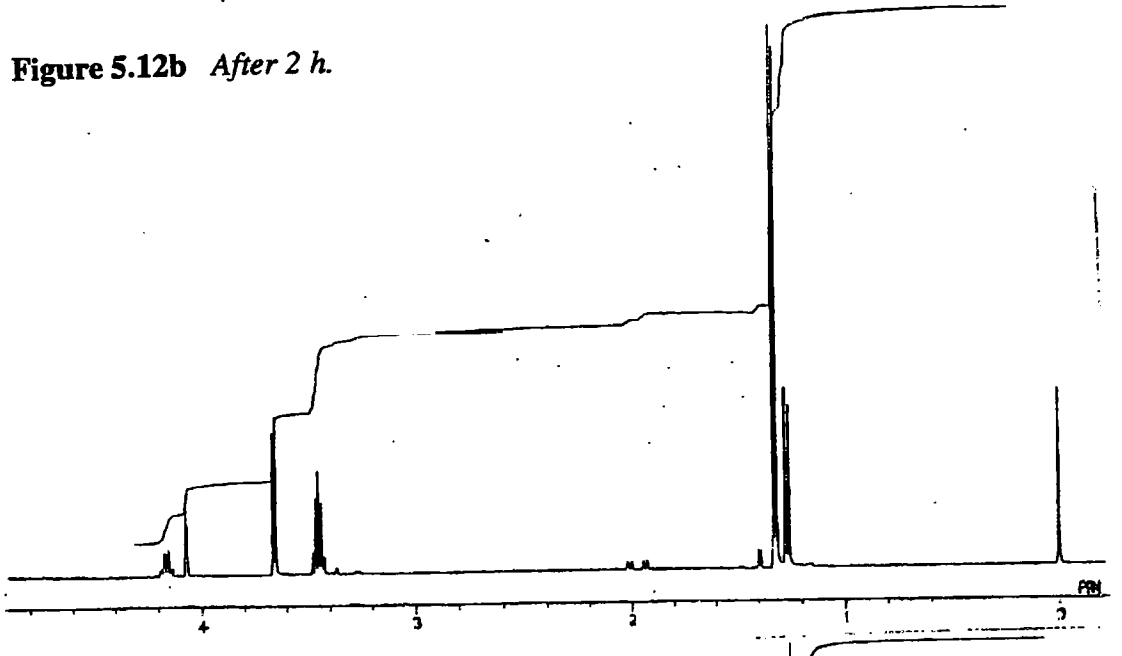

Figure 5.12c *After 2 d.*

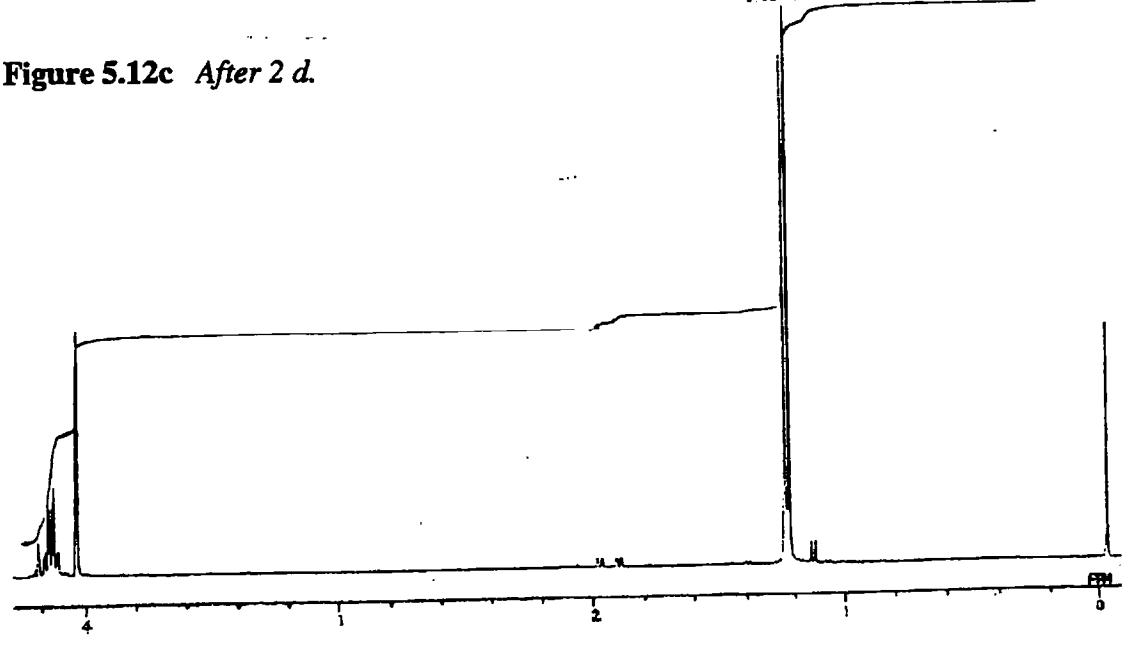

formation of new signals from a single, major product. The ^{1}H-nmr parameters are summarised in Table 5.4 and are entirely consistent with (5.3) as the major product. In particular, the chemical shifts for the two -CH resonances of diol product (5.3) {δ = 4.17, and 4.07} are more deshielded than the two -CH resonances of epoxide *cis*-(4.15) {δ = 3.43 and 3.36 ppm}, by the two adjacent hydroxyl groups.

Table 5.4 400 MHz ^{1}H-nmr Data for (5.3) in 0.1 M $DClO_4$

Assignment	δ, ppm	m	J, Hz
-CH(C*H*$_3$)OH	1.26	d	6.0
H_2NOC-C*H*OH-CH-	4.07	d	2.4
-CH-C*H*OH(CH_3)	4.17	m	

5.3.2 Decomposition of *cis*-(4.15) in Dilute NaOH

From the results in Section 5.2.2, the approximate $t_{1/2}$ for the decomposition of *cis*-(4.15) in 1 M NaOD at 37 °C is 5 h. The 400 MHz ^{1}H-nmr spectra of these reactions at t = 0, 2.5 h., 1 d. and 10 d. are shown as Figures 5.13a-d, respectively. The ^{1}H-nmr parameters of the reactant and products, summarised in Table 5.5, show that epoxide *cis*-(4.15) reacts to form an intermediate product B with signals at δ =1.28, 3.36, and 3.54 ppm as reported in Section 5.2.2. Figure 5.13d shows prolonged incubation of the solution over 10 d. produces a second product C with signals at δ = 1.21, 3.81 and 4.00 ppm and diminution of the signals due to intermediate B. Thus, the decomposition of *cis*-(4.15) in NaOD must be a two step process probably involving sequential hydrolysis of the oxirane ring and the amide group. Two pathways are therefore possible, both producing (5.5) as the final product (Scheme 5.3), and depending on the relative rates for k_1 and k_2, the intermediate (B) must be either (5.3) or (5.4).

Figure 5.13a *400 MHz ^{1}H-nmr Spectrum of cis-(4.15) in 1.0 M NaOD in D_2O at 37 °C: At t = 0*

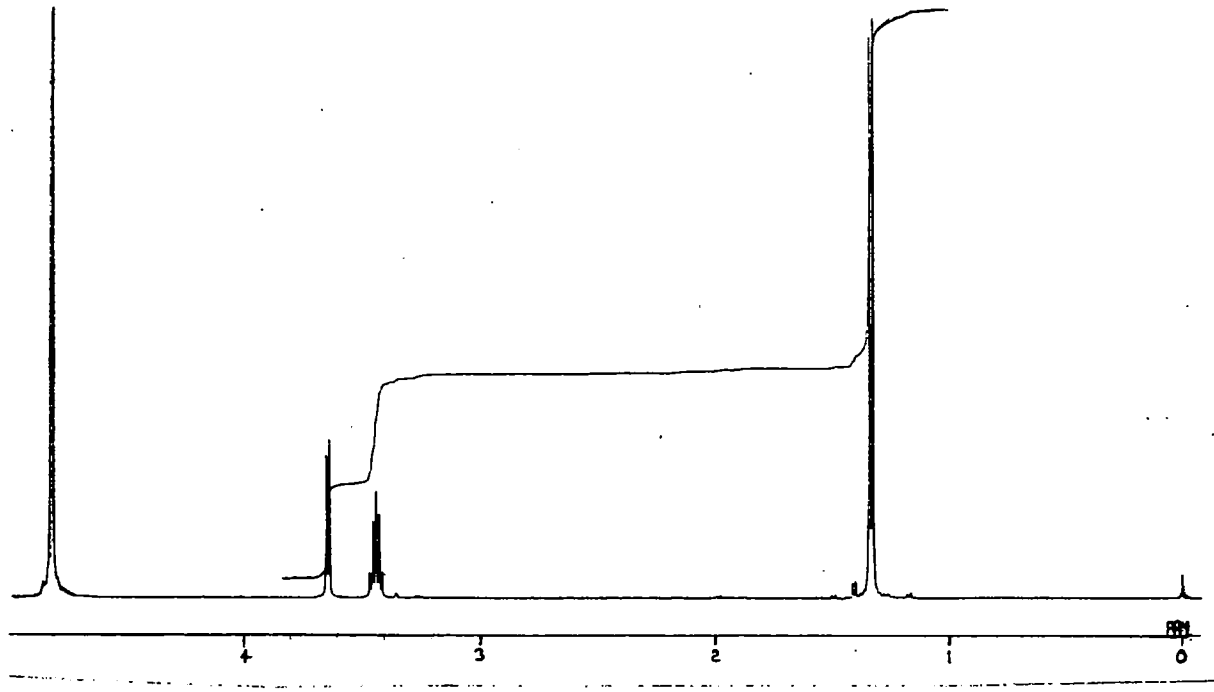

Figure 5.13b *After 2.5 h.*

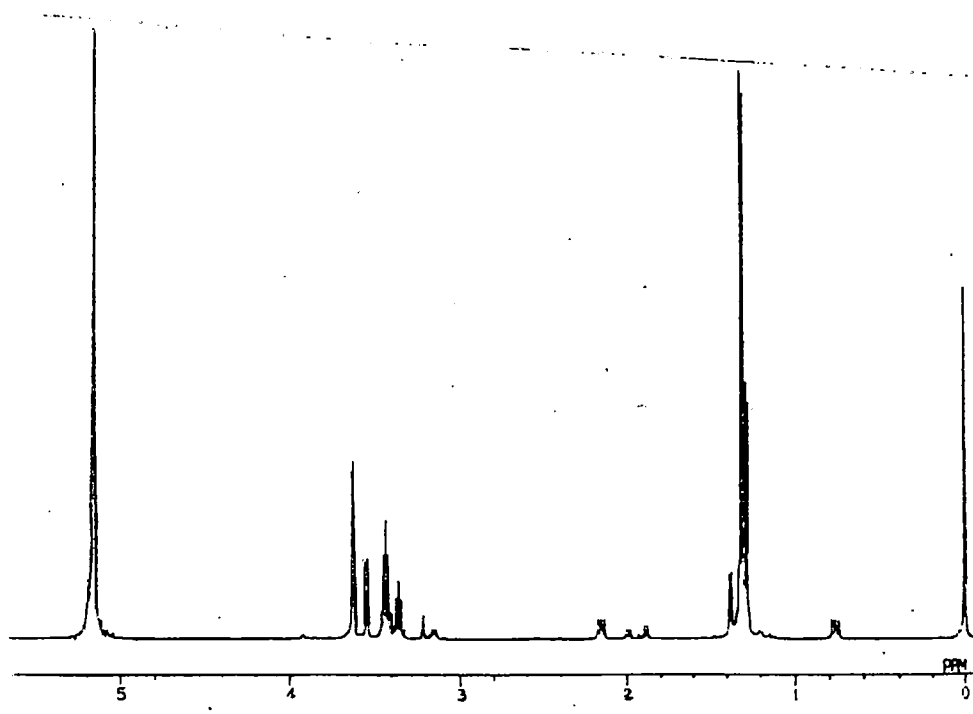

Figure 5.13c *After 1 d.*

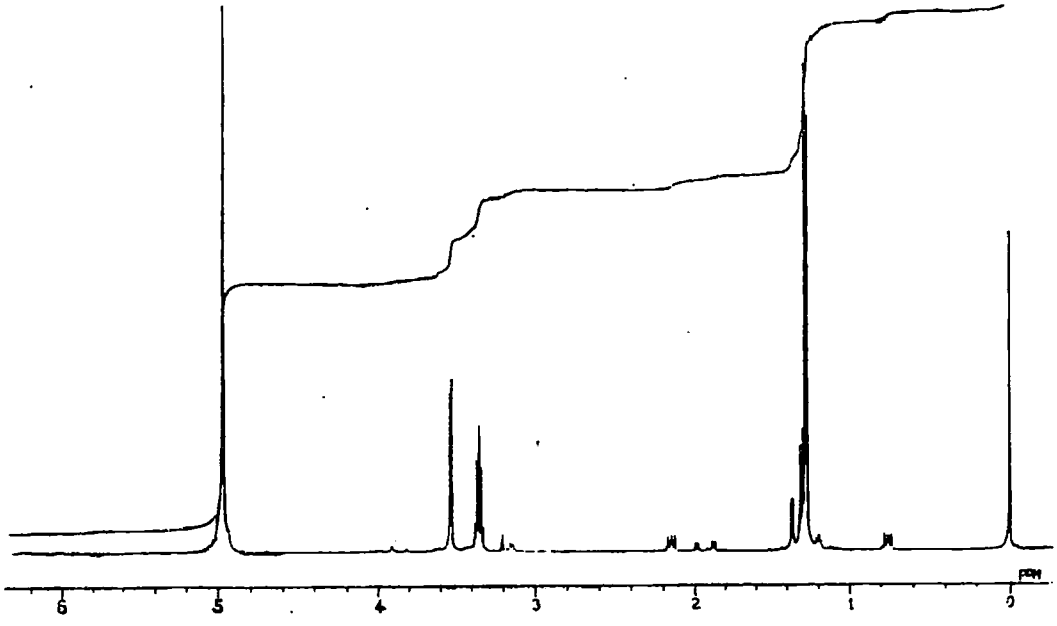

Figure 5.13d *After 10 d.*

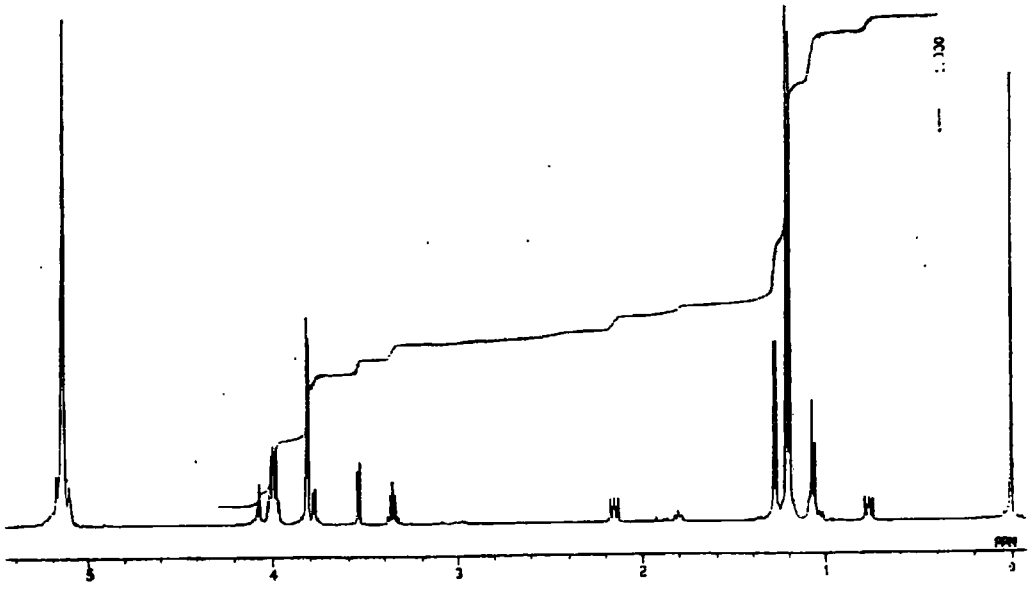

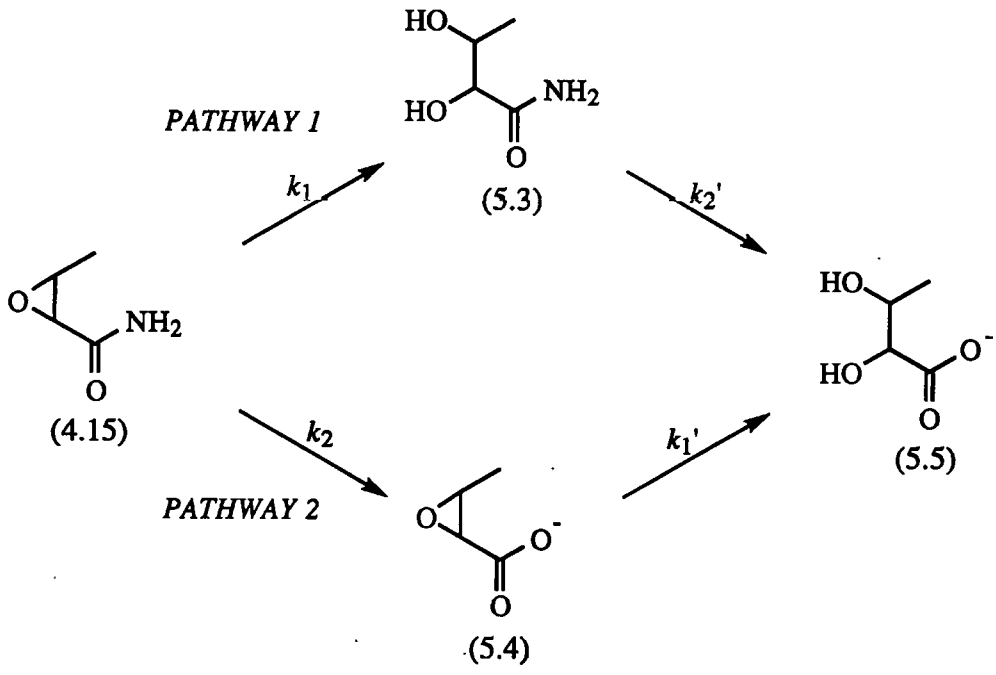

Scheme 5.3 *Alternative Pathways for the Hydrolysis of (4.15) in Dilute NaOH*

Table 5.5 ^{1}H-nmr Data for the Decomposition of *cis*-(4.15) in Dilute NaOD in D_2O at 37 °C

Assignment		*cis*-2,3-Epoxy-butanamide (4.15)	Intermediate B	2,3-Dihydroxy-butanoic acid (5.5)	
-CH-CH$C\!H_3$	δ	1.31	1.28	1.21	ppm
		d	d	d	
	J	5.2	5.2	6.4	Hz
-CH-C$\!H$CH$_3$	δ	3.42	3.36	4.00	ppm
		m	m	m	
-C$\!H$-CHCH$_3$	δ	3.61	3.54	3.81	ppm
		d	d	d	
	J	5.2	5.2	3.6	Hz

From the ^{1}H-nmr data summarised in Table 5.5, *cis*-(4.15) and intermediate (B) show similar spectra and give identical coupling constants for H_{ab} (J = 5.2 Hz) and H_{ac} (J = 5.2 Hz). Thus, intermediate (B) is probably structure *cis*-(5.4) with an intact oxirane ring.

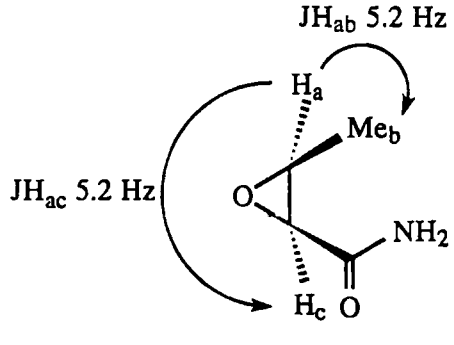

X = HH_2 or O^-

Further, the slight upfield shifts in all ^{1}H-resonances for intermediate (B) relative to *cis*-(4.15) is also consistent with the *cis*-(5.4) structure corresponding to increased shielding from the carboxylate group relative to the amide group. The ^{1}H-nmr spectra (Figures 5.13a-d) show intermediate (5.3) is not formed by the alkaline hydrolysis of *cis*-(4.15) in contrast to hydrolysis in dilute perchloric acid (Section 5.3.1). Under alkaline conditions, decomposition follows *PATHWAY 2* of Scheme 5.3 with an initial amide hydrolysis of *cis*-(4.15) to intermediate *cis*-(5.4), followed by much slower oxirane hydrolysis to give final product (5.5).

Interestingly, the accidental equivalence of JH_{ab} and JH_{ac} for *cis*-(4.15) and *cis*-(5.4) causes the H_a signal to appear as a 1:4:6:4:1 pentet, instead of a more complex multiplet where $JH_{ab} \neq JH_{ac}$. As reported in Section 5.3.3.1, the complex multiplet is observed for *trans*-(4.15) and *trans*-(5.4) where $JH_{ab} = 5.2$ and $JH_{ac} = 2.4$ Hz, and the H_a signal is observed as the 1:1:3:3:3:3:1:1 quartet of doublets shown in Figure 5.14.

Figure 5.14

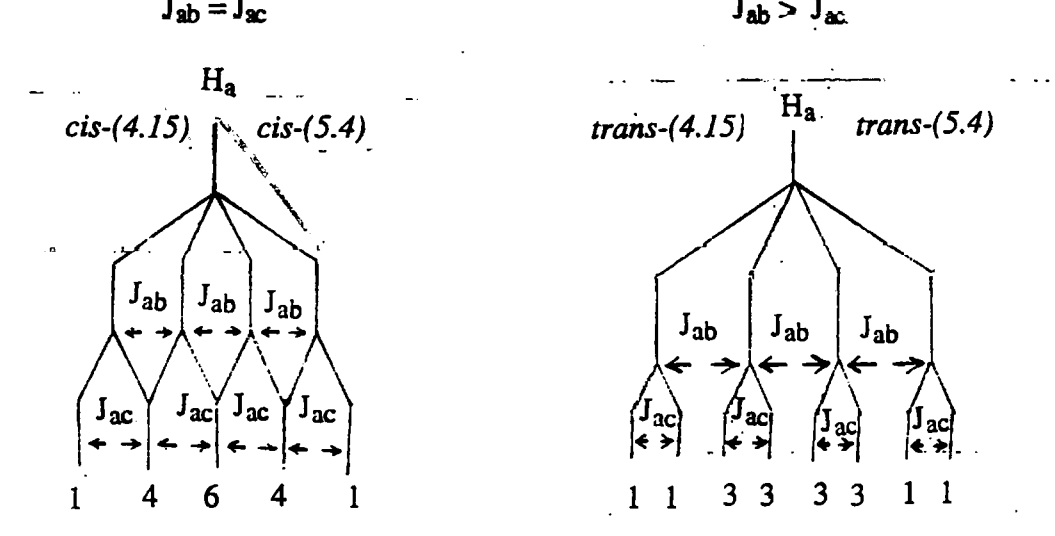

The products from the incubation of *cis*-(4.15) in 1M NaOH at 37 °C for 10 d. were also examined by FAB mass spectrometry. The reaction was neutralised with CO_2, freeze-dried, and the white solid residue (mainly sodium carbonate) was extracted with ethanol, as described in Section 7.4.2.2. Evaporation of the solvent gave a white solid residue for mass spectral analysis. The FAB negative mode spectrum (Figure 5.15) shows two strong signals at m/z = 101 and 119, consistent with M-H parent ions $^{-}O_2CCH\text{-}(O)\text{-}CHCH_3$ and $^{-}O_2CCH(OH)CH(OH)CH_3$ of intermediate *cis*-(5.4) and final product (5.5), respectively. Further, loss of CO_2 is observed at m/z = 57 and 75, respectively. Thus, the mass spectral information is consistent with the ^{1}H-nmr data above.

Figure 5.15 *FAB Mass Spectrum of Products from the Reaction of cis-(4.15) in 1 M NaOH at 37 °C After 10 d.*

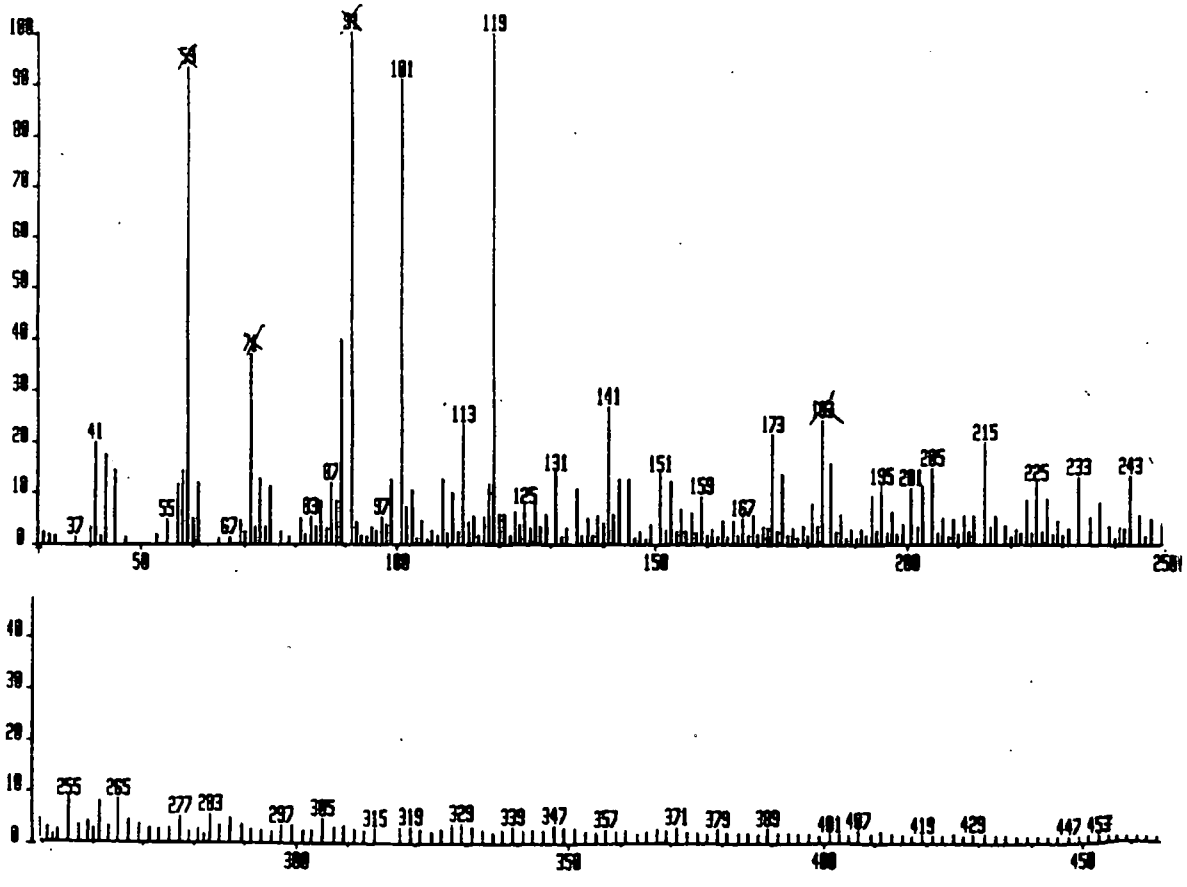

Independent Synthesis of Products

Confirmation that 2,3-epoxybutanoic acid (5.4) and 2,3-dihydroxybutanoic acid (5.5) were the intermediate and final products, respectively, from the hydrolysis of (4.15) in dilute NaOH was sought by independent synthesis.

5.3.2.1 Synthesis of *trans*-2,3-Epoxybutanoic acid (5.4)

The *trans*-epoxide (5.4) was synthesised in satisfactory yield (38 %) by reaction of *trans*-crotonic acid with hydrogen peroxide using sodium tungstate as the *syn*-epoxidation catalyst in slightly acidic media (see Section 7.5.4.1) {Scheme 5.4}.[128]

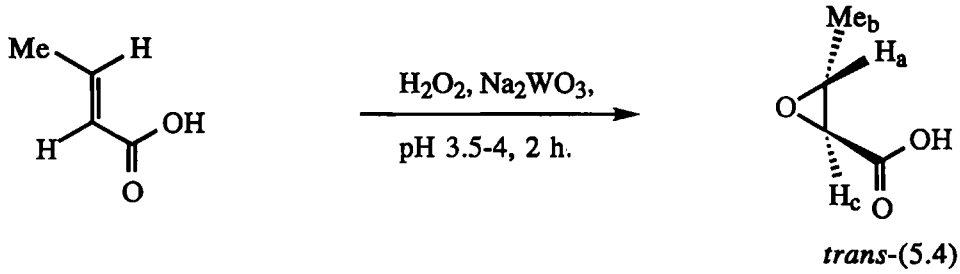

trans-(5.4)

Scheme 5.4

The FAB negative mode mass spectrum of the product (Figure 5.16) shows a strong M-H^+ ion at m/z = 101 (100 %) which loses CO_2 to give the fragment ion at m/z = 57 (20 %). The mass spectrum of *trans*-(5.4) also shows the presence of the dimer {$(M)_2$-H^+}, trimer {$(M)_3$-H^+}and tetramer {$(M)_4$-H^+} cluster ions at m/z = 203, 305 and 407, respectively. This behaviour is very similar to that of intermediate (B) from the hydrolysis of *cis*-(4.15) in dilute NaOH.

The 400 MHz ^{1}H-nmr spectrum of *trans*-(5.4) in Figure 5.17, however, shows considerable differences from that of intermediate (B) {*cis*-(5.4)}, as expected. In

Figure 5.16 *FAB Mass Spectrum of trans-2,3-Epoxybutanoic acid (5.4)*

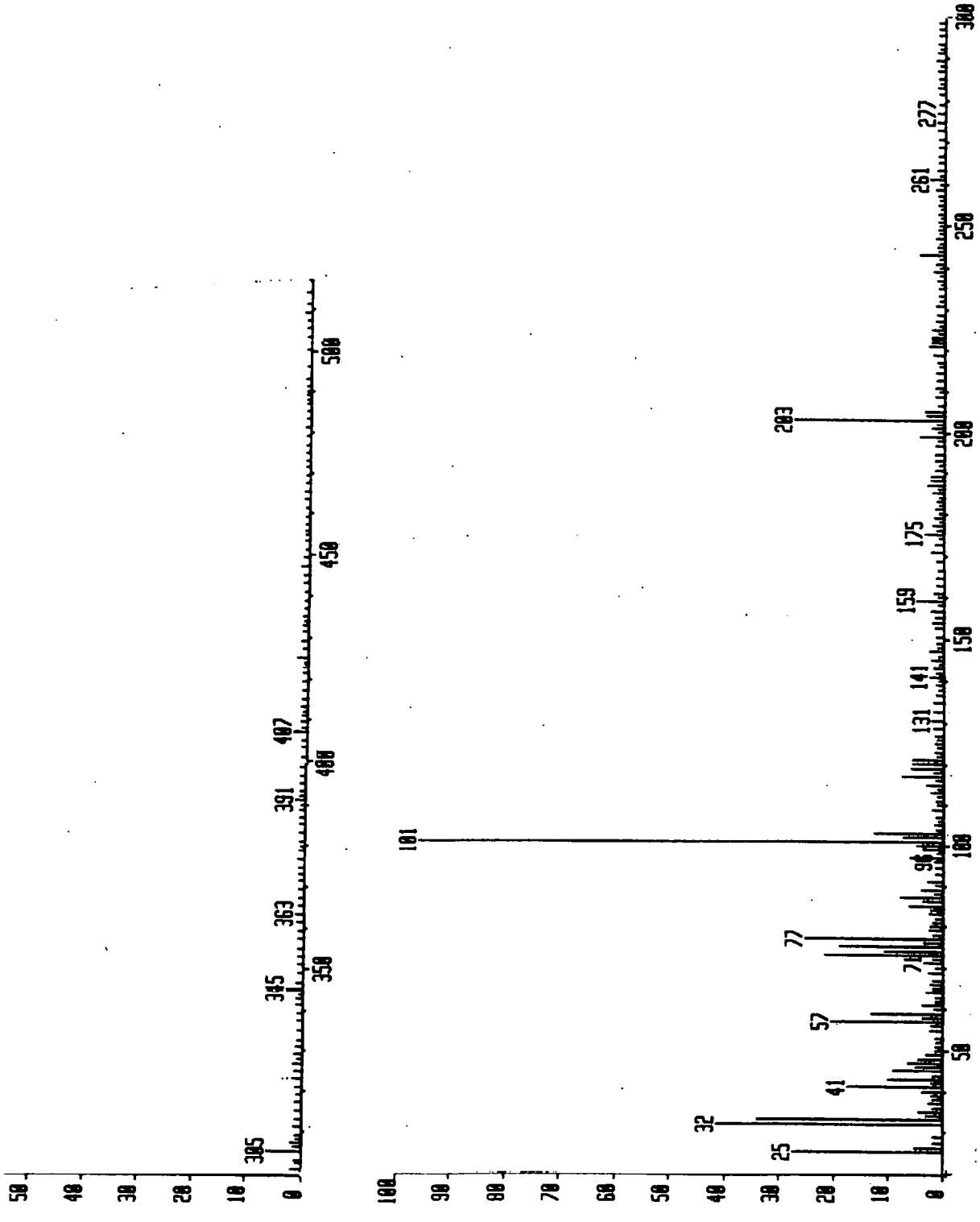

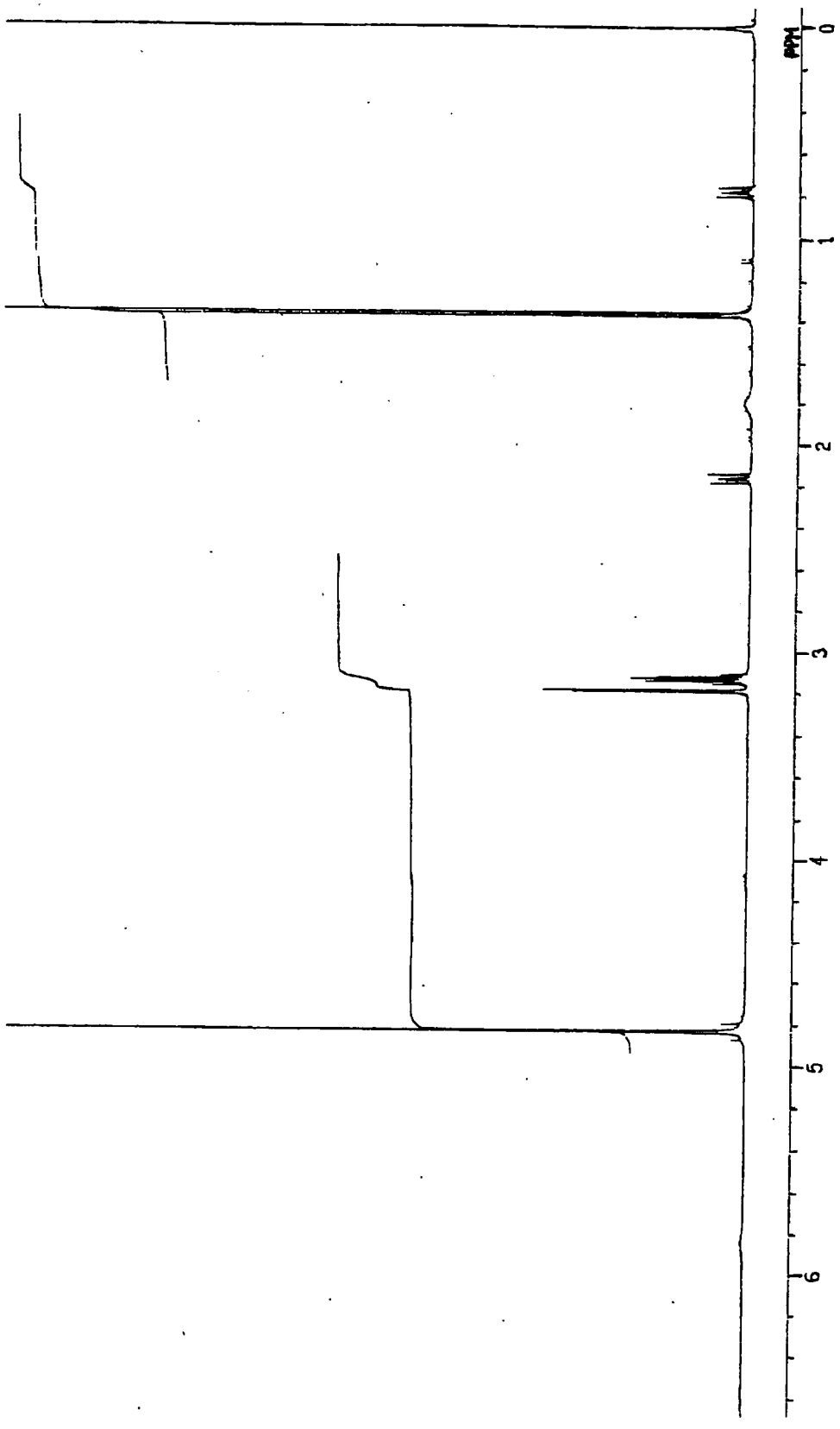

Figure 5.17 *400 MHz ^{1}H-nmr Spectrum of trans-2,3-Epoxybutanoic acid (5.4) in 0.1 M NaOD in D_2O*

particular, the two -CH resonances of authentic *trans*-(5.4) have smaller shift differences, are more shielded, and show smaller JH_{ac} (2.4 Hz) relative to *cis*-(5.4), as expected for the *trans* stereoisomer. The ^{1}H-nmr data for *trans*-(5.4) are summarised in Table 5.6.

Unfortunately, time was not available to synthesise *cis*-2,3-epoxybutanoic acid (5.4) independently, but the data for *trans*-(5.4) leaves little doubt about the identity of the intermediate (B) as *cis*-(5.4). Interestingly, close inspection of Figures 5.13b and 5.13c suggests that a small amount of the *trans*-(5.4) intermediate is formed in the alkaline hydrolysis of (4.15), corresponding to *ca.* 10 % of the *trans* isomer in the reactant (4.15).

Table 5.6 400 MHz ^{1}H-nmr Data for *trans*-(5.4) in 0.1 M NaOD in D_2O

Assignment	δ, ppm	m	J, Hz
-CH-CH(CH_3)	1.37	d	5.6
-CH-C*H*(CH_3)	3.14	m	
$^-$$_2$OCC*H*-CH-	3.20	d	2.4

5.3.2.2 Synthesis of 2(*R*),3(*S*)-Dihydroxybutanoic acid (5.5)

Diol 2(*R*),3(*S*)-(5.5) {plus 2(*S*),3(*R*)-(5.5)}was synthesised by *syn*-hydroxylation of *trans*-crotonic acid using an osmium tetroxide catalyst (see Section 7.5.4.2) as outlined in Scheme 5.5.

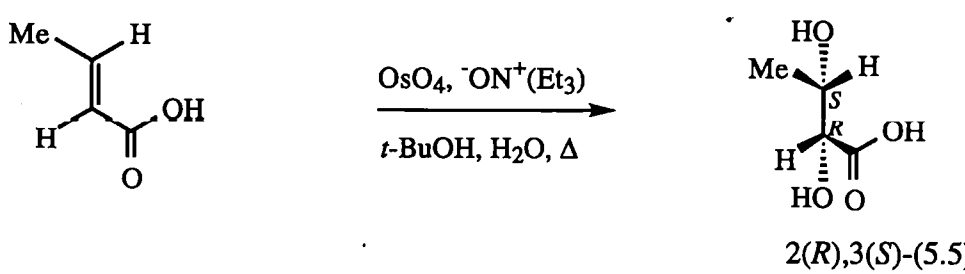

2(*R*),3(*S*)-(5.5)

Scheme 5.5

The FAB negative mode mass spectrum of the product (Figure 5.18) gives a strong M-H^+ ion at m/z = 119 (100 %) with loss of CO_2 to give a fragment ion at m/z = 75 (19 %), and is very similar to the mass spectrum of final product C (Figure 5.15).

The 400 MHz ^{1}H-nmr spectrum of authentic 2(*R*),3(*S*)-(5.5) shown as Figure 5.19 is identical to that for final product C (see Figure 5.13d and Table 5.5.). This suggests that *cis*-(4.15) hydrolyses to form the intermediate *cis*-(5.4) which then undergoes further (oxirane) hydrolysis to form the 2(*R*),3(*S*) {plus 2(*S*),3(*R*)} diastereoisomer of diol (5.5).

The corresponding hydrolysis product of *trans*-(5.4) in 1 M NaOD gives a significantly different 400 MHz ^{1}H-nmr spectrum (Figure 5.20) to that of 2(*R*),3(*S*)-(5.5) from *cis*-(5.4), as expected, but an identical FAB negative mode mass spectrum. This is consistent with formation of the 2(*S*),3(*S*)-(5.5) {plus 2(*R*),3(*R*)} diol diastereoisomer. The 400 MHz ^{1}H-nmr data of the 2(*S*),3(*R*)-(5.5) and 2(*S*),3(*S*)-(5.5) diastereoisomers are summarised in Table 5.7.

Table 5.7 400 MHz ^{1}H-nmr Data for Diol (5.5) Diastereoisomers in 0.1 M NaOD in D_2O

Assignment		2(*R*),3(*S*)	2(*S*),3(*S*)	
-CH-CH(CH_3)	δ	1.21	1.10	ppm
		d	d	
	J	6.4	6.4	Hz
-CH-C*H*(CH_3)	δ	4.00	4.10	ppm
		m	m	
$^-$$_2$OCC*H*-CH-	δ	3.81	4.08	ppm
		d	d	
	J	3.6	2.4	Hz

Figure 5.18 *FAB Mass Spectrum of 2(R),3(S)-Dihydroxybutanoic acid (5.5)*

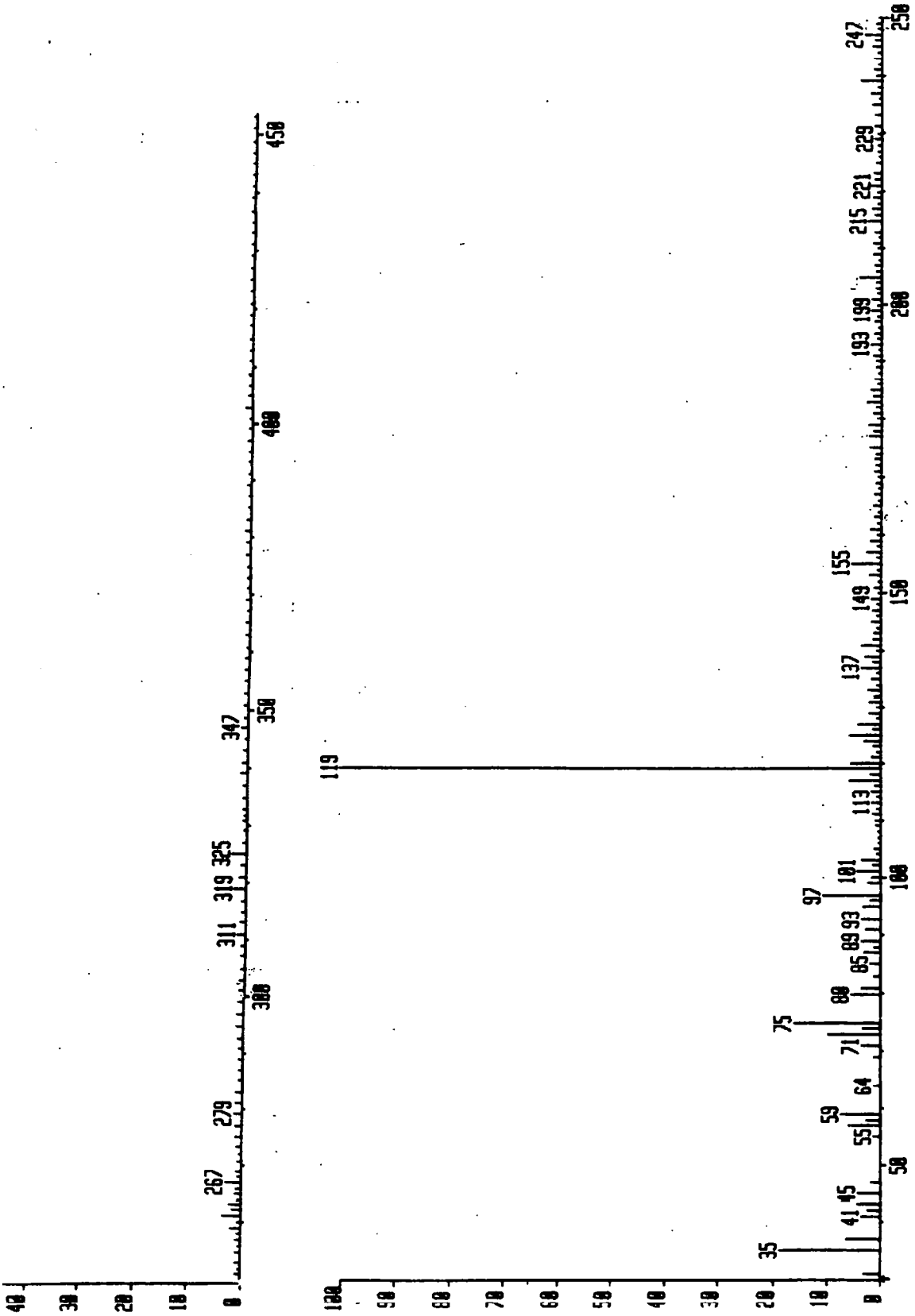

Figure 5.19 *400 MHz ^{1}H-nmr Spectrum of 2(R),3(S)-Dihydroxybutanoic acid (5.5) in 0.1 M NaOD in D_2O*

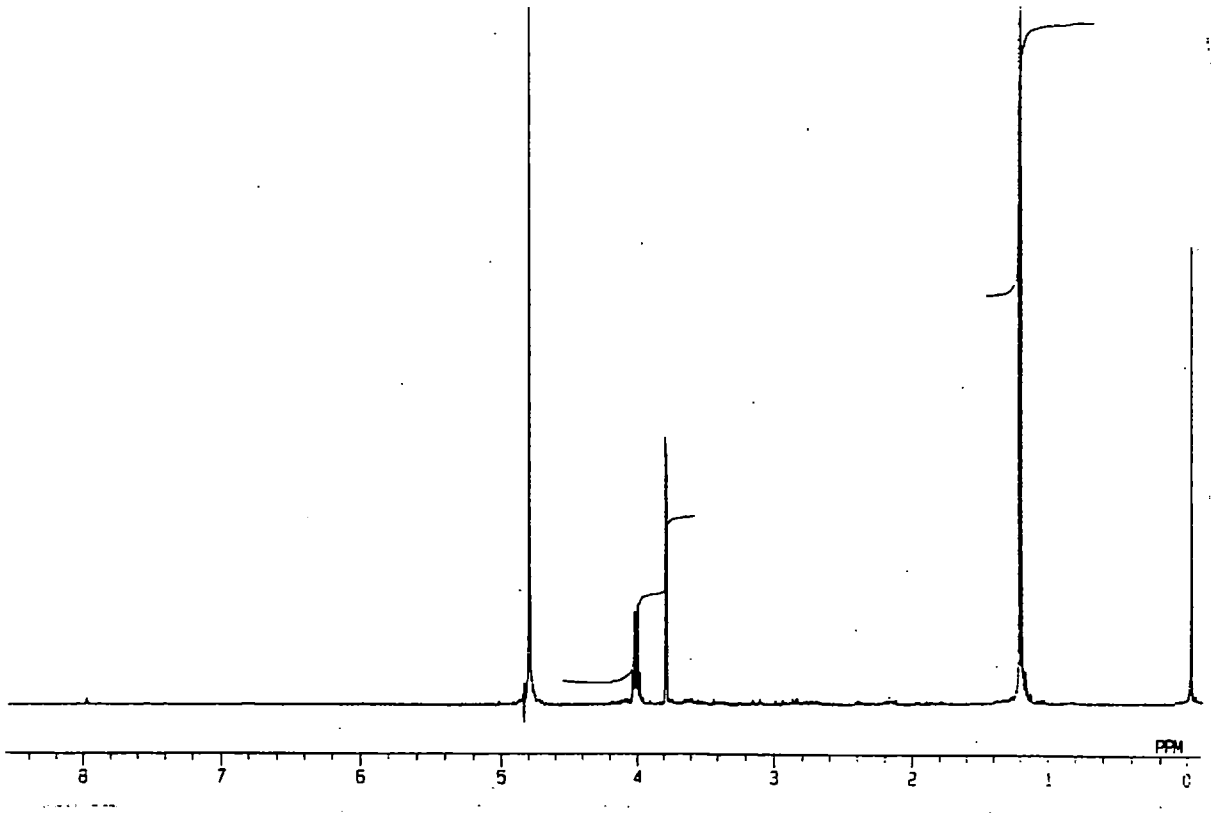

Figure 5.20 *400 MHz ^{1}H-nmr Spectrum of trans-2,3-Epoxybutanoic acid (5.4) in 2 M NaOD in D_2O*

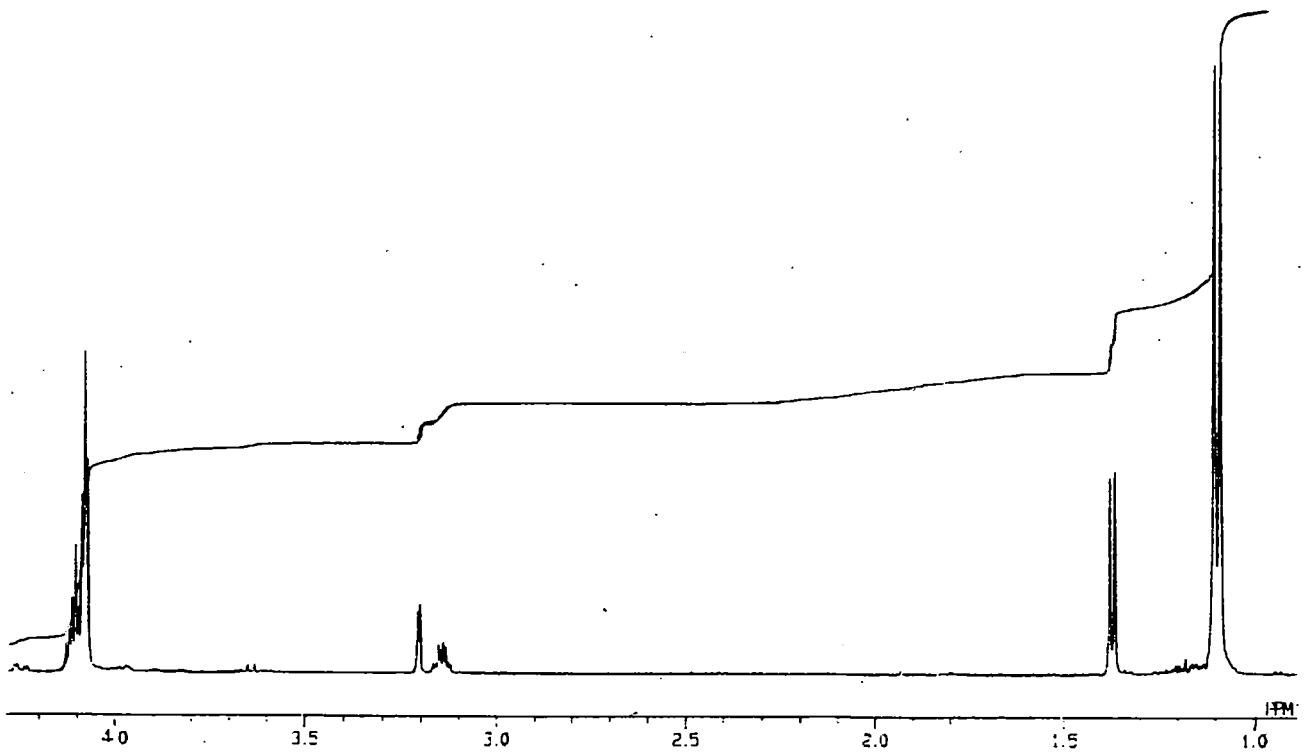

5.3.2.3 Summary

The product studies confirm that rate measurements in dilute NaOD at 37 °C relate to amide hydrolysis of *cis*-(4.15) rather then oxirane hydrolysis. The subsequent oxirane hydrolysis of intermediate *cis*-(5.4) is much slower. Brief time-dependent studies following the loss of *cis*-(5.4) in 1 M NaOD at 37 °C by 400 MHz ^{1}H-nmr gave k_2 *ca.* 2.0 x 10^{-6} $M^{-1}s^{-1}$, *ca.* 60 times slower than the alkaline hydrolysis of the amide group, *ca.* 40 times slower than oxirane ring opening by morpholine in aqueous media at pH 10.9 and *ca.* 200 times slower than oxirane hydrolysis of *cis*-(4.15) in $HClO_4$.

5.3.3 Reaction of *cis*-(4.15) in Aqueous Morpholine

The products from the reaction of *cis*-(4.15) with aqueous 0.1 M morpholine at 37 °C and pH 10.9 over 10 d. were also examined by FAB m/s and ^{1}H-nmr spectroscopy. These products were obtained from the reaction mixture as a white solid residue after removal of water and excess morpholine by freeze-drying (see Section 7.4.2.3).

The FAB mass spectra, shown as Figure 5.21, suggest formation of a single product with m/z = 189 (63 %) for the MH^+ and m/z = 187 (100 %) for the $M\text{-}H^+$, consistent with either structure (5.6) or (5.7).

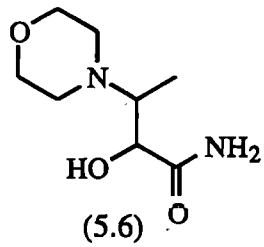

(5.6)

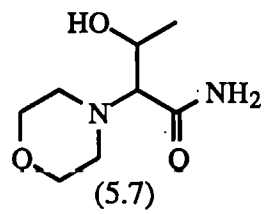

(5.7)

Further, there is no indication of the diol hydrolysis product (5.3). Fragment ions in the FAB positive mode mass spectrum at m/z = 114 (100 %) and m/z = 144 (7 %) are

Figure 5.21 *FAB Mass Spectrum of Products from the Reaction of cis (4.15) in 0.1 M Aqueous Morpholine at 37 °C After 10 d.*

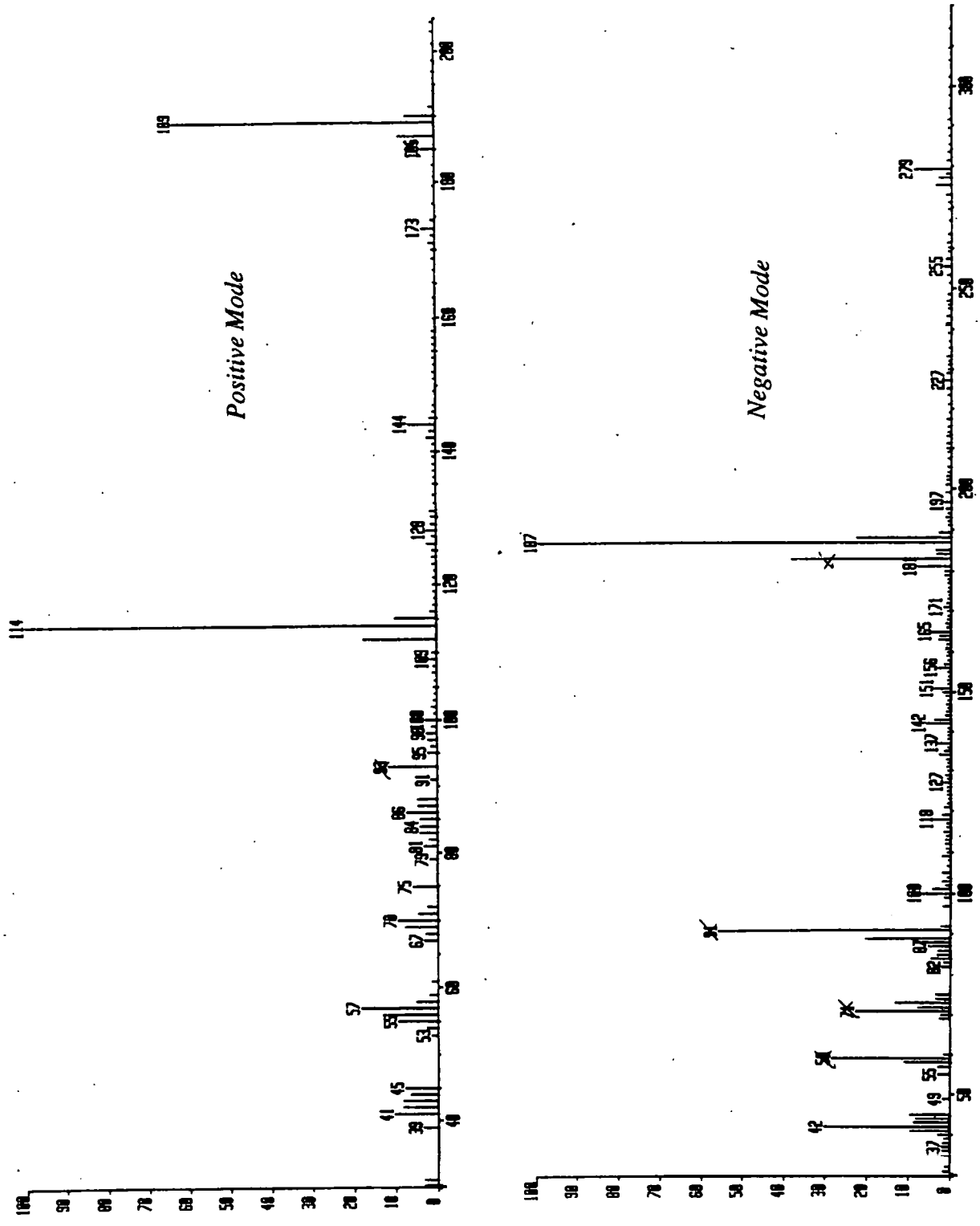

consistent with the $H_3CHC{=}\overset{+}{N}$ 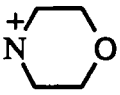 and 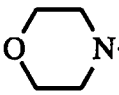 $N\text{-}\,CH(CH_3)CH{=}\overset{+}{O}H$ moities, respectively, and therefore with structure (5.6) for the single product. There was no evidence for the 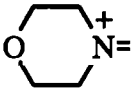 $\overset{+}{N}{=}\,CHCONH_2$ fragment ion at m/z = 143 derived from potential product (5.7).

From the results in Section 5.2.3, decomposition of *cis*-(4.15) in aqueous 0.1 M morpholine at 37 °C proceeds with $t_{1/2}$ *ca.* 24 h. Hence, a similar reaction solution in D_2O was monitored by 400 MHz ^{1}H-nmr and the spectra at t = 0, 24 h. and 7 d. are reported as Figures 5.22a-c, respectively. Figure 5.22a for unreacted *cis*-(4.15) in 0.1 M morpholine shows the *N*- and *O*-methylene triplets of the morpholine ring at δ = 2.82 and 3.71 ppm, respectively. Figure 5.22b for *ca.* 50 % reaction shows the appearance of new signals at δ = 1.10, 2.60, 3.43, 3.63 and 3.76 ppm, suggesting epoxide ring cleavage with formation of single a morpholine substituted product. Figure 5.22c for *ca.* 100 % reaction shows complete loss of substrate *cis*-(4.15) and formation of a single product, which is consistent with the m/s data. Compared with the epoxide *cis*-(4.15) substrate, the product with morpholine shows three important chemical shift differences:

1) The product -CH-C*H*(CH_3) multiplet at δ = 2.84 ppm is significantly more shielded (and partially masked by the intense *N*-methylene resonance of morpholine) than the corresponding multiplet of *cis*-(4.15) at δ = 3.43 ppm.

2) The product -C*H*-CH(CH_3) doublet at δ = 4.01 ppm is more deshielded than the corresponding doublet of *cis*-(4.15) at δ = 3.63 ppm.

3) The product -CH-CH(C*H*$_3$) doublet at δ = 1.10 ppm is more shielded than the corresponding doublet of *cis*-(4.15) at δ = 1.32 ppm.

These data are consistent with structure 2(*S*),3(*R*)-(5.6) {refer also to Section 7.5.4.3} for the single product, where relative to epoxide *cis*-(4.15), the -C*H*(CH_3)-N- resonances are shielded by an adjacent morpholine substituent and the H_2NOC-C*H*(OH)-CH-

Figure 5.22a *400 MHz ^{1}H-nmr Spectrum of cis-(4.15) in 0.1 M Morpholine in D_2O at 37 °C: At t = 0*

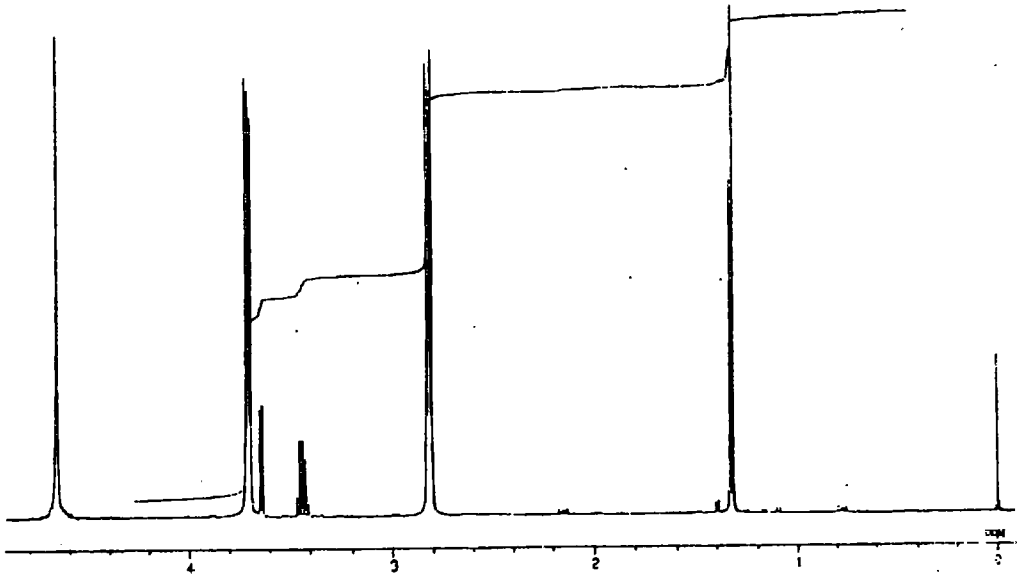

Figure 5.22b *After 1 d.*

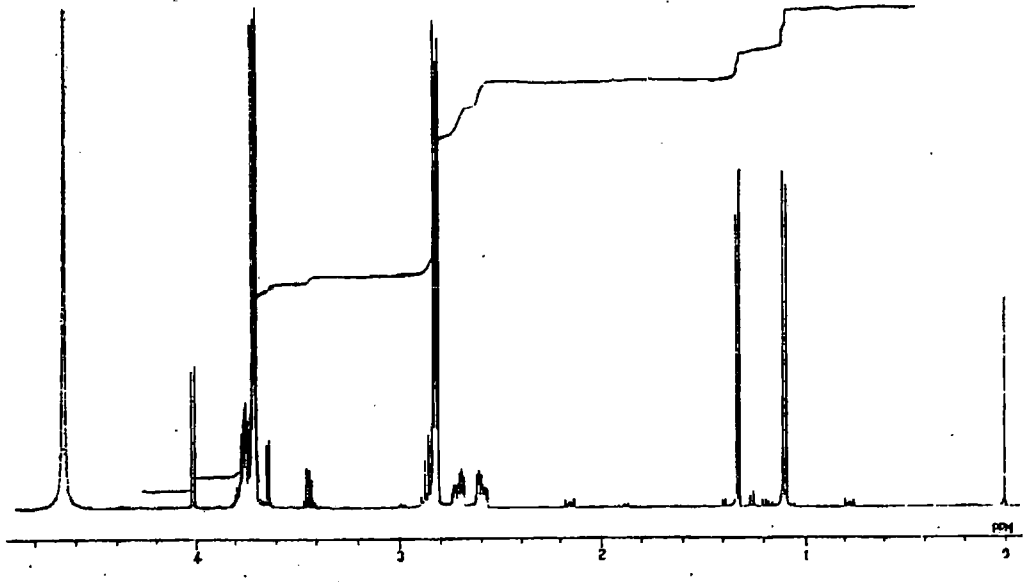

Figure 5.22c *After 7 d.*

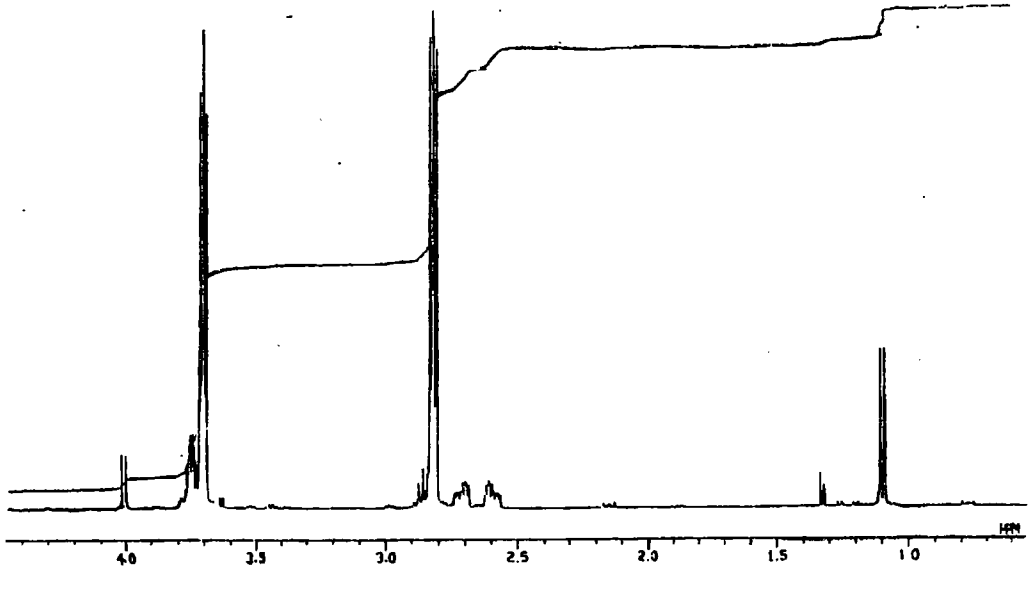

resonance is deshielded by an adjacent hydroxyl group. As no other products are observed, nucleophilic attack by morpholine must occur exclusively at the -*C*H(CH_3) carbon atom of epoxide *cis*-(4.15). The ^{1}H-nmr data for product (5.6) are summarised in Table 5.8.

Table 5.8 400 MHz ^{1}H-nmr Data for (5.6) in D_2O

Assignment	δ, ppm	m	J, Hz	Rel. Integral
-CH(C*H*$_3$)	1.10	d	7.2	3
-CH-N(C*H*$_2$)$_2$-	2.71, 2.60	m, m		2 x 2
-CH-C*H*(CH_3)	2.84	m		1
H_2NOC*H*-CH-	4.01	d	6.8	1
O(C*H*$_2$)$_2$-	3.76	m		4

An interesting feature of the ^{1}H-nmr spectrum of product (5.6) is the presence of two complex multiplets at δ = 2.71 and 2.60 ppm, each corresponding to two protons. These multiplets relate to two pairs of non-equivalent, diastereotopic *N*-methylene morpholine ring protons (H_a and H_b), which lie in different chemical environments because they are adjacent to the -N-*C*H(CH_3)- chiral centre. The H_a and H_b signals of (5.6) are more shielded than those of morpholine because of the tertiary morpholino N-atom. The four non-diastereotopic, *O*-methylene morpholine ring protons of (5.6) appear as a single muliplet, centred at δ = 3.76 ppm, due to coupling with diastereotopic H_a and H_b.

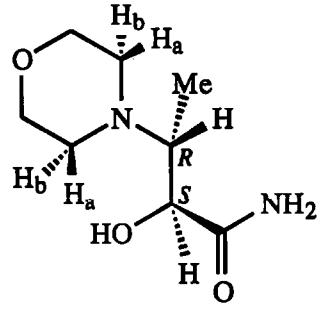

(5.6)

5.4 Discussion

The above results are indicative of S_N2 pathways with inversion of stereochemistry at C_3 for the oxirane ring opening of *cis*-(4.10) and *cis*-(4.15) by water (in both acidic and basic media) and by morpholine.

In aqueous acid, hydrolysis probably occurs *via* an A2 mechanism involving an initial equilibrium between the epoxide and its conjugate acid (which is more reactive than the epoxide itself), followed by nucleophilic attack by water with inversion of stereochemistry. The nucleophilic attack probably occurs at C_3 where partial positive charge development can be stabilised by the inductive effect of the methyl group (Scheme 5.6). Attack at C_2 should be less favourable because of steric hinderance and positive charge destabilisation by the carbonyl residue X. This conclusion is supported by the higher stability of epoxides derived from seryl rather than threonyl peptides in dilute acid, which lack the C_3 methyl substituent (see Section 5.2.1).

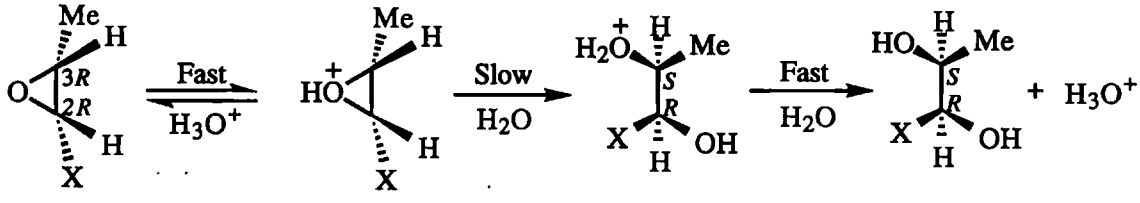

Where X = $CONH_2$, CO_2^-, CONHR

Scheme 5.6 *Mechanism for Epoxide Hydrolysis in dilute Acid*

In aqueous base, oxirane hydrolysis is *ca.* 200 times slower than in aqueous acid. The results in Section 5.3.2 are consistent with an S_N2 pathway involving attack of hydroxyl ion at either C_2- or C_3-atoms with inversion of stereochemistry (Scheme 5.7). The nucleophilic attack probably occurs at the less hindered C_3-atom, although reaction at the C_2-atom is not discounted by the present results. Thus, nucleophilic attack at the 'harder

acid' C_2-site may be preferred by hydroxyl ion and potential for S_N2 transition state stabilisation by π bond overlap with the carbonyl group also exists. This question can be resolved by further work using enantiomerically pure *cis*- or *trans*-epoxides (as in Scheme 5.7) and ^{1}H-nmr with the addition of chiral shift reagents to separate the diol enantiomers.

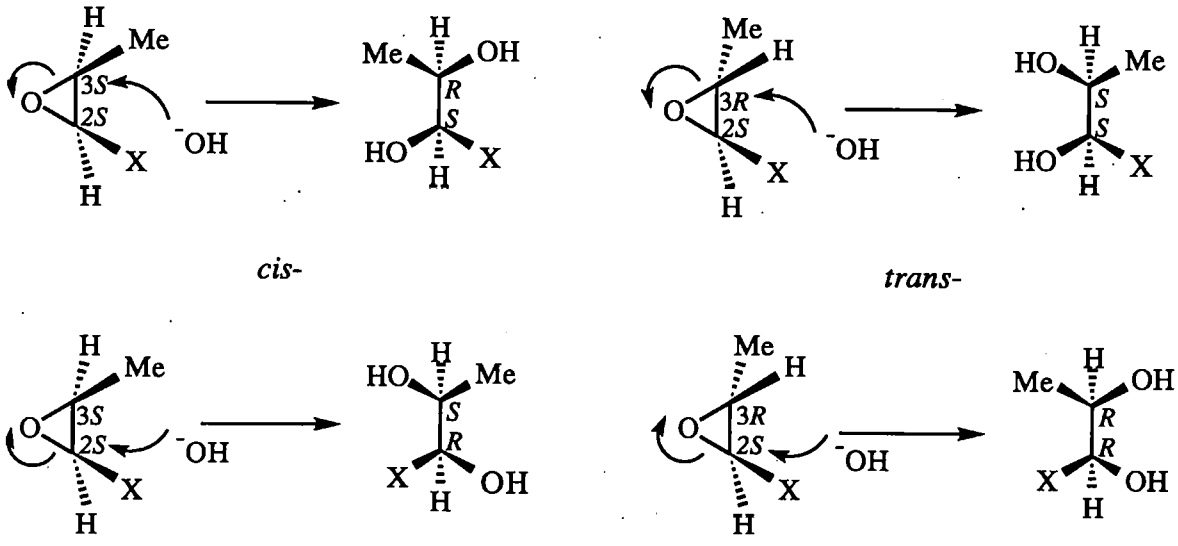

Scheme 5.7 *Stereochemistry of Diol Products from Base Hydrolysis of Epoxides*

The results in Section 5.3.3 show that amines facilitate cleavage of epoxide (4.15). In aqueous morpholine at pH 10.9; ring opening is *ca.* 40-fold faster than in aqueous NaOH and there is no evidence for concurrent formation of the diol hydrolysis product (5.5). The exclusive substitution product (5.6), arises from nucleophilic attack by morpholine at the C_3-atom of *cis*-(4.15). The reaction with morpholine probably proceeds *via* an S_N2 pathway, and the relatively 'soft' amine base prefers to react at the 'softer acid' C_3-site to give 2(*S*)-hydroxy-3(*R*)-*N*-morpholinobutanamide (5.6) as the single product (see Section 7.5.4.3) {Scheme 5.8}.

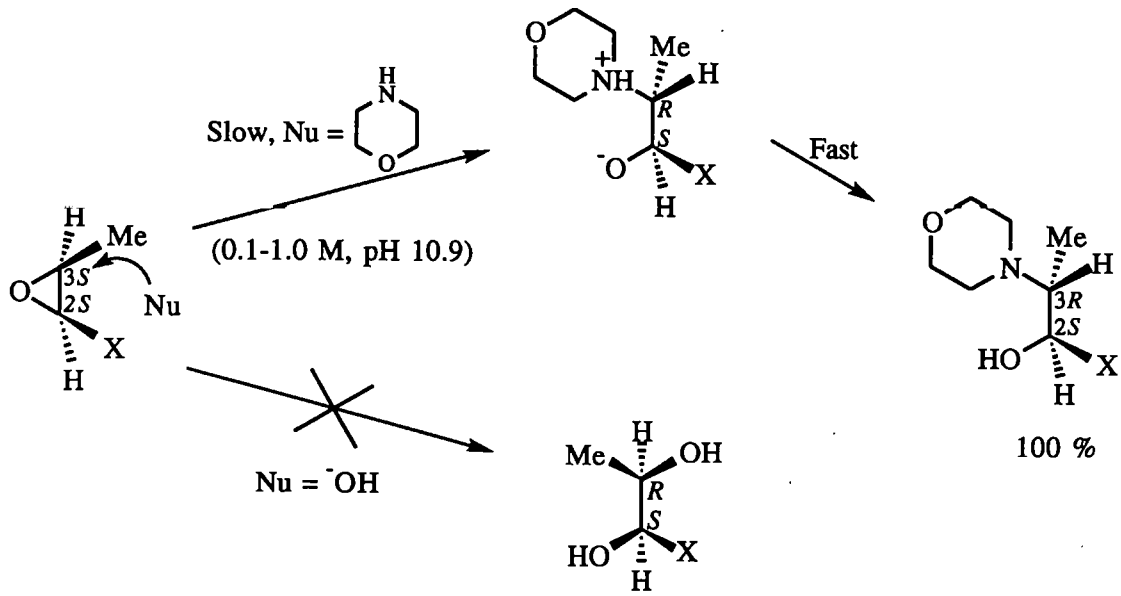

Scheme 5.8 *Pathways for the Reaction of cis-Epoxides with aqueous Morpholine at pH 10.9*

The present results suggest that epoxide products derived *via* the nitrosation of seryl and threonyl peptides are sufficiently stable to survive gastric conditions and to act as potential circulating carcinogens after absorption into the bloodstream. The relatively facile alkylation of morpholine by *cis*-(4.15) in aqueous media suggests they may also alkylate DNA, which bears on the potential cytotoxicity of the diazo derivatives of seryl and threonyl peptides. The most potent carcinogenic agents appear to alkylate DNA *via* S_N1 pathways, contrary to the behaviour of epoxide *cis*-(4.15). In independent studies, however, *N*-(2,3-epoxypropanoyl)glycine ethyl ester (4.14) gives a positive Ames Test (TA100) for mutagenic activity. The results in Table 5.9 show that (4.14) is mutagenic both with and without S-9 activation, giving a similar response to some diazopeptides.[122]

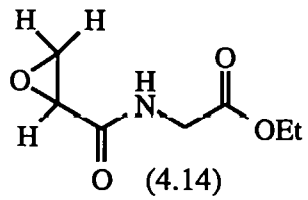

(4.14)

Table 5.9 Ames Test Data for *N*-(2,3-Epoxypropanoyl)glycine ethyl ester (4.14) with TA100

Epoxide (4.14)	Mean Revertants	
µg/plate	Without S-9 Activation	With S-9 Activation
50	127	141
100	136	131
500	228	200
1000	281	310
5000	619	647
+ve	537	1287

6. Summary and Conclusions

6.1 Introduction

The work in this thesis is part of an on-going programme to evaluate the causal role of diazopeptides in human cancer. Specifically, it was aimed at understanding aspects of the chemistry of diazopeptides decomposition such as the rates of reaction and products formed.

6.2 Kinetics and Mechanism of Acid-Catalysed Diazopeptide Decomposition

In Chapter 2, detailed kinetic studies for the decomposition of several diazopeptides in aqueous acid and buffer solutions at 25 °C are in excellent agreement with earlier work by Shuja[18] and extend mechanistic understanding about the decomposition of diazopeptides. Thus, these reactions are subject to general-acid-catalysis, which, along with other kinetic dependencies, is consistent with decomposition *via* a common pathway where the rate-limiting step is dependent upon the structure of the α-substituent to the diazo group (see Scheme 2.1). The kinetic form of the catalysis, however, is dependent on the type of acid.

In dilute perchloric acid (Section 2.4), reaction rates show a linear dependence on acid concentration, and diazopeptide stability is dependent upon the nature of the substituent (R) adjacent to the diazo group. For non-glycyl diazopeptides ($R \neq H$), those with electron-withdrawing α-substituents {e.g. CH_2OH, $-CH(CH_3OH)$} are most stable, whereas compunds bearing electron-donating α-substituents {e.g. $R = CH(CH_3)_2$} are *ca.* 5-fold more reactive. These findings are entirely consistent with decomposition *via* an AS_E2 mechanism, where protonation of the diazpeptide is rate-limiting and stability is related to the basisity of the α-C-atom adjacent to the diazo group.

In aqueous buffer solutions (Section 2.2), however, reaction rates show a non-linear dependence on buffer-acid concentration, and because rates attenuate at high concentrations, curved plots are obtained in agreement with Shuja's observations.[18] This behaviour is evident for both glycyl (R = H) and non-glycyl (R ≠ H) diazopeptides in formate, acetate and phosphate buffers, but not in pyridine buffers. The non-linear catalysis is probably related to a competing reaction pathway involving generation of a metastable azo-ester intermediate (Section 2.5.1), which retards diazopeptide decomposition at high buffer-acid concentrations. Analysis of the non-linear kinetic data *via* Line-Weaver Burke plots gave the equilibrium constants for azo-ester formation reported in Table 2.12.

Although the unusual kinetics provide good evidence for azo-ester formation by diazopeptides, independent confirmatory evidence is required, such as ^{15}N-nmr spectral analysis of reaction solutions using isotopically labelled diazo substrates.

6.3 Reactions of Diazopeptides with Amines

The linear general-acid-catalysis reported for the decomposition of diazopeptides in pyridine buffers in Chapter 2, is rationalised as evidence for the formation of a very unstable, positively charged triazene ion *via* nucleophilic addition of pyridine to the diazopeptide (see Section 2.5.1). It follows that more stable, neutral triazenes should result from analogous addition reactions of primary and secondary amines (Scheme 3.1). There is evidence to this effect for many other diazo compounds (especially diazonium ions), but not for diazopeptides. The results reported in Chapter 3 are aimed at providing this evidence for reactions of diazopeptides with aromatic amines in aqueous buffer solutions. Triazene (3.1) could not be detected by uv/visible spectrophotometry for the interaction of *N*-(2-diazoacetyl)glycine ethyl ester (1.3) with aniline in phosphate buffers,

but attenuation of the rate of acid-catalysed decomposition by added aniline is consistent with its formation (see Section 3.3). Triazene (3.2) was detected by uv/visible spectrophotometry, however, for the analogous reaction using sulphanilic acid (see Section 3.4). One explanation for the different behaviour is that aniline forms triazene (3.1) as a transient which reacts with a second diazopeptide to give a penta-azadiene, whereas sulphanilic acid forms a stable triazene (3.2) bearing a strong electron-withdrawing -SO_3H aryl substituent which minimises further coupling.

Triazene (3.2) was synthesised independently by coupling the sulphanilic acid diazonium ion with glycine ethyl ester in aqueous media. Attempts to isolate and quantitate triazene (3.2) from reaction of *N*-(2-diazoacetyl)glycine ethyl ester (1.3) with sulphanilic acid, however, proved difficult due to the high aqueous solubility inferred by the -SO_3H group. Triazene (3.2) was therefore isolated as the less soluble silver-triazene complex (3.2a), which could be precipitated from the reaction mixture by the addition of silver nitrate and acetone (see Section 3.7.1). Although this precipitate contained much inorganic impurity, silver-triazene complex (3.2a) was successfully characterised spectroscopically (see Section 3.8), and it showed analogous properties to both independently synthesised micro-analytically pure triazene (3.3) and silver-triazene (3.3a).

A k ey question to address in future studies is whether triazene products result from the interaction of amines with diazopeptides in aqueous media. Some evidence for the formation of triazenes (3.1) and (3.3) comes from uv/visible spectrophotometry of reactions of *N*-(2-diazoacetyl)glycine ethyl ester (1.3) with aniline and sulphanilic acid, respectively, but independent synthesis, isolation and purification of triazene (3.2) from the reaction of diazopeptide (1.3) and sulphanilic acid is required. Because of its high aqueous solubility, however, isolation and purification of triazene (3.2) may prove difficult, and it might be more practical to focus on alternative triazenes which are easier to isolate and purify.

6.4 Diazopeptide Decomposition Products

Chapter 4 identifies and quantitates the major products from the acid-catalysed decomposition of three non-glycyl diazopeptides, *N*-(2-diazo-3-methylbutanoyl)glycine ethyl ester (2.2), *N*-(2-diazo-3-hydroxybutanoyl)glycine ethyl ester (2.1), and *N*-(2-diazo-3-carbamoyl)glycine benzyl ester (4.1). Because H^+-transfer is rate-limiting for these reactions (see Section 2.5.1), information about the subsequent product-forming steps and the incidence of neighbouring group interactions can be gained by product studies. For diazopeptides containing α-alkyl substituents such as diazopeptide (2.2), the product studies show that substitution, elimination and perhaps rearrangement reactions typical of a very reactive carbocation intermediate occur. Diazopeptides such as (2.1) and (4.1) containing nucleophilic α-substituents, however, also gave cyclic products resulting from intramolecular trapping of the carbocation intermediate by the nucleophilic substituent. Importantly, neither the structure nor yields of the major decomposition products for any of the diazopeptide substrates varied significantly with the type of acid-catalyst or the pH of the solution. This implies that the carbocation derived from the diazopeptide is very reactive and non-discriminatory.

As the product-forming steps are post rate-limiting, it is difficult to assign mechanisms for them. Some information is forthcoming, however, from diazopeptide (2.1) synthesised from the natural amino acid *L*-threonine and therefore enantiomerically pure with two adjacent chiral centres. The product stereochemistry of the diol and epoxide products reveals the nature of the intermolecular and intramolecular substituent reactions, respectively. The results in Section 4.3.4 show that both of these reactions are non-stereoselective with both *cis*- and *trans*-epoxide (4.10), with 2(*R*),3(*R*)- and 2(*S*),3(*R*)-diol (4.8) products formed in approximately equal amounts. This suggests that both the intramolecular and the intermolecular nucleophilic substitution reactions are S_N1-like occurring *via* a fully-formed carbocation intermediate (Scheme 6.1).

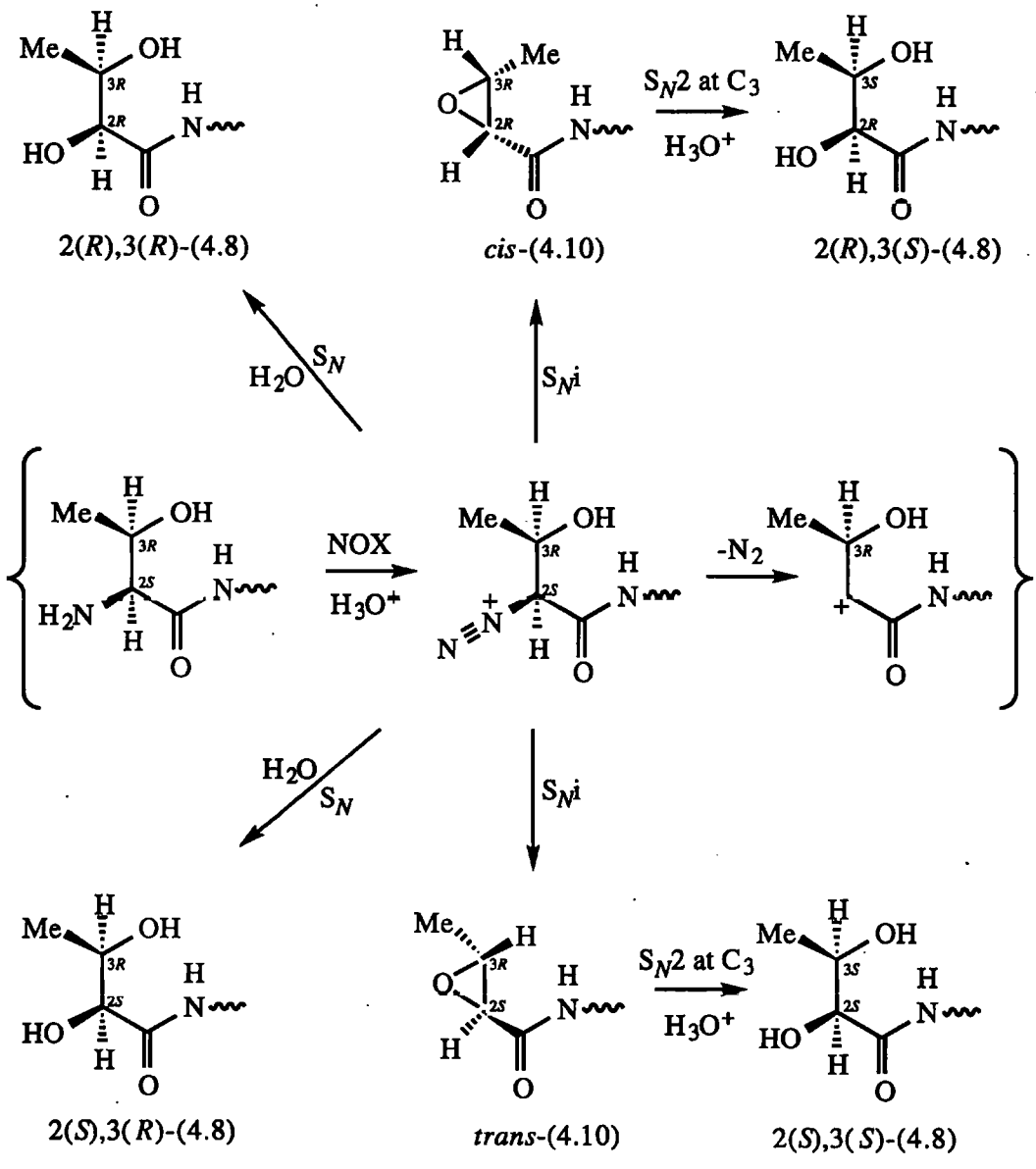

Scheme 6.1

Interestingly four diol stereoisomers may form in acidic reaction solutions (see Scheme 6.1): Initially the 2(*R*),3(*R*) and the 2(*S*),3(*R*) diastereoisomers form directly *via* nucleophilic attack on the carbocation intermediate by water but the corresponding 2(*S*),3(*S*) and the 2(*R*),3(*S*) enantiomers may also form *via* bimolecular hydrolysis at C_3 (see Section 5.4) of the *trans* and *cis*-epoxides, respectively (much slower reaction ,see Section 5.2.1). These additional diol products would of course give identical analytical hplc and 400 MHz ^{1}H-nmr spectra to the first pair of diols, hence only two diol products can be detected by the methods used here.

The formation of relatively stable epoxides *via* decomposition of diazoseryl- and diazothreonyl-peptides is important to the cancer hypothesis, because they may act as stabilised, circulating alkylating agents as discussed in Section 5.4.

The results in Section 4.4 suggest that β-lactam (4.2) may be the principal product from the decomposition of *N*-(2-diazo-3-carbamoyl)glycine benzyl ester (4.1) in organic media. As β-lactams are the building blocks of penicillin antibiotics, this finding could be of synthetic importance to the pharmaceutical industry. The identification of β-lactam (4.21) from spectral analysis of partially purified reaction mixtures requires confirmation *via* independent synthesis, but potentially, these products offer a useful, one step route to β-lactam antibiotics.

6.5 Toxicity

Although diazopetides and diazoamino acids are powerful mutagens,[13,17,115] they are highly acid-labile and unlikely to persist long enough in the gastric environment to interact with genetically sensitive material. The present work, however, suggest two ways by which diazopeptides may exert toxicity. Thus, studies reported in Chapters 2 and 3 strongly suggest that diazopeptides react with nucleophiles such as carboxylate and amino groups to form azo-ester and triazene compounds, respectively. Although not well known, these reversible reactions may generate azo-esters and triazenes as stabilised, transportable forms of cytotoxic diazonium ions. Evidence to support this hypothesis is the correlation between the rate of hydrolysis of dimethyltrazienes and their ability to induce tumours at the site of administration.[85]

Further studies reported in Chapters 4 and 5 show that diazothreonyl- and diazoasparaginyl-peptides also generate cyclic decomposition products able to act as

stabilised alkylating agents. For seryl-peptides and therefore probably threonyl-peptides, the cyclic epoxide product has proven to be mutagenic by the Ames Test (Section 5.4).

Chapter 5 also reports preliminary studies to assess the stability and the alkylating ability of the epoxide product (4.10) in aqueous media. In dilute perchloric acid, epoxide (4.10) is *ca.* 10^5-fold more stable than the parent diazopeptide (2.1) and in aqueous solution, it readily alkylates amines. Since epoxide (4.10) is probably mutagenic by the Ames Test, it seems feasible that decomposition products derived from diazoseryl- and diazothreonyl-peptides may be involved in dietary related cancer.

Further work to elucidate the potential risk from the endogenous nitrosation of dietary peptides should assess the extent of diazopeptide and cyclic product formation under simulated gastric conditions, and the cytotoxicity of both the diazopeptide addition products and cyclic decomposition products.

7. Experimental

7.1 General Instrumentation

Melting points were measured on an Electrothermal digital apparatus and are uncorrected. Elemental analyses were obtained from Medac Ltd. (Bruncl). pH Measurements were made on a Universal PT15 digital meter using a combination electrode calibrated against two standard buffer solutions (pH 4 and 7). Ultra violet/visible spectra were recorded using either Kontron Uvikon 810 or Cecil 599 spectrophotometers calibrated with a holmium filter and fitted with Grant thermostatted circulators to control the cell compartment temperature to ± 0.1 °C.

i.r. Spectra, as either nujol mulls or thin films using sodium chloride plates, in solution using cells with either sodium chloride or sapphire windows and as KBr discs, were recorded on either a Perkin Elmer 1710 Fourier transform spectrometer (equipped with triglycine sulphate and mercury cadmium telluride detectors and data processing *via* 7500 computer using DS-3 applications software) or on a Nicollet Model 205 FTIR spectrometer.

^{1}H and ^{13}C-nmr data, recorded on Jeol EX400 and Jeol FX90 Fourier transform spectrometers, were provided by Mr. Gordon Howell of the Chemistry Department. ^{1}H-nmr data were also recorded on a Jeol PMX60 spectrometer. Tetramethylsilane was used as internal standard with organic deuteriated solvents and tetramethylsilanepropionate (sodium salt) similarly with deuterium oxide solutions.

Mass spectra, recorded on a VG20-250 quadrupole instument equipped with both an EI probe and an Ion Tech fast atom bombardment (FAB) gun, were provided by Mr. Brandon Cook of the Chemistry Department. FAB ionization using xenon gas was

normally used for the analyses of amino acid and peptide derivatives in a dry glycerol matrix, but less nucleophilic matrices (e.g. tetraethylene glycol diethyl ether) were used for labile compounds.

7.2 Reagents and Reactants

Regular laboratory reagents and solvents were obtained from commercial sources and where necessary, were purified by standard procedures. Hplc grade solvents (May and Baker), amino acids and peptides (Aldrich and Sigma) were used as supplied. Dinitrogen tetroxide (BOSG, 99 %) was used without further purification.

Stock buffer solutions were prepared gravimetrically in distilled water from Analar grade reagents. Working buffer solutions for kinetic experiments were prepared by volumetric dilution of the stock solutions. Their ionic strength was adjusted with Analar sodium perchlorate (BDH).

Aqueous dilute perchloric acid solutions were prepared by volumetric dilution of Analar 70 % (w/w) $HClO_4$ (Fisons) and standardised against Analar sodium hydroxide solutions (0.1-1 M) {BDH} using phenyl red as indicator.

7.3 Kinetic Methods

7.3.1 Decomposition of Diazopeptides

The diazopeptides were decomposed in both aqueous buffer solutions and dilute acid at 25 °C. These reactions were followed by monitoring the decrease in the uv/visible absorbance of the diazo group of the substrate (λ_{max} 250 or 390 nm) with respect to time. Two different methods were used depending on the rapidity of the reaction, which in turn, depended on the structure of the diazopeptide substrate, the pH and the buffer concentration.

7.3.1.1 Slow reactions ($t_{1/2}$ > 60 s)

These measurements were made using a conventional uv/visible spectrophotometer with a thermostatted cell block. Aliquots (3 cm^3) of the buffer solution in the cuvettes (1 cm^3 path length) were thermally equilibrated to 25 (± 0.1) °C in the cell block of the spectrophotometer. The reactions were started by adding an aliquot (typically 30 µl) of a stock solution of the diazopeptide in ethanol to give an initial concentration of *ca.* 5 x 10^{-5} M diazopeptide and an initial absorbance of *ca.* 1 for reactions monitored at λ = 250 nm.

For reactions monitored at λ = 380 nm (pyridine, aniline and sulphanilic acid buffer solutions gave a uv cut off at *ca.* 300 nm), 100 µl of a 0.1 M diazopeptide stock solution in ethanol was usually added to 3 cm^3 of reaction solution in the cuvette, giving an initial diazopeptide concentration of *ca.* 3 x 10^{-3} M and an initial absorbance of *ca.* 0.1. After mixing thoroughly, the uv absorbance was monitored with time until either constant or in the case of very slow reactions, over at least four half-lives before adding a

drop of conc. HCl to the cuvette to obtain the infinity absorbance value (typically 0.010 to 0.030).

The pH of the cuvette contents was checked after each reaction. Values of the *pseudo* first-order rate coefficient k_o (Rate = k_o [Substrate]) were determined from plots of $\ln(A_t - A_\infty)$ *vs.* time, where A_t and A_∞ = absorbance at time t and infinity, respectively. The kinetic runs were carried out in duplicate and an average value of k_o was taken. The k_o values were reproducible to ± 2 % for reactions monitored at λ = 250 nm and to ± 5 % for reactions monitored at λ = 380 nm. Absorbance readings were less reliable for reactions using higher diazopeptide concentrations due to the formation of gas bubbles in the cuvettes. Fortunately, most reactions were sufficiently slow to briefly remove the cuvette from the spectrophotometer and to shake gas bubbles to the surface before the next uv scan. Sufficient dead space was left in the cuvette for this purpose and reproducible results were obtained.

A typical kinetic plot for the reaction of *N*-(2-diazoacetyl)glycinamide in 0.5 M phosphate buffer at pH 6.20 and 25 °C is shown in Figure 2.1. The slope of this plot gives $k_o = 1.90 \times 10^{-4}$ sec^{-1}.

7.3.1.2 Fast reactions ($2s < t_{1/2} < 60s$)

The acid-catalysed decomposition of some diazopeptides was too fast to be measured accurately with a conventional uv/visible spectrophotometer. Thus, a Nortech (Type SF-32) stopped-flow unit equipped with a Hitech (TDI-43) timer delay was used, and the results were processed on-line by computer. An aqueous solution of the diazopeptide (*ca.* 1.0×10^{-4} M) adjusted to pH 7.0 with a pinch of solid Na_2HPO_4, and the appropriate

buffer solution (*i.e.* twice the required buffer concentration and ionic strength to allow for the 2-fold dilution on mixing) were placed in separate reactant reservoirs from which two syringes were filled with each solution. In a single operation, equal volumes of the reactant solutions were passed manually through the mixing chamber and into the uv cell. After transfer of *ca.* 0.5 cm^3 of each solution, the flow of reactants was stopped mechanically and the subsequent absorbance of the reaction solution recorded with respect to time. Measurements were continued until the absorbance became constant (time infinity). The flow unit, mixing chamber and uv cell were thermostatted at 25 ± 0.1 °C.

The absorbance results were analysed by a computer program which calculated a *pseudo* first-order rate coefficient (k_o) by a regression procedure. A mean value of k_o was taken from the duplicated kinetic runs which agreed to ± 5 %. Finally, the pH of the solution collected from the mixing cell was determined for each reaction.

7.3.2 Decomposition of *cis*-*N*-(2,3-Epoxybutanoyl)glycine ethyl ester (4.10) in Dilute $HClO_4$ at 37 °C

The decomposition of *cis*-(4.10) in aqueous $HClO_4$ was followed by monitoring its loss by hplc. The hplc system comprised an LDC Constametric 3000 pump and Spectromonitor 3010 variable wavelength uv detector coupled to an LDC CI10B computing integrator. The assay was carried out on a Jones Apex II ODS column (25 cm x 4.0 mm i.d.) using 15 % (v/v) methanol in water eluent at a flow rate of 1 cm^3/min., with monitoring at λ = 210 nm. Under these conditions, *cis*-(4.10) gave R_f = 12.7 min. A typical chromatogram for *ca.* 1 mM *cis*-(4.10) in 0.1 M $HClO_4$ is shown in Figure 5.2. Independent experiments established that the concentration of *cis*-(4.10) was proportional to both the height and area of the peak at 12.7 min. A calibration curve showing peak area *vs.* concentration of *cis*-(4.10) in Figure 7.1 was linear.

For the kinetic experiments, solutions of *cis*-(4.10) {*ca.* 1 mmol, 25 cm^3} in the appropriate $HClO_4$ were prepared in a volumetric flask and thermally equilibrated at 37 °C (± 0.1 °C) in a water bath. Aliquots (20 µl) were withdrawn at timed intervals and assayed for *cis*-(4.10) by hplc. The reactions were followed until the peak at

Figure 7.1 *Calibration Curve for cis-N-(2,3-Epoxybutanoyl)glycine ethyl ester (4.10) by Hplc Assay*

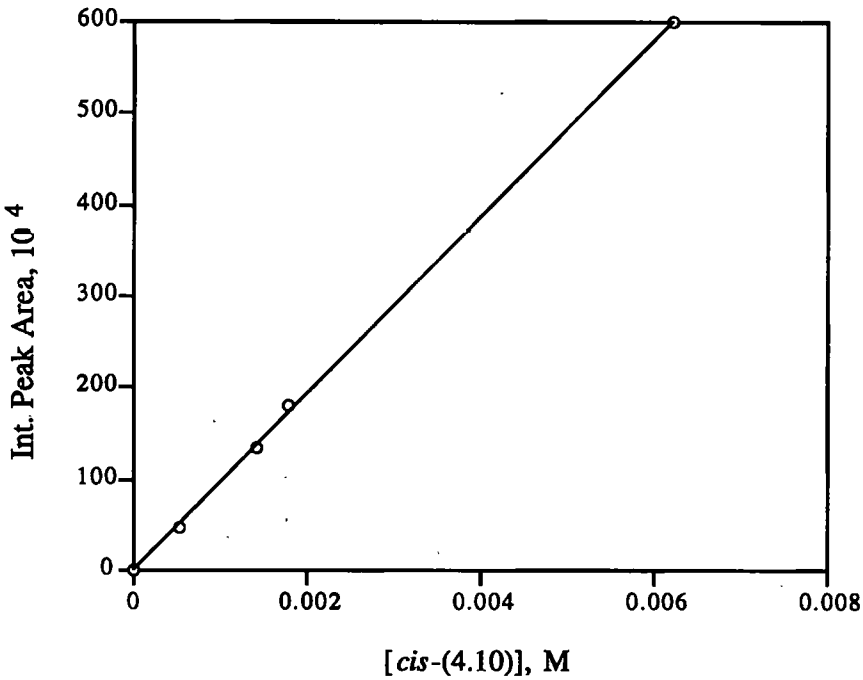

R_f = 12.7 min. had decreased to almost zero. Values of k_o (Rate = k_o [Substrate]) were determined from plots of ln(peak area or peak height) *vs.* time. These showed good linearity as shown for a typical decomposition of *cis*-(4.10) in 0.1 M $HClO_4$ at 37 °C in Figure 5.1 giving a value for k_o of 4.05 x 10^{-5} sec^{-1}. Usually, the reactions were carried out in duplicate, and values of k_o were reproducible to ± 10 %.

7.3.3 Decomposition of *cis*-2,3-Epoxybutanamide (4.15)

7.3.3.1 In Aqueous NaOD at 37 °C

Rates of decomposition of *cis*-(4.15) in aqueous NaOD were determined by 400 MHz

^{1}H-nmr using TSP as an internal standard, following the loss of *cis*-(4.15) from the decrease in the integrals of two signals assigned to ring protons of *cis*-(4.15) {*i.e.* -O-C*H*-CONH$_2$ at δ = 3.64 ppm and -O-C*H*(CH$_3$) at δ = 3.44 ppm}, with respect to time. Typically, dilute solutions of NaOD were prepared by volumetric dilution of 10 M NaOD (Sigma) with D_2O. Solutions of *cis*-(4.15) {*ca.* 1 mmol, 25 cm^3} in the appropriate NaOD solution were prepared in a volumetric flask. Aliquots (2 cm^3) of the solution were transferred to 5 cm^3 nmr tubes thermostatted at 37 °C (± 1.0) by the VT control within the nmr probe. These solutions were scanned at timed intervals until the ^{1}H-nmr signals at δ = 3.64 and 3.44 ppm had disappeared. The concentration of *cis*-(4.15) was assumed to be proportional to the ^{1}H-nmr integrals, and they were observed to decrease to zero. A typical nmr spectrum of *cis*-(4.15) in 0.3 M NaOD at 37 °C, is shown in Figure 5.6.

Values of k_o (Rate = k_o [Substrate]) were determined from plots of ln (Peak Integral) *vs.* time. Duplicate experiments showed values of k_o were reproducible to ± 10 %. A typical plot for the decomposition of *cis*-(4.15) in 0.3 M NaOD at 37 °C shown in Figure 5.5 is linear, giving a value of $k_o = 2.7 \times 10^{-5}$ sec^{-1}.

7.3.3.2 In Aqueous Morpholine at 37 °C

These reactions were also carried out by monitoring the loss of *cis*-(4.15) by hplc. The hplc assay used 5 % (v/v) methanol in aqueous 0.05 M K_2HPO_4 as eluent with a Jones Apex II ODS column (25 cm x 4.0 mm i.d.) at a flow rate of 1 cm^3/min. Under these conditions, *cis*-(4.15) gave a retention time of 4.8 min.

The kinetic studies were carried out similarly to those for the decomposition of epoxide *cis*-(4.15) in aqueous $HClO_4$ (Section 7.3.2) using solutions of *cis*-(4.15) {*ca.* 1 mmol,

25 cm^3} in aqueous morpholine thermally equilibrated at 37 °C (± 0.1 °C). Values of k_o (Rate = k_o [Substrate]) were also determined from plots of ln (peak height) *vs.* time. At t_∞, the peak at R_f = 4.8 min. had invariably disappeared, and values of k_o were reproducible to ± 10 %. A typical plot and chromatogram for the decomposition of *ca.* 1 mM *cis*-2,3-epoxybutanamide (4.15) in 0.2 M aqueous morpholine at 37 °C and pH 10.9 are shown in Figures 5.8 and 5.9, respectively. The plot is linear giving a value of $k_o = 1.46 \times 10^{-5}$ sec^{-1}.

7.4 Product Analyses

7.4.1 Diazopeptide Decomposition Products

7.4.1.1 From *N*-(2-Diazo-3-methylbutanoyl)glycine ethyl ester (2.2)

N-(2-Diazo-3-methylbutanoyl)glycine ethyl ester (2.2) {0.02 g, 0.1 mmol} was decomposed in aqueous $HClO_4$ (25 cm^3, 0.1 M) at ambient temperature. After standing for *ca.* 10 min., the mixture was neutralised to pH 7-8 by the addition of solid sodium bicarbonate.

Aliquots (10 µl) of the neutralised reaction solution were assayed for products by reverse-phase hplc using a Jones Apex II ODS column (25 cm x 4.0 mm i.d.) with isocratic elution using 30 % (v/v) methanol in water at a flow rate of 1 cm^3/min. and uv detection at λ = 210 and 250 nm. The single, major product with R_f = 12.6 min. (see Figure 4.1) was subsequently identified as *N*-(3-methylbut-2-enoyl)glycine ethyl ester (4.5).

The product was isolated *via* semi-preparative hplc using a Waters Delta Prep-3000 system (consisting of a quaternary pump, 600E system controller, 484 tunable absorbance detector (λ = 210 nm) and a 745 B data module) from a more concentrated reaction of *N*-(2-diazo-3-methylbutanoyl)glycine ethyl ester (2.1) {0.2 g, 1 mmol} in 0.1 M $HClO_4$ (25 cm^3), which had been neutralised with solid sodium bicarbonate. Manual injections (2 cm^3) were made on to a Jones Apex Prepsil ODS column (25 cm x 25 mm) using 30 % (v/v) methanol in water eluent at a flow rate of 25 cm^3/min. Under these conditions, *N*-(3-methylbut-2-enoyl)glycine ethyl ester (4.5) gave R_f = 12.8 min.,

and the fraction eluting from 12 to 14 min. was collected. Methanol was removed from the combined fractions *via* a rotary evaporator, and water was then removed by freeze-drying to give a white solid. The isolated product was identified by 400 MHz ^{1}H-nmr and FAB mass spectrometry.

Quantitation of Product (4.5)

Yields of *N*-(3-methylbut-2-enoyl)glycine ethyl ester (4.5) were quantitated by analytical hplc following the procedure described above. In independent experiments using authentic (4.5), the calibration curve shown as Figure 4.7 was generated for peak area *vs.* concentration of (4.5). The % yield of (4.5) was deduced from this calibration curve using peak areas. The assay was carried out in triplicate for each decomposition reaction, and a mean value taken. The assays agreed to ± 5 %.

7.4.1.2 From *N*-(2-Diazo-3-hydroxybutanoyl)glycine ethyl ester (2.1)

N-(2-Diazo-3-hydroxybutanoyl)glycine ethyl ester (2.1) {0.02 g, 0.1 mmol} was decomposed in $HClO_4$ (25 cm^3, 0.1 M) at ambient temperature. After standing for *ca.* 10 min., the mixture was neutralised to pH 7-8 with solid sodium bicarbonate. Aliquots (10 µl) of the neutralised solution were analysed by reverse-phase hplc using a Jones Apex II ODS column (25 cm x 4.0 mm i.d.) with isocratic elution using 15 % (v/v) methanol in water at a flow rate of 1 cm^3/min., and uv detection at λ = 210 and 250 nm. Five major peaks at R_f = 6.2, 7.9, 8.9, 12.7 and 13.5 min. were found as shown by the typical chromatogram presented as Figure 4.8.

The products with R_f = 6.2, 7.9, and 8.9 min. were isolated by semi-preparative hplc from more concentrated solutions of *N*-(2-diazo-3-hydroxybutanoyl)glycine ethyl

ester (2.1) {0.2 g, mmol} in 0.1 M $HClO_4$ (25 cm^3), using the same method as that described above (see Section 7.4.1.1). As before, for each of the three products, the methanol was removed by vacuum evaporation and the water by freeze-drying. The residues were then investigated by 400 MHz ^{1}H-nmr and FAB mass spectrometry.

Quantitation of Products *SR*-(4.8), (4.9) and *cis*-(4.10)

The yields of products 2(*S*),3(*R*)-(4.8), (4.9) and *cis*-(4.10) from decomposition reactions of *N*-(2-diazo-3-hydroxybutanoyl)glycine ethyl ester (2.1) were quantitated by analytical hplc following the procedure described above.

The % yields were deduced from calibration curves of peak area *vs.* concentration generated from authentic 2(*S*),3(*R*)-(4.8), (4.9) and *cis*-(4.10), prepared by independent synthesis. The assay was carried out in triplicate for each decomposition reaction, and a mean value taken. The assays agreed to ± 5 %.

7.4.1.3 From *N*-(2-Diazo-3-carbamoylpropanoyl)glycine benzyl ester (4.1)

N-(2-Diazo-3-carbamoylpropanoyl)glycine benzyl ester (4.1) was generated *in situ* by aprotic nitrosation of *L*-asparaginylglycine benzyl ester trifluoroacetate (4.4), and then allowed to decompose under controlled conditions. Typically, *L*-asparaginylglycine benzyl ester (4.4) {2.0g, 5 mmol} in THF (150 cm^3) and triethylamine (1.4 cm^3, 10 mmol), was reacted with liquid N_2O_4 (0.4 cm^3, 7 mmol) at -40 °C, in a similar way to that used in the preparation of *N*-(2-diazo-3-methylbutanoyl)glycine ethyl ester (2.2). The reaction mixture was allowed to warm to ambient temperature with stirring, which facilitated decomposition of the diazopeptide (*ca.* 2 h. from monitoring the loss of the diazo group at ν_{max} *ca.* 2100 cm^{-1} by FTIR). The THF was removed under vacuum, the

oily residue was taken up in ethyl acetate (150 cm^3), washed sequentially with sat. sodium bicarbonate solution (20 cm^3) and brine (20 cm^3), then dried over anhyd. sodium sulphate. Evaporation of the ethyl acetate gave a pale yellow oil, which was analysed by reverse-phase hplc using a Jones Apex II ODS column (25 cm x 4.0 mm i.d.), 40 % (v/v) methanol in water eluent, at a flow rate of 1 cm^3/min., and uv detection at λ = 258 nm.

Two major product peaks eluting at R_f = 6.3, and 16.3 min. were apparent as shown in Figure 4.27. Larger amounts of these products were obtained by semi-preparative hplc of more concentrated samples of the crude reaction mixture (0.5 g) dissolved in 40 % (v/v) methanol in water (10 cm^3), using a Jones Apex Prepsil ODS column (25 cm x 25 mm) and 40 % (v/v) methanol in water eluent at a flow rate of 25 cm^3/min., with uv detection at λ = 258 nm. Methanol, from combined fractions of each isolated product, was removed on a rotary evaporator, and water by freeze-drying. The residues were examined by 400 MHz ^{1}H-nmr and FAB mass spectrometry for structure elucidation.

7.4.2. *cis*-2,3-Epoxybutanamide (4.15) Decomposition Products

7.4.2.1 In $HClO_4$

cis-2,3-Epoxybutanamide (4.15) {0.1 g, 1.0 mmol} dissolved in 0.10 M $HClO_4$ (25 cm^3) was incubated at 37 °C for 5 h. The solution was neutralised with sodium bicarbonate and then freeze-dried to give a white crystalline solid (mainly sodium perchlorate). The solid was extracted with ethyl acetate (3 x 10 cm^3), and evaporation of the solvent gave a white solid residue which was analysed by FAB mass spectrometry.

cis-2,3-Epoxybutanamide (4.15) {0.05 g, 0.5 mmol} was also dissolved in D_2O (25cm^3, n_D = 0.995) plus $HClO_4$ (15 µl, 70 % w/w). The solution therefore contained *ca.* 0.1 M

$DClO_4$ and a D atom fraction (n_D) *ca.* 0.995. The reaction mixture was incubated at 37 °C and aliquots of the solution (2 cm^3) were analysed by 400 MHz ^1H-nmr over 2 d. for both loss of the *cis*-2,3-epoxybutanamide (4.15) substrate and formation of products. A typical 400 MHz ^1H-nmr spectrum for reaction of *cis*-(4.15) in 0.1 M $DClO_4$ after 2 d. is shown as Figure 5.12c.

7.4.2.2 In NaOH

cis-2,3-Epoxybutanamide (4.15) {0.1 g, 1.0 mmol) dissolved in 1 M NaOH (25 cm^3) was incubated at 37 °C for 10 d. The solution was neutralised with CO_2, then freeze-dried to give a white crystalline solid (mainly sodium carbonate). The solid was extracted with ethanol (3 x 10 cm^3) to give a white solid residue, which was examined by FAB mass spectrometry.

cis-2,3-Epoxybutamide (4.15) {0.05 g, 0.5 mmol} was also dissolved in 1 M NaOD (25 cm^3), prepared by volumetric dilution of a stock NaOD solution (Sigma) with D_2O. The solution therefore contained 1 M NaOD and n_D *ca.* 0.995. The reaction mixture was incubated at 37 °C, and aliquots of the solution (2 cm^3) were analysed by 400 MHz ^1H-nmr over 10 d. for both loss of substrate and formation of products. A typical 400 MHz ^1H-nmr spectrum for the reaction of *cis*-(4.15) with 1 M NaOD at 37 °C after 10 d. is shown as Figure 5.13d.

7.4.2.3 In Aqueous Morpholine

cis-2,3-Epoxybutanamide (4.15) {0.1 g, 1.0 mmol} dissolved in 0.1 M aqueous morpholine (25 cm^3) was incubated at 37 °C for 7 d. Water and morpholine were removed by freeze-drying to give a white solid residue, which was examined by FAB mass spectrometry.

cis-2,3-Epoxybutanamide (4.15) {0.05 g, 0.5 mmol} and morpholine (0.2 g, 2.3 mmol) were also dissolved in D_2O (25 cm^3, $n_D = 0.995$). The solution therefore contained 0.1 M morpholine and n_D *ca.* 0.90. The reaction mixture was incubated at 37 °C, and aliquots of the solution (2 cm^3) were analysed by 400 MHz ^{1}H-nmr over 7 d. for both loss of substrate and formation of products. A typical 400 MHz ^{1}H-nmr spectrum for the reaction of *cis*-(4.15) with 0.1 M morpholine in D_2O at 37 °C after 7 d. is shown as Figure 5.22c.

7.5 Syntheses

7.5.1 Synthesis of Diazopeptides

7.5.1.1 *N*-(2-Diazoacetyl)glycine ethyl ester (1.3)

Aq. sodium nitrite (5 M, 10 cm^3) was added to a solution of glycylglycine ethyl ester hydrochloride (5.0 g, 25 mmol) in 2 M sodium acetate (20 cm^3) at 0 °C. DCM and glacial acetic acid were added, and the mixture was stirred at 0 °C for 4 h. The DCM layer was separated, washed sequentially with sat. sodium bicarbonate solution (20 cm^3), brine (20 cm^3), dried with anhyd. sodium sulphate, concentrated to *ca.* 20 cm^3 and cooled to give yellow crystals of *N*-(2-diazoacetyl)glycine ethyl ester (1.3). Yield 2.4 g, (56 %); m.p. 106-107 °C (lit. m.p. 107 °C [42]); λ_{max} (EtOH) 250 (ε 20,520), 374 nm (ε 17 $dm^3mol^{-1}cm^{-1}$); ν_{max} (nujol) 3280 (NH amide), 2110 (C=N=N), 1740 (C=O ester), 1610 cm^{-1} (C=O amide); δ^1H (400 MHz, $CDCl_3$) 1.3 (3H, t, $-CH_2CH_3$, J = 7.2 Hz), 4.1 (2H, d, $-NHCH_2CO_2Et$, J = 5.6 Hz), 4.2 (2H, q, CH_2CH_3, J = 7.2 Hz), 4.8 (1H, s, $-CH{=}N_2$); m/z (FAB +ve ion) 172 (MH^+, 44 %), 116 ($MH^+ - N_2 - CH_2{=}CH_2$, 13), 104 ($[H_3NCH_2CO_2Et]^+$, 50).

7.5.1.2 *N*-(2-Diazoacetyl)glycinamide (1.4)

N-(2-Diazoacetyl)glycine ethyl ester (1.0 g, 5 mmol) was suspended in water (4 cm^3) at ambient temperature and 35 % ammonia solution (2.5 cm^3, 50 mmol) was added with stirring. The solution was cooled to give *N*-(2-diazoacetyl)glycinamide (1.4) as a yellow, crystalline solid. The product was washed with acetone and recrystallised from ethanol. Yield 0.35 g, (55 %); m.p. 160 °C (lit. m.p. 160 °C [42]); λ_{max} (H_2O) 250 (ε 21,500), 380 nm (ε 20.9 $dm^3mol^{-1}cm^{-1}$); ν_{max} (nujol) 3300, 3170 (NH_2), 2100 (C=N=N), 1650

(C=O primary amide), 1610 (C=O secondary amide), 1550 cm^{-1} (C-N amide); δ^1H (400 MHz, d_6 DMSO) 3.70 (2H, d, -NHC$H_2$$CO_2$Et, J = 5.6 Hz), 5.40 (1 H, s, -C$H$$N_2$); m/z (FAB +ve ion) 143 (MH^+, 20 %).

7.5.1.3 *N*-(2-Diazo-3-methylbutanoyl)glycine ethyl ester (2.2)

i) *N*-α-Carbobenzyloxy-*L*-valylglycine ethyl ester (7.1)

METHOD 1

N-α-Carbobenzyloxy-*L*-valine (10.0 g, 40 mmol) and triethylamine (5 cm^3, 44 mmol) were stirred in dry THF (150 cm^3) and cooled to -10 °C for 30 min. Ethylchloroformate (3.8 cm^3, 40 mmol) in THF (30 cm^3) was added dropwise with stirring at -10 °C, and the mixture was left to stir for 30 min. A solution of ethylglycinate in THF was prepared from the hydrochloride salt (5.9 g, 57 mmol) by the addition of triethylamine (0.8 cm^3, 57 mmol) and added dropwise to the mixed anhydride at -10 °C, and then left to stir at ambient temperature for 1 h. The solution was filtered, the filtrate evaporated to give an oil which was dissolved in DCM (100 cm^3), washed with 0.1 M HCl (10 cm^3), sat. sodium bicarbonate solution (10 cm^3) and brine (10 cm^3), and then dried over anhyd. sodium sulphate. Evaporation of the solvent gave the protected dipeptide ethyl ester as a white solid. Yield 5.6 g, (42 %); m.p. 163-65 °C.

METHOD 2

To a mixture of *N*-α-carbobenzyloxy-*L*-valine (10.0 g, 40 mmol) and glycine ethyl ester hydrochloride (6.0 g, 44 mmol) in DMF (250 cm^3), was added diphenylphosphorylazide {DPPA} (9.4 cm^3, 44 mmol) in DMF (30 cm^3) at 0 °C dropwise with stirring for 1 h.

Triethylamine (11.6 cm^3, 84 mmol) was then added dropwise at 0 °C, and the mixture was stirred at 0 °C for 5 h. and then at ambient temperature for 24 h. The solution was filtered and the DMF removed under vacuum. The crude white solid was taken up in ethyl acetate (200 cm^3) and washed with sat. sodium bicarbonate (30 cm^3) and brine (30 cm^3). Removal of the solvent under vacuum gave a white crystalline solid, which was recrystallised from a 1:1 (v/v) mixture of ether and ethyl acetate. Yield 9.8 g (73 %); m.p. 164-65 °C; ν_{max} (nujol) 3300 (NH amide), 1760 (C=O ester), 1710 (C=O carbamate ester), 1650 (C=O amide), 1225 (C-O ester), 710 cm^{-1} (CH arom); δ^1H (400 MHz, CD_3OD) 0.94, 0.97 (6H, d, $(CH_3)_2$ isopropyl, J = 6.8 Hz), 1.3 (3H, t, $-CH_2CH_3$, J = 7.2 Hz), 2.15 (1H, m, $(CH_3)_2CH$-, J = 6.8 Hz), 4.0-4.1 (3H, d & dd, -NHCHCO, $-NHCH_2CO_2Et$), 4.2 (2H, q, $-CH_2CH_3$, J = 7.2 Hz), 5.1 (2H, s, $PhCH_2$-O-), 5.4 (1H, br. s, -NH-CHCONH), 6.5 (1H, br. s, $-NHCH_2CO_2Et$), 7.3 (5H, s, Ph); $\delta^{13}C$ (CD_3OD, 100 MHz) 14.1 ($-CH_2CH_3$), 17.7, 19.2 ($(CH_3)_2$, isopropyl,) 31.0 ($-CH(CH_3)_2$), 41.3 ($-NHCH_2CO_2Et$), 60.4 (-NH-CH-CONH-), 61.6 ($-CH_2CH_3$), 67.1 ($PhCH_2$-O-), 128.2 (CH Ph), 156.4 (CO carbamate), 169.6 (CO amide), 171.4 (CO ester); m/z (FAB +ve ion) 337 (MH^+, 8 %), 91 ($[PhCH_2]^+$, 32).

ii) *L*-Valylglycine ethyl ester hydrochloride (4.2)

N-α-Carbobenzyloxy-*L*-valylglycine ethyl ester (7.1) {4.0 g, 12 mmol} was dissolved in ethanol (200 cm^3), and 5 M aqueous HCl (2.5 cm^3, 12 mmol) plus 10 % Pd/C (200 mg) catalyst was added. Hydrogen was sparged through the stirred solution at ambient temperature for 5 h. The solution was filtered and the solvent removed under vacuum. The oily residue was washed with ether (100 cm^3), and left under hard vacuum for 2 h. to give a white hygroscopic solid. Yield 2.4 g, (85 %); ν_{max} (nujol) 3210 (NH amide), 1740 (C=O ester), 1682 (C=O amide), 1205 cm^{-1} (C-O ester); δ^1H (60 MHz, CD_3OD) 1.1-1.4 (9H, d & t, $-CH(CH_3)_2$, $-CH_2CH_3$), 2.2 (1H, m, $-CH(CH_3)_2$), 3.8 (1H, d, $^+H_3NCHCO$), 4.05 (2H, d, $-NHCH_2COEt$), 4.2 (2H, q, $-CH_2CH_3$);

m/z (FAB +ve ion) 203 (MH^+ -HCl, 100 %), 104 ($[H_3NCH_2CO_2Et]^+$, 8.2).

iii) *N*-(2-Diazo-3 methylbutanoyl)glycine ethyl ester (2.1)

L-Valylglycine ethyl ester hydrochloride (2.2) {2.0 g, 8.4 mmol} was dissolved in dry THF (150 cm^3) plus triethylamine (3.6 cm^3, 26.0 mmol). Anhyd. sodium sulphate (5 g) was added and the solution cooled to *ca.* -40 °C with stirring under an atmosphere of N_2. Liquid N_2O_4 (0.6 cm^3, 92 mmol) in THF (30 cm^3) pre-cooled to *ca.* -40 °C in a jacketed, pressure-equalising dropping-funnel was added to the mixture dropwise over 20 min. with stirring. The solution was then stirred for a further 1 h. at *ca.* -40 °C. The resulting yellow-green solution was allowed to warm to room temperature and filtered before the THF was removed under vacuum. The residual yellow oil was taken up in dry ethyl acetate (150 cm^3) and washed sequentially with water (10 cm^3), sat. sodium bicarbonate solution (10 cm^3), and brine (10 cm^3) and then dried over anhyd. sodium sulphate. The solvent was evaporated to give the diazopeptide as a yellow oil which was purified by silica-column chromatography using 1:1 (v/v) light petroleum/ether as eluent. Yield 0.75 g, (42 %); λ_{max} (EtOH) 255 (ε 8,310), 380 nm (ε 8.2 $dm^3mol^{-1}cm^{-1}$); ν_{max} (thin film) 3350 (amide NH), 2080 (C=N=N), 1750 (C=O ester), 1620 (C=O amide), 1200 cm^{-1} (C-O ester); δ^1H (400 MHz, $CDCl_3$), 1.16 (6H, d, $-CH(CH_3)_2$, J = 6.8 Hz), 1.31 (3H, t, $-CH_2CH_3$, J = 7.2 Hz), 2.7 (1H, m, $-CH(CH_3)_2$), 4.10 (2H, d,$-NHCH_2CO_2Et$, J = 5.6 Hz), 4.22 (2H, q, $-CH_2CH_3$, J = 7.2 Hz); m/z (FAB +ve ion) 214 (MH^+, 22 %), 186 (MH^+ -N_2, 88), 168 (MH^+ -EtOH, 6), 140 (MH^+ -HCO_2Et, 9), 104 ($[H_3NCH_2CO_2Et]^+$, 9), 83 (N_2=$CCH(CH_3)_2]^+$, 100).

7.5.1.4 *N*-(2-Diazo-3-hydroxybutanoyl)glycine ethyl ester (2.1)

i) *N*-α-Carbobenzyloxy-*L*-threonylglycine ethyl ester (7.2)

A solution of DECP (4.0 g, 24 mmol) in DMF (20 cm^3) was added to a mixture of *N*-α-carbobenzyloxy-*L*-threonine (5.0 g, 20 mmol) and glycine ethyl ester hydrochloride (3.05 g, 22 mmol) in DMF (150 cm^3) at 0 °C. A solution of triethylamine (5.6 cm^3, 40 mmol) in DMF (20 cm^3) was added over 5 min., and the mixture stirred at 0 °C for 2 h. and then at room temperature for 2 d. After most of the DMF had been removed under vacuum, the oily residue was taken up in ethyl acetate (200 cm^3) washed sequentially with 0.1 M HCl (20 cm^3), sat. sodium bicarbonate (20 cm^3), and brine (20 cm^3), and then dried over anhyd. sodium sulphate. Evaporation of the solvent gave the product as an off-white solid, which was recrystallised from ethyl acetate to give a white crystalline solid. Yield 4.2 g, (42 %); m.p. 95.5-96.5 °C; ν_{max} (KBr) 3200-3300 (br. NH amide and OH alcohol), 1750 (C=O ester), 1690 (C=O carbamate), 1650 (C=O amide), 1200 cm^{-1} (C-O ester); δ^1H (60 MHz, CD_3OD) 1.3 (6H, overlapping t & d, -CH_2CH_3, -$CH(CH_3)OH$), 3.9-4.5 (6H, overlapping m, d, d & q, -$CH(CH_3)OH$, -$CHCONH$-, -CH_2CO_2Et, -CH_2CH_3), 5.1 (2H, s, $PhCH_2$-O-), 7.3 (5H, s, Ph); m/z (FAB +ve ion) 339 (MH^+, 2 %), 91 ($[PhCH_2]^+$, 100).

ii) *L*-Threonylglycine ethyl ester hydrochloride (4.3)

This compound was prepared by catalytic hydrogenation of *N*-α-carbobenzyloxy-*L*-threonylglycine ethyl ester (7.2) {1.75 g, 5.2 mmol} in ethanol (100 cm^3) plus 5 M HCl (1.25 cm^3, 6.3 mmol), using 10 % Pd/C catalyst (100 mg) in the same way as for compound (4.2). The product was isolated as a white hygroscopic solid. Yield 1.15 g, (93 %); ν_{max} (nujol) 3200-3300 (br. NH amide and OH alcohol), 1750 (C=O ester), 1625 (C=O amide), 1205 cm^{-1} (C-O ester); δ^1H (400 MHz, CD_3OD) 1.27

(3H, t, -CH_2CH_3, J = 7.2 Hz), 1.37 (3H, d, -CH(OH)CH_3, J = 4.0 Hz), 3.73 (1H, d, -CHCONH-, J = 6.8 Hz), 3.93-4.12 (2H, ABq, -NH-CH_2CO_2Et), 4.04 (1H, m, -CH(OH)CH_3), 4.19 (2H, q, CH_2CH_3, J = 7.2 Hz); δ^{13}C (100 MHz, CD_3OD) 14.5 (-CH_2CH_3), 20.2 (-CH(OH)CH_3), 42.1 (NHCH_2CO_2Et), 60.4 (-CH(OH)CH_3), 62.5 (-CH_2CH_3), 67.5 (-CHCONH-), 169.1 (*C*O amide), 170.9 (*C*O ester); m/z (FAB +ve ion) 206 (MH^+ -HCl, 25 %); (FAB -ve ion) 204 ($M-H^+$, 20 %).

iii) *N*-(2-Diazo-3-hydroxybutanoyl)glycine ethyl ester (2.1)

This compound was prepared in the same way as *N*-(2-diazo-3-methylbutanoyl)glycine ethyl ester (2.2) by aprotic nitrosation using liquid N_2O_4 (0.53 cm^3, 8.4 mmol) from *L*- threonylglycine ethyl ester (4.3) {1.83 g, 7.6 mmol} and triethylamine (3.16 cm^3, 23 mmol). The product was purified by silica-column chromatography using ether as eluent. Yield 0.73 g, (45 %); λ_{max} (EtOH) 255 nm (ε = 18490 $dm^3mol^{-1}cm^{-1}$); ν_{max} (thin film) 3300-3500 (NH amide and OH alcohol), 2980 (CH_3 stretch), 2093 (C=N=N), 1749 (C=O ester), 1625 (C=O amide), 1209 cm^{-1} (C-O ester); δ^1H (400 MHz, $CDCl_3$) 1.30 (3H, t, -CH_2CH_3, J = 7.2 Hz), 1.45 (3H, d, -CH(CH_3)OH, J = 6.2 Hz), 4.05, 4.15 (2H, dd, -CH_2CO_2Et), 4.20 (2H, q, -CH_2CH_3, J = 7.2 Hz), 4.91 (1H, q, -CH(OH)CH_3, J = 6.2 Hz); δ^{13}C (100 MHz, $CDCl_3$) 14.1 (-CH_2CH_3), 20.8 (-CH (CH_3)OH), 41.0 (-CH_2CO_2Et), 61.6 (-CH_2CH_3), 128.6 (-*C*=N=N), 166.5 (*C*O amide), 170.6 (*C*O ester); m/z (FAB +ve ion) 216 (MH^+, 18 %), 188 (MH^+ -N_2, 16), 170 (MH^+ -EtOH, 27), 142 (MH^+ -N_2 -H_2O -CH_2=CH_2, 21), 130 ([$CONHCH_2CO_2Et$]$^+$, 100), 104 ([$H_3NCH_2CO_2Et$]$^+$, 77); (FAB -ve ion) 214 ($M-H^+$, 39 %), 186 ($M-H^+$ -N_2, 29).

7.5.1.5 *N*-(2-Diazo-3-hydroxybutanoyl)sarcosine ethyl ester (2.4)

i) *N*-α-Carbobenzyloxy-*L*-threonylsarcosine ethyl ester (7.3)

This compound was prepared from *N*-α-carbobenzyloxy-*L*-threonine (5.0 g, 20 mmol) and sarcosine ethyl ester hydrochloride (2.83 g, 20 mmol) using DECP (4.0 g, 24 mmol) in the presence of triethylamine (5.6 cm^3, 40 mmol), using the same method as described for the synthesis of *N*-α-carbobenzyloxy-*L*-threonylglycine ethyl ester (7.2). The product was purified by silica-column chromatography using ethyl acetate as eluent (R_f = 0.4) and isolated as a colourless oil. Yield 5.5 g, 80 %; ν_{max} (thin film) 3400 (OH alcohol), 3300 (NH amide), 1750 (C=O ester), 1690 (C=O carbamate ester), 1650 (C=O amide), 1200 cm^{-1}; δ^1H (60 MHz, $CDCl_3$) 1.2-1.6 (6H, overlapping d & t, -CH(OH)C*H*$_3$, -CH_2CH_3), 3.3 (3H, s, -N-C*H*$_3$), 3.7 (1H, d, -C*H*-CO-), 3.9-4.4 (5H, overlapping d, t & m, -C*H*$_2$-CO_2Et, -C*H*$_2CH_3$ and CH_3(OH)C*H*-CH-), 5.1 (2H, s, Ph-C*H*$_2$-O-), 7.3 (5H, s, Ph); m/z (FAB +ve ion) 353 (MH^+, 2 %), 335 (MH^+ - H_2O, 3), 91([$PhCH_2$]$^+$, 100).

ii) *L*-Threonylsarcosine ethyl ester hydrochloride (7.4)

This compound was prepared by catalytic hydrogenation of the *N*-α-carbobenzyloxy-*L*-threonylsarcosine ethyl ester (7.3) {2.5 g, 7.35 mmol} in ethanol (150 cm^3) plus 5 M HCl (1.62 cm^3, 8.1 mmol), using 10 % Pd/C catalyst (100 mg) in the same way as for compound (4.2). The product was isolated as a white hygroscopic solid after the removal of ethanol under vacuum. Yield 1.53 g, (85 %); ν_{max} (nujol) 3300-3000 (NH amide and OH alcohol), 1750 (C=O ester), 1670 (C=O amide), 1200 cm^{-1} (C-O ester); δ^1H (400 MHz, $CDCl_3$) 1.27 (3H, t,-CH_2CH_3, J = 7.2 Hz), 1.37 (3H, d, -CH(OH)C*H*$_3$, J = 4.0 Hz), 3.06 (3H, s, C*H*$_3$N-), 3.72 (1H, d, -C*H*-CH(OH)CH_3, J = 6.8 Hz), 3.93-4.12 (2H, ABq, -C*H*$_2$$CO_2$Et), 4.05 (1H, m, -C*H*(OH)CH_3), 4.19 (2H, -C*H*$_2$$CH_3$, J = 7.2 Hz);

m/z (FAB +ve ion) 219 (MH^+ -HCl, 100 %), 201 (MH^+ -H_2O, 80), 155 (MH^+ -H_2O -EtOH, 24), 127 (MH^+ -H_2O -EtOH -CH_2=CH_2, 16).

iii) *N*-(2-Diazo-3-hydroxybutanoyl)sarcosine ethyl ester (2.4)

This compound was prepared in the same way as *N*-(2-diazo-3-methylbutanoyl)glycine ethyl ester (2.2) by aprotic nitrosation using liquid N_2O_4 (0.5 cm^3, 7.2 mmol), *L*-threonylglycine sarcosine ester (7.4) {1.4 g, 5.5 mmol} and triethylamine (2.3 cm^3, 16.5 mmol). The product was purified by silica-column chromatography using 1:1 (v/v) ethyl acetate/DCM (R_f = 0.4), and isolated as a bright yellow oil. Yield 0.49 g, (39 %); λ_{max} (EtOH) 255 nm (ε 12,846 $dm^3mol^{-1}cm^{-1}$); ν_{max} (thin film) 3300-3500 (NH amide and OH alcohol), 2070 (C=N=N), 1740 C=O ester), 1625 (C=O amide), 1205 cm^{-1} (C-O ester); δ^1H (400 MHz, $CDCl_3$) 1.27 (3H, t, -CH_2CH_3, J = 7.2 Hz), 1.37 (3H, d, -CH(OH)CH_3, J = 4.0 Hz), 3.07 (3H, s, CH_3-N-), 3.98-4.16 (2H, ABq, -CH_2CO_2Et), 4.24 (2H, q, -CH_2CH_3, J = 7.2 Hz), 4.95 (1H, m, -CH(OH)CH_3); $\delta^{13}C$ (100 MHz, $CDCl_3$) 14.2 (-CH_2CH_3), 18.8 (-CH(OH)CH_3), 37.3 (-N-CH_3), 50.5 (-CH_2CO_2Et), 61.5 (-CH_2CH_3), 64.4 (-CH(OH)CH_3), 128.2 (-C=N=N), 167.9 (CO amide), 169.0 (CO ester); m/z (FAB +ve ion) 230 (MH^+, 4 %), 202 (MH^+ -N_2, 63), 184 (MH^+ -EtOH, 18), 156 (MH^+ -EtOH -CH_2=CH_2, 28), 116 ([$N(CH_3)$-CH_2CO_2Et]$^+$, 100); (FAB -ve ion), 228 (M-H, 20 %), 200 (M-H -N_2, 29), 184 (M-H^+ -N_2 -H_2O, 27), 172 (M-H^+ -N_2 -CH_2=CH_2, 18), 156 (M-H^+ -N_2 -H_2O -CH_2=CH_2, 100).

7.5.1.6 *N*-(2-Diazo-3-carbamoylpropanoyl)glycine benzyl ester (4.1) {formed *in situ*, see Section 7.4.1.3}

i) Glycine benzyl ester *p*-toluenesulphonate salt (7.5)

Glycine toluene-4-sulphonic acid monohydrate (11.4 g, 0.19 mol) and benzyl alcohol (120 cm^3) in toluene (120 cm^3) were heated under reflux using a Dean & Stark head until the production of water had ceased (4 h.). After cooling to room temperature, ether (200 cm^3) was added and the mixture was left in an ice bath for 2 h. Off-white crystals of glycine benzyl ester toluene-4-sulphonate were filtered off and air-dried to give a white crystalline solid. The product was recrystallised from ethanol to give a white crystalline solid. Yield 28.4 g, (64 %); m.p. 131-32 °C; ν_{max} (nujol) 1740 (C=O ester), 1200 cm^{-1} (C-O ester); δ^1H (60 MHz, d_6 DMSO) 2.2 (3H, s, -NC*H*$_3$), 3.7 (2H, s, H_3N^+C*H*$_2CO_2$Bz), 5.0 (2H, s, Ph-C*H*$_2$O-), 6.95 (2H, d, Ar), 7.2 (5H, s, Ph), 7.65 (2H, d, Ar), 8.1 (3H, br. s, H_3N^+); m/z (FAB +ve ion) 166 ($[H_3N^+CH_2CO_2CH_2Ph]^+$), 91 ($[PhCH_2]^+$, 100 %); (FAB -ve ion) 171 ($[CH_3PhSO_3]^-$), 80 ($[SO_3]^-$, 100 %).

ii) *N*-α-*t*-Butoxycarbonyl-*L*-asparaginylglycine benzyl ester (7.6)

This was prepared from *N*-α-*t*-butoxycarbonyl-*L*-asparagine (10.0 g, 38 mmol), glycine benzyl ester *p*-toluenesulphonate salt (7.5) {12.7 g, 38 mmol} and DECP (7.4 g, 45 mmol) in the presence of triethylamine (10.5 cm^3, 76 mmol), using the same method and work up as for compound (7.2). The product was obtained as a chalky white solid and used without further purification. Yield 11.8 g, (88 %); m.p. 135-136 °C; ν_{max} (KBr) 3400 (NH amide), 3300 (NH carbamate), 1740 C=O ester), 1680 (primary amide), 1660 (C=O secondary amide), 1570 (secondary carbamate), 1190 (C-O ester); δ^1H (400 MHz, CD_3OD) 1.44 (9H, s, C(C*H*$_3$)$_3$), 2.6 (2H, dd, -C*H*$_2CONH_2$), 3.99 (2H, dd, -HNC*H*$_2CO_2$Bz), 4.48 (1H, t, -HNC*H*(CH_2CONH_2)-CO-), 5.01 (2H, s, Ph-C*H*$_2$O-), 7.28 (5H, s, Ph); m/z (FAB +ve ion) 380 (MH^+, 1 %), 280 (MH^+ -$(CH_3)_3COCO$, 14), 91 ($[PhCH_2]^+$, 100).

iii) *L*-Asparaginylglycine benzyl ester trifluoroacetate (4.4)

Deprotection of the *N*-α-*t*-butoxycarbonyl-*L*-asparaginylglycine benzyl ester (7.6) {2.0 g, 5.5 mmol} using trifluoroacetic acid (6.0 cm^3, 50 mmol) gave this compound. The reaction solution was diluted with dry DCM (50 cm^3) and stirred at ambient temperature for 30 min. The organic solvents were removed by rotary evaporation to leave an oily residue. On addition of dry ether (100 cm^3), the residue transformed to a white hygroscopic solid. The ether was decanted and the solid was dried under vacuum. Yield 2.0 g, (95 %); ν_{max} (KBr); 3400 (NH amide), 1740 (C=O ester), 1680 (C=O primary amide), 1660 (C=O secondary amide), 1190 (C-O ester); δ^1H (400 MHz, CD_3OD) 2.50-2.70 (2H, dd, -C*H*$_2$CONH$_2$), 3.70-3.90 (2H, ABq, -NHC*H*$_2$CO$_2$Bz), 4.04 (1H, dd, -HNC*H*(CH$_2$CONH$_2$)-CO-, J = 6.4 Hz), 5.01 (2H, s, PhC*H*$_2$-), 7.28 (5H, s, Ph); m/z (FAB +ve ion) 280 (MH^+ -CF_3CO_2H, 11 %), 263 (MH^+ -NH_3, 4), 91 ($[PhCH_2]^+$, 76); (FAB -ve ion) 113 ($[CF_3CO_2]^-$, 100 %).

7.5.1.7 *N*-(2-Diazo-3-carbamoylpropanoyl)glycine ethyl ester (4.17) {formed *in situ*, see Section 7.4.1.3}

i) *N*-α-Carbobenyloxy-*L*-asparaginylglycine ethyl ester (7.7)

This was prepared from *N*-α-carbobenzyloxy-*L*-asparagine (10.0 g, 41 mmol), glycine ethyl ester hydrochloride (5.8 g, 41 mmol) and DECP (8.0 g, 50 mmol) in the presence of triethylamine (11.4 cm^3, 82 mmol), using the same method as described for the synthesis of *N*-α-carbobenzyloxy-*L*-threonylglycine ethyl ester (7.6). The product was obtained as a white solid, and was recrystallised from ethanol to give a white crystalline solid. Yield 11.0 g, (83 %); m.p. 184-85 °C; ν_{max} (KBr) 3410 (NH amide), 3300 (NH carbamate), 1740 (C=O ester), 1670 (C=O primary amide), 1650 (C=O secondary amide), 1540 cm^{-1} (C=O secondary carbamate); δ^1H (60 MHz, d_6 DMSO) 1.2 (3H, t, -CH$_2$C*H*$_3$, J = 7.2 Hz), 2.6 (2H, d, -C*H*$_2$CONH$_2$), 3.3 (2H, s, -CONH$_2$), 3.8 (1H, m,

-C*H*CH_2CONH_2), 4.1 (2H, d, -HNC*H*$_2CO_2Et$), 4.2 (2H, q, -C*H*$_2CH_3$, J = 7.2 Hz), 5.0 (2H, s, PhC*H*$_2$O-), 7.3 (5H, s, Ph); m/z (FAB +ve ion) 352 (MH^+, 6 %), 91 ($[PhCH_2]^+$, 100).

ii) *L*-Asparaginylglycine ethyl ester hydrochloride (4.18)

This was prepared by catalytic hydrogenation of *N*-α-carbobenzyloxy-*L*-asparaginylglycine ethyl ester (7.7) {4.0 g, 11.4 mmol} in methanol (200 cm^3) with 12 M HCl (1.1 cm^3, 2.5 mmol), using 10 % Pd/C catalyst (200 mg) in the same way as for compound (4.2). The product was isolated as a white hygroscopic solid. Yield 2.7 g, (93 %); ν_{max} (KBr) 3400 (NH amide), 1740 (C=O ester), 1680 (C=O primary amide), 1660 (C=O secondary amide), 1208 cm^{-1} (C-O ester); δ^1H (60 MHz, CD_3OD) 1.3 (2H, t, -CH_2C*H*$_3$, J = 7.2 Hz), 3.0 (2H, d, -C*H*$_2CONH_2$), 4.1 (2H, d, -HNC*H*$_2CO_2Et$), 4.2 (2H, q, -C*H*$_2CH_3$, J = 7.2 Hz); m/z (FAB +ve ion) 218 (MH^+ -HCl, 100 %), 201 (MH^+ -NH_3, 40).

7.5.2 Synthesis of Triazenes and Related Products

7.5.2.1 *N*-(4-Nitrophenylazo)glycylglycine ethyl ester (3.3)

4-Nitroaniline (2.0 g, 14 mmol) was dissolved in 2 M HCl (30 cm^3), diluted with water (40 cm^3), and diazotised at 0 °C over a period of 1-2 h. with sodium nitrite (1.0 g, 14 mmol) dissolved in water (10 cm^3). The 4-nitrophenyl diazonium salt solution was filtered and then reacted with glycylglycine ethyl ester hydrochloride (2.85 g, 14 mmol) in water (10 cm^3). After stirring the mixture at 0 °C for 20 min., a ten-fold molar excess of sodium acetate trihydrate (20 g) was added to slowly precipitate the *N*-(4-*N*-nitrophenylazo)glycylglycine ethyl ester (3.3) from the reaction mixture. The product was filtered, dried over magnesium sulphate and recrystallised from 2:1 (v/v) chloroform/hexane. Yield 3.0 g, (68 %); m.p. 106-106.5 °C, decomp.; (Found: C, 44.46; H, 4.97; N, 20.47 %. Calc for $C_{12}H_{15}N_5O_5$: C, 45.16; H, 5.05; N, 20.93 %); λ_{max} (EtOH) 350 nm (ε 20,827 $dm^3mol^{-1}cm^{-1}$); ν_{max} (KBr); 3400-3600 (NH amide), 1740 (C=O ester), 1652 (C=O amide), 1548 (N=N azo), 1516, 1338 (NO), 1214 cm^{-1} (C-O ester); δ^1H (400 MHz, $CDCl_3$) 1.28 (3H, t, -CH_2CH_3, J = 7.2 Hz), 4.12 (2H, d, -NHCH_2CO_2Et, J = 4.8 Hz), 4.23 (2H, q, -CH_2CH_3, J = 7.2 Hz), 4.46 (2H, br. s, ArN=N-NHCH_2CO-), 6.84, 7.52 (2H, br. s, Ar), 8.24 (2H, d, Ar); $\delta^{13}C$ (100 MHz, $CDCl_3$) 14.1 (-CH_2CH_3), 41.3 (NHCH_2CO_2Et), 61.8 (-CH_2CH_3), 125.8 (*C*H Ar), 168.1 (*C*O amide), 170.4 (*C*O ester); m/z (FAB +ve ion) 310 (MH^+, 9 %), 150 ([O_2N-Ph-N_2^+], 32), 104 ([$H_3NCH_2CO_2Et]^+$, 12); (FAB -ve ion) 308 (M-H^+, 100 %), 205 (M -[$H_3NCH_2CO_2Et]^+$, 12), 159 (M -O2NPh-N_2^+, 14).

7.5.2.2 *N*-(4-Nitrophenyl)glycylglycine ethyl ester silver salt (3.3a)

The *N*-(4-nitrophenylazo)glycylglycine ethyl ester (3.3) {1.0 g, 3.2 mmol} dissolved in ethanol (30 cm^3) was added with stirring to a solution of silver nitrate (2.7 g, 16 mmol)

in water (10 cm^3) to give an immediate bright yellow precipitate. The solid was filtered, washed with ethanol and dried under vacuum. Yield 0.7 g, 52 %; m.p. 168-169 °C, decomp.; (Found: C, 34.40; H, 3.36; N, 16.58 %, Calc. for $AgC_{12}H_{15}N_5O_5$: C, 34.55; H, 3.62; N, 16.79 %); ν_{max} (KBr); 1728 (C=O ester), 1645 (C=O amide), 1545 (N=N azo), 1500, 1330 (NO), 1218 cm^{-1} (C-O ester); δ^1H (400 MHz, d_6 DMSO) 1.21 (3H, t, $-CH_2CH_3$, J = 7.2 Hz), 4.04 (2H, d, $-HNCH_2CO_2Et$, J = 5.6 Hz), 4.10 (2H, q, $-CH_2CH_3$, J = 7.2 Hz), 4.61 (2H, s, $ArN{=}N{-}NHCH_2CO-$), 7.60 (2H, d, Ar, J = 8.8 Hz), 8.10 (2H, d, Ar, J = 8.8 Hz), 8.94 (1H, br. t, $-NHCH_2CO_2Et$); m/z (FAB +ve ion) 310 (MH^+ -Ag, 3 %), 150 ($[O_2NPhN_2]^+$, 14), 59 ($[HO{=}CHOEt]^+$, 100); (FAB -ve ion) 308 ($M{-}H^+$, 20 %), 137 ($[O_2NPhNH]^-$, 29).

7.5.2.3 *N*-(4-Sulphonylphenylazo)glycylglycine ethyl ester silver salt (3.2a)

Sulphanilic acid (2.0 g, 11.6 mmol) was dissolved in 2 M $HClO_4$ (30 cm^3), diluted with water (40 cm^3), and then diazotised at 0 °C over a period of 1 h. with sodium nitrite (0.8 g, 12 mmol) dissolved in water (10 cm^3). The diazonium salt solution was reacted at 0 °C with aqueous, neutral glycylglycine ethyl ester prepared *in situ* by the addition of silver nitrate (2.0 g, 11.6 mmol) to glycylglycine ethyl ester hydrochloride (2.0 g, 11.6 mmol) in water (10 cm^3), followed by filtration of the precipitated silver chloride. The reaction solution was stirred at 0 °C, and the pH raised to 7 by the dropwise addition of 5 M sodium hydroxide to give a yellow orange solution. This solution was then treated at 0 °C with silver nitrate (4.0 g, 25 mmol) in water (10 cm^3), which caused a colour change to bright yellow. Addition of acetone (30 cm^3) to the reaction solution at 0 °C gave a fine yellow precipitate. Yield 2.10 g, 40 %; m.p. 155 °C, decomp.; ν_{max} (KBr) 1749 (C=O ester), 1655 cm^{-1} (C=O amide), 1548 (N=N azo), 1381, 1122 (S=O), 1209 (C-O ester); δ^1H (400 MHz, d_6 DMSO) 1.21 (3H, t, $-CH_2CH_3$, J = 7.2 Hz), 4.00 (2H, d, $-HNCH_2CO_2Et$), 4.12 (2H, q, $-CH_2CH_3$, J = 7.2 Hz), 4.54 (2H, s, $-PhN{=}N{-}NHCH_2CO-$), 7.36 (2H, d, Ar, J = 8.0), 7.49 (2H, br. s, Ar), 8.79 (1H, br. s, $-NHCH_2CO_2Et$); m/z (FAB -ve ion) 343 ($M{-}H^+$, 12 %), 315 ($M{-}H^+ - N_2$, 7), 293 ($M{-}H - N_2 - CH_2{=}CH_2$, 25).

7.5.2.3 *N*-(2-*N*-Morpholinoacetyl)glycine ethyl ester (3.4)

i) 2-(*N*-Morpholino)ethanoic acid (3.8)

Morpholine (3.8 cm^3, 42 mmol) was added to chloroacetic acid (2.0 g, 21 mmol) dissolved in absolute ethanol (100 cm^3), and the mixture was heated under reflux for 5 h. The ethanol was then removed under vacuum to give the morpholino salt of (3.8) as a pale brown solid. The crude salt was recrystallised from 1:1 (v/v) ethyl acetate/ethanol to give a white crystalline solid. Yield 4.8 g, (85 %); m.p. 141-142 °C; ν_{max} (KBr) 3200-2400 (NH quarternary salt), 1600 (C=O carboxylate), 1210 cm^{-1} (C-O ether); δ^1H (400 MHz, d_6 DMSO) 2.66 (4H, t, -(CH_2)$_2$N$CH_2CO_2^-$ (ring), J = 4.8 Hz), 3.06 (4H, t, -CH_2-NH_2^+-CH_2- (ring), J = 4.8 Hz), 3.21 (2H, s, -NH-$CH_2CO_2^-$), 3.63 (4H, t, -CH_2-O-CH_2-CH_2-N-$CH_2CO_2^-$ (ring), J = 4.8 Hz), 3.80 (4H, t, -CH_2-O-CH_2-CH_2-NH_2^+- (ring), J = 4.8 Hz); δ^{13}C (100 MHz, d_6 DMSO) 42.4 (-$CH_2CO_2^-$), 52.0 (-(CH_2)$_2$-N-$CH_2CO_2^-$ (ring)), 58.6 ((CH_2)$_2$-N^+H_2- (ring)), 63.1 (-CH_2-O-CH_2- (ring)), 64.9 (-CH_2-O-CH_2- (ring)), 169.7 ($CH_2CO_2^-$); m/z (FAB +ve ion), 231 (MH^+), 100 (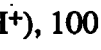); (FAB -ve ion) 229 (M-H^+), 201 (M-H^+ -CH_2=CH_2), 183 (M-H^+ -EtOH).

ii) *N*-(2-*N*-Morpholinoacetyl)glycine ethyl ester (3.4)

DECP (2.2 g, 13.5 mmol) in DMF (20 cm^3) was added to a cooled solution of (3.8) {3.0 g, 11.2 mmol} and glycine ethyl ester hydrochloride (1.87 g, 13.5 mmol) in DMF (100 cm^3). A solution of triethylamine (5.4 cm^3, 39 mmol), in DMF (20 cm^3) was then added over 5 min., and the whole mixture stirred at 0 °C for 2 h. and then at room temperature for 2 d. The solution was filtered and the DMF removed under vacuum. The colourless oil was taken up in ethyl acetate (100 cm^3), washed sequentially with water (20 cm^3) and brine (20 cm^3), and then dried over anhyd. sodium sulphate. The

solvent was vacuum evaporated to give a residual, pale yellow oil which was purified by silica-column chromatography using ethyl acetate as eluent ($R_f = 0.2$). After vacuum evaporation of the ethyl acetate, (3.4) was isolated as a white crystalline solid. Yield 2.0 g, (75 %); m.p. 72.5-73.5 °C; (Found: C, 51.76; H, 7.88; N, 12.01 %; Calc. for $C_{10}H_{18}N_2O_4$: C, 52.16; H, 7.88; N, 12.17 %); ν_{max} (KBr) 3280 (NH amide), 1750 (C=O ester), 1660 cm^{-1} (C=O amide); δ^1H (400 MHz, $CDCl_3$) 1.29 (3H, t, $-CH_2CH_3$, J = 7.2 Hz), 2.58 (4H, $-NCH_2-$ (ring), J = 4.4 Hz), 3.06 (2H, s, $-NCH_2CONH-$), 3.75 (4H, t, $-OCH_2-$ (ring), J = 4.4 Hz), 4.07 (2H, d, $-NHCH_2CO_2Et$, J = 5.2 Hz), 4.20 (2H, q, $-CH_2CH_3$, J = 7.2 Hz); $\delta^{13}C$ (100 MHz, $CDCl_3$) 14.2 ($-CH_2CH_3$), 40.2($-CH_2CO_2Et$), 53.8 ($-CH_2-N-CH_2-$ (ring)), 61.5 ($-NCH_2CONH-$), 61.7 ($-CH_2CH_3$), 67.0 ($-CH_2-O-CH_2-$ (ring)), 169.9 (CO amide), 170.3 (CO ester); m/z (FAB +ve ion) 231 (MH^+, 80 %), 100 ( , 100); (FAB -ve ion) 229 ($M-H^+$, 100 %), 201 ($M-H^+ -CH_2=CH_2$, 94), 183 ($M-H^+$ -EtOH, 72).

7.5.3 Synthesis of Authentic Products from Diazopeptide Decompositions

7.5.3.1 *N*-(2-Methylbut-2-enoyl)glycine ethyl ester (4.5)

This was prepared from 3,3-dimethylacrylic acid (5.0 g, 50 mmol) and glycine ethyl ester hydrochloride (7.0 g, 50 mmol) and DPPA (10.7 cm^3, 50 mmol) in the presence of triethylamine (7.0 cm^3, 50 mmol) using the same method as described for the synthesis of *N*-α-carbobenzyloxy-*L*-valylglycine ethyl ester (7.1). The reaction solution was filtered, and the DMF was removed in vacuo, to leave a pale yellow oil, which was taken up in ethyl acetate (200 cm^3), washed sequentially with sat. sodium bicarbonate solution (10 cm^3), water (10 cm^3) and brine (10cm^3), and then dried over anhyd. sodium sulphate. After vacuum evaporation of the solvent, tlc of the crude oily product using 1:1 (v/v) 40-60 pet. ether/ethyl acetate as eluent indicated 4 spots, including the product at R_f = 3.9. The product was purified by silica-column chromatography using 1:1 (v/v) 40-60 pet. ether/ethyl acetate as eluent, and recrystallised from ether/pentane (6:1 v/v) to give a white crystalline solid. Yield 2.4 g, (30 %); m.p. 37-38 °C; (Found: C, 58.10; H, 8.12; N, 7.52 %. Calc. for $C_9H_{15}NO_3$: C, 58.36; H, 8.16; N, 7.56 %); ν_{max} (nujol) 3300 (NH amide), 1750 (C=O ester), 1660 (C=O amide & C=C), 1225 (C-O ester), 810 cm^{-1} (=CH); δ^1H (400 MHz, $CDCl_3$) 1.28 (3H, t, -CH_2CH_3, J = 7.2 Hz), 1.86 (3H, s, $CH_3C(CH_3)$=CH-), 2.16 (3H, s, $CH_3C(CH_3)$=CH-), 4.07 (2H, d, -$NHCH_2CO_2Et$, J = 5.6 Hz), 4.22 (2H, q, -CH_2CH_3, J = 7.2 Hz), 5.63 (1H, s, $(CH_3)_2CH$=CH-CO-), 5.84 (1H, br. s, NH); δ^{13}C (100 MHz, $CDCl_3$) 14.1 (-CH_2CH_3), 19.9 (=$C(CH_3)CH_3$), 27.2 (=$C(CH_3)CH_3$), 41.2 (-CH_2CO_2Et), 61.5 (-CH_2CH_3), 117.6 ($(CH_3)_2C$=), 152.3 (=CHCO-), 166.8 (CO amide), 170.3 (CO ester); m/z (FAB +ve ion) 186 (MH^+, 100 %), 140 (MH^+ -EtOH, 10), 112 ($[(CH_3)_2C$=$CHCONHCH_2]^+$, 3), 83 ($[(CH_3)_2C$=$CHCO]^+$, 100).

7.5.3.2 *N*-(2(*S*),3(*R*)-Dihydroxybutanoyl)glycine ethyl ester (4.8)

i) *trans*-*N*-(But-2-enoyl)glycine ethyl ester (4.12)

A solution of DECP (10.4 g, 64 mmol) in DMF (30 cm^3) was added to a stirred solution at 0 °C of *trans*-crotonic acid (5.0 g, 58 mmol) plus glycine ethyl ester hydrochloride (8.1 g, 58 mmol) in DMF (150 cm^3). A solution of triethylamine in DMF (16 cm^3, 116 mmol) was then added over 5 min., and the mixture stirred first at 0 °C for 2 h. and then at ambient temperature for 2 d. The solution was filtered and the DMF removed under vacuum. The oily residue was taken up in ethyl acetate (150 cm^3), washed sequentially with sat. sodium bicarbonate solution (10 cm^3), brine (10 cm^3), and then dried over anhyd. sodium sulphate. Evaporation of the solvent gave *trans*-*N*-(but-2-enoyl)glycine ethyl ester (4.12) as a white crystalline solid. Yield 6.5 g, (69 %); m.p. 50-52 °C; ν_{max} (nujol) 3300 (br. NH amide), 1760 (C=O ester), 1680 (C=O amide), 1200 cm^{-1} (C-O ester); δ^1H (400 MHz, $CDCl_3$) 1.3 (3H, t, -CH_2CH_3, J = 7.2 Hz), 1.9 (3H, d, CH_3CH=CH-, J = 6.8 Hz), 4.1 (2H, d, -CH_2-CO_2Et, J = 6.2 Hz), 4.3 (2H, q, -CH_2CH_3, J = 7.2 Hz), 5.8 (1H, d, -CH=$CHCH_3$, J = 12.8 Hz), 6.6 (1H, m, CH_3CH=CH-); m/z (FAB +ve ion) 172 (MH^+, 100 %), 126 (MH^+ -EtOH, 62), 104 ($[H_3NCH_2CO_2Et]^+$, 12), 69 ($[CH_3CH=CHCO]^+$, 89); (FAB -ve ion) 170 ($M\text{-}H^+$, 76 %), 142 ($M\text{-}H^+$ -CH_2=CH_2, 57), 124 ($M\text{-}H^+$ -EtOH, 44).

ii) *N*-(2(*S*),3(*R*)-Dihydroxybutanoyl)glycine ethyl ester (4.9)

To a solution of *trans*-*N*-(but-2-enoyl)glycine ethyl ester (4.12) {2.5 g, 14.6 mmol}, triethylamine *N*-oxide dihydrate (2.21 g, 20 mmol), pyridine (1 cm^3), water (7.5 cm^3) and *t*-butanol (50 cm^3), was added a 2.5 % (w/v) solution of osmium tetroxide in *t*-butanol (0.58 cm^3). The reaction mixture was heated under reflux for 48 h. After cooling to ambient temperature, aq. sodium metabisulphite was added (20 % (v/v),

8.0 cm^3). The mixture was concentrated to *ca.* 20 cm^3 on a rotary evaporator, and then extracted with ethyl acetate (3 x 50 cm^3). The combined extracts were washed sequentially with water (20 cm^3) and brine (20cm^3), and then dried over magnesium sulphate. The product was isolated after silica-column chromatography using ethyl acetate as eluent (R_f = 0.3) as a white crystalline solid. Yield 0.9 g, (30 %); m.p. 96-97 °C; (Found: C, 46.6; H, 7.4; N, 6.7%. Calc. for $C_{18}H_{15}NO_5$: C, 46.8; H, 7.4; N, 6.8 %); ν_{max} (nujol) 3300 (br. NH amide and OH), 1734 (C=O ester), 1650 (C=O amide), 1210 cm^{-1} (C-O ester); δ^1H (400 MHz, CD_3OD) 1.23-1.29 (6H, d & t, -C*H*$_3$ and -CH_2C*H*$_3$), 3.88 (1H, d, -C*H*(OH)-CO-, J = 3.2 Hz), 3.90-4.06 (2H, ABq, -C*H*$_2$$CO_2$Et), 4.04 (1H, m, -C*H*O$HCH_3$), 4.19 (2H, q, -C*H*$_2$$CH_3$, J = 7.2 Hz); δ^{13}C (100 MHz, CD_3OD), 14.5 (-CH_2C*H*$_3$), 19.5 (-CHOHC*H*$_3$), 41.8 (-C*H*$_2$$CO_2$Et), 62.4 (-C*H*$_2$$CH_3$), 69.6 (-C*H*OHCO-), 76.5 (-C*H*OHCH_3), 171.4 (-C=O ester), 176.1 (C=O amide); m/z (FAB +ve ion) 206 (MH^+, 100 %), 160 (MH^+ -EtOH, 19), 104 ([$H_3NCH_2CO_2Et$]$^+$, 52); (FAB -ve ion) 204 ($M-H^+$, 100 %), 176 ($M-H^+$ -CH_2=CH_2, 9), 158 ($M-H^+$ -EtOH, 12).

7.5.3.3 *N*-(3-Ketobutanoyl)glycine ethyl ester (4.9)

i) *N*-(3-Hydroxybutanoyl)glycine ethyl ester (4.13)

This was prepared from sodium 3-hydroxybutyrate (4.0 g, 32 mmol) and glycine ethyl ester hydrochloride (4.9 g, 32 mmol) and DECP (5.2 g, 32 mmol) in the presence of triethylamine (9.0 cm^3, 64 mmol), using the same method as described for the synthesis of *N*-(2(*S*),3(*R*)-dihydroxybutanoyl)glycine ethyl ester (4.8). The reaction mixture was filtered and the DMF removed under vacuum. The residual pale yellow oil was taken up in ethyl acetate (150 cm^3), washed sequentially with sat. sodium bicarbonate solution (10 cm^3), brine (10 cm^3), and then dried over anhyd. sodium sulphate. The solvent was evaporated, and tlc of the oily mixture using ethyl acetate as eluent, indicated 3 spots

including the product at $R_f = 0.5$. The *N*-(3-hydroxybutanoyl)glycine ethyl ester was purified by silica-column chromatography using ethyl acetate as eluent and isolated as a white semi-solid. Yield 2.4 g, (56 %); m.p. 35-37 °C; ν_{max} (thin film) 3300-3600 (br. NH amide and OH alcohol), 1749 (C=O ester), 1657 (C=O amide), 1207 cm^{-1} (C-O ester); δ^1H (400 MHz, $CDCl_3$) 1.21 (3H, d, -CHOHC*H*$_3$, J = 6.4 Hz), 1.30 (3H, t, -CH_2CH_3, J = 7.2 Hz), 2.35 (2H, dd, -C*H*$_2$CHOHCH$_3$), 3.98 (1H, m, -C*H*(OH)CH_3), 4.07 (2H, dd, -C*H*$_2$$CO_2$Et, J = 5.2 Hz), 4.17 (2H, q, -C*H*$_2$$CH_3$, J = 7.2 Hz); m/z (FAB +ve ion) 190 (MH^+), 172 (MH^+ -H_2O), 144 (MH^+ -EtOH), 116 ($[CH_3CH(OH)CH_2CONHCH_2]^+$, 87 ($[CH_3CH(OH)CH_2CO]^+$).

ii) *N*-(3-Ketobutanoyl)glycine ethyl ester (4.9)

This was prepared from the above alcohol using Collin's oxidation.[126] Thus, chromium (vi) oxide (4.5 g, 44.4 mmol) was suspended in dry DCM (100 cm^3) and cooled to 0 °C. Pyridine (7.2 cm^3, 88.8 mmol) was added with stirring over 5 min., and the mixture was further stirred at ambient temperature for 30 min. *N*-(3-Hydroxybutanoyl)glycine ethyl ester (1.2 g, 6.4 mmol) in DCM (25 cm^3) was then added in one portion, and the mixture stirred vigorously for 3 h. The reaction was followed by tlc ($R_f = 0.5$ for product) using ethyl acetate as eluent. The mixture was added to diethyl ether (100 cm^3) and then filtered. The black residue was extracted with ether (3 x 50 cm^3), and silica gel (*ca.* 10 g) was added to the combined ether extracts until the solution clarified. The solvent was removed under vacuum, and the residual oily product purified by silica-column chromatography using ethyl acetate as eluent, to give a white semi-solid. Yield 0.44 g, (40 %); m.p. 40 °C; (Found: C, 50.18; H, 6.98; N, 6.99 %. Calc. for $C_8H_{13}NO_4$: C, 51.33; H, 7.00; N, 7.48 %); ν_{max} (thin film) 3312 (NH amide), 2980 (CH_3, stretch), 1749 (C=O ester and CH_3C=O overlap), 1662 (C=O amide), 1205 cm^{-1} (C-O ester); δ^1H (400 MHz, $CDCl_3$) 1.26 (3H, t, -CH_2CH_3, J = 7.2 Hz), 2.9 (3H, s, -COC*H*$_3$), 3.5 (2H, s, CH_3COC*H*$_2$-), 4.04 (2H, d, -C*H*$_2$$CO_2$Et, J = 5.6 Hz), 4.22 (2H, q, -C*H*$_2$$CH_3$, J = 7.2 Hz);

$\delta^{13}C$ (100 MHz, $CDCl_3$) 14.1 (-CH_2CH_3), 30.9 (CH_3CO-), 41.1 (CH_3COCH_2-), 49.9 (-CH_2CO_2Et), 61.6 (-CH_2CH_3), 165.9 (*C*O, amide), 169.6 (*C*O ester), 204.6 (CH_3CO-); m/z (FAB +ve ion) 188 (MH^+, 82 %), 142 (MH^+ -EtOH, 48), 114 (MH+ -EtOH -CH_2=CH_2, 41), 104 ([$H_3NCH_2CO_2Et$]$^+$, 100), 85 ([CH_3COCH_2CO]$^+$, 13); (FAB -ve ion) 186 (M-H^+, 79 %), 158 (M-H^+ -CH_2=CH_2, 54), 140 (M-H^+ -EtOH, 30).

7.5.3.4 *cis-N*-(2,3-Epoxybutanoyl)glycine ethyl ester (4.10)

i) *cis*-2,3-Epoxybutanamide (4.15)

To a 3-necked flask equipped with dropping-funnel, thermometer and a combination electrode connected to a pH meter, was added crotononitrile (33.6 g, 0.5 mol, 50:50 % *cis* and *trans* mixture), water (300 cm^3) and 30 % hydrogen peroxide (67 cm^3, 0.6 mol). The mixture was stirred at 35 °C while 1 M aqueous NaOH was added *via* a dropping-funnel to maintain the pH at 7.3-7.5. After 9 h., the pH became constant indicating completion of reaction. The mixture was then treated with 5 % Pd/C (100 mg) and stored overnight at 5 °C. After filtration, most of the water was removed under vacuum. The colourless, oily residue was extracted with ethyl acetate (300 cm^3) and dried over magnesium sulphate. The solvent was removed under vacuum, and the crude off-white solid was recrystallised from ether/hexane (4:1 v/v) to give a white crystalline solid. Yield 12.6 g, (28 %); m.p. 88-90 °C; (Found: C, 47.26; H, 6.94; N, 13.52 %. Calc. for $C_4H_7NO_2$: C, 47.52, H 6.98, N 13.85 %); ν_{max} (KBr) 3350, 3175 (NH_2), 3010 (CH epoxide), 2850 (CH_3 stretch), 1650 (C=O amide), 1140 cm^{-1} (C-O epoxide); δ^1H (400 MHz, $CDCl_3$) 1.32 (3H, d, -CHC*H*$_3$, J = 5.2 Hz), 3.44 (1H, m, -O-C*H*CH_3), 3.64 (1H, d, -C*H*$CONH_2$, J = 5.2 Hz), 6.22 (2H, br. s, N*H*$_2$); $\delta^{13}C$ (100 MHz, $CDCl_3$) 13.2 (-*C*H_3), 54.17 (-O-*C*HCH_3), 55.1 (-*C*$HCONH_2$), 170.4 (*C*O); m/z (FAB +ve ion) 102 (MH^+, 100 %), 85 (MH^+ -NH_3, 47); (FAB -ve ion) 100 (M-H^+, 100 %).

ii) *cis*-*N*-(2,3-Epoxybutanoyl)glycine ethyl ester (4.10)

To a stirred solution of *cis*-2,3-epoxybutanamide (4.15) {1.0 g, 10 mmol}, LDA (1.4 g, 13 mmol) and 12-crown-4-ether (2 cm^3, 1.3 equiv.) in dried THF (100 cm^3) under an atmosphere of N_2 at -40 °C, was added ethylbromoacetate (1.5 cm^3, 13 mmol) in THF (25 cm^3) dropwise over 30 min. The reaction mixture was stirred at -40 °C for a further 30 min., and then at ambient temperature for 30 min. The reaction was followed by analytical hplc (see Section 7.4.1.2). On completion, the solvent was removed under vacuum and the crude solid residue was washed with hexane (3 x 20 cm^3). The product was dissolved in 15 % (v/v) methanol in water, and then purified by semi-preparative hplc with uv detection at λ = 210 nm, using a Jones Apex Prepsil ODS column (25 cm x 25 mm) eluting with 15 % (v/v) methanol in water eluent, and collecting the fraction with R_f = 12.7 min. From the pooled fractions of eluent, methanol was evaporated under vacuum and water was removed by freeze-drying to leave an oily residue. The preparative hplc was repeated on the oily residue to obtain a purer product. Yield 0.36 g, (21 % isolated, but 68 % by anal. hplc); ν_{max} (thin film) 1750 (C=O ester), 1625 (C=O amide), 1210 cm^{-1} (C-O ester); δ^1H (400 MHz, $CDCl_3$) 1.30 (3H, t, -CH_2CH_3, J = 7.2 Hz), 1.42 (3H, d, CH_3CH-O-, J = 5.2 Hz), 3.33 (1H, m, -O-C*H*CH_3), 3.53 (1H, d, -O-C*H*-CO-, J = 4.8 Hz), 3.93, 4.24 (2H, dd, -NHC*H*$_2CO_2Et$), 4.20 (2H, q, -CH_2CH_3, J = 7.2 Hz), 6.67 (1H, br. s, N*H*); δ^{13}C (100 MHz, $CDCl_3$) 13.1 (CH_3CHCO-), 14.1 (-CH_2CH_3), 40.6 (-O-CHCO-), 54.7 (CH_3-CH-O-), 55.3 (-CH_2CO_2Et), 61.7 (-CH_2CH_3), 167.8 (CO amide), 169.3 (CO ester); m/z (FAB +ve ion) 188 (MH^+, 100 %), 142 (MH^+ -EtOH, 27), 130 ([OCNHCH$_2$CO$_2$Et]$^+$, 10), 114 ([CH_3CHOCHCONHCH$_2$]$^+$, 34), 104 ([H_3NCH$_2$CO$_2$Et]$^+$, 34).

7.5.1.5 *N*-(2,3-Epoxypropanoyl)glycine ethyl ester (4.14)

i) 2,3-Epoxypropanamide (7.8)

This was prepared from acrylonitrile (26.5 g, 0.5 mol) and 30 % hydrogen peroxide (67 cm^3, 0.6 mol) using the same method and work up as described for the preparation of *cis*-2,3-Epoxybutanamide (4.15).[127] The product was recrystallised from ether/hexane (4:1 v/v) to give a white crystalline solid. Yield 23 g (53 %); m.p. 33.5 °C (lit. m.p. 32-34 °C[127]).

ii) *N*-(2,3-Epoxypropanoyl)glycine ethyl ester (4.14)

This was prepared from 2,3-epoxypropanamide (7.8) {1.75 g, 20 mmol}, LDA (2.38 g, 23 mmol) and ethylbromoacetate (2.55 cm^3, 23 mmol) using the same method and work up as described for the preparation of *cis*-*N*-(2,3-epoxybutanoyl)glycine ethyl ester (4.10). The product was purified by preparative hplc (R_f = 8.0 min.) to give a white crystalline solid. Yield 0.63g (18 % isolated, but 55 % by anal. hplc); ν_{max} (nujol) 1730 (C=O ester), 1640 (C=O amide), 1206 cm^{-1} (C-O ester); δ^1H (400 MHz, $CDCl_3$) 1.24 (3H, t, CH_2CH_3, J = 7.2 Hz), 2.82 (1H, m, -O-CH(*H*)), 2.95 (1H, m, -O-C*H*(H)), 3.45 (1H, m, -O-C*H*CO-), 3.95 (2H, ABq, -HNCH_2CO_2Et), 4.15 (2H, q, -CH_2CH_3, J = 7.2 Hz); m/z (FAB +ve ion) 174 (MH^+, 25 %), 146 (MH^+ -CH_2=CH_2, 11), 128 (MH^+ -EtOH, 28), 104 $[H_3NCH_2CO_2Et]^+$, 40), 100 (MH^+ -EtOH -CH_2=CH_2, 44); (FAB -ve ion) 172 ($M-H^+$, 65%), 144 ($M-H^+$ -EtOH, 26), 98 ($M-H^+$ -EtOH -CH_2=CH_2, 35).

7.5.4 Synthesis of Authentic Products from the Decomposition of *cis*-2,3-Epoxybutanamide (4.15)

7.5.4.1 *trans*-2,3-Epoxybutanoic acid (5.4)

This was prepared *via* a literature method[128] involving the epoxidation of *trans*-crotonic acid by hydrogen peroxide in the presence of sodium tungstate catalyst in a slightly acidic medium. Thus, to an aq. solution (50 cm^3) of *trans*-crotonic acid (4.30 g, 0.05 mol) and sodium hydroxide (1.0 g), was added sodium tungstate dihydrate (0.92 g, 0.005 mol) with warming to effect dissolution. Hydrogen peroxide in water (27.5 %, w/v) {7.5 cm^3, 0.065 mol} was added dropwise with stirring, and the pH was maintained above 4 by the dropwise addition of 5 M sodium hydroxide solution. After 1 h., 30 % sulphuric acid was added dropwise to give pH *ca.* 2.5. The solution was then saturated with ammonium sulphate, and extracted with ether (3 x 50 cm^3). The combined organic extract was dried with anhyd. sodium sulphate, and the solvent evaporated under vacuum to give a crude oily product. *cis*-2,3-Epoxybutanoic acid was purified by silica-column chromatography eluting with ethyl acetate to give a colourless oil. Yield 1.94 g (38 %); ν_{max} (thin film) 3600-3200 (OH), 1740 cm^{-1} (C=O acid); δ^1H (400 MHz, 0.2 M NaOD) 1.37 (3H, d, C*H*$_3$, J = 5.6 Hz), 3.14 (1H, m, -O-C*H*CH$_3$), 3.20 (1H, d, -O-C*H*CO$_2$D, J = 2.4 Hz); m/z (FAB -ve ion) 101 (M-H$^+$, 100 %), 57 (M-H$^+$ -CO$_2$, 25).

7.5.4.2 2(*R*),3(*S*)-Dihydroxybutanoic acid (5.5)

This was prepared from *trans*-crotonic acid (3.0 g, 35 mmol), triethylamine *N*-oxide dihydrate (5.3 g, 48 mmol) and 2.5 % (w/v) solution of osmium tetroxide in *t*-butanol (1.40 cm^3) using the same method and work up as described for the preparation of *N*-(2(*S*),3(*R*)-dihydroxybutanoyl) glycine ethyl ester (4.8). The product was purified by silica-column chromatography using 5:1 (v/v) ethyl acetate/ethanol as eluent to give the

product as a pale yellow oil. Yield 1.8 g, (42 %); ν_{max} (thin film) 3000-3600 (OH), 1730 cm^{-1} (C=O acid); δ^1H (400 MHz, 0.2M NaOD) 1.23 (3H, d, C*H*$_3$, J = 6.4 Hz), 3.90 (1H, d, -C*H*OHCO-, J = 2.8 Hz), 4.00 (1H, m, -C*H*OHCH$_3$); m/z (FAB -ve ion) 119 (M-H^+, 100 %), 101 (M-H^+ -H_2O, 5), 75 (M-H^+ -CO_2, 18).

7.5.4.3 2(*S*)-Hydroxy-3(*R*)-*N*-Morpholinobutanamide (5.6)

cis-2,3-Epoxybutanamide (4.15) {100 mg, 1 mmol} dissolved in aqueous morpholine (25 cm^3, 1.0 M) was heated at 37 °C for 4 d. The water and excess morpholine were then removed by freeze-drying to give a fluffy white crystalline solid. The product was recrystallised from chloroform/hexane (3:1 v/v). Yield 165 mg, (88 %); m.p. 139-140 °C; (Found: C, 50.20; H, 8.44; N, 14.20 %. Calc. for $C_8H_{16}N_2O_3$: C, 51.05; H, 8.57; N, 14.88 %); ν_{max} (KBr) 3400, 3150 (NH_2 amide and OH overlap) 1680 cm^{-1} (C=O amide); δ^1H (400 MHz, D_2O) 1.10 (3H, d, -C*H*$_3$, J = 7.2 Hz), 2.59 (2H, m, -H_2CNC*H*$_2$- ring), 2.72 (2H, m, -*H*$_2$CNCH$_2$- (ring)), 2.88 (1H, m, -C*H*(CH$_3$)N-), 3.77 (4H, m, -C*H*$_2$OC*H*$_2$- (ring)), 4.01 (1H, d, -C*H*OHCO-, J = 6.8 Hz), 5.4 (1H, br. s, -NH(*H*)), 6.98 (1H, br. s, -N*H*(H)); $\delta^{13}C$ (100 MHz, $CDCl_3$) 10.1 (-*C*H$_3$), 62.7 (-*C*H(OH)CO-), 67.2 (-H_2*C*NCH$_2$- (ring)), 71.1 (-*C*H$_2$O*C*H$_2$- (ring)), 169.0 (*C*O amide); m/z (FAB +ve ion) 189 (MH^+, 63 %), 144 ([O(C_4H_8)N-CH(CH$_3$-CH(OH)]$^+$, 6), 114 ([O(C_4H_8)N-CH(CH$_3$)]$^+$, 100); (FAB -ve ion) 187 (M-H^+, 100 %).

8. References

1. P. N. Magee & J. M. Barnes, *Adv. Cancer Res.*, 1976, **10**, 163.

2. P. N. Magee, R. Montesano & R. Preussmann, '*Chemical Carcinogens*,' ed. C. E. Searle, ACS Monograph 173, American Chemical Society, Washington D.C., 1976, p.491.

3. S. S. Mirvish, *Toxicol. Appl. Pharmacol.*, 1975, **31**, 325.

4. J. H. Ridd, *Quart. Rev.*, 1961, **15**, 418.

5. C. L. Walters, *Oncology*, 1980, **37**.

6. P. I. Reed, P. L. R. Smith, K. Haines, F. R. House & C. L. Walters, *Lancet.*, 1981, **ii**, 550.

7. S. E. Shepherd, C. H. Schlatter & W. K. Lutz, in '*Relevance of N-Nitroso-Compounds to Human Cancer, and Mechanisms*,' eds. H. Bartsch, I. K. O' Neill & R. Schultz-Hermann, IARC Scient. Publ. No. 84, IARC, Lyon, France, 1987, p. 292.

8. S. E. Shepherd, C.H. Schlatter & W. K. Lutz, *Fd. Chem. Toxicol*, 1987, **25**, 91.

9. E. P. Steffey & B. Tarkington, *Amer. Rev. Resp. Dis.*, 1977, **115**, 403.

10. D. Hoffman, J. D. Adams, K. D. Brunneman & S. S. Hecht, '*ACS Symposium Series 174, N-Nitroso-Compounds*,' eds. R. A. S. R. Tannebaum, ACS, Washington D.C., 1981, p. 247.

11. B. C. Challis, B. R. Glover & J. R. A. Pollock, in ref. 7, p. 345.

12. L. Baldini & G. Brambilla, *Cancer Res.*, 1966, **26**, 1727.

13. E. Banfi, M. Tamero, B. Pani & C. Monti-Bragadin, *Boll, Inst. Sieroter, Milan*, 1974, **531**, 632.

14. G. Brambilla, M. Cavanno, A. Maura, S. Parodi, A. Furlani & I. De Fant, *Mutat. Res.*, 1980, **78**, 375.

15. L. Giraldi, C. Monti-Bragadin & R. Della-Loggia, *Experentia*, 1974, **30**, 496.

16. G. Sava, T. Giraldi & L. Baldini, *Cancer Treat. Rep.*, 1979, **66**, 179.

17. C. Monti-Bragadin, M. Tamaro & E. Banfi, *Anticromb. Agents and Chemotherapy*, 1974, **6**, 655.

18. S. Shuja, *PhD Thesis*, The Open University, 1993.

19. B. C. Challis, in '*Cancer Surveys*,' S. Forman, D. Shuker, D.E.G. eds. O.U. Press, Oxford, 1989, Vol. **8**, p. 362.

20. B. C. Challis, J. R. Milligan & R. C. Mitchell, *J. Chem. Soc., Chem. Commun.*, 1984, 1050.

21. B. C. Challis, A. R. Hopkins, J. R. Milligan, R. C. Massey, D. Anderson & S. D. Blowers, *Toxicol. Lett.*, 1985, **26**, 89.

22. W. Kubacka, L. M. Libbey & R. A. Scanlan, *J. Agric. Food Chem.*, 1984, **32**, 401.

23. A. R. Tricker, M. Jo, R. C. Massey & D. J. McWenny, *Food Add. Contam.*, 1984, **1**, 307.

24. K. Bott, *Angew. Chem. Int. Edn.*, 1979, **18**, 259.

25. M. Regitz, *Synthesis*, 1972, 351.

26. T. Aoyama, M. Kabeya, A. Fukushima & T. Shioiri, *Heterocycles*, 1985, **23**, 2363.

27. H. Zollinger, '*Azo and Diazo Chemistry*,' Interscience, N.Y., 1961.

28. For a comprehensive review, see '*The Chemistry of the Diazonium and Diazo Groups*,' ed. S. Patai, Wiley, Chichchester, 1978.

29. G. W. Cowell & A. Ledwith, *Quart. Rev.*, 1970, **24**, 119.

30. M. Regitz, '*The Chemistry of Diazonium and Diazo Groups*,' Part 2, ed. S. Patai, John Wiley Interscience, Bristol, 1978, p. 659.

31. T. Curtius and A. Dapravsky, *Chem Ber.*, 1906, **39**, 1373.

32. W. Rundell, *Angew. Chem.*, 1962, **74**, 496.

33. T. Curtius, *Chem. Ber.*, 1889, **22**, 2161.

34. W. R. Bamford & S. Stevens, *J. Chem. Soc.*, 1952, 4735.

35. S. M. Hecht & J. W. Kozarich, *Tetrahedron Lett.*, 1972, **50**, 5147.

36. B. R. Brown & D. L. Hammick, *J. Chem. Soc.*, 1947, 1384.

37. T. Curtius, *Chem. Ber.*, 1883, **16**, 2230.

38. T. Curtius & J. Thompson, *Chem. Ber.*, 1906, **39**, 1379.

39. T. Curtius & L. Callen, *Chem. Ber.*, 1910, **43**, 2447.

40. T. Curtius & J. Thompson, *Chem. Ber.*, 1906, **39**, 4140.

41. J. H. Looker & J. W. Carpenter, *Canad. J. Chem.*, 1967, **45**, 1727.

42. B. C. Challis & F. Latif, *J. Chem. Soc., Perkin Trans. I*, 1990, 1005.

43. E. H. White, *J. Amer. Chem. Soc.*, 1955, **77**, 6008.

44. R. C. Weast, Ed., '*CRC Handbook of Chemistry & Physics*,' 60 ed., CRC Press, Boca Raton, Florida, 1979, p.218.

45. D. A. Ben-Etraim, in ref. 28 , p.149.

46. O. Dimroth, M. Eble & W. Gruhl, *Ber.*, 1907, **40**, 2390.

47. T. A. Daniels, S. Sidi & K. Vaughan, *Canad. J. Chem.*, 1977, **55**, 3751.

48. T. P. Ahern & K. Vaughan, *J. Chem. Soc., Chem. Commun.*, 1973, 701.

49. N. S. Isaacs & E. Rannala, *J. Chem. Soc. Perkin Trans II*, 1974, 899.

50. R. Baumgarten, *J. Org. Chem.*, 1966, **32**, 484.

51. J. F. McGarrity, *J. Chem. Soc., Chem Commun.*, 1974, 558.

52. G. N. Okfao, *PhD Thesis*, London, 1989.

53. G. B. Neurath, M. Dungar & F. G. Pein, *IARC Scientific Publ. No. 14*, IARC, Lyon, 1976, 215.

54. C. Smith & C. H. Watts, *J. Chem. Soc.*, **97**, 562, 1910.

55. O. Dimroth, *Chem. Ber.*, 1905, **38**, 670.

56. O. Dimroth, *Chem. Ber.*, 1905, **38**, 2329.

57. E. G. Rukdadze, T. V. Ershova, S. A. Fedorova & A. P. Terent'ev, *Zhur. Obschei. Khim.*, 1969, **39**, 303 (Chem. Abs., 1969, **71**, 3451z).

58. L. D. Brown & J. A. Ibers, *J. Amer. Chem. Soc.*, 1976, **98**, 1957.

59. G. Bombier, A. Immirzi & L. Toniolo, *J. Inorg. Chem.*, 1976, **15**, 2428.

60. M. Corbett & B. F. Hoskins, *J. Chem. Soc., Chem. Commun.*, 1968, 1602.

61. J. Kuyper, P. I. van Vliet & K. Vieze, *J. Organometallic Chem.*, 1976, **105**, 317.

62. M. Corbett, B. F. Hoskins, N. J. McLeod & B. P. O' Day, *Austral. J. Chem.*, 1975, **28**, 2377.

63. S. C. De Sanctis, L. Tonido, T. Boschi & G. Deganollo, *Inorg. Chim. Acta.*, 1975, **12**, 251.

64. E. Phieffer, J. Kuyper & K. Vieze, *J. Organometallic Chem.*, 1976, **105**, 371.

65. P. I. van Vliet, J. Kuyper & K. Vrieze, *J. Organometallic Chem.*, 1976, **122**, 99.

66. G. F. Kolar, in '*Mass Spectroscopy in Biochemistry and Medicine*,' ed. Frigerio and Castagnoli, Raven Press, N. Y., 1974, 267.

67. T. P. Ahern, H. Fong & K. Vaughan, *Canad. J Chem.*, 1977, **55**, 1701.

68. N. S. Isaacs & E. Rannala, *J. Chem. Soc., Perkin Trans. II*, 1974, 899.

69. K. Vaughan, *J. Chem. Soc., Perkin Trans. II*, 1977, 17.

70. K. Albert, K. M. Dangel, A. Rieker, H. Iwamura & Y. Imahashi, *Bull. Chem. Soc. Japan*, 1976, **49**, 2537.

71. H. Iwamura, K. Albert & A. Rieker, *Tetrahedron Lett.*, 1976, 2627.

72. D. Dadzi & J. Jan, *Spectroscopy Letters*, 1968, **1**, 139.

73. W. J. Abery, A. N. Campbell-Crawford & K. S. Hobbs, *J. Chem. Soc., Perkin Trans II*, 1972, 2180.

74. R. J. W. Le Fevre & T. H. Liddecoet, *J. Chem. Soc.*, 1951, 2743.

75. R. Preussman, A. von Hodenberg & H. Hengy, *Biochem. Pharmacol.*, 1969, **18**, 1.

76. T. Ong & F. J. De Serres, *Mutation Research*, 1971, **13**, 276.

77. H. Druckrey, S. Ivankovic, R. Preussman & U. Brunner, *Experientia*, 1967, **23**, 1042.

78. I. V. Zlochevskaya, E. G. Rukhadze, T. S. Bobkavol & L. N. Checkunova, *Vestn. Mosk. Univ. Biol Pochvoved*, 1973, **28**, 42 (*Chem Abs.*, 1974, **81**, 21539*N*).

79. F. A. Schmid & D. J. Hutchinson, *Cancer Research*, 1974, **34**, 1671.

80. D. A. Clarke, B. K. Barclay, C. C. Stock & C. S. Rondestvedt, *Proc. Soc. Exp. Biol. Med.*, 1955, **90**, 484.

81. S. K. Carter & M. A. Friedman, *European J. Cancer*, 1972, **8**, 85.

82. K. Hano, A. Akashi, I. Yamamoto, S. Narumi & H. Iwati, *Gann.*, 1968, **59**, 207.

83. R. C. S. Audette, T. A. Connors, H. G. Mandel, K. Merani & W. C. J. Ross, *Biochem. Pharmacol.*, 1973, **22**, 1855.

84. W. J. Dunn, M. J. Greenberg & S. S. Callejas, *J. Med. Chem.*, 1976, **19**, 1299.

85. G. F. Kolar & R. Preussman, *Z. Naturforsch*, 1971, **26B**, 950.

86. B. C. Challis, M. H. R. Fernandes, B. R. Glover & F. Latif, in ref. 7, p.308.

87. W. J. Albery & R. P. Bell, *Trans. Faraday Soc.*, 1961, **57**, 1942.

88. W. J . Albery & M. H. Davies, *Trans. Faraday Soc.*, 1969, **65**, 1066.

89. W. J. Albery, J. E. C. Hutchins, R. M. Hyde & R. H. Johnson, *J. Chem. Soc.*, ***B***, 1968, 219.

90. M. M Kreevoy and D. E. Konasewich, *J. Phys. Chem.*, 1970. **74**, 4464.

91. B. R. Glover, *PhD Thesis*, London, 1969.

92. P. Brewser, F. Hiron, E. D. Hughes, C. K. Ingold & P. A. D. S. Rao, *Nature*, 1950, **166**, 178.

93. C. K. Ingold, '*Structure and Mechanism in Organic Chemistry*,' G. Bell and Sons Ltd., London, 1963, p. 381.

94. M. Larcheveque & Y. Petit, *Tetrahedron Lett.*, 1984, **25**, 3705.

95. *'Asymmetric Synthesis-Construction of Chiral Molecules using Amino Acids,'* eds. G. M. Coppola & H. F. Schoster, John Wiley and Sons Inc., N.Y., 1987.

96. S. Henerot, M. Larcheveque & Y. Petit, *Synth. Commun.*, 1986, **16**, 183.

97. M. B. Takeo & A. Eiichi, see *Chem. Abs.*, 1983 (**23**), 193732 *K*.

98. E. H. White, *J. Amer. Chem. Soc.*, 1955, **77**, 6008.

99. A. T. Austin & J. Howard, *J. Chem Soc.*, 1961, 3278.

100. J. H. Markgraf & H. A. Davies, *J. Chem. Ed.*, 1990, **67**, 173.

101. H. Sachs & E. Brand, *J. Amer. Chem. Soc.*, 1954, **76**, 3601.

102. A. T. Austin & J. Howard, *Chem. Ind.*, 1959, 1413.

103. A. T. Austin & J. Howard, *J. Chem. Soc.*, 1961, 3593.

104. C. D. Maycock & R. J. Stoodley, *J. Chem. Soc. Chem. Commun.*, 1976, 234.

105. C. D. Maycock & R.J. Stoodley, *J. Chem. Soc. Perkin Trans. I*, 1979, 1852.

106. J. S. Sandhu (unpublished results).

107. N. C. Carmen, *PhD Thesis,* The Open University, 1991.

108. J. H. Markgraf & H. A. Davies, *J. Chem. Soc.*, 1990, **67**, 173.

109. J. R. A. Pollock, *'N-Nitroso Compounds: Occurence and Biological Effects,'* eds. H. Bartsch, I. K. O' Neill & M. Castegnaro, IARC, Scient. Publ. No. 41, p. 81.

110. A. R. Tricker & R. Preussman, *Carcinogenesis*, 1986, **7**, 1523.

111. J. R. A. Pollock, *Fd. Chem. Toxicol.*, 1985, **23**, 701.

112. T. Curtius & J. Thompson, *Chem. Ber.*, 1906, **39**, 4140.

113. O. Dimroth, *Ann.*, 1910, **373**, 336.

114. B. C. Challis, B. R. Glover & J. R. A. Pollock (unpublished results).

115. B. Pani, N. Bahudri, F. Bartoli-Klugmann, S. Venturini & I. De Fant, *Mutat. Res.*, 1980, **78**, 375.

116. G. Sava, T. Giraldi & L. Baldini, *Cancer Treat. Rep.*, 1979, **66**, 179.

117. T. Giraldi, C. Nisi & G. Savana, *European J. Cancer*, 1979, **13**, 1321.

118. T. Giroldi, A. M. Guarino, C. Nisi and L. Baldini, *European J. Cancer.*, 1979, **15**, 603.

119. S. Parodi, M. Picca, C. Bolognesi, M. Cavanna, P. Carlo, R. Finollo & G. Brambilla, *Pharmacol. Res. Commun.*, 1977, **9**, 621.

120. G. Brambilla, M. Cavanna, S. Parodi and L. Baldini, *European J. Cancer*, 1972, **8**, 127.

121. G. Brambilla, M. Cavanna, S. Parodi & L. Baldini, *Transplantation*, 1972, **10**, 100.

122. F. Latif, *PhD Thesis*, University of London, 1986.

123. W. J. Baron, M. R. De Camp, M. E. Hendrick, M. Jones Jr., R. H. Levin & M. B. Sohn, '*Carbenes*,' Vol I, eds. M. Jones Jr., R. A. Moss, John Wiley & Sons, N.Y., 973, p.1.

124. H. Chaimovich, R. J. Vaughan & F. H. Westheimer, *J. Amer. Chem. Soc.*, 1968, **90**, 4088.

125. J. C. Collins, W. W. Hess, F. J. Frank, *Tetrahedron Lett.*, 1968, 3363.

126. A. B. Smith, P. A. Levenberg, *Synthesis*, 1981, 567.

127. G. B. Payne & P. H. Williams, *J. Org. Chem.*, 1961, **26**, 651.

128. G. Foulds, *U.S. Pat.* 3,651,136, 1972, Ser. No. **874,716**.

129. J. W. Daley, D. M. Jerina & B. Witkop, *Experientia*, 1972, **28**, 1129.

130. D. M. Jerina & J. W. Daley, *Science*, 1974, **185**, 573.

131. T. C. Bruice & P. Y. Bruice, *Acc. Chem. Res.*, 1976, **9**, 378.